1. "I wish to discuss the strength of hollow solids, which are employed in art - and still oftener in nature - in a thousand operations for the purpose of greatly increasing strength without adding to weight; examples of these are seen in the bones of birds and in many kinds of reeds which are light and highly resistant both to bending and breaking".

   - Galileo Galilei

2. Omission, in the current design recommendations, of the distortional failure for full width unstiffened T-joints of rectangular hollow sections loaded with an out-of-plane bending moment is unsafe.

3. The current CIDECT recommendation for the multiplanar load effect of multiplanar joints should be corrected for small $\beta$ values and large negative load ratios.

4. In evaluating databases of static strength of connections not only the material and geometrical properties, the modelling and the definition of the ultimate load (moment) capacities should be considered, but also the boundary conditions and the testing method.

5. Every PhD student in Civil Engineering should work in practice for 6 months, to bridge the gap between researchers and designers and to accelerate the introduction of new research results into design practice.

6. Standing by a stream, Confucius said: "Ah! that which is passing is just like this, never ceasing day or night".
   Looking back at the past, a PhD student says: "Time is flying just like a passing stream, never ceasing day or night".

7. Governments, industries and researchers should make more effort in the development of environmentally friendly energy sources based on sun, wind, water and other inexhaustible resources.

8. "To be" a mother *as a housewife* "or not to be" a mother *as a working woman* should not be a question in a modern society, because women as an important productive force should not be forced to play the tragedy of Shakespeare.

9. The Dutch title system is very confusing for a foreign student. A female law student works four years to put a male title before her name (mevrouw mr.), which in English means Mrs. Mr. A male master degree student (drs.) works four years more in order to get a degree one letter less (dr.).

10. Sometimes circular is better, sometimes square...
    (TV-advertisement Bokma jenever)

# STELLINGEN

behorende bij het proefschrift

# The Static Strength of Uniplanar and Multiplanar Connections In Rectangular Hollow Sections

Y. Yu

Delft, December 1997    •

1.  "Ik wil de sterkte bespreken van holle structuren die in de kunst - en nog vaker in de natuur - op duizend verschillende manieren worden toegepast teneinde de sterkte te vergroten zonder gewichtstoename; voorbeelden hiervan zijn te vinden in de botten van vogels en in vele soorten riet, die licht zijn en zeer goed bestand tegen buigen en breken".

    - Galileo Galilei

2.  Doordat in de huidige rekenregels voor T-verbindingen van rechthoekige buisprofielen, belast op een moment uit het vlak, een controle op distorsie ontbreekt, zijn deze rekenregels onveilig.

3.  De huidige CIDECT richtlijnen voor ruimtelijke verbindingen voor kleine breedteverhoudingen, waarbij de wandstaven tegengesteld belast zijn, moeten worden aangepast.

4.  Bij het analyseren van databestanden van de statische sterkte van buisverbindingen moet niet alleen aandacht worden besteed aan de materiaal- en geometrische eigenschappen, het modelleren en het criterium waarop de uiterste sterkte is bepaald, maar ook aan de randvoorwaarden en de methode van beproeven.

5.  Alle promovendi in de Civiele Techniek zouden een half jaar in een bedrijf moeten werken om de afstand tussen onderzoekers en ontwerpers te verkleinen en nieuwe onderzoeksresultaten sneller in de praktijk te kunnen toepassen.

6.  Bij een stromende beek staande, zei Confucius: "Ah! al wat geschiedt is wat u hier ziet, het gaat dag en nacht door."
    Naar het verleden kijkend zegt een promovendus: "De promotietijd vliedt voorbij als een stromende beek, zonder ophouden, dag en nacht."

7.  Ten behoeve van een beter milieu voor toekomstige generaties dienen overheid, industrie en onderzoekers snel een revolutie op het gebied van energieopwekking te bewerkstelligen, die gebaseerd is op zon, wind, stromend water en andere onuitputtelijke bronnen.

8.  "To be" een moeder *als huisvrouw* " or not to be" een moeder *als werkende vrouw* zou tegenwoordig geen punt van discussie meer mogen zijn, omdat de vrouw als een belangrijke produktieve kracht niet in de rol van Shakespeare's tragedie zou mogen worden gedwongen.

9.  De Nederlandse titulatuur is uiterst verwarrend voor buitenlandse studenten. Een vrouwelijke rechtenstudent werkt vier jaar om een mannelijke titel voor haar naam te krijgen (mevrouw mr.), wat in het Engels "mevrouw meneer" zou betekenen. Een doctoraal student (drs.) moet nog vier jaar werken om één letter van de titel af te krijgen (dr.).

10. Soms is rond beter, soms vierkant...    (TV-reclame Bokma jenever)

# THE STATIC STRENGTH OF UNIPLANAR AND MULTIPLANAR CONNECTIONS IN RECTANGULAR HOLLOW SECTIONS

# THE STATIC STRENGTH OF UNIPLANAR AND MULTIPLANAR CONNECTIONS IN RECTANGULAR HOLLOW SECTIONS
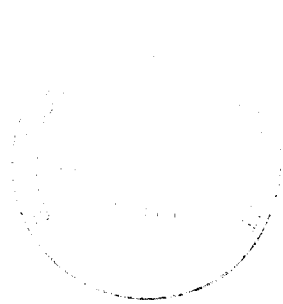
PROEFSCHRIFT

door

**Yanrong YU**

civiel ingenieur

geboren te Pingshan, Hebei, China

Dit Proefschrift is goedgekeurd door de promotor:
Prof. dr. ir. J. Wardenier

Samenstelling promotiecommissie:

Rector Magnificus        :   Voorzitter
Prof. dr. ir. J. Wardenier :   Faculteit der Civiele Techniek,
                             Technische Universiteit Delft, promotor
Prof. ir. J.W.B. Stark    :   Faculteit der Civiele Techniek,
                             Technische Universiteit Delft
Prof. ir. J. Witteveen    :   Em. (1997) hgl. Faculteit der Civiele Techniek,
                             Technische Universiteit Delft
Prof. dr. G. Den Ouden   :   Scheikundige Technologie en Materiaalkunde,
                             Technische Universiteit Delft
Prof. ir. H.H. Snijder    :   Faculteit der Bouwkunde,
                             Technische Universiteit Eindhoven
Prof. dr. ir. R.S. Puthli  :   Versuchsanstalt für Stahl, Holz und Steine,
                             Universität Karlsruhe, Duitsland

## ACKNOWLEDGEMENTS

# TABLE OF CONTENTS

# SYNOPSIS

Rectangular hollow sections (RHS) can be found in many applications, among which are industrial buildings, towers, masts, bridges, crane booms and mechanical equipments etc. with various types and configurations of connections. Little information was available on the static behaviour of multiplanar connections until the end of the 1980s. Furthermore, for uniplanar connections under complicated loading conditions, limited evidence was available. This research programme aims to provide design recommendations on the static strength for such connections.

This thesis presents the results of analytical, experimental and numerical studies on the static strength of uniplanar and multiplanar welded connections in rectangular hollow sections.

In the analytical study, a set of formulae is developed for full width X-joints loaded with axial forces, in-plane bending moments and out-of-plane bending moments respectively, based upon a so called "4-hinge yield line and chord web crippling" model. Furthermore, the influence of the bending moments in the chord on the ultimate load capacity of the joint is studied analytically.

In the experimental research programme, the multiplanar geometrical stiffening effect due to the existence of the out-of-plane braces and the multiplanar load effect due to the loads applied on the out-of-plane braces have been studied.

A numerical model (finite element model) has been developed and calibrated with the experimental results. The numerical modelling and calibration considered the following aspects: the element types, the modelling of the weld, the modelling of the members and the behaviour of material and geometrical non-linearities.

The finite element model is further used for a series of extensive parameter studies for uniplanar X-, T- and multiplanar XX- and TX-joints under different loading conditions. Furthermore, additional studies on the influence of boundary conditions on uniplanar K-joints are included. Based upon the analytical formulae for uniplanar joints and the experimental and numerical results for each type of joint considered, design recommendations for the static strength of uniplanar and multiplanar connections in rectangular hollow sections are proposed.

# KEYWORDS

Static Strength, Rectangular Hollow Sections, Uniplanar Connection, Multiplanar Connection, Welded Connection, Analytical Model, Experiments, Numerical Modelling.

## SYMBOLS



$$\alpha = 2l_0/b_0$$
$$\beta = b_1/b_0$$
$$2\gamma = b_0/t_0$$
$$\tau = t_1/t_0$$
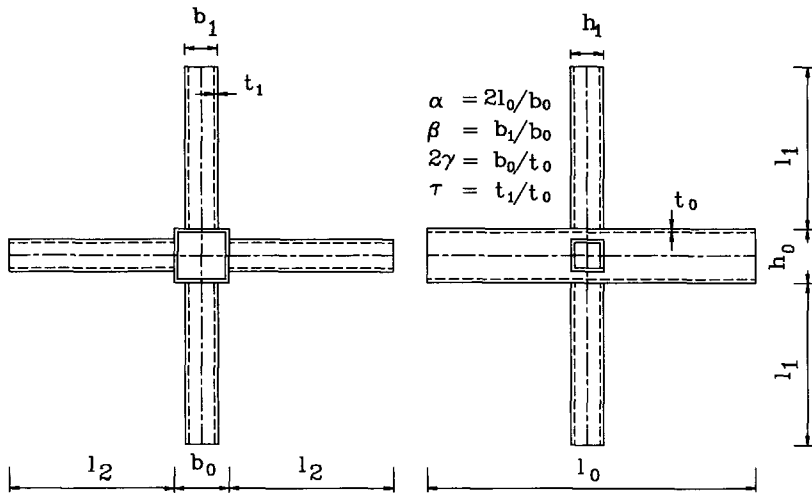
<u>Greek Letters</u>

| | | |
|---|---|---|
| $\alpha$ | : | 2 times the chord length to width ratio $2l_0/b_0$; |
| $\alpha$ | : | Angle between two yield lines; |
| $\alpha_s$ | : | Shape factor of the cross section; |
| $\alpha_x$ | : | Critical chord length to width value to form a distortion mechanism. |
| $\beta$ | : | Brace to chord width ratio $b_1/b_0$; |
| $\gamma$ | : | Half width to thickness ratio of the chord, $b_0/(2t_0)$; |
| $\gamma_g$ | : | Action load factor; |
| $\gamma_M$ | : | Partial safety factor of the joint; |
| $\gamma_{M0}$ | : | Partial safety factor of the section resistance (class 1, 2 3); |
| $\gamma_{M1}$ | : | Partial safety factor of the section resistance (class 4); |
| $\delta$ | : | Chord top face indentation; |
| $\delta$ | : | Chord distortion displacement; |
| $\delta_{3\%b0}$ | : | Chord top face indentation at $3\%b_0$; |
| $\delta_{max}$ | : | Chord top face indentation at maximum load or moment capacity; |
| $\delta_u$ | : | Chord top face indentation at ultimate load capacity or ultimate moment capacity of the joints; |
| $\varepsilon_E$ | : | Engineering strain; |
| $\varepsilon_T$ | : | Logarithm strain; |
| $\eta$ | : | Brace depth to chord width ratio $h_1/b_0$; |
| $\theta$ | : | Angle between brace and chord; |
| $\kappa$ | : | Reduction factor for buckling; |
| $\bar{\lambda}$ | : | Non-dimensional slenderness of a column or chord side wall; |
| $\lambda$ | : | Slenderness of a column or chord side wall; |
| $\lambda_E$ | : | Eulerian slenderness; |
| $\xi$ | : | Moment reduction factor for the chord webs due to shear; |
| $\rho$ | : | Moment reduction factor for the chord section due to shear; |

| | | |
|---|---|---|
| $\sigma_0$ | : | Stresses in the chord; |
| $\sigma_E$ | : | Engineering stress; |
| $\sigma_T$ | : | True stress; |
| $\tau$ | : | Wall thickness ratio between brace and chord members $\tau = t_1/t_0$; |
| $\phi$ | : | Angle between planes of multiplanar joints; |
| $\phi$ | : | Joint rotation angle: $\phi = \delta/(h_1/2)$ or $\phi = \delta/(b_1/2)$; |
| $\phi_0$ | : | Distortion angle of the chord wall; |
| $\phi_{0.1}$ | : | Joint rotation angle at 0.1 rad.; |
| $\phi_i$ | : | Rotation angle of yield line i; |

Latin Letters

| | | |
|---|---|---|
| a | : | Throat thickness of the weld; |
| A | : | Section area of a member; |
| $A_0$ | : | Section area of the chord; |
| $A_{eff}$ | : | Effective area of the cross-section; |
| $a_h$ | : | Projected length of the weld along the chord face; |
| $A_u$ | : | Updated section area of a member; |
| $a_v$ | : | Projected length of the weld along the brace face; |
| $b_0$ | : | External width of the chord; |
| $b_1$ | : | External width of the brace; |
| $b_i$ | : | External width of member i (i=0, chord; i=1, in-plane brace; i=2, out-of-plane brace); |
| $c_m$ | : | Factor for the multiplanar geometrical stiffening effects; |
| E | : | Modulus of elasticity; |
| $f(J_{AA})$ | : | Function for the multiplanar load effects; |
| $f(J_{II})$ | : | Function for the multiplanar load effects; |
| $f(J_{IA})$ | : | Function for the multiplanar load effects; |
| $f(J_m)$ | : | Reduction function for the ultimate load capacity due to the chord bending moment; |
| $f(n)$ | : | Reduction function for the ultimate load capacity due to the chord axial preloading; |
| $f_{u0}$ | : | Ultimate strength of the chord in longitudinal direction; |
| $f_{y0}$ | : | Yield strength of the chord in longitudinal direction; |
| $f_{y1}$ | : | Yield strength of the brace in the longitudinal direction; |
| $h_0$ | : | External depth of the chord; |
| $h_1$ | : | External depth of the brace; |
| $h_i$ | : | External depth of member i (i=0, chord; i=1, in-plane brace; i=2, out-of-plane brace); |
| $J_{AA}$ | : | Load ratio between axial loads applied to the out-of-plane and in-plane braces: $J_{AA} = N_2/N_1$; |
| $J_{II}$ | : | Moment ratio between the in-plane bending moments applied to the out-of-plane and the in-plane braces: $J_{II} = M_2/M_1$; |
| $J_{IA}$ | : | Load ratio between the axial load applied to the out-of-plane braces and the in-plane bending moment applied to the in-plane braces: $J_{IA} = N_2/(M_1/h_1)$; |

| | | |
|---|---|---|
| $J_m$ | : | Moment ratio incorporating the moment applied to the chord, equation (5.47) or (7.28); |
| $k_0$ | : | Reduction factor for the warping stress due to torsional shear stresses; |
| $l_0$ | : | Length of the chord; |
| $l$ | : | length of a member; |
| $l_1$ | : | Length of the in-plane brace; |
| $l_2$ | : | Length of the out-of-plane brace; |
| $l_i$ | : | Length of yield line i; |
| $M_0$ | : | Chord bending moment; |
| $M_1$ | : | In-plane bending moment applied to the in-plane braces; |
| $M_{1,ipb}$ | : | In-plane bending moment applied to the in-plane braces; |
| $M_{1,ipb,k}$ | : | Characteristic moment strength of the joints loaded with in-plane bending moments; |
| $M_{1,ipb,Rd}$ | : | Design resistance moment of the joints loaded with in-plane bending moments; |
| $M_{1,ipb,u}$ | : | Ultimate moment capacity of uniplanar joints loaded with in-plane bending moments; |
| $M_{1,ipb,u}(J_{II})$ | : | Ultimate moment capacity of multiplanar joints loaded with moment ratio $J_{II}$; |
| $M_{1,ipb,u}(J_{II}=0)$ | : | Ultimate moment capacity of multiplanar joints loaded with moment ratio $J_{II}=0$; |
| $M_{1,ipb,u}(J_{IA})$ | : | Ultimate moment capacity of multiplanar joints loaded with load ratio $J_{IA}$; |
| $M_{1,ipb,u}(J_{IA}=0)$ | : | Ultimate moment capacity of multiplanar joints loaded with load ratio $J_{IA}=0$; |
| $M_{1,opb}$ | : | Out-of-plane bending moment applied to the in-plane brace; |
| $M_{1,opb,k}$ | : | Characteristic moment strength of the joints loaded with out-of-plane bending moments; |
| $M_{1,opb,Rd}$ | : | Design resistance moment of the joints loaded with out-of-plane bending moments; |
| $M_{1,opb,u}$ | : | Ultimate moment capacity of uniplanar joints loaded with out-of-plane bending moments; |
| $M_{1,u}$ | : | Ultimate moment capacity of the joints; |
| $M_2$ | : | In-plane bending moment applied to the out-of-plane braces; |
| $M_{el,Rd}$ | : | Elastic design resistance moment for class 3 section without reduction by shear; |
| $M_{f,Rd}$ | : | Moment resistance of the flange; |
| $M_i$ | : | Plastic moment of yield line i; |
| $m_p$ | : | Plastic moment per unit length $m_p=f_{y0}t_0^2/4$; |
| $m_{pi}$ | : | Plastic moment per unit length of yield line i; |
| $M_{pl,Rd}$ | : | Plastic moment resistance for class 1 and 2 sections without reduction by shear; |
| $M_s$ | : | Moment capacity of the joints at the serviceability deformation limit; |
| $M_{Sd}$ | : | Design moment for the chord; |
| $M_t$ | : | Torsional moment; |
| $M_{tp}$ | : | Plastic torsion capacity under pure torsion; |
| $M_u$ | : | Ultimate moment capacity of the joint; |
| $M_{V,e,Rd}$ | : | Moment resistance for class 3 sections reduced by shear; |

| | | |
|---|---|---|
| $M_{V,Rd}$ | : | Moment resistance for class 1 and 2 sections reduced by shear; |
| $M_{w,e,Rd}$ | : | Moment resistance of the web for class 3 sections; |
| $M_{w,Rd}$ | : | Moment resistance of the web for class 1 and 2 sections; |
| n: | : | Chord axial preloading ratio, $n=N_0/(f_{y0}*A_0)$; |
| $N_0$ | : | Axial force in the chord; |
| $N_{0(in\ gap)}$ | : | Axial load in the gap of the chord; |
| $N_{0,m}$ | : | Axial load applied to the top and the bottom flanges of the chord; |
| $N_{0,Rd}$ | : | Design compression resistance of the chord; |
| $N_1$ | : | Axial load applied to the in-plane braces; |
| $N_{1,k}$ | : | Characteristic strength of the joints; |
| $N_{1,Sd}$ | : | Design axial load on brace 1; |
| $N_{2,Sd}$ | : | Design axial load on brace 2; |
| $N_{1,Rd}$ | : | Design resistance load of uniplanar joints; |
| $N_{1,u}$ | : | Ultimate load capacity of uniplanar joints; |
| $N_{1,u}(J_{AA})$ | : | Ultimate load capacity of multiplanar joints loaded with axial forces with a load ratio $J_{AA}$; |
| $N_{1,u}(J_{AA}=0)$ | : | Ultimate load capacity of multiplanar joints loaded with axial forces with a load ratio $J_{AA}=0$; |
| $N_{1,u}(J_m)$ | : | Ultimate load capacity of the joint including the chord bending moment; |
| $N_{1,u}(J_m=0)$ | : | Ultimate load capacity of the joint excluding the effect of the chord bending moment; |
| $N_{1,u}(n)$ | : | Ultimate load capacity of the joint with chord preloading ratio n; |
| $N_{1,u}(n=0)$ | : | Ultimate load capacity of the joint with n=0; |
| $N_2$ | : | Axial load applied on the out-of-plane braces; |
| $N_k$ | : | Characteristic strength of the joint; |
| $N_{pl,Rd}$ | : | Design plastic resistance of the chord section; |
| $N_{Rd}$ | : | Design resistance of the joint; |
| $N_s$ | : | Load capacity of the joints at the serviceability deformation limit; |
| $N_{Sd}$ | : | Design axial load on the chord; |
| $N_u$ | : | Ultimate load capacity of the joints; |
| $N_{V,e,Rd}$ | : | Brace axial load corresponding to $M_{V,e,Rd}$ for class 3 sections; |
| $N_{V,Rd}$ | : | Brace axial load corresponding to $M_{V,Rd}$ for class 1 and 2 sections; |
| $n_{w,b}$ | : | Reaction force per unit length of the web at buckling; |
| $n_{w,y}$ | : | Reaction force per unit length of the web at yielding; |
| P | : | Force applied to the section area; |
| $r_i$ | : | Internal corner radius of the chord or braces; |
| $r_o$ | : | External corner radius of the chord or braces; |
| $t_i$ | : | Wall thickness of the member i |
| $t_r$ | : | Wall thickness at the curved corners of the chord or the braces; |
| $t_w$ | : | Thickness of the weld in the FE model; |
| V | : | Shear load on the chord; |
| $V_{pl,Rd}$ | : | Plastic shear resistance of the chord; |
| $V_{Sd}$ | : | Design shear load on the chord; |
| $W_{el}$ | : | Elastic section modulus; |
| $W_i$ | : | Internal energy dissipation; |
| $W_{pl}$ | : | Plastic section modulus; |
| x | : | Length to form the failure mechanism in Figure 7.23, Chapter 7; |

Abbreviations

| | | |
|---|---|---|
| AWS | : | American Welding Society; |
| CIDECT | : | Comité International pour le Développement et l'Étude de la Construction Tubulaire; |
| ECSC | : | European Community of Steel and Coal; |
| FE | : | Finite Element; |
| IIW | : | International Institute of Welding; |
| ipb | : | In-plane bending; |
| mp | : | Multiplanar; |
| opb | : | Out-of-plane bending; |
| RHS | : | Rectangular hollow section; |
| up | : | Uniplanar. |

# 1   INTRODUCTION

Tubular structures made of structural hollow sections are not only aesthetically attractive but also have structural, economical and other advantages, e.g. as McGilvray (1994) states: The qualities of tubular structures are their power to evoke in their occupants a sense of lightness, vigour, delight, order, comfort, shelter and protect.

Structural hollow sections with a rectangular, square or circular cross-section offer outstanding static properties with regard to resisting tension, compression, torsion and biaxial bending and consequently result in a considerable saving in material compared to structures of open sections. Furthermore, structural hollow sections have smaller and smoother surfaces than open sections without sharp edges and the required corrosion protection can be applied more economically.

A connection, also referred to as a joint, can be formed by joining several structural hollow sections together by welding. The welding procedure for joints of rectangular hollow sections (RHS) is fairly straightforward, because profiling is not required for RHS which is necessary for circular hollow sections. Rectangular hollow sections can be found in industrial buildings, towers, masts, bridges, crane booms, mechanical equipment and agricultural applications etc. with various types and configurations of joints.

Since the first preliminary tests on joints of RHS in the sixties, many experimental and analytical investigations have been carried out on uniplanar joints. However, very little information was available on the static behaviour of multiplanar joints until the end of the 1980s. Furthermore, for uniplanar joints under complicated loading conditions, limited evidence was available. In order to thoroughly investigate the static behaviour of uniplanar and multiplanar joints, this PhD research programme was set up.

## 1.1   OBJECTIVES AND SCOPE

This PhD research programme aims to provide design recommendations on the static strength of uniplanar and multiplanar connections in rectangular hollow sections. Basically there are two approaches in doing research: the theoretical approach and the experimental approach. The first can be further divided into an analytical approach (eg. the yield line method) and a numerical approach (eg. the finite element method). The current research work reflects a combination of the theoretical and experimental approaches. The experimental approach is time consuming and expensive. The yield line theory can be used in the derivation of solutions of a mechanism under some assumptions. In some cases, no direct analytical formula can be derived due to the complexity of the problem. In the last decade, there has been an increasing growth of the use of non-linear finite element techniques to analyse the static behaviour of connections of structural hollow sections.

In 1988, an ECSC (European Community of Steel and Coal) research programme entitled "The development of design methods for the cost-effective applications of multiplanar connections" started to fill up the lack of information on the static behaviour of multiplanar joints. This research programme consists of both experimental tests and numerical simulations of uniplanar X- and T-joints and multiplanar XX-, TX- and KK-joints. Furthermore, a

numerical study was carried out within the framework of CIDECT (Comité International pour le Développement et l'Étude de la Construction Tubulaire) programme No. 5BG entitled "The static strength of multiplanar joints of square hollow sections". This PhD study covers the last mentioned programme and a part of the ECSC research programme.

Based upon the experimental results from the ECSC research project, a numerical model (finite element model) is developed which is fully calibrated against the experimental results. The finite element model is further used for a series of extensive parameter studies of uniplanar and multiplanar connections under different loading conditions. Based upon the analytical solutions and the experimental and numerical results for each type of joint, design recommendations for the static strength of uniplanar and multiplanar connections in rectangular hollow sections are proposed.
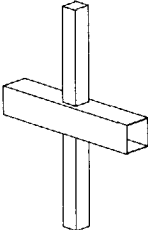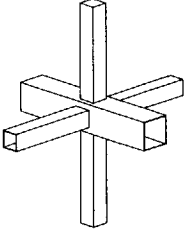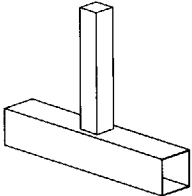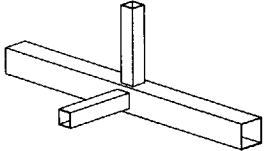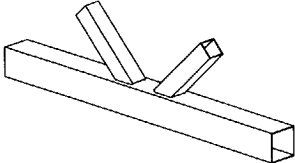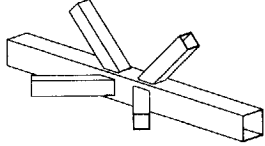
## 1.2     TERMINOLOGY

### 1.2.1   Classification of joints

The joint types studied in this thesis contain unstiffened welded uniplanar and multiplanar connections between rectangular hollow sections. The classification of the joints is summarised in Table 1.1.

An uniplanar joint consists of a chord member and one or more brace members in one single plane. A multiplanar joint consists of a chord member and brace members in more than one planes. For each type of joint, different loads can be applied.

**Table 1.1    Classification of joints in RHS**

| Uniplanar joints | | Multiplanar joints | |
|---|---|---|---|
| X-joint |  | XX-joint |  |
| T-joint |  | TX-joint |  |
| | | TT-joint |  |
| K-joint |  | KK-joint |  |

### 1.2.2   Determination of the design strength of the joint

The bases for design and general principles for the determination of the design strength of predominantly statically loaded joints made of hollow sections is given by Wardenier (1982a) where the variables in the strength functions were assumed as normal distribution. In Annex Z of EC3 (1993a), a log-normal distribution is assumed for all variables of a strength function. Adopting a log-normal distribution has the advantage that no negative values can occur for the geometrical and strength variables which is physically correct. The basic ideas of the two are comparable, because if a variable r has a log-normal distribution, ln(r) has then a normal distribution. The formulae for a normal distribution can be transferred to those for a log-normal distribution. Several terms with regard to the joint strength should be distinguished which are: the serviceability deformation limit, the "ultimate" deformation limit, the serviceability load capacity, the ultimate load (moment) capacity, the characteristic strength and the design strength (design resistance) of the joint.

### The serviceability and the "ultimate" deformation limit

The serviceability deformation limit is generally accepted as a local deformation of $1\%b_0$ for hollow sections (Wardenier 1982a and IIW 1989). The "ultimate" deformation limit is defined as a local deformation of $3\%b_0$ of the joint (Lu 1994[*]). For a joint loaded with bending moment, the joint rotation angle corresponding to the "ultimate" deformation limit should not be larger than 0.1 rad, see Chapter 4.

### The serviceability load capacity

The serviceability load capacity of the joint is defined as the load at the serviceability deformation limit.

### The ultimate load or moment capacity (the ultimate strength)

The ultimate load (moment) capacity of the joint is defined as the maximum load (moment) if the local deformation at the maximum load (moment) is smaller than the "ultimate" deformation limit, or is defined as the load (moment) at the "ultimate" deformation limit if no maximum load is reached. The determination of the ultimate load (moment) capacity of the joint can be found in Chapter 4.

### The characteristic strength

The characteristic strength is defined as the strength with a probability of failure of 5%. The procedure to determine the characteristic strength from a given ultimate strength formula can be found in Annex Z of EC3 (1993a).

---

[*]:       For the clearness of reading, only the name of the first author is mentioned. The names of the coauthors can be found in the references.

**The design strength (design resistance)**

In Limit States Design, the design load should not exceed the design strength. The procedure to determine the design strength from a given ultimate strength function (ultimate load or moment capacity formula) can be found in Annex Z of EC3 (1993a) and Sedlacek (1991). The same procedure as for the characteristic strength can be used to determine the design strength by replacing the characteristic fractile coefficient by the design fractile coefficient (Annex Z of EC3 1993a), or if the partial safety factor of the joint is known beforehand, the design strength is equal to the characteristic strength divided by the partial safety factor (Wardenier 1982a). The relationship between the design strength and the characteristic strength is given as:

$$N_{Rd} = \frac{N_k}{\gamma_M} \tag{1.1}$$

Where $N_{Rd}$ is the design resistance of the joint; $N_k$ is the characteristic strength of the joint and $\gamma_M$ is the partial safety factor of the joint.

## 1.3   OUTLINE OF THE THESIS

This thesis contains eleven chapters.

Chapter 1 gives an introduction of the research work.

Chapter 2 summarises the current design guidance and the existing literature on the static behaviour of uniplanar and multiplanar connections in rectangular hollow sections.

Chapter 3 gives experimental evidence on uniplanar X- and T-joints and multiplanar XX- and TX-joints.

Chapter 4 discusses the calibration of the numerical model and the general aspects about the numerical parameter study.

Chapter 5 includes the existing analytical formulae and gives the newly developed analytical formulae for full width joints ($\beta$=1.0) under different load cases. The influence of chord bending moments is also studied analytically based upon the yield line theory.

Chapter 6 deals with a parameter study on uniplanar X-joints loaded with axial forces, in-plane bending moments and out-of-plane bending moments. Furthermore, the influence of axial preloading and bending moments in the chord is studied. Ultimate load (moment) capacity formulae are given for uniplanar X-joints which form a basis for the formulae from the parameter study of the corresponding multiplanar XX-joints.

Chapter 7 includes a parameter study on uniplanar T-joints loaded with axial forces, in-plane and out-of-plane bending moments which forms a basis for the study of multiplanar TX-joints.

The influence of chord bending moments is also investigated. For unstiffened full width T-joints loaded with out-of-plane bending moment, a distortional failure mode is observed. The ultimate moment capacity formula is derived on the basis of an analytical and a numerical study. The ultimate load (moment) capacity formulae of uniplanar T-joints are related to those of uniplanar X-joints.

Chapter 8 considers the multiplanar geometrical stiffening effect and multiplanar load effect of multiplanar XX-joints loaded with three different multiplanar load combinations. Ultimate load (moment) capacity formulae for multiplanar joints loaded with three load cases are established.

Chapter 9 deals with a parameter study on multiplanar TX-joints. The influence of restraints on the out-of-plane braces is studied. The multiplanar geometrical effect and the multiplanar load effect of TX-joints excluding chord bending moments are related to those of XX-joints. Additionally, based upon available evidence on uniplanar K-joints, the influence of boundary conditions is studied. The experimental results of multiplanar KK-joints are compared with the CIDECT design resistance formula and the existing mean ultimate load capacity formula.

Chapter 10 gives conclusions and recommendations. Ultimate load (moment) capacity formulae for each type of joint and each load case are summarised in tables.

Chapter 11 lists the references with regard to the static strength of connections of rectangular hollow sections and other relevant literature.

The geometrical parameters and the loading cases for each type of joint in this PhD study of Chapters 6 to 9 are outlined in Tables 1.2 to 1.4. The symbols used can be found in the list of symbols.

**Table 1.2    Parameter studies for X- and XX-joints under difference loading cases**
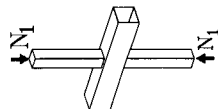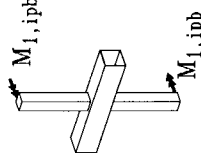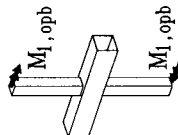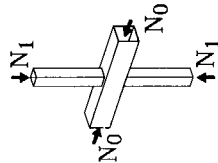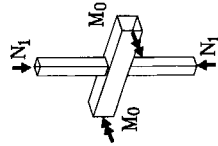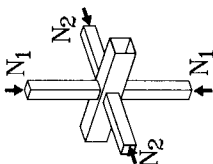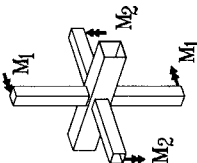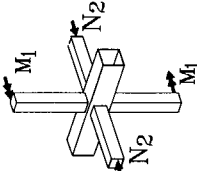
| | | | | | |
|---|---|---|---|---|---|
| **Uniplanar** | Loads $N_1$ | Loads $M_1$ $M_{1,ipb}$ | Loads $M_1$ $M_{1,opb}$ | Loads $N_1, N_0$ | Loads $N_1, M_0$ |
| **Multiplanar** | Loads $N_1, N_2$ | Loads $M_1, M_2$ | Loads $M_1, N_2$ | | |
| **Load ratios** | $J_{AA}=N_2/N_1=$ $-1, -0.5, 0, 0.5, 1.0$ | $J_{II}=M_2/M_1=$ $-1, -0.5, 0, 0.5, 1.0$ | $J_{IA}=N_2 h_1/M_1=$ $-1, -0.5, 0, 0.5, 1.0$ | | |
| **Parameters** | $\alpha=12$; | $\beta=0.2, 0.4, 0.6, 0.8, 1.0$; | $2\gamma=15, 24, 35$ | | |

**Table 1.3    Parameter studies for T- and TX-joints under different loading cases**
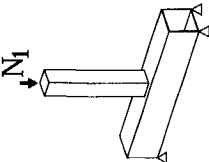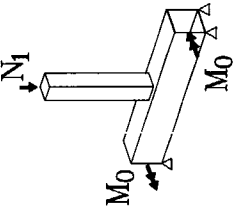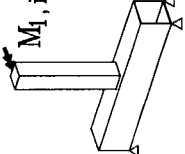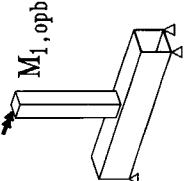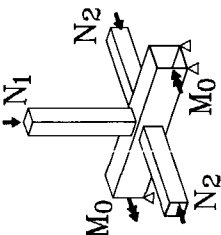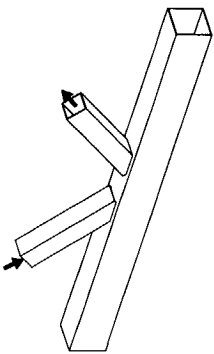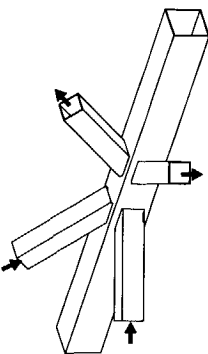
| | Axial loads including bending | Axial loads excluding bending | In-plane bending | Out-of-plane bending |
|---|---|---|---|---|
| Uniplanar | $N_1$ | $N_1$, $M_0$, $M_0$ | $M_{1,ipb}$ | $M_{1,opb}$ |
| Multiplanar | | $N_1$, $N_2$, $N_2$, $M_0$, $M_0$ | | |
| Load ratios | | $J_{AA} = N_2/N_1 =$ <br> $-1, -0.5, -0.25, 0, 0.25, 0.5$ | | |
| Parameters | $\alpha = 6, 9, 12, 18, 24, 40;$ | $\beta = 0.4, 0.6, 0.8, 1.0;$ | $2\gamma = 15, 24, 35$ | |

**Table 1.4    Axially loaded uniplanar K-joints and multiplanar KK-joints**

| Uniplanar | Multiplanar |
|---|---|
|  |  |

$\beta = 0.4, 0.6, 1.0;$
$2\gamma = 15, 24, 30;$
$g = 13, 23, 30, 65;$
$\theta = 45°$

# 2 SUMMARY OF EXISTING LITERATURE

## 2.1 INTRODUCTION

Since the first tests on connections of rectangular hollow sections by Stewarts and Lloyds in 1965 (now British Steel Corporation), extensive series of experiments have been carried out on uniplanar X- T- and K-joints from the sixties to the eighties. Most of them were tests on isolated joints loaded with axial forces. Some of the tests were joints loaded with in-plane and out-of-plane bending moments. The number of corresponding girder tests were limited. During that period, design equations for the static strength of uniplanar joints were derived based on the experiments and the analytical approaches, for instance, the yield line theory.

At the end of the eighties the subject of multiplanar connections was targeted as a key area where research had lagged behind the needs of industry. The lack of design guidance was identified as an obstacle to the development of the market. In 1988, an ECSC research programme entitled "The development of design methods for the cost-effective applications of multiplanar connections" was started which included both multiplanar joints of circular and rectangular hollow sections. The research programme contained two phases: phase 1 and phase 2. Phase 1 (SCI 1989) gave a state-of-the-art technical and economic review and programme definition study. A detailed survey of the construction industry in the UK revealed that RHS multiplanar connections under static loading regime are encountered frequently. Due to the absence of sufficient test evidence on the static behaviour of multiplanar connections, phase 2 of the programme was formulated. The objectives of phase 2 were to investigate and establish the fundamental multiplanar influences on the static strength of welded hollow section joints and to develop a numerical model, fully calibrated against experimental results, which could be used in the future development of design guidance and hence costly test programmes could be reduced. This PhD research work was initiated as part of the above ECSC programme Phase 2. The numerical study was carried out within the framework of CIDECT programme No. 5BG entitled "Static Strength of Multiplanar Joints of Square Hollow Sections".

In this chapter, the existing design guidance and the experimental, numerical and analytical evidences with regard to the static behaviour of uniplanar and multiplanar connections in rectangular hollow sections are summarised briefly.
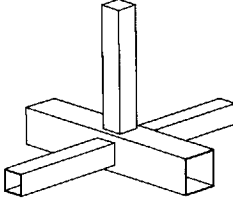
## 2.2 CURRENT DESIGN GUIDANCE

In the 1980s and early 1990s, design recommendations for statically-loaded welded connections of rectangular hollow sections have been developed by IIW (1981 and 1989), Wardenier (1982a) and CIDECT (Giddings 1985a, 1985b, Packer 1992a) etc. These recommendations have been implemented in standards of Canada (Packer 1984a, 1992b), Japan (AIJ 1990), the USA (AWS 1992) and all EC member countries (EC3 1993b, Annex K). Since most of the design recommendations for uniplanar connections of rectangular hollow sections are based on those of IIW (1989) and CIDECT (Packer 1992a), only the CIDECT design formulae are used for comparison in the present study.

In the CIDECT design guide, little information is available about the influence of bending moments in the chord on the static strength of the joints. For most cases, identical design formulae have been recommended for axially loaded uniplanar X- and T-joints. However, the static behaviour of axially loaded T-joints is obviously influenced by the chord length, thus by the bending moment in the chord. The current CIDECT formula for the influence of chord prestressing is mainly based upon the experimental results of K-joints (Wardenier 1982a). For full width uniplanar T-joints loaded with out-of-plane bending moments, distortion of the unstiffened chord section is a dominant failure mode which is not yet included in the CIDECT design guide.

For the static strength of multiplanar joints of rectangular hollow sections, it is indicated in the CIDECT design guide (Packer 1992a) that if the ratio between the axial loads applied to the out-of-plane braces and those applied to the in-plane braces is negative, the design resistance of the multiplanar TT-, XX- and KK-joints will be reduced by 10% compared to that of their uniplanar counterparts, see Table 2.1. This multiplanar effect is only roughly considered, since insufficient evidence was available. However the ultimate load capacity of multiplanar joints is obviously influenced by the magnitude of the load ratios, the geometrical parameters and the joint configurations.

**Table 2.1    Correction factors for RHS multiplanar joint strength (CIDECT, Packer 1992a)**

| Type of connection | Correction factor to uniplanar connection formulae |
|---|---|
| KK<br><br>$60° \leq \phi \leq 90°$ | 0.9 |
| | also, for gap KK connections, check that:<br><br>$\left(\dfrac{N_{0(\text{in gap})}}{A_0 f_{y0}}\right)^2 + \left(\dfrac{V}{A_0 f_{y0}/\sqrt{3}}\right)^2 \leq 1.0$ |
| TT, XX<br><br>$60° \leq \phi \leq 90°$ | 0.9 |

In EC3 (1993b), different correction factors for multiplanar joints have been given depending upon the joint configurations, see Table 2.2. This recommendation was based upon the results of multiplanar connections between circular hollow sections (Paul 1989) and some initial investigations on multiplanar rectangular hollow section joints (Bauer 1983, 1984, 1985), Coutie (1983), British Steel (1985) and Redwood (1983).

**Table 2.2    Correction factors for RHS multiplanar joint strength (EC3 1993b)**

| Type of joint | Correction factor to uniplanar connection formulae |
|---|---|
| TT-joint<br><br>$60°\leq\phi\leq90°$ | 0.9 |
| XX-joint | $0.9(1+0.33\ N_{2,Sd}/N_{1,Sd})$ |
| KK-joint<br><br>$60°\leq\phi\leq90°$ | 0.9<br>provided that, in a gap-type joint, the chord satisfies:<br><br>$\left(\dfrac{N_{Sd}}{N_{pl,Rd}}\right)^2 + \left(\dfrac{V_{Sd}}{V_{pl,Rd}}\right)^2 \leq 1.0$ |

## 2.3    RESEARCH WORK BEFORE 1982

A thorough bibliography of the literature regarding welded joints in structural hollow sections was given by Wardenier (1982a). Only some references in the period before 1982 are summarised in this thesis, because these references form an important background for the present research.

The first design equations which were based upon some amount of experimental evidence were provided by Eastwood (1970a, 1970b, 1971). These equations were based on the results of experiments where the actual dimensions and the actual material properties of the joints were not measured. Furthermore, these equations showed a scale effect which is not likely for the static strength.

From 1973 until the beginning of the 1980s, an extensive experimental and analytical research programme was carried out in the Netherlands which covered isolated T-, X-, K-, N- and KT-joints and some additional girder tests. All the results of this programme were reported in many interim reports which have been summarised by Wardenier (1978) and de Koning (1979). At the same period of time, experimental tests and analytical investigations were also carried out in Germany (K-joints), the U.K. (K-joints), Italy (girder tests), Poland (T-, X and K-joints), Canada (T-joints) and Japan (T-joints) etc. Many of these programmes have been coordinated by CIDECT and benefited from the additional financial support of CIDECT Member Companies, national governments and the European Community of Steel and Coal.

Based on all these test results and analytical investigations design recommendations were given by IIW (1981) and Wardenier (1982a) which were the basis for the present design recommendations. The design recommendations for uniplanar T- and X-joints were based upon the yield line theory (Johansen 1962, Mouty 1978 and Wardenier 1982a etc.) for joints with $\beta\leq0.85$ and semi-empirical formulae (effective width, punching shear and chord side wall failure) for joints with $0.85\leq\beta\leq1.0$ (Wardenier 1982a). Theoretical formulae based upon a yield line approach for uniplanar K-joints excluding the membrane and work hardening effects were found very conservative compared to the experimental results (Davies 1975, 1977). The

membrane action and work hardening effects for K-joints have been considered by Packer (1978). Taking these effects into account leads to extremely complicated functions which can only be solved with the help of a computer. Thus, no direct formula could be deduced. The analytical studies for K-joints were only used to study the influence of various parameters of the joints.

## 2.4 RESEARCH WORK AFTER 1982

Based upon IIW (1981) and Wardenier (1982a), current design recommendations on uniplanar joints of rectangular hollow sections have been established which are CIDECT Monograph No. 6 (Giddings 1985a and Packer 1992a), IIW (1989) and EC3 (1993b). These recommendations with minor modifications have been widely implemented in standards of many countries as mentioned in Section 2.2.

### Uniplanar joints

From 1983 until now, publications on the static strength of uniplanar connections of rectangular hollow sections are summarised in Table 2.3. It can be seen from this table that much work has been done on overview and implementations of design recommendations. Most of publications dealing with an overview and implementations of design guidance are consistent with the IIW or the CIDECT design guide. One of the most important developments during this period of time was the use of finite element techniques in the analysis of the joint behaviour. Studies of uniplanar connections during this period include:

- Joints under combined axial and moment loading (Davies 1986, Panjeh Shahi 1983 and Szlendak 1984).

- Web crippling of full width joints (Crocket 1994, Davies 1987a, Packer 1984b, 1987, Yu 1996c, Zhang 1989 and Zhao 1992).

- Distortion of full width T-joints under out-of-plane bending (Niemi 1986).

- Influence of the chord bending moments or chord axial forces of a T- or an X-joint (Zhao 1991, 1993a, 1993b and Yu 1995, 1996d).

- Influence of the brace angle (Davies 1986 and 1996a).

- Influence of the welds (Davies 1994, Yu 1994a, 1994b).

- Behaviour of joints under low temperature (Niemi 1989).

- Behaviour of joints made of stainless steel (Rasmussen 1993).

- Finite element analyses (Crockett 1994, Davies 1989, 1994 and 1996a, Koskimäki 1989, Owen 1996, Partanen 1989, Yu 1993, 1994a, 1994b, 1995, 1996c, 1996d and Zhang 1989, 1993, 1994 etc.).

**Table 2.3     Publications on uniplanar joints of rectangular hollow sections after 1982**

| Authors | T-joints | X-joints | K-joints |
|---|---|---|---|
| Burdekin (1993) | | | 1,3 |
| Crockett (1994) | 3 | | 3 |
| Czechowski (1989) | 4 | 4 | 4 |
| Davies (1984, 1986) | | 1,2 | |
| Davies (1987a) | 1,2,4 | 1,2,4 | 1,2,4 |
| Davies (1987b) | 4 | 4 | 4 |
| Davies (1989) | | 3 | |
| Davies (1994) | | | 3 |
| Davies (1996a) | | 3 | 3 |
| Giddings (1985a, 1985b,1986) | 4 | 4 | 4 |
| Koning (1983) | | | 2 |
| Koning (1984) | | | 2 |
| Koskimäki (1989) | | | 3 |
| Kurobane (1984) | 4 | 4 | 4 |
| Linderman (1990) | 4 | 4 | 4 |
| Marshall (1991) | 4 | 4 | 4 |
| Niemi (1986) | 1,2 | | |
| Niemi (1989) | | | 1 |
| Owen (1996) | 3 | | |
| Packer (1983,1984a) | 4 | 4 | 4 |
| Packer (1984b) | 1,2 | | |
| Packer (1985) | 4 | 4 | 4 |
| Packer (1987) | 1,2,4 | 1,2,4 | |
| Packer (1989) | 4 | 4 | 4 |
| Packer (1992a, 1992b, 1992c, 1993) | 4 | 4 | 4 |
| Panjeh Shahi (1983) | 1, 2 | | |

Note:   1. Tests.          2. Theory.
        3. FEM.           4. Overview or recommendations of design formulae

*:     For the clearness of reading, only the first author is mentioned. The names of the coauthors can be found in the references.

**Table 2.3     (Continued)**

| Authors | T-joints | X-joints | K-joints |
|---|---|---|---|
| Partanen (1989) | 2,3 | | 2,3 |
| Partanen (1993) | 1,2 | | 1,2 |
| Rasmussen (1993) | | | 1 |
| Reusink (1989) | 4 | 4 | 4 |
| Szlendak J. (1983, 1984, 1985) | 1,2 | 1,2 | |
| Wardenier (1985, 1988) | 4 | 4 | 4 |
| Wardenier (1989) | 2,4 | 2,4 | 2,4 |
| Wardenier (1991,1993) | 4 | 4 | 4 |
| Yeomans (1989) | 4 | | |
| Yu (1993, 1994a, 1994b, 1995) | 3 | 3 | |
| Yu (1996c, 1996d) | 2,3 | 2,3 | |
| Zhang (1989) | 2,3 | 2,3 | |
| Zhang (1993) | | | 3 |
| Zhang (1994) | 3 | | |
| Zhao (1991, 1992, 1993a, 1993b) | 1,2 | | |
| Zhao (1996) | 4 | | |

Note:   1. Tests.              2. Theory.
        3. FEM.               4. Overview or recommendations of design formulae

**Multiplanar joints**

The earliest studies on the static behaviour of multiplanar joints were carried out by Bauer (1983, 1984 and 1985) and Redwood (1983) in order to investigate the static behaviour of a triangular truss. Sixteen TT-joints and seven KK-joints were included in the experimental tests. The $\beta$ values of the joints investigated range from 0.2 to 0.6. The equations for uniplanar T- and K-joints based upon the yield line mechanisms were modified and adapted to TT- and KK-joints. Due to the limited information about the static behaviour of multiplanar joints, design recommendations were not included until the beginning of the 1990s (Wardenier 1991, 1993, Packer 1992a and EC3 1993b). The multiplanar effects in the current design guidance were only roughly considered. Within the ECSC research programme as mentioned before, experimental tests and numerical simulations of multiplanar XX-, TX- and KK-joints were carried out. Additionally, the current extensive numerical study was carried out within the framework of CIDECT programme No. 5BG entitled "Static strength of multiplanar joints of square hollow sections". Publications about the static behaviour of multiplanar joints are summarised in Table 2.4.

**Table 2.4**     **Publications on multiplanar joints of rectangular hollow sections after 1982**

| Authors | TT-joints | TX-joints | XX-joints | KK-joints |
|---|---|---|---|---|
| Bauer (1983) | | | | 1 |
| Bauer (1984) | 1 | | | |
| Bauer (1985) | 2 | | | 2 |
| Bauer (1988, 1989) | 4 | | | 4 |
| British Steel (1985) | | | | 1 |
| Crockett (1994) | | 3 | | |
| Davies (1991a) | | | 2 | |
| Davies (1991b, 1992a, 1992b, 1993a, 1993b) | | 1,3 | | |
| Davies (1996a) | | 3 | | |
| EC3 (1993b) | 4 | | 4 | 4 |
| Koning (1992) | | | 1,3 | |
| Liu (1993) | | | 1,3 | |
| Liu (1998) | | | | 3 |
| O'Connor (1993) | | | | 3 |
| CIDECT (1992) | 4 | | 4 | 4 |
| Packer (1992a) | 4 | | 4 | 4 |
| SCI (1989) | 4 | 4 | 4 | 4 |
| SCI (1995) | | 1,3 | 1,3 | 1,3 |
| Redwood (1983) | 2 | | | 2 |
| Wardenier (1991,1993) | 4 | 4 | 4 | 4 |
| Yeomans (1993) | | | | 1 |
| Yu (1993a, 1993b) | | 3 | | |
| Yu (1996a, 1996b) | | | 3 | |
| Yu (1998) | | | 3 | |

Note:  1. Tests.          2. Theory.
          3. FEM.          4. Overview or recommendations of design formulae

In summary, the following literature is relevant for multiplanar connections:

-       Axially loaded multiplanar TT-joints including experimental tests and analytical
        studies (Bauer 1984, 1985 and Redwood 1983).

-       Axially loaded XX-joints including analytical studies, experimental tests, finite
        element calibrations and numerical parameter studies (Davies 1991a, de Koning 1992,
        Liu 1993, SCI 1995 and Yu 1993a, 1993b, 1996b).

-       XX-joints loaded with in-plane bending moments on both in-plane and out-of-plane
        braces including numerical parameter study (Yu 1996a).

-       XX-joints loaded with in-plane bending moments on the in-plane braces and axial
        forces on the out-of-plane braces including experimental tests, finite element
        calibration and numerical parameter studies (de Koning 1992, Liu 1993, SCI 1995 and
        Yu 1998).

-       Axially loaded TX-joints including experimental tests, finite element calibration and
        numerical parameter studies (Crockett 1994, Davies 1991b, 1992a, 1992b, 1993a,
        1993b, 1996b, SCI 1995 and Yu 1993a, 1993b).

-       Axially loaded KK-joints including analytical studies, experimental tests and finite
        element calibrations (Bauer 1983, 1985, British Steel 1985, O'Connor 1993, Liu
        1998b, Yeomans 1993 and SCI 1995).

-       Overview and implementations of design recommendations (Bauer 1988, 1989, EC3
        1993b, Packer 1992a, SCI 1989, Wardenier 1991, 1993).

# 3    EXPERIMENTAL WORK

## 3.1    INTRODUCTION

The experimental work has been carried out within an ECSC programme "The Development of Design Methods for the Cost-Effective Application of Multiplanar Joints". The first objective of the experimental work is to study the fundamental multiplanar interactions affecting the static strength of joints between rectangular hollow sections (RHS). The second objective is to develop numerical models fully calibrated against the experimental results in order to reduce the need for future costly test programmes.
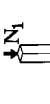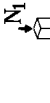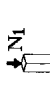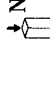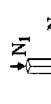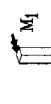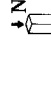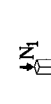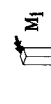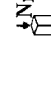
A series of 24 full scale joint tests on uniplanar X-, T- and multiplanar XX- TX-joints and multiplanar KK-joints has been carried out at TNO in The Netherlands, University of Nottingham and British Steel's Swinden Laboratories in the United Kingdom. Full details of all the tests can be found in the reports of de Koning (1992), Davies (1992a, 1992b) and TS&MD (1992). The experimental investigation concerns the determination of:

-       The influence of the unloaded out-of-plane braces of multiplanar XX- or TX-joints in comparison with their uniplanar counterparts (the multiplanar geometrical stiffening effect).

-       The influence of different load ratios between the loads applied on the out-of-plane braces and the loads applied on the in-plane braces of multiplanar XX- and TX-joints (the multiplanar loading effects).

-       The influence of the restraints applied on the out-of-plane braces of multiplanar TX-joints in order to keep the out-of-plane braces horizontal.

-       The influence of the geometrical parameters for multiplanar KK-joints.

## 3.2    RESEARCH PROGRAMME

The research programme for uniplanar X- and T- joints and for multiplanar XX- and TX-joints is outlined in Table 3.1. Eight tests on uniplanar X-joints and multiplanar XX-joints have been carried out at TNO and seven tests on uniplanar T-joint and multiplanar TX-joints have been carried out at University of Nottingham. The joint parameters in Table 3.1 are fixed at $\beta=0.6$, $2\gamma=24$, $\tau=1$. These above two test series are used to examine the multiplanar geometrical stiffening effects and the multiplanar loading effects of multiplanar joints under different loading conditions. The third test series consists of nine multiplanar KK-joints which have been tested at British Steel's Swinden Laboratory. The joint specimens for the third test series are divided into three groups dependent upon the brace to chord width ratios ($\beta$). This chapter includes only the tests on X- and T-joints and their multiplanar counterparts. The test results of multiplanar KK-joints are discussed in Chapter 9.

**Table 3.1    Experiments of X-, XX-, T- and TX-joints in RHS**

| | X-Joints | | T-joints | |
| --- | --- | --- | --- | --- |
| | Loads: $N_1$, $N_2$ | Loads: $M_1$, $N_2$ | Loads: $N_1$, $N_2$ | Loads: $N_1$, $N_2$ |
| Uniplanar | X1 | X5 | MPJT1A | |
| Multiplanar | DX2 | DX6 | MPJT2 | MPJT5 |
| | DX3 | DX7 | MPJT4 | MPJT7 |
| | DX4 | DX8 | MPJT3 | MPJT6 |

## 3.3    TESTS FOR X- AND XX-JOINTS

### 3.3.1    Specimen Geometry

The X-joints are fabricated from hot finished RHS 150 x 150 x 6.3 and 90 x 90 x 6.3 in grade S355 according to the current European standard EN 10210-1. The joint parameters are $\beta$=0.6 and $2\gamma$=24. To prevent failure of the braces before joint failure, the $\tau$ ratio is taken as 1.0. The measured thicknesses and the yield strength of the chord and the braces are listed in Tables 3.2 and 3.3. The length of the braces is 5 times the width of the brace and the length of the chord is 6 times the chord width. The specimen parameter ratios are chosen as being typical of practical joints and provide a good starting point for the study of multiplanar interactions.

All brace members for a specimen are from the same production batch. The braces are welded to the chords with fillet welds with a throat thickness equal to the wall thickness of the connected brace. The welds are carried out using a low hydrogen electrode. The weld sequence is such that the welds start and finish at the mid-sides of the member.

### 3.3.2    Test procedure

For the axially loaded joints (X1, DX2, DX3 and DX4), a schematic illustration of the test arrangement is given in Figure 3.1. The compressive axial load $N_1$ is applied at the ends of the pin-ended in-plane braces. The out-of-plane braces are unloaded for joint DX2. Proportional compression and tension loads $N_2$ are applied on the out-of-plane braces for specimens DX3 and DX4 respectively. The axial loads on the in-plane braces and the proportional loads on the out-of-plane braces are applied at the same time with a proportional ratio of 0.6. The joints have been loaded incrementally to failure (maximum load or excessively large deformation). The chord is supported in the lateral and the longitudinal directions, to prevent displacement in both directions. As the in-plane loads are applied equally to the top and the bottom chord faces, no significant rotation of the out-of-plane chord faces should take place. Therefore, it is sufficient for the majority of the tests to keep the out-of-plane braces unrestrained. However, to ensure that no significant secondary moments occur for specimen DX3 under out-of-plane compression loads, the out-of-plane braces are adjusted to remain in-line with the centre of the specimen throughout the test. During the tests, the change in distance between two points of the upper and the lower in-plane braces is measured which is approximately equal to the indentation of the chord top face plus the indentation of the chord bottom face. Thus, the indentation of one chord face is half of the change in distance measured. The measured points which are close to the chord faces are in the middle of the brace faces parallel to the longitudinal axis of the chord, see Figure 3.1.

For joints loaded with in-plane bending moments (specimens X5, DX6, DX7, DX8), a compression force is applied to one end of the chord and the specimen is simply supported at the ends of the in-plane braces as shown schematically in Figure 3.2. The chord is supported in two directions by lateral supports, to prevent lateral displacements in any directions. The out-of-plane braces of joint DX6 are unloaded. Proportional compression and tension loads have been applied on the out-of-plane braces of specimens DX7 and DX8 respectively. The out-of-plane loads are applied in such a way that at each stage of the test

the axial stresses in the out-of-plane braces are 30% (i.e. 0.6 x 50%) of the bending stresses in the in-plane braces at the intersection of the chord. The value of the out-of-plane loads are calculated as 2.613 times the vertical load applied to the end of the chord. During the tests, the vertical displacements at two points on each of the in-plane braces have been measured. From these measurements, the rotation angle $\phi$ of the in-plane braces can be calculated as shown in Figure 3.2. Furthermore, the indentation of the chord faces on the compression side and the push-out of chord faces on the tension side is measured to check the rotation.
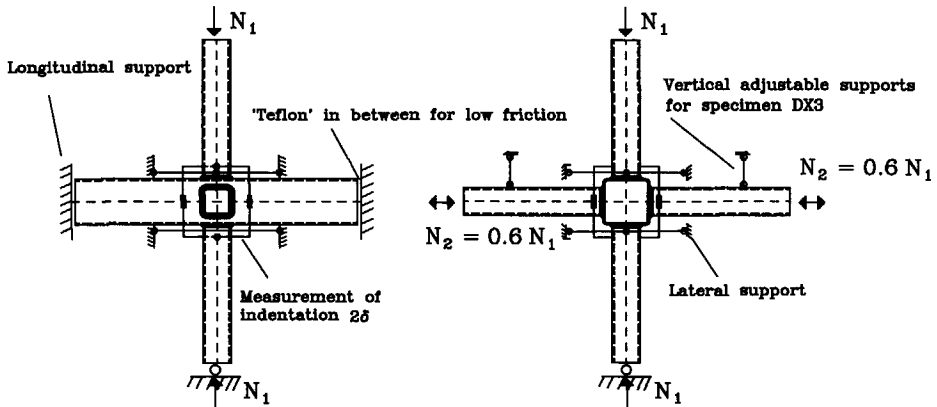


**Figure 3.1      Test arrangement for the axially loaded XX-joints**
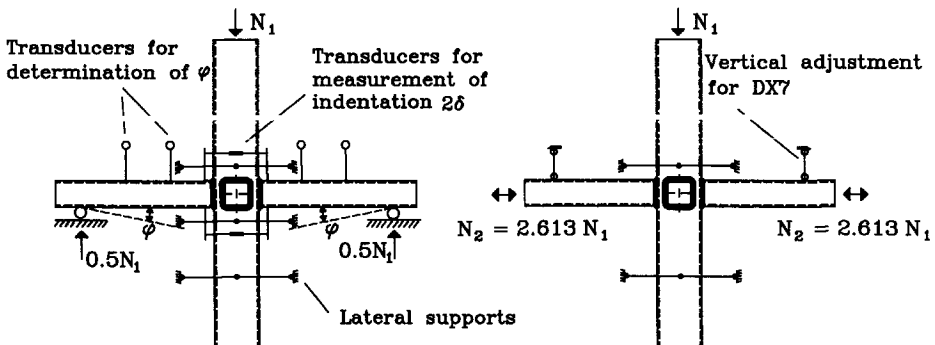


**Figure 3.2      Test arrangement for XX-joints loaded with in-plane bending moments**

It should be mentioned that for the joints loaded with in-plane bending moments, rotation of the out-of-plane braces occurs due to asymmetry in loading condition. If the out-of-plane braces are free for rotation and loaded by tension, the secondary bending moments reduce the rotation somewhat which may result in a small positive effect on the ultimate moment capacity of the joint. If the out-of-plane braces are free for rotation and loaded by compression, the secondary bending moments enlarge the rotation which may result in a large negative effect on the ultimate moment capacity of the joint. If the out-of-plane braces are restrained for rotation and loaded in compression, this may result in a positive influence on the ultimate moment capacity of the joint. Thus, for joints loaded with compression on the out-of-plane braces, the ultimate moment capacity of the joint is largely influenced by the boundary conditions of the out-of-plane braces. This effect is further studied in Section 8.3 of Chapter 8. During the test, vertical adjustable supports are only applied for specimen DX7 in order to prevent such rotation (the out-of-plane braces are kept in level), see Figure 3.2. This may result in a stronger multiplanar loading effect because keeping the out-of-plane braces in level means applying favourable bending moments on them.

**Table 3.2    Test results for axially loaded X- and XX-joints**

| Joints | $\beta$ | $2\gamma$ | $t_0$ mm | $f_{y0}$ N/mm$^2$ | $f_{y1}$ N/mm$^2$ | $\delta_u$ mm | $N_2/N_1$ | $N_s$ kN | $N_{1,u}$ kN |
|--------|------|------|------|------|------|------|------|------|------|
| X1 | 0.6 | 24 | 6.12 | 411 | 444 | 4.5 | - | 171 | 205 |
| DX2 | 0.6 | 24 | 6.12 | 411 | 444 | 4.5 | 0.0 | 180 (1.05)* | 220 (1.07)* |
| DX3 | 0.6 | 24 | 6.12 | 411 | 444 | - | 0.6 | 250 (1.40)** | (272)*** (1.24)** |
| DX4 | 0.6 | 24 | 6.12 | 411 | 444 | 4.5 | -0.6 | 132 (0.73)** | 177 (0.80)** |

*:      Ratio to the load of uniplanar joint X1.
**:     Ratio to the load of multiplanar joint DX2.
***:    Load for joint DX3 at the end of the test.

**Table 3.3        Test results for X- and XX-joints loaded with in-plane bending moments**

| Joints | $\beta$ | $2\gamma$ | $t_0$ mm | $f_{y0}$ N/mm² | $f_{y1}$ N/mm² | $\phi_{0.1}$ rad. | $\delta_u$ mm | $M_s$ kNm | $M_{1,u}$ kNm |
|--------|---------|-----------|----------|----------------|----------------|-------------------|---------------|-----------|---------------|
| X5 | 0.6 | 24 | 6.12 | 411 | 406 | 0.1 | 4.5 | 10.4 | 14.5 |
| DX6 | 0.6 | 24 | 6.12 | 411 | 406 | 0.1 | 4.5 | 10.4 (1.00)* | 14.6 (1.01)* |
| DX7 | 0.6 | 24 | 6.12 | 411 | 406 | 0.1 | 4.5 | 15.4 (1.48)** | 18.80 (1.29)** |
| DX8 | 0.6 | 24 | 6.12 | 411 | 433 | 0.1 | 4.5 | 10.5 (1.01)** | 15.8 (1.08)** |

*:       Ratio to the load of uniplanar joint X5.
**:     Ratio to the load of multiplanar joint DX6.


### 3.3.3    Test results and discussions

The load *vs.* chord face (one face) indentation curves for the four axially loaded X- and XX-joints are given in Figure 3.3. The moment *vs.* in-plane rotation curves for the four X- and XX-joints under in-plane bending moments are given in Figure 3.4. The serviceability deformation limit of $1\%b_0$ and the ultimate deformation limit of $3\%b_0$ are indicated in the two figures. The relationship between the in-plane rotation and the chord face indentation can be approximately written as follows:

$$\phi = \frac{\delta}{h_1/2} \tag{3.1}$$
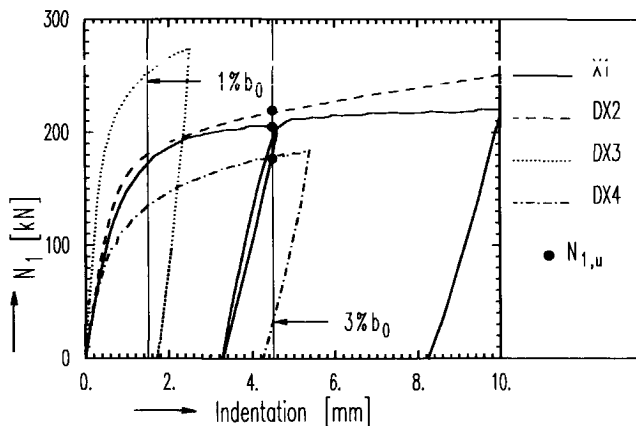


**Figure 3.3    Test results of axially loaded X- and XX-joints**
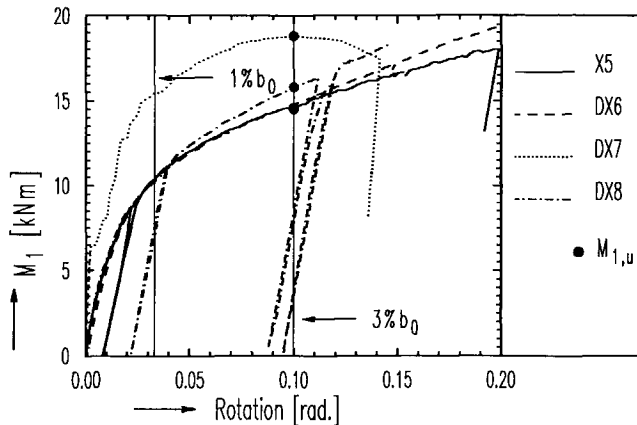
**Figure 3.4    Test results of X- and XX-joints loaded with in-plane bending moments**

Detailed description of the deformation limits and the determination of the ultimate load (moment) capacity of the joint can be found in Chapter 4. The serviceability load capacity and the ultimate load capacity are listed in Table 3.2. The serviceability moment capacity and ultimate moment capacity are shown in Table 3.3.

The failure mode for both axially loaded and moment loaded joints is usually plastification of the chord faces with excessive chord face indentation. For joints loaded with in-plane bending moments (X5, DX6, DX7 and DX8), cracking occurs in the tension side chord wall at the weld toe. Cracking in the chord initiates very close to or even after the ultimate deformation limit.

From the results of axially loaded X- and XX-joints listed in Table 3.2, it can be concluded that:

-    For the joint with the out-of-plane braces unloaded (DX2), the multiplanar geometrical stiffening effect is 5% at the serviceability limit and 7% at the ultimate deformation limit, compared to uniplanar joint X1.

-    For the joint with the out-of-plane braces loaded in compression (DX3), the serviceability load capacity is increased by 40% compared to that of the joint with the out-of-plane braces unloaded (DX2). Comparison between the results of joint DX3 and DX2 at the ultimate deformation limit is hampered by the premature stop of the test for joint DX3. However, it can be found from the load vs. indentation curve in Figure 3.3 that there is a large enhancement of the load capacity for joint DX3 too in comparison with that for joint DX2. For indication, the load at the end of the test for joint DX3 is listed in Table 3.2 which is already 24% higher than the ultimate load capacity of joint DX2.

-       For the joint with the out-of-plane braces loaded in tension (DX4), the serviceability
        load capacity is decreased by 27% and the ultimate load capacity is decreased by 20%
        compared to joint DX2.


For the results of X- and XX-joints loaded with in-plane bending moments, it is concluded
that:

-       For the joint with the out-of-plane braces unloaded (DX6), the geometrical stiffening
        effect can be neglected at both serviceability limit and ultimate deformation limit in
        comparison with joint X5.

-       For the joint with the out-of-plane braces loaded in compression (DX7), the
        multiplanar loading effect is significant (with 48% and 30% enhancement of moment
        capacity at serviceability deformation limit and ultimate deformation limit respectively
        in comparison with joint DX6). As mentioned before, this strong effect is mainly due
        to the vertical adjustment of the out-of-plane braces for DX7.

-       For the joint with the out-of-plane braces loaded in tension (DX8), there is a slight
        enhancement of the load capacity due to the reduced rotation of the out-of-plane
        braces.

## 3.4    TESTS FOR T- AND TX-JOINTS

### 3.4.1    Specimen geometry

The nominal steel grade and joint geometrical parameters are the same as for the tests of X- and XX-joints. The measured yield strength of the chord is 420 N/mm$^2$ and that the braces is 430 N/mm$^2$. All brace members for a specimen are from the same production batch. The braces are welded to the chords with fillet welds with a throat thickness equal to the wall thickness of the brace. The welds are made using a low hydrogen electrode of yield strength 460 N/mm$^2$ and ultimate tensile strength of 570 N/mm$^2$. The weld sequence is such that the welds start and finish at the mid-sides of the member cross sections. The measured dimensions of the hollow sections and the weld sizes are listed in Tables 3.4 and 3.5 respectively.

**Table 3.4  Measured Dimensions of the chord and the braces (mm)**

| Specimen | | b x h x t | $t_r$ | $r_i$ | $r_o$ |
|---|---|---|---|---|---|
| MPJT1A | chord | 149.2 x 149.8 x 6.42 | 7.50 | 4.17 | 12.00 |
| | in-pl. brace | 89.5 x  90.5 x 6.15 | 7.96 | 2.78 | 9.63 |
| MPJT2 | chord | 150.0 x 149.5 x 6.20 | 7.70 | 2.20 | 10.10 |
| | in-pl. brace | 90.5 x  89.5 x 6.20 | 8.01 | 2.31 | 10.13 |
| | out-of-pl. brace | 90.5 x  89.5 x 6.20 | 8.03 | 2.52 | 9.85 |
| MPJT3 | chord | 150.0 x 150.0 x 6.20 | 7.96 | 2.25 | 9.43 |
| | in-pl. brace | 91.0 x  90.0 x 6.30 | 8.09 | 2.28 | 9.63 |
| | out-of-pl. brace | 91.0 x  90.0 x 6.30 | 8.11 | 2.33 | 9.68 |
| MPJT4 | chord | 149.5 x 149.5 x 6.20 | 7.92 | 2.25 | 8.93 |
| | in-pl. brace | 90.5 x  89.5 x 6.20 | 8.06 | 1.98 | 8.33 |
| | out-of-pl. brace | 90.5 x  89.5 x 6.20 | 8.32 | 2.58 | 8.39 |
| MPJT5 | chord | 149.7 x 149.3 x 6.42 | 7.70 | 2.20 | 10.10 |
| | in-pl. brace | 90.1 x  89.6 x 6.19 | 8.01 | 2.31 | 10.13 |
| | out-of-pl. brace | 90.1 x  89.6 x 6.19 | 8.03 | 2.52 | 9.85 |
| MPJT6 | chord | 149.1 x 149.7 x 6.36 | 7.96 | 2.25 | 9.43 |
| | in-pl. brace | 90.7 x  89.7 x 6.13 | 8.09 | 2.28 | 9.63 |
| | out-of-pl. brace | 90.7 x  89.7 x 6.13 | 8.11 | 2.33 | 9.68 |
| MPJT7 | chord | 149.1 x 149.7 x 6.37 | 7.92 | 2.25 | 8.93 |
| | in-pl. brace | 89.8 x 89.8 x 6.16 | 8.06 | 1.98 | 8.33 |
| | out-of-pl. brace | 89.8 x 89.8 x 6.16 | 8.32 | 2.58 | 8.39 |

**Table 3.5  Measured dimensions of the welds (mm)**

| Specimen | Brace | Flat side | | Corner | |
|----------|-------|-----------|-----------|--------|--------|
| | | $a_h$ | $a_v$ | $a_h$ | $a_v$ |
| MPJT1A | in-pl. | 9.72 | 9.72* | 9.3 | 9.3* |
| MPJT2 | in-pl. | 9.90 | 9.90* | 9.90 | 9.90* |
| | out-of-pl. | 9.78 | 9.78* | 9.78 | 9.78* |
| MPJT3 | in-pl. | 10.00 | 10.00* | 9.44 | 9.44* |
| | out-of-pl. | 9.44 | 9.44* | 9.44 | 9.44* |
| MPJT4 | in-pl. | 9.88 | 9.88* | 9.69 | 9.69* |
| | out-of-pl. | 9.81 | 9.81* | 9.78 | 9.78* |
| MPJT5 | in-pl. | 9.88 | 10.00 | 9.75 | 9.75 |
| | out-of-pl. | 9.26 | 9.57 | 9.16 | 9.47 |
| MPJT6 | in-pl. | 10.13 | 9.25 | 9.38 | 8.43 |
| | out-of-pl. | 10.57 | 9.44 | 9.57 | 8.78 |
| MPJT7 | in-pl. | 9.38 | 9.38* | 9.38 | 9.38* |
| | out-of-pl. | 9.41 | 9.41* | 8.91 | 8.91* |

\* In case where $a_v$ is not measured, $a_v = a_h$ is assumed.

### 3.4.2  Test procedure

The behaviour of axially loaded T- and TX-joints differs from that of X- and XX-joints in two aspects.

1.      The axial load on the in-plane brace of a T- or TX-joint is balanced by the supports of the chord ends. The reaction forces cause overall bending moment in the chord. Premature chord bending failure should be prevented. The chord length between two reaction plates is chosen as 850 mm which is, for the joint geometrical parameters used, short enough to prevent overall bending failure before joint failure, but long enough to minimise end effects on the joint behaviour (Davies 1991b).

2.      Due to asymmetry in geometry and loading in-plane, rotation of the out-of-plane braces occurs for TX-joints during axial loading which results in secondary bending moments on the out-of-plane braces. The rotation of the out-of-plane braces can be restrained in such a way that they are always kept horizontal during the test. Two sets of tests are carried out: one with the out-of-plane braces restrained another with the out-of-plane braces free to rotate in order to examine the restraining effect.

A schematic illustration of the test arrangement is given in Figure 3.5. Compression axial load is applied on the in-plane brace.

On each of the out-of-plane braces of joints MPJT2, MPJT3 and MPJT4, two dial gauges are arranged (gauges A and B and gauges C and D). At particular load increments the test is halted, the position of the out-of-plane braces is adjusted based upon the readings from the dial gauges in order to keep the out-of-plane braces horizontal. For joint MPJT2, the out-of-plane braces are unloaded. While for joints MPJT3 and MPJT4, the out-of-plane braces are loaded in tension and compression respectively. The loads on the out-of-plane braces when applicable are applied at the same time as the load on the in-plane brace with an absolute loading ratio of 0.56.

The tests for joints MPJT5, MPJT6 and MPJT7 correspond to the tests for joints MPJT2, MPJT3 and MPJT4 respectively. The difference is that the out-of-plane braces for MPJT5 to MPJT7 are free to rotate, i.e. no position adjustment of the out-of-plane braces.

The test is continued until a peak occurs in the in-plane load versus chord face indentation curve or the chord face indentation reaches unacceptably large values whichever is the sooner.
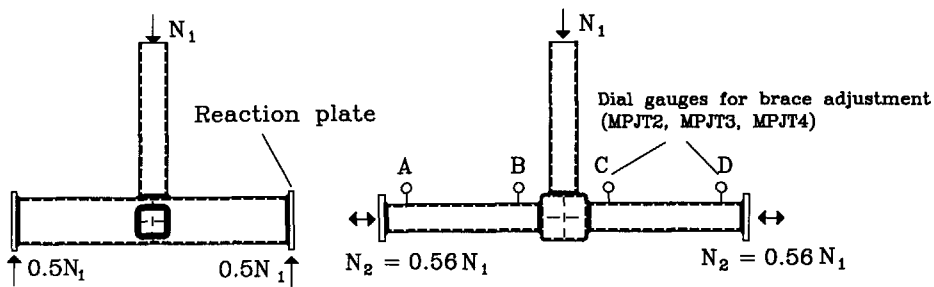


**Figure 3.5  Test arrangement for axially loaded TX-joints**

### 3.4.3   Test results and discussions

Joint failure is usually by excessive chord top face indentation, i.e. plastification of the joint. When the out-of-plane braces are in tension (MPJT3 and MPJT6) some cracking occurs in the chord side faces at the weld toes. Cracking initiates close to or later than the ultimate deformation limit. For joints with the out-of-plane braces kept in horizontal position, the in-plane load vs. chord top face indentation curves are illustrated in Figure 3.6. For joints with the out-of-plane braces free to rotate, the results are illustrated in Figure 3.7. The load capacity of each joint at the serviceability deformation limit and the ultimate deformation limit is listed in Tables 3.6 and 3.7. The influence of the restraints on the out-of-plane braces is listed in Table 3.8.

**Table 3.6    Test results for axially loaded T- and TX-joints with the out-of-plane braces kept horizontal**

| Joints | $\beta$ | $2\gamma$ | $t_0$ mm | $f_{y0}$ N/mm$^2$ | $f_{y1}$ N/mm$^2$ | $\delta_u$ mm | $N_2/N_1$ | $N_s$ kN | $N_{1,u}$ kN |
|--------|------|------|------|-----|-----|-----|------|-----|-----|
| MPJT1A | 0.6 | 23.2 | 6.42 | 420 | 430 | 3.9 | - | 189 | 210 |
| MPJT2 | 0.6 | 24.2 | 6.20 | 420 | 430 | 4.5 | 0.0 | 202 $(1.07)^*$ | 251 $(1.20)^*$ |
| MPJT3 | 0.6 | 24.2 | 6.20 | 420 | 430 | 4.5 | -0.56 | 165 $(0.82)^{**}$ | 210 $(0.84)^{**}$ |
| MPJT4 | 0.6 | 24.1 | 6.20 | 420 | 430 | 4.5 | 0.56 | 227 $(1.12)^{**}$ | 264 $(1.05)^{**}$ |

$^*$: Ratio to the load of uniplanar joint MPJT1A.
$^{**}$: Ratio to the load of multiplanar joint MPJT2.

**Table 3.7    Test results for axially loaded T- and TX-joints with the out-of-plane braces unrestrained**

| Joints | $\beta$ | $2\gamma$ | $t_0$ mm | $f_{y0}$ N/mm$^2$ | $f_{y1}$ N/mm$^2$ | $\delta_u$ mm | $N_2/N_1$ | $N_s$ kN | $N_{1,u}$ kN |
|--------|------|------|------|-----|-----|-----|------|-----|-----|
| MPJT1A | 0.6 | 23.2 | 6.42 | 420 | 430 | 3.9 | - | 189 | 210 |
| MPJT5 | 0.6 | 23.3 | 6.42 | 420 | 430 | 4.5 | 0.0 | 191 $(1.01)^*$ | 225 $(1.07)^*$ |
| MPJT6 | 0.6 | 23.4 | 6.36 | 420 | 430 | 4.5 | -0.56 | 150 $(0.79)^{**}$ | 190 $(0.84)^{**}$ |
| MPJT7 | 0.6 | 23.3 | 6.37 | 420 | 430 | 4.5 | 0.56 | 232 $(1.21)^{**}$ | 258 $(1.15)^{**}$ |

$^*$: Ratio to the load of uniplanar joint MPJT1A
$^{**}$: Ratio to the load of multiplanar joint MPJT5

**Table 3.8    Influence of the restraints on the out-of-plane braces**

| Indentation | $\dfrac{N_{MPJT2}}{N_{MPJT5}}$ | $\dfrac{N_{MPJT3}}{N_{MPJT6}}$ | $\dfrac{N_{MPJT4}}{N_{MPJT7}}$ |
|-------------|------|------|------|
| 1%b$_0$ | 1.06 | 1.10 | 0.98 |
| $\delta_u$ | 1.12 | 1.11 | 1.02 |
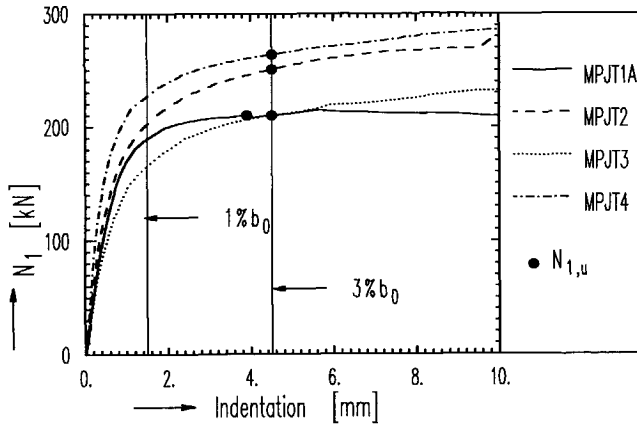
**Figure 3.6** **Test results of axially loaded T- and TX-joints with the out-of-plane braces kept horizontal**
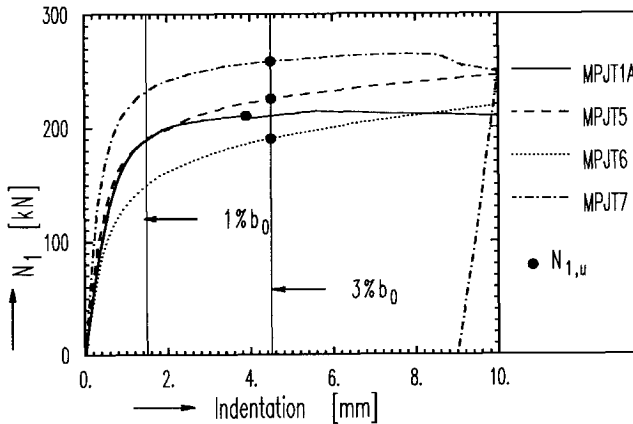


**Figure 3.7** **Test results of axially loaded T- and TX-joints with the out-of-plane braces free to rotate**

From Figures 3.6 to 3.7 and Tables 3.6 to 3.8, the following conclusions can be drawn:

- For the joint with the out-of-plane braces **unloaded and restrained** (MPJT2), the multiplanar geometrical stiffening effect is 7% at the serviceability deformation limit and 20% at the ultimate deformation limit. The multiplanar geometrical stiffening effect is much stronger at the ultimate deformation limit than at the serviceability

deformation limit. The reason is partly due to the larger vertical adjustment forces applied at the ultimate deformation limit in order to keep the out-of-plane braces horizontal. For the joint with the out-of-plane braces **unloaded and unrestrained** (MPJT5), the multiplanar geometrical stiffening effect is 1% and 7% respectively at the serviceability and the ultimate deformation limits. Thus, smaller geometrical stiffening effect is found if no restraints are applied on the out-of-plane braces.

- For the joint with the out-of-plane braces loaded in **tension and restrained** (MPJT3), the load capacity is decreased by 18% and 16% respectively at the serviceability and the ultimate deformation limits compared to that of joint MPJT2 with the out-of-plane braces unloaded. For the joint with the out-of-plane braces loaded in **tension and unrestrained**, the load capacity at the serviceability and the ultimate deformation limits is decreased by 21% and 16% respectively compared to that of joint MPJT5.

- For the joint with the out-of-plane braces loaded in **compression and restrained** (MPJT4), the load capacity is increased by 12% and 5% respectively at the serviceability and the ultimate deformation limits compared to joint MPJT2. For joint with the out-of-plane braces loaded in **compression and unrestrained** (MPJT7), the load capacity at the serviceability and the ultimate deformation limits is 21% and 15% increased respectively compared joint MPJT5.

- The effect of the restraints used to keep the out-of-plane braces horizontal is within 12%.

# 4 NUMERICAL CALIBRATION AND GENERAL ASPECTS ABOUT THE PARAMETER STUDY

## 4.1 INTRODUCTION

Experimental testing is expensive and time consuming. In the last decade, there has been an increasing awareness that the use of non-linear techniques represents a much more economic tool for ultimate strength estimations of hollow section joints. For predicting the ultimate strength, the following major influences should be taken into account for modelling tubular joints (Puthli 1981 and Cofer 1992): the constitutive laws for elasto-plastic behaviour including the strain hardening behaviour (material nonlinearity); large displacement and large strain behaviour (geometrical nonlinearity); the ability to reproduce the weld profile in order to take into account its influence on the static strength of tubular joints. There is no problem of including the first two by using the general purpose FE programme MARC. For modelling of the weld, different ways may be adopted which will be further discussed in this chapter. Of course, experiments need to be carried out within the range of parameters being investigated in order to: check the preliminary numerical results; calibrate the numerical models for accuracy; give sufficient proof of the validity of the results. Once a numerical model is well established and well calibrated, a large number of numerical parameter studies can be carried out which are cheaper and faster than the experimental investigations.

This chapter contains the following work:

- software and hardware used for the numerical study, Section 4.2.
- selection of a suitable numerical model, Section 4.3.
- calibration of the numerical model with the experimental results, Section 4.4.
- general aspects about the numerical parameter study, Section 4.5.

## 4.2 SOFTWARE AND HARDWARE

Using the pre- and post precessing package SDRC-IDEAS (level IV and V), the FE models have been generated on SUN SPARC Workstations. The numerical analyses have been performed using the general purpose FE programme MARC (Versions K5 and K6) on a CONVEX Super Computer or on an IBM RS/6000-350 Workstation. Converting IDEAS files to MARC files and vice versa has been carried out using MARC's pre- and post processor MENTAT (Version 5.4).

## 4.3 SELECTION OF THE MOST SUITABLE NUMERICAL MODEL

### 4.3.1 Literature review

In order to choose the best FE strategy, available literature (de Koning 1992, van der Vegte 1991) has been reviewed. The following aspects have been considered:

- the finite element mesh refinement.
- the use of material and geometrical non-linearities.
- the modelling of the weld.

-        the modelling of the rounded corners of the rectangular hollow sections.
-        the choice of a finite element type.

In order to guarantee the mesh accuracy, three different meshes have been modelled for joint X1 with the number of elements equalling to 160, 270 and 362 (de Koning 1992), see Figure 4.1. The geometrical and material properties of joint X1 can be found in Chapter 3. It was concluded that the model with 160 elements for joint X1 is sufficiently accurate for the problem at a relatively low cost. Thus, similar mesh refinement is used for uniplanar T-joints.
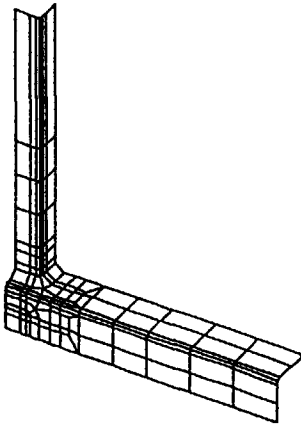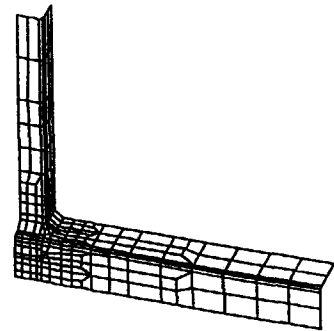


1) No. of elements: 160                     2) No. of elements: 270
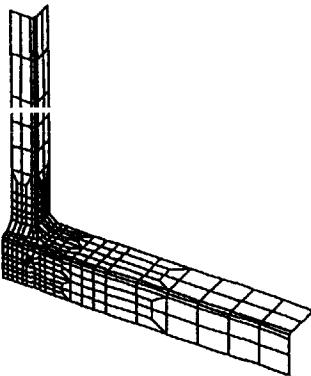


3) No. of elements: 362

**Figure 4.1  Different element meshes (de Koning 1992)**

As mentioned before, both material and geometrical non-linearities should be included for the prediction of the joint ultimate load capacity .

The presence of the weld may have a strong influence on the strength of the joint, so that the weld should be included in the numerical modelling. The degree of weld penetration has little influence on the strength of the joint. Therefore, the gap between the chord and the brace due to partial fillet weld penetration can be neglected in the numerical modelling.

The rounded corners of chord and braces may have a strong influence on the strength of the joint, and have to be included in the modelling.

The choice of an element type is not only structural dependent but also limited by other factors such as the disk space, the CPU time and the software etc. In principle, the following element types can be used for this study: solid elements, shell elements or a combination of the two through transition elements. It is well known that a numerical model with the combination of solid, shell and transition elements needs much more disk space and CPU time than a model with only solid or shell elements (Yu 1994a, Van der Vegte 1995) if the same mesh refinement is used. Using the FE programme ABAQUS, Davies (1993b) concluded that using solid elements to model the weld and shell elements to model the brace and the chord gives a good simulation of the joint behaviour compared to the experimental results. However, in the FE programme MARC, using solid elements to model the fillet weld overestimates the load capacity of the RHS joints. This will be further discussed in this section. Van der Vegte (1991) indicated that using eight noded thick shell elements to model the <u>butt</u> weld, the chord and the braces for circular hollow section joints gives a good agreement with the experimental results. In his model, the throat thickness of the fillet part of the butt weld is used as the thickness of the finite elements representing the weld. However, using this approach for <u>fillet</u> welded joints of RHS sections, it is found that the load capacity is overestimated compared to the experimental results, see Figure 4.2.
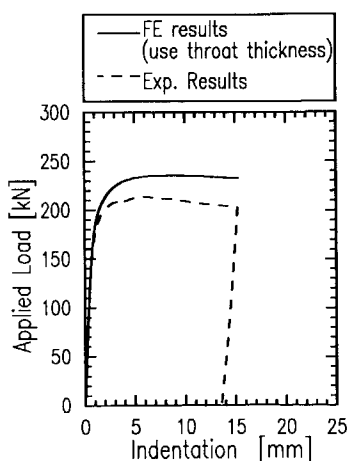


**Figure 4.2**     **Comparison between numerical and experimental results of fillet welded joint of rectangular hollow sections (joint MPJT1A in Chapter 3)**

In order to demonstrate the sensitivity of the FE analyses to different approaches in modelling the RHS joints, six models with different types of elements available in the general purpose FE computer programme MARC are used to model the joint in different ways, see Table 4.1. In Table 4.1, one uniplanar T-joint (MPJT1A) with measured dimensions and material properties is considered, see Tables 3.4 to 3.6 in Chapter 3. The hollow section members and the welds are modelled using: two types of solid elements (model 1 and 2); three types of shell elements (model 3, 4 and 5); and one type of solid and shell elements together with transition elements in between (model 6).

**Table 4.1. Element types used in the six models**

| Models | | Element Types |
|---|---|---|
| Solid models | Model 1 | 20-noded solid (Element 21) |
| | Model 2 | 20-noded solid with reduced integration (Element 57) |
| Shell Models | Model 3 | 8-noded thick shell (Element 22) |
| | Model 4 | 8-noded thin shell (Element 72) |
| | Model 5 | 4-noded thick shell (Element 75) |
| Shell+Solid+Transition Model | Model 6 | 20-noded solid+8-noded thick shell+15-noded solid (Element 22 + Element 57) |

## 4.3.2   Description of different element types

**Solid elements**

Solid elements can model both relatively thin objects such as steel hollow sections and thick objects such as welds between hollow sections. With the midside nodes, twenty noded solid elements can be used for high accuracy problems. Two types are used here for comparison.

Model 1     20-noded solid elements (MARC element type 21): Each has three translational degrees of freedom; Quadratic interpolation polynomials are used for the coordinates and the displacements; 27 Gaussian integration points are used in order to elaborate the element stiffness matrix, thus 3 integration points in each of three directions. No reduced integration technique is used. Shear locking may occur for using such an element. Because of the existence of the midside nodes, it is an element with a high order accuracy.

Model 2     20-noded solid element (MARC element type 57): Each has three translational degrees of freedom; Quadratic interpolation polynomials are used for the

coordinates and the displacements; By using reduced integration, shear locking can be prevented; Due to the application of reduced integration, 8 Gaussian integration points are used for elaborating the element stiffness matrix, i.e., 2 integration points in each of the three directions. It is also a high accuracy element because of the existence of midside nodes.

It should be mentioned that it is not possible to have more than three integration points for either of the above two solid elements in the thickness direction of the chord and the brace walls. This will cause difficulties in adequately describing the plastic stress pattern in the thickness direction for nonlinear analyses, and is not suitable for no-linear analysis. These two elements are used for comparison purposes to clearly demonstrate the erroneous results.

### Shell elements
Shell elements can be used for relatively thin structures such as steel hollow sections. However, for the welds at the tubular joints, it is difficult to exactly describe the geometrical shape, because shell element nodes are located in the middle plane of the element. It is necessary to choose the thickness of the weld carefully in the FE analysis in order to describe the joint behaviour correctly. It is possible to select an adequate number of integration points in the thickness direction of the shell elements and the non-linear stress pattern in the thickness direction of the tubular joints can be better described.

Model 3        8-noded thick shell element (MARC element type 22): Each has three translational and two rotational degrees of freedom. Quadratic interpolation polynomials are used for the coordinates, displacements and rotations. For defining the strain and stress distribution adequately, 7 Simpson integration points (called layers in MARC) are used in the thickness direction of the elements, and 2x2 Gaussian integration points are used in each layer of the elements with the reduced integration scheme. It is a high order accuracy element because of the existence of the midside nodes. Thick shell elements are also called Mindlin shell elements in which the transverse shear strains are taken into account (Puthli 1981).

Model 4        8-noded thin shell element (MARC element type 72): Each corner has three degrees of freedom for translation. At midside nodes, rotation of the edge about itself is allowed. Although coordinates may be specified at the midside nodes, they will be ignored and the edges set up as straight lines. Bilinear interpolation is used both for displacements and coordinates. Because of the bilinear interpolation for displacements and coordinates, it is a lower accuracy element compared to element 22. Thin shell elements are also called Kirchhoff elements where transverse shear strains are ignored. 7 Simpson integration points are used in the thickness direction of the elements and 5 Gaussian integration points are used in each layer. This type of element is suitable for tubular joints with very thin chord and brace members.

Model 5        4-noded thick shell element (MARC element type 75): Each has three translational and two rotational degrees of freedom. Bilinear interpolation is used for the coordinates, displacements and rotations. With the absence of

midside nodes, it is a lower accuracy element compared to MARC element type 22. Again, 7 Simpson integration points are used in the thickness direction of the elements, and 2x2 Gaussian integration points are used in each layer of the elements. Transverse shear strains are included.

**Transition elements**

Model 6          Another possibility of modelling the RHS joints is to combine solid and shell elements in one model. Namely, the weld areas are modelled as solid elements and other parts are modelled as shell elements. Automatic constraints are used for transitions between solid and shell elements. The transition element is a special case of MARC element type 57 degenerated as 15-nodes, as shown in Figure 4.3.
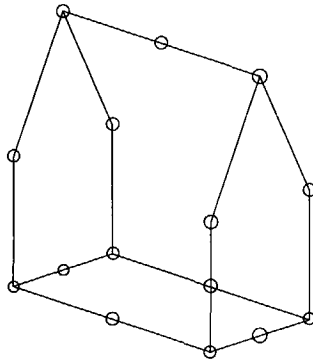


**Figure 4.3  15-noded transition element**

### 4.3.3   Modelling of the weld area

Corresponding to the six models, there are different ways to model the weld area, as shown in Figure 4.4. In Figure 4.4,  (b) corresponds to models 1 and 2 with solid elements; (c) to models 3 and 4 with 8-noded thick shell and 8-noded thin shell elements respectively; (d) to model 5 with 4-noded thick shell elements; and e) to model 6 with solid, shell and transition elements.

For models 3, 4 and 5, the thickness of the shell elements for the fillet weld is taken as its average thickness $t_w$ (see Figure 4.5). The average thickness $t_w$ was also used in the earlier reports and papers (de Koning 1992, Liu 1993, Yu 1993a, Yu 1993b).

(a) Weld area

(b) Solid Elements
(Model 1, Model 2)

(c) 8-node Shell Elements
(Model 3, Model 4)

(d) 4-node Shell Elements
(Model 5)

(e) Solid+Transition+Shell Elements
(Model 6)
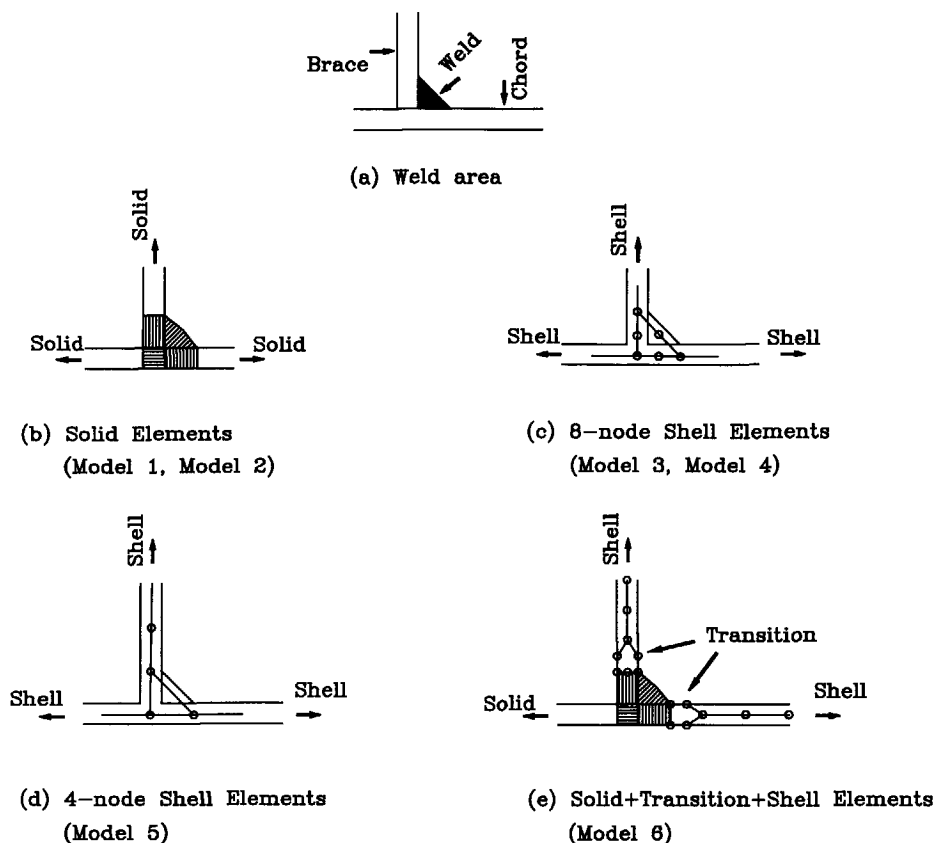
**Figure 4.4  Modelling of the weld area**
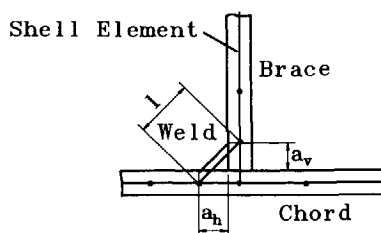
**Figure 4.5    Average thickness of fillet weld $t_w$**
**($t_w = 0.5 * a_v * a_h / l$)**
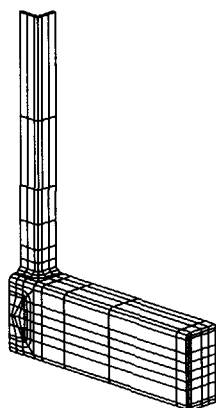
**Figure 4.6  Solid element meshes (Models 1 and 2 in Table 4.1)**

### 4.3.4    FE meshes for different models

Considering symmetry in load (axial compressive load applied on the brace) and geometry, only one quarter of a T-joint is analysed. Figure 4.6 gives the element meshes for models 1 and 2 where only solid elements are used. Figure 4.7 shows the element meshes for models 3 and 4 where only 8-noded shell elements are used. For model 5, the same element grid is used as in Figure 4.7. However there are only four nodes per element. In Figure 4.8, the shaded elements are 15-noded degenerated solid elements with automatic constraints (the transition elements, see Figure 4.3). The weld, the chord wall underneath the weld, the chord wall underneath or surrounded by the brace and the brace adjacent to the weld are modelled as 20-noded solid elements (element 57). Other parts of the joint are modelled as 8-noded thick shell elements.
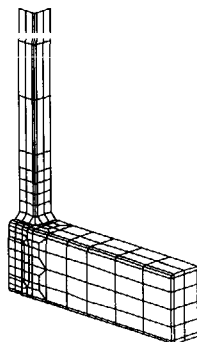


**Figure 4.7  Shell element meshes (Models 3, 4 and 5 in Table 4.1)**
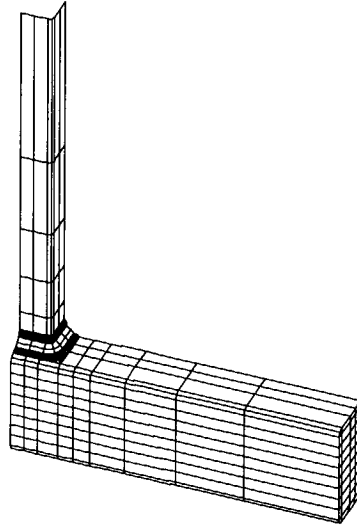
**Figure 4.8  Solid + shell + transition element meshes (Model 6 in Table 4.1)**

### 4.3.5   Geometrical and material non-linearities

**Geometrical non-linearities**
In order to describe large displacement problem, an updated Lagrange procedure is used so that a new frame of reference is defined at the beginning of each increment.

**Material non-linearities:**
For finite strain problems, the true stress-strain curves should be used for the work hardening data. For an uniaxial tensile specimen, the true strain (logarithm strain) is the integration of the deformation rate along its length:

$$\varepsilon_T = \int_{l}^{l+\Delta l} \frac{dx}{x} = \ln\frac{l+\Delta l}{l} = \ln(1+\varepsilon_E) \tag{4.1}$$

The true stress:

$$\sigma_T = \frac{P}{A_u} = \frac{P}{A}\frac{A}{A_u} = \frac{A}{A_u}\sigma_E \tag{4.2}$$

Note that for an approximate incompressible material behaviour,

$$A_u(1+\varepsilon_E)=A \tag{4.3}$$

Where,

        l        : Member length;
        $A_u$    : Updated section area of a member;
        A     : Section area of a member;
        P     : Force applied to the section area;
        $\varepsilon_E$    : Engineering strain, $\varepsilon_E=\Delta l/l$;
        $\varepsilon_T$    : Logarithm strain;
        $\sigma_E$    : Engineering stress;
        $\sigma_T$    : True stress;

Hence, the expression for the true stress may then be approximated by

$$\sigma_T=(1+\varepsilon_E)\sigma_E \tag{4.4}$$

First, the engineering stress-strain curves are determined by tensile testing of material from the chord and the brace in the longitudinal direction of the members (Davies 1992b). The engineering stress-strain curve reaches its maximum when necking occurs in the specimen, see Figure 4.9. However, for the true stress-strain curve, the true stress will still increase after the maximum engineering stress, due to the decreasing of the section area .
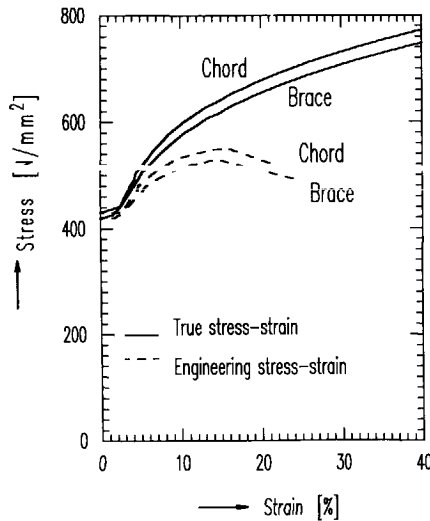


Figure 4.9   The stress-strain curves of the chord and the braces

Thus, two approaches have been used to convert the engineering stress-strain curves into true stress-strain ones:

-        Directly use formulae (4.1) and (4.4). These formulae can only be used until maximum is reached in the stress-strain curve, see Figure 4.9.

-        After the maximum is reached in the engineering stress-strain curve, the Ramberg-Osgood power law is recommended to be used (Background Document of EC3 1992 and van der Vegte 1991):

$$\varepsilon_T/\varepsilon = a*(\sigma_T/\sigma)^{\frac{1}{n}} \tag{4.5}$$

Where a and n are coefficients to be determined using the least square method based upon the test results of the engineering stress-strain. $\sigma$ and $\varepsilon$ are the reference stress and reference strain (here taken as engineering stress and engineering strain respectively).

The engineering stress-strain curves and the corresponding true stress-strain curves are shown in Figure 4.9. The true stress-strain curves are used for the work hardening data in the numerical investigation. Furthermore, the isotropic work hardening rule and the Von Mises yield criterion have been chosen.

### 4.3.6   Solution techniques used for the numerical analysis

**Loading**
The axial loads are applied by the displacement control procedure. With this method, an axial displacement at the end nodes of the in-plane brace is prescribed which in turn results in nodal forces at these nodes. The displacements are applied with increments and within each increment, iterations are needed until the prescribed convergence criteria are reached. Full Newton-Raphson technique has been used for the iterative-incremental solution procedure.

**Convergence criteria**
The convergence criteria used here are based on the ratio of residual forces and the ratio of residual moments (the maximum residual force divided by the maximum reaction force and the maximum residual moment divided by the maximum reaction moment respectively). Both convergence ratios are set to 0.01.

**Bandwidth optimization of the stiffness matrix**
In order to reduce CPU time, the Cuthill-McKee algorithm is used to optimize the bandwidth of the stiffness matrix.

### 4.3.7   Comparisons between the results of six models investigated

**Results from models with solid elements**
In Figure 4.10, the numerical results from the different solid element models (model 1, 2 and 6) are compared with the experimental result of joint MPJT1A (Davies 1992b). The horizontal

axis represents the chord top face indentation at the joint intersection and the vertical axis represents the axial load applied on the in-plane brace.
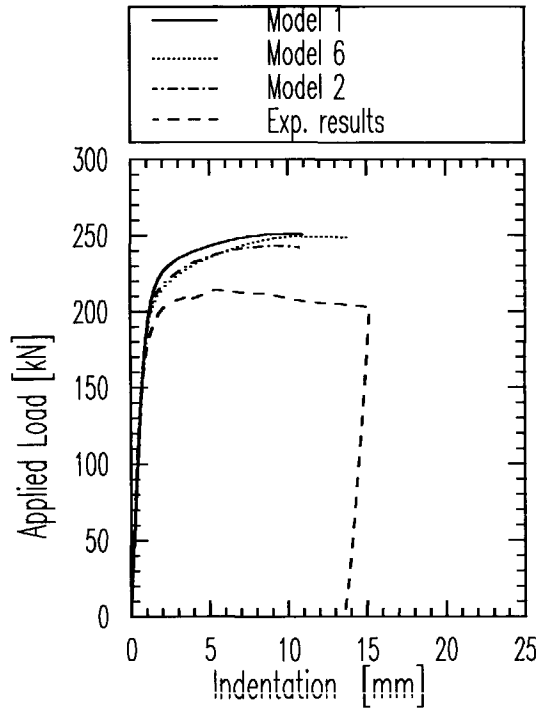


**Figure 4.10    Comparison between the results of models with different solid elements and the experimental result (β=0.6 2γ=23.8)**

It can be seen that the load capacity obtained for all the three models (models 1, 2 and 6) is much higher than that from the experiment. Model 1 using 20-noded solid elements gives the highest load capacity among the three models, because a reduced integration technique is used for models 2 and 6. Model 1, without using the reduced integration technique, overestimates the transverse shear strain capacity of the elements. The load capacities from models 2 and 6 are very close to each other in most part of the load vs. indentation curve.

Using solid elements or combining solid and shell elements with automatic constraints gives too high load capacity compared to the experimental result. The reason is because there are no more than three integration points in the area of the weld modelled with solid elements. In that case, the stress distribution in the thickness direction of the elements can not be appropriately described.
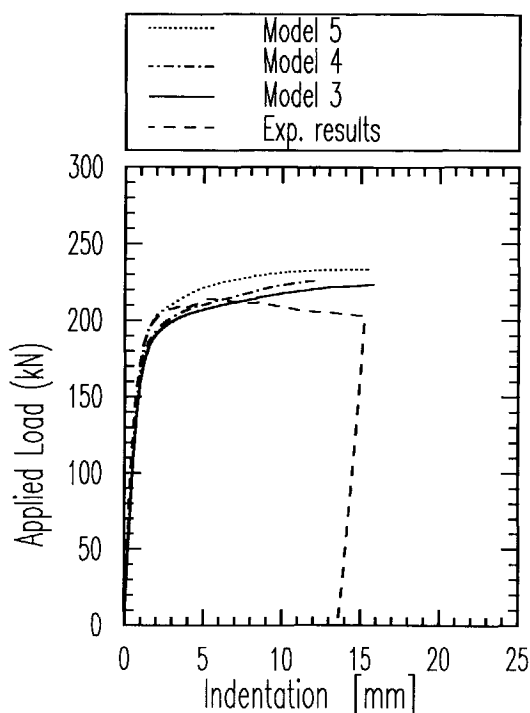
**Figure 4.11    Comparison between the results of models using different shell elements and the experimental result ($\beta$=0.6 2$\gamma$=23.8)**


**Results from models with different shell elements**

Figure 4.11 shows the comparison between the results from the models with shell elements (models 3, 4 and 5) and the experimental result of joint MPJT1A. The load capacity from model 5 with 4-noded thick shell elements gives the highest value. The load capacity from model 4 with 8-noded thin shell elements is higher than that from model 3 with 8-noded thick shell elements. The difference in load capacities between model 3 and model 4 is, however, only 1%, although the load capacity of the latter is a little bit higher for the investigated joint geometry ($\beta$=0.6 and 2$\gamma$=23.8). Thus, for a joint with a 2$\gamma$ value larger than 24, model 4 is an alternative choice to model 3, although the latter is theoretically speaking more accurate, because the transverse shear strain of the element is considered. For a smaller 2$\gamma$ value of 15, the ultimate load capacity of model 4 with 8-noded thin shell elements is about 6% higher than that of model 3 with 8-noded thick shell elements, see Figure 4.12.

The load capacity of model 5 with 4-noded thick shell elements is also close to that of the experimental results before the kink of the load vs. indentation curve. However, with the increase of the indentation, the numerical result is higher than the experimental one.
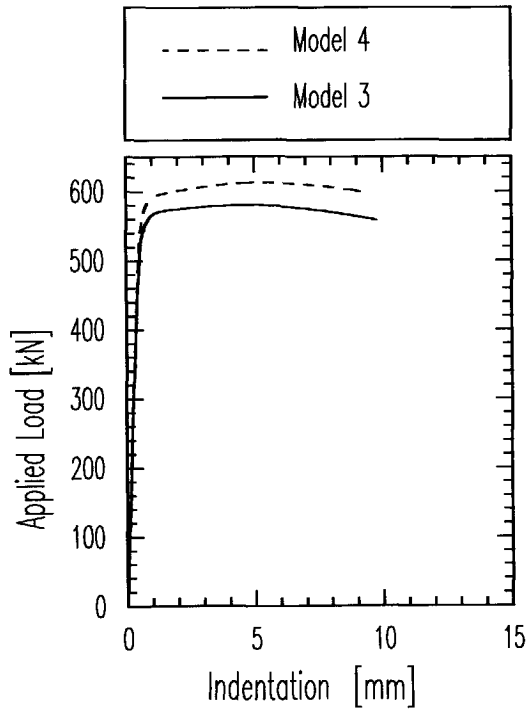
**Figure 4.12**    **Comparison between the results of Models 3 and 4 (for β=0.8, 2γ=15)**

The load capacities from the models with 8-noded thin (model 4) and 8-noded thick (model 3) shell elements are close to each other and close to the experimental results for the investigated joint geometry (β=0.6, 2γ=23.8). However, as already mentioned, the difference between the numerical results from model 3 and model 4 will be larger for lower 2γ values, as shown in Figure 4.12. In Table 4.2, the numerical results from different models are quantitatively compared to the experimental result.

**Table 4.3  Comparisons between the results from six models**

| Models | Element No. | $f_{y0}$ N/mm$^2$ | $t_0$ mm | Ultimate load capacity | |
|---|---|---|---|---|---|
| | | | | $N_{1,u}$ kN | relative $N_{1,u}$ to exp. results |
| Model 1 (20-node solid) | 276 | 419.7 | 6.42 | 243 | 1.16 |
| Model 2 (20-noded solid with reduced integration) | 276 | 419.7 | 6.42 | 235 | 1.12 |
| Model 3 (8-noded thick shell) | 270 | 419.7 | 6.42 | 206 | 0.98 |
| Model 4 (8-noded thin shell) | 270 | 419.7 | 6.42 | 209 | 0.99 |
| Model 5 (4-noded thick shell) | 270 | 419.7 | 6.42 | 219 | 1.04 |
| Model 6 (8-noded thick shell + 20-noded solid + 15-noded solid) | 267 | 419.7 | 6.42 | 233 | 1.11 |
| Exp. results (MPJT1A) | | 419.7 | 6.42 | 210 | 1.00 |

### 4.3.8  Summary and recommendation for the numerical modelling

Six models with different types of elements have been used to model the RHS joints. The results are summarised as follows:

- Using solid elements or a combination of solid and shell elements through transition elements to model RHS joints gives an unacceptably high load capacity of the joint compared to the experimental results. The reason is that there are no more than three integration points in each direction of the solid elements, particularly in the thickness direction. The stress distribution in the elements after yielding cannot therefore be described exactly.

- Models with solid elements or model with a combination of solid and shell elements through transition elements require much more computer time than models with shell elements. Between the models with shell elements, an 8-noded thin shell element model requires the smallest amount of CPU time and a 4-noded thick shell element model the smallest disc working space (Yu 1994a, Van der Vegte 1995).

- The numerical results using the 4-noded thick shell elements are higher than those using the 8-noded thin and thick shell elements.

- Theoretically speaking, an 8-noded thick shell element is more accurate because the transverse shear strain of the element is considered. For most cases, model 3 with 8-noded thick shell elements is recommended to model the hollow sections and the welds if the disc working space and CPU time are not limited. For large models (large number of nodes) with $2\gamma$ value higher than 24, model 4 with 8-noded thin shell elements can be an alternative model, in order to save computing time and disc working space.

- For modelling of the fillet weld, an average thickness $t_w$ can be used, see Figure 4.5. For modelling of the butt weld, the throat thickness of the fillet part of the weld has been proved to be suitable (Van der Vegte 1991).

## 4.4 CALIBRATION OF THE NUMERICAL MODEL WITH THE EXPERIMENTAL RESULTS

### 4.4.1 General remarks

A numerical model has been recommended in Section 4.3. In this section, the same model is used for the calibration with the experimental results of multiplanar TX-joints described in Chapter 3. The numerical calibration of uniplanar X- and multiplanar XX-joints has also been carried out in a similar way (de Koning 1992) but is not included in this section. General remarks regarding the numerical calibration are as follows:

- In order to simulate the experiments as accurately as possible, the measured dimensions and material properties of each joint are used. The measured dimensions and material properties can be found in Tables 3.4 to 3.7, Chapter 3. The loading conditions for each joint can be found in Table 3.1, Chapter 3.

- The rounded corners of the chord and the braces are modelled.

- The plates attached to the ends of the chord and the ends of the out-of-plane braces are also modelled, using the material properties of the chord.

- 8-noded thick shell elements are used for the chord, the braces and the weld. The thickness of the weld is taken as the average thickness defined in Figure 4.5.

- For the work hardening data, the stress-strain curves of the material are modelled as a multilinear relationship which are obtained by converting the engineering stress-strain curves into true stress-strain curves, see Figure 4.9. The engineering stress-strain curves are determined by tensile tests of the chord and the brace members in the longitudinal direction (Davies 1992a, 1992b). The work hardening data for the braces is also used for the weld. The Von Mises yield criterion and the isotropic strain hardening rule are adopted.

- Large displacement and finite strain options are chosen. The updated Lagrange procedure is used.

### 4.4.2 Finite element meshes and boundary conditions

T-joints differ from X-joints in the way forces are transferred through the hollow section chord. In X-joints with balanced forces, axial forces are transferred across the chord from one brace to another, without imposing shear forces or bending moments in the chord. In X-joints, the local chord face deformation is doubly symmetric, so that no bending of the brace members occurs. In T-joints, however, the in-plane brace force is transferred to the supports. This gives rise to shear and bending in the chord. Due to the non-symmetric distortion of the chord cross section, rigid body rotation of the out-of-plane braces occurs, if their ends are free as shown in Figure 4.13 or bending occurs in the out-of-plane braces if the out-of-plane braces are restrained from vertical displacement at the ends.
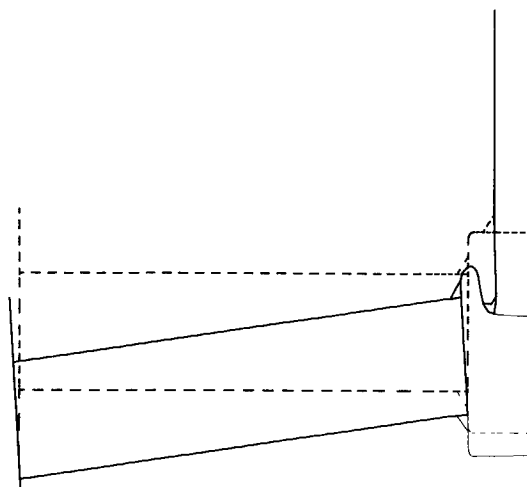
**Figure 4.13  Rigid body motion of the out-of-plane braces**

For both uniplanar T-joint and multiplanar TX-joints, a quarter of a joint has been modelled. As an example, Figure 4.14 shows the finite element meshes and boundary conditions for multiplanar joints (MPJT2, MPJT3, MPJT4) with the out-of-plane braces kept horizontal. The origin of the coordinate system is at the centre of the chord.

For multiplanar joints of MPJT2 to MPJT4 shown in Figure 4.14, points A1 and A2 indicate positions where transducers are attached in the experimental work for the measurement of the vertical displacements of the out-of-plane braces. Small forces are applied at A3 to maintain equal vertical displacements at points A1 and A2 during the experiment. In order to simulate these forces, point A3 is tied to point A1 in the vertical direction. As a result, the out-of-plane braces are kept horizontal.

For multiplanar joints of MPJT5 to MPJT7, the same element meshes and boundary conditions are used except that no restraints are applied on the out-of-plane braces.

### 4.4.3   Simulation for the loading

For uniplanar joint and multiplanar joints with the out-of-plane braces unloaded, the compressive load at the end of the in-plane brace is applied by displacement control.

For multiplanar joints with the out-of-plane braces loaded, all the loads are applied by load control, because the loads applied to the out-of-plane braces are to be maintained proportional (0.56 times the in-plane brace load), as in the experiment.

**Tying for loading**

$A_1$

$A_2$

$A_3$

**Support**

| BOUNDARY CONDITIONS | | | |
|---|---|---|---|
| Degree of freedom | Nodes on plane X=0.0 | Nodes on plane Z=0.0 | Nodes on support |
| $u_x$ | 0. | free | free |
| $u_y$ | free | free | 0. |
| $u_z$ | free | 0. | free |
| $\Phi_x$ | free | 0. | free |
| $\Phi_y$ | 0. | 0. | free |
| $\Phi_z$ | 0. | free | free |
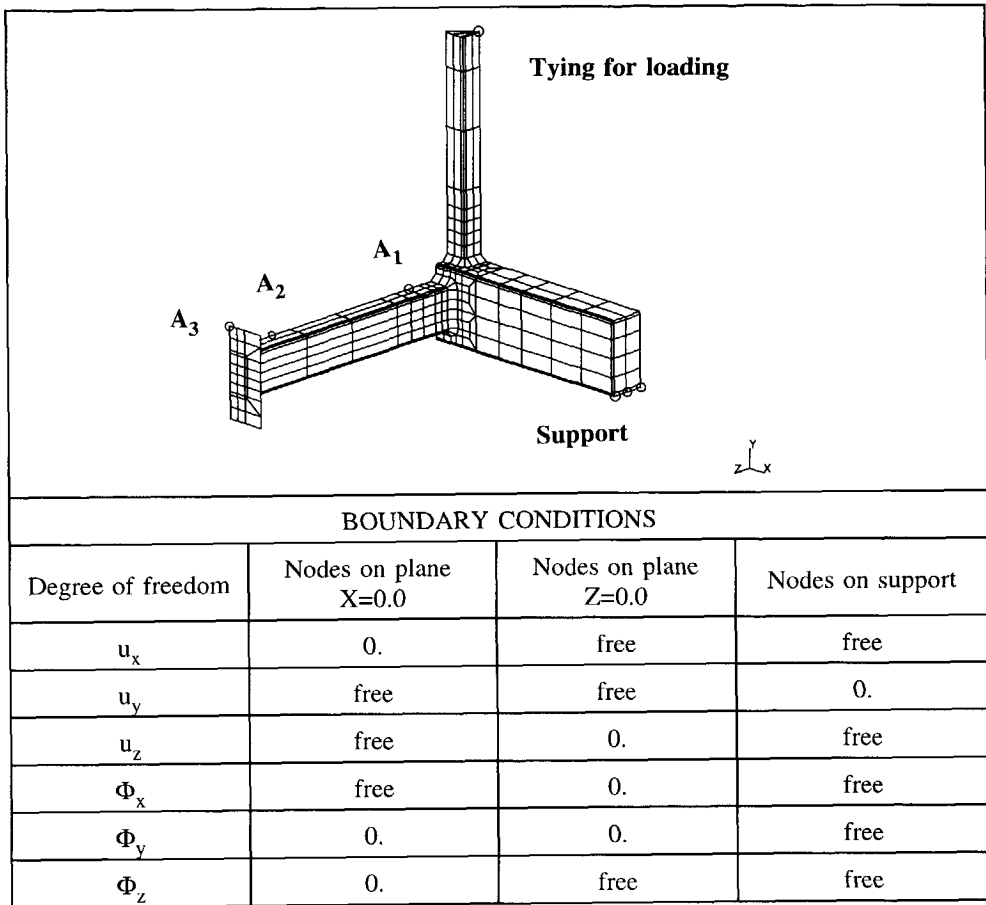
**Figure 4.14    FE meshes and boundary conditions for multiplanar joints**

### 4.4.4    Numerical results

The numerical results are illustrated with the in-plane brace load versus chord top face indentation curves in Figure 4.15. The local indentation of the chord top face is measured as the in-plane brace displacement (at a position of 100 mm above the chord top face) minus the bottom face displacement of the chord, as in the experiments. This load versus indentation relationship has been included in a FORTRAN subroutine for the output.

### 4.4.5    Comparison between the numerical and the experimental results

Comparison between the numerical and the experimental results is shown in Figure 4.15. A quantitative comparison between the numerical and the experimental results with regard to the serviceability load capacity and the ultimate load capacity is listed in Tables 4.3 and 4.4.
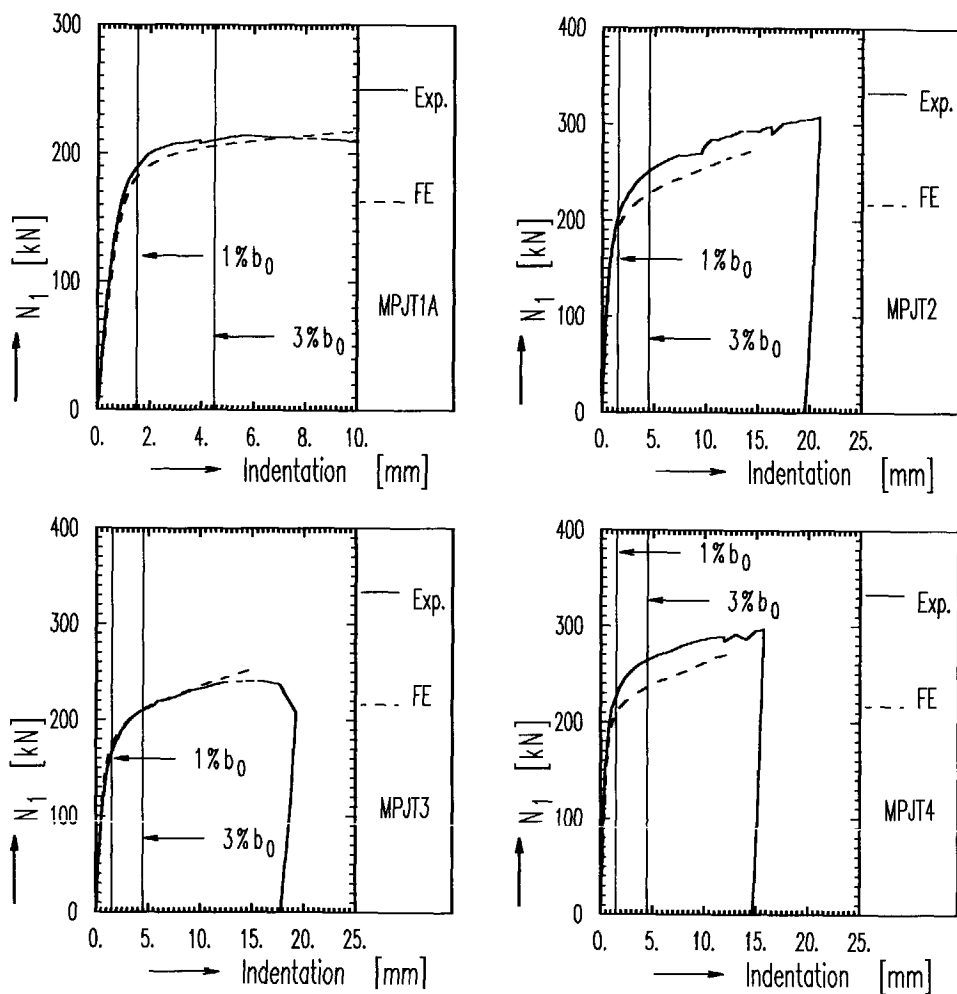
**Figure 4.15    Calibration of the numerical model with the experimental results**
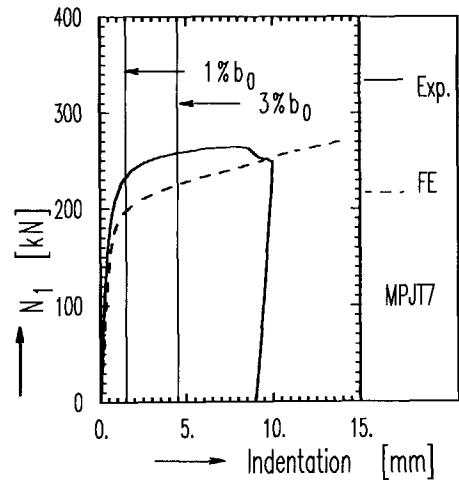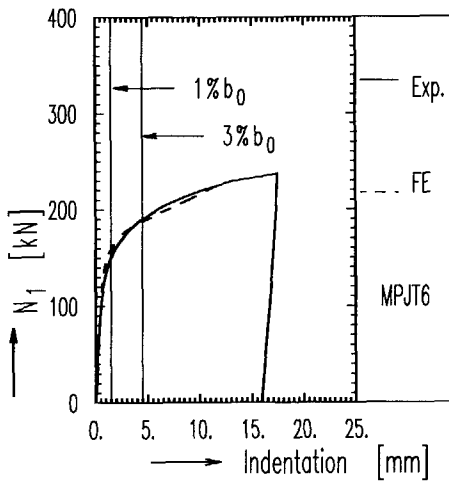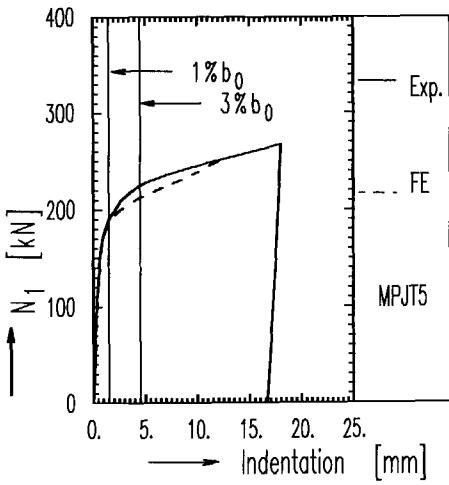
**Figure 4.15**   **(Continued)**

**Table 4.3**   **Comparison between the numerical and the experimental results at the serviceability load capacity**

| Joint | $N_{s,num.}$ kN | $N_{s,exp.}$ kN | $\dfrac{N_{s,num.}}{N_{s,exp.}}$ |
|---|---|---|---|
| MPJT1A | 182 | 189 | 0.96 |
| MPJT2 | 192 | 202 | 0.95 |
| MPJT3 | 174 | 165 | 1.05 |
| MPJT4 | 209 | 227 | 0.92 |
| MPJT5 | 187 | 191 | 0.98 |
| MPJT6 | 159 | 150 | 1.06 |
| MPJT7 | 197 | 232 | 0.85 |

**Table 4.4**   **Comparison between the numerical and the experimental results at the ultimate load capacity**

| Joint | $N_{u,num.}$ kN | $N_{u,exp.}$ kN | $\dfrac{N_{u,num.}}{N_{u,exp.}}$ |
|---|---|---|---|
| MPJT1A | 206 | 210 | 0.98 |
| MPJT2 | 228 | 251 | 0.91 |
| MPJT3 | 211 | 210 | 1.00 |
| MPJT4 | 236 | 264 | 0.89 |
| MPJT5 | 213 | 225 | 0.95 |
| MPJT6 | 188 | 190 | 0.99 |
| MPJT7 | 225 | 258 | 0.87 |

At the serviceability deformation limit ($1\%b_0$ indentation), there is a good agreement between the numerical results and the experimental ones for most of the cases except for joint MPJT7 where a difference of 15% occurs, which is, however, conservative compared to the experimental result.

At the ultimate deformation limit ($3\%b_0$ indentation), the numerical results agrees well with the experimental ones for most of the cases. A maximum difference of 13% occurs for joint MPJT7 which is again conservative compared to the experimental result. It should be

mentioned that for joint MPJT7, there was a horizontal rotation of the out-of-plane braces during the experiment. This rotation can be found in Figure 3.7.5 of page 71 in the Nottingham report (Davies 1992b). The experimental test for joint MPJT7 has been stopped when the out-of-plane braces had become unstable. The horizontal rotation of the out-of-plane braces may influence the load capacity of the joint.

For the numerical calibration of uniplanar X- and multiplanar XX-joints, similar results have been found (de Koning 1992).

In conclusion, the numerical model recommended gives either good agreements or is somewhat conservative with respect to the experimental results.

## 4.5    GENERAL ASPECTS ABOUT THE NUMERICAL PARAMETER STUDY

### 4.5.1    The numerical model

- The nominal dimensions of the joints are used for the parameter study. For all the joints investigated, the depth of the chord is fixed at 150 mm. The external and internal corner radii of a rectangular hollow section are two and one times its thickness respectively. Unless indicated, the length of the chord is 6 times its width and the length of the braces is 5 times their width. Butt welds are used in the numerical parameter study. The weld dimensions for butt welds are shown in Figure 4.16. The leg length of the fillet part of the butt weld along the chord is taken as $0.5t_1$ and the leg length of the butt weld along the brace is $(2+t_1)$ mm.

- 8-noded thick shell elements are used for the chord, the braces and the welds as recommended in Section 4.3. The modelling of the butt weld is shown in Figure 4.17. The thickness of the weld in the FE modelling is taken as the throat thickness of the fillet part of the butt weld.

- The steel grade of the chord members is S355 with $f_{y0}=355$ N/mm$^2$ and $f_{u0}=510$ N/mm$^2$. In order to prevent brace failure before chord failure, a higher yield strength of 690 N/mm$^2$ (StE 690) for the brace members has been chosen. For the same reason, the yield strength of the weld is also used as 690 N/mm$^2$. The engineering stress - strain curves and the corresponding true stress - strain curves for S355 and StE 690 are shown in Figure 4.18. In reality, if brace failure does not occur before joint failure, there is little influence of the brace yield strength on the joint ultimate load.
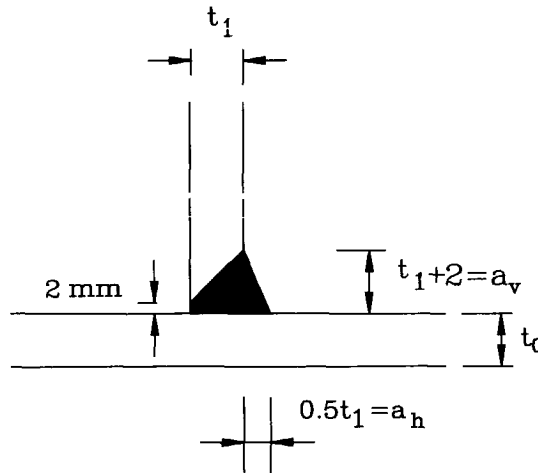


**Figure 4.16  Dimensions of the butt weld**
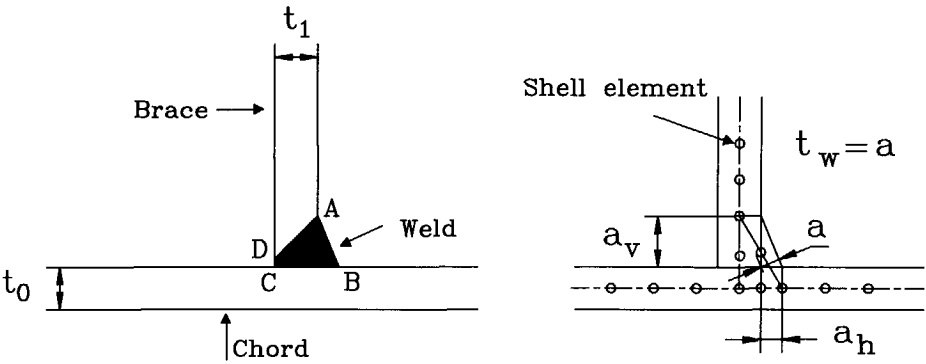
**Figure 4.17 FE modelling of the butt weld**
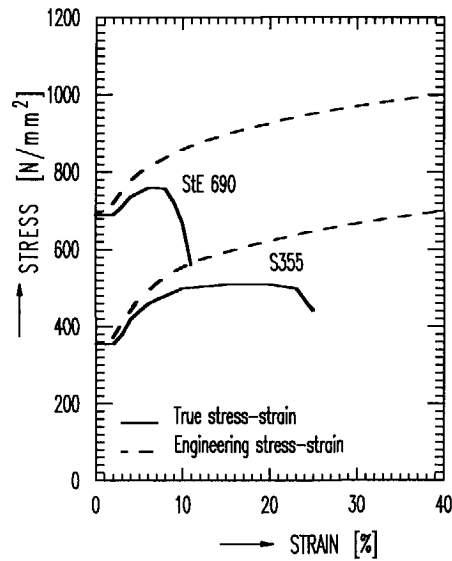


**Figure 4.18 Engineering and true stress - strain curves of S355 and StE 690**

### 4.5.2    Determination of the "ultimate" load and the "ultimate" moment capacity

**The "ultimate" load capacity**

For axially loaded joints, the chord top face "indentation" is shown in Figure 4.19. The static behaviour of the joint is described using the typical load (on the in-plane brace) vs. chord face indentation curves. For joint with small to medium $\beta$ values, no maximum load is reached. The load is increasing with the increase of indentation due to the membrane effect. In such a case, an "ultimate" deformation limit is needed to define the "ultimate" load capacity of the joints. The local deformation of $1\%b_0$ for hollow sections is generally accepted as the serviceability deformation limit (Wardenier 1982a and IIW 1989). The load $N_s$ at the serviceability multiplied by the load factor $\gamma_g$ should not exceed the design resistance load $N_{Rd}$ of the connection:

$$\gamma_g N_s \leq N_{Rd} \tag{4.6}$$

According to Eurocode 3 (EC3, 1992), the minimum value of $\gamma_g$ should be taken as 1.35, considering the combination of the different unfavourable action loads on the structures. If the ultimate loads $N_u$ at the ultimate deformation limit from the numerical analyses would be considered as the characteristic values, the design loads can be obtained by dividing the characteristic value by the joint partial safety factor $\gamma_M$ which is generally taken as 1.1 (Lu 1994). Consequently, if the ratio between the ultimate load capacity and the serviceability load capacity is less than or equal to 1.5 (=1.35 x 1.1), the serviceability criterion will not be critical:

$$\frac{N_u}{N_s} \leq \gamma_g \gamma_M = 1.5 \tag{4.7}$$

In this case, the check at the serviceability deformation limit can be ignored. Based upon an extensive study on different types of connections with different load conditions, an "ultimate" deformation limit of $3\%b_0$ has been recommended (Lu 1994). The procedure to determine the ultimate load capacity of joints loaded with axial forces is illustrated in Figure 4.20.
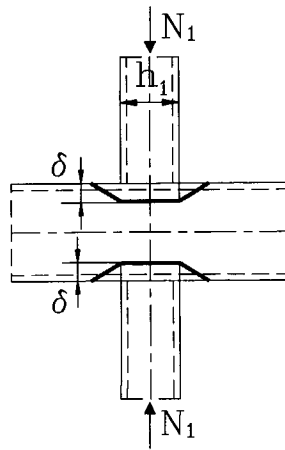
**Figure 4.19 "Indentation" of chord top face of joints loaded with axial forces**
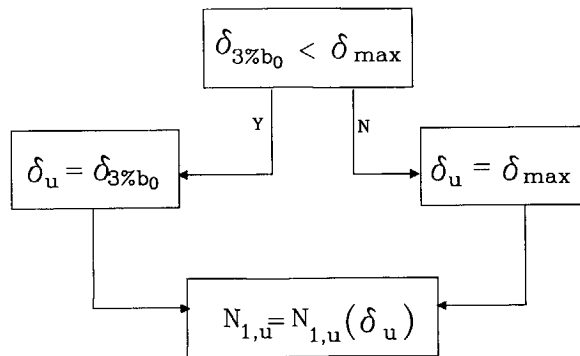


**Figure 4.20 Procedure to determine the "ultimate" load capacity**

**The "ultimate" moment capacity**

For joints loaded with bending moments, the same problem exists as for axially loaded joints. In such a case, the "indentation" represents the chord top face "push-in" at the compression side, see Figure 4.21.
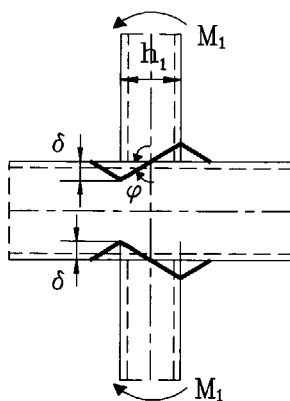
**Figure 4.21    "Indentation" and "rotation" of the chord top face loaded with in-plane bending moments**

The "ultimate" deformation limit of $3\%b_0$ can be translated into a rotation angle of the joint:

$$\phi = \frac{3\%b_0}{h_1/2} = \frac{0.06}{\eta} \tag{4.8}$$

According to equation (4.8), an unrealistic large joint rotation will be obtained for joints with small $\eta$ values. For example, for a joint with $\eta=0.6$, $\phi=0.1$ rad., while for a joint with $\eta=0.2$, $\phi=0.3$ rad. The same problem exists for moment connections between I-beams to a rectangular hollow section chord (Lu 1995) and I-beams to a circular hollow section chord (de Winkel 1994). Equation (4.8) should be restricted so that no unrealistic large rotation occurs for all these connections.

For joints between RHS to RHS loaded with in-plane or out-of-plane bending moments, the numerically determined ultimate moment capacity according to the ultimate deformation limit is firstly determined for joints with medium $\eta$ or $\beta$ values. Then a regression formula can be obtained for these ultimate moment capacity which is a function of $\beta$ or $\eta$ values. By extrapolation of the formula to joints with small $\beta$ or $\eta$ values, the corresponding ultimate moment capacity can be determined for such joints. With the obtained ultimate moment capacity as a reference, the rotation angle of the joint can be found according to the moment vs. rotation (or indentation) curves of the numerical results. This rotation angle is about $\phi=0.1$ for joints with small $\beta$ or $\eta$ values.

For connections between I-beams to a circular hollow section column (CHS) or CHS to CHS, there is nearly no difference in the ultimate moment capacity if the rotation angle is between $\phi=0.08$ to 0.13 (de Winkel 1994 and van der Vegte 1995).

Based upon these considerations, a rotation angle of $\phi=0.1$ rad. is used as a restriction to the

deformation limit of equation (4.8). The procedure for the determination of the ultimate moment capacity is summarised in Figure 4.22.
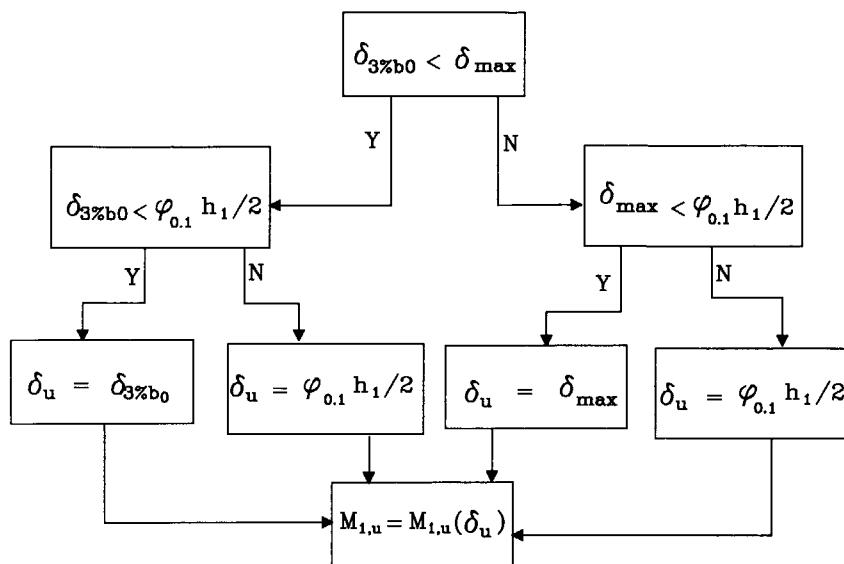


**Figure 4.22  Procedure to determine the "ultimate" moment capacity**

Based upon the procedures described in Figures 4.20 and 4.22, the ultimate load capacity and the ultimate moment capacity can be determined which will be used to establish the ultimate load and ultimate moment capacity formulae respectively.

### 4.5.3  The analytical models

The analytical models described in Chapter 5 will be used as a basis for the analyses of the numerical results in Chapters 6 to 9.

### 4.5.4  The regression analyses

Non-linear regression analyses are performed using the numerical results in order to determine the ultimate load or ultimate moment capacity formulae for each type of joint with different loading cases. The regression formulae are based upon the analytical approaches described in Chapter 5. After each regression analysis, the regression constants are determined and the statistical results such as the mean normalised error, the coefficient of variation (CoV), and the correlation coefficient $R^2$ etc. are given. The non-linear regression analyses are carried out with the program NONLIN, developed at the Stevin Laboratory for Steel Structures, Delft University of Technology.

The statistical formulae used for the regression analysis are given as follows:

The mean value:

$$\overline{y} = \frac{1}{n} \sum_{i=1}^{n} \frac{y_i}{y_{F,i}} \tag{4.9}$$

Where

$y_i$     :     the value from the numerical result;
$y_{F,i}$     :     the value from the formula;
$n$     :     number of data points.

The standard deviation:

$$\sigma = \sqrt{\frac{1}{n-1} \sum_{i=1}^{n} \left(\frac{y_i}{y_{F,i}} - \overline{y}\right)^2} \tag{4.10}$$

The coefficient of variation:

$$CoV = \frac{\sigma}{\overline{y}} \tag{4.11}$$

The correlation coefficient:

$$R^2 = \frac{\sum_{i=1}^{n} y_i^2 - \frac{1}{n}\left(\sum_{i=1}^{n} y_i\right)^2 - \sum_{i=1}^{n}\left(y_i - y_{F,i}\right)^2}{\sum_{i=1}^{n} y_i^2 - \frac{1}{n}\left(\sum_{i=1}^{n} y_i\right)^2} \tag{4.12}$$

# 5 ANALYTICAL MODELS FOR X-JOINTS

## 5.1 AXIALLY LOADED X-JOINTS

### 5.1.1 General description of different failure modes

For axially loaded uniplanar X-joints of rectangular hollow sections, failure mechanisms can be described as follows (Wardenier 1982a):

a.      Plastification of the chord top face (small to medium $\beta$ values).
b.      Cracking of the chord face around the brace (punching shear, $\beta \leq 1.0\text{-}1.0/\gamma$).
c.      Cracking in the welds or in the brace by tension (effective width).
d.      Local buckling in the brace by compression (effective width).
e.      Chord web bearing or buckling ($\beta=1.0$).

According to Wardenier (1982a), plastification of the chord top face (mode a) can be analysed using the yield line theory and cracking of the chord face (mode b) be analysed with the punching shear model. Failure modes c and d are combined together under the term "effective width failures", and treated identically since the connection resistance in both cases is determined by the effective cross section of the brace members. Failure modes c and d are due to the non-uniform local stress distribution in the braces caused by the different support conditions provided by the side walls and top faces of the chord. Weld failure can be avoid by choosing suitable weld sizes and material qualities. According to EC3 (1992), when forces applied to one flange and transferred through the web in I, H or U sections to the other flange, both web crushing (or bearing) and web buckling should be checked in order to determine the web resistance to the transverse forces. However, according to Wardenier (1982a), one combined formula including both chord web bearing and buckling can be used for failure mode e.

Because cracking is not simulated in the FE analyses, the punching shear model and the effective width model due to cracking cannot be calibrated with the FE results. Thus, this study will concentrate on the failure modes of chord face plastification (mode a), and chord web yielding or buckling (mode e).

### 5.1.2 Analytical model for chord face plastification

The yield line model has been used by many researchers in dealing with the plastic mechanism failure of RHS joints. The most commonly used method is the simplified yield line theory which ignores membrane action and strain hardening effects of the material. This method is adopted in several design guides such as IIW (1989), AWS (1992), EC3 (1993b) and CIDECT (Packer, 1992a) etc. Several researchers have tried to include the membrane action and the strain hardening behaviour. However, this led to extremely complicated analytical formulae as far as it was possible to include this effect. In this study, the simplified yield line method is used as the basis for the analysis, considering its simplicity. For axially loaded X-joints of RHS, the yield line pattern for the chord top face plastification is shown in Figure 5.1.
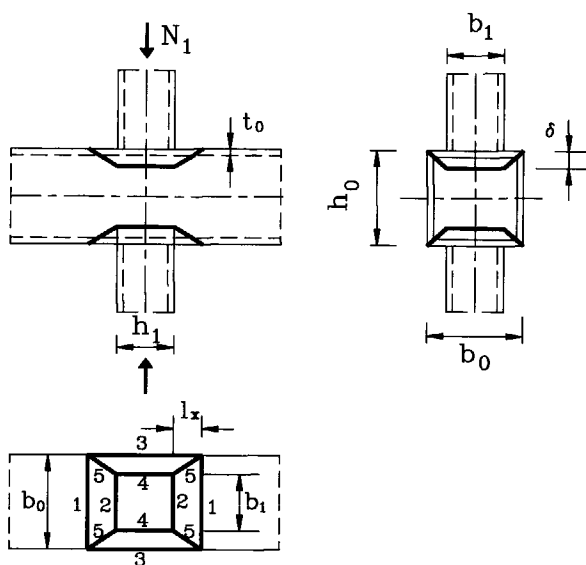
**Figure 5.1   Chord face plastification model**

The mechanism failure load of X-joints with $\theta=90°$ is taken as the design resistance:

$$N_{1,Rd} = \frac{2f_{y0}t_0^2}{1-\beta}(\eta + 2\sqrt{1-\beta})$$                     (5.1)

Rewriting it in non-dimensional form:

$$\frac{N_{1.Rd}}{f_{y0}t_0^2} = \frac{2}{1-\beta}(\eta + 2\sqrt{1-\beta})$$                     (5.2)

Equation (5.2) will be used as a basis for the analyses in Chapter 6.

### 5.1.3   Analytical models for chord web yielding or buckling

For X-joints of RHS with $\beta=1.0$, failure of the chord with stocky webs is caused by yielding of the web and the flange directly under the applied load. However, for joints with relatively thin webs, failure may occur by web buckling or the combination of the two. The models to describe the failure mechanism of such joints can be summarised as follows:

-      Chord web crippling failure (Mouty 1978), shown in Figure 5.2;
-      Frame instability model (Kato 1981), shown in Figure 5.3;
-      Combined check of chord web bearing (shown in Figure 5.4) and chord web buckling

failures (Wardenier 1982a);
- "4-hinge yield line and web buckling" model (Yu 1996c).

Other models used for connections between I-chord or other sections:

- Web crippling model used for cold formed hat sections (Bakker 1992);
- "4-hinge yield line" mechanism used for slender plate girders under in-plane patch loading (Roberts 1979); This model has been also used in EC3 (1992) in determining the web resistance to transverse forces where the webs are in I, H or U sections;
- "4-hinge yield line" mechanism used for plate to I-chord connections with the membrane action excluded (Zoetemeyer 1982) or included (Wardenier 1982b).

For the chord web crippling mechanism, the yield line patterns shown in Figure 5.2 was given by Mouty (1978). Because of the complexity in calculating the minimum mechanism failure load, an iteration procedure has to be used in solving the equation, thus, no direct analytical formula can be obtained according to this yield mechanism. The same problem exists in the web crippling model used by Bakker (1992).

The frame instability model (Kato 1981) may give a good analytical basis but it leads to a very comprehensive formula.

The combined check procedure for chord web bearing and buckling (Wardenier 1982a) is used as a comparison in this study. This model is found to be very conservative for high web slenderness compared to the results from the finite element analyses, see Chapter 6.

The "4-hinge yield line and web buckling" model was introduced (Yu 1996c) based upon the "4-hinge yield line" mechanism. A detailed description is given in this section.



$\beta = 1$
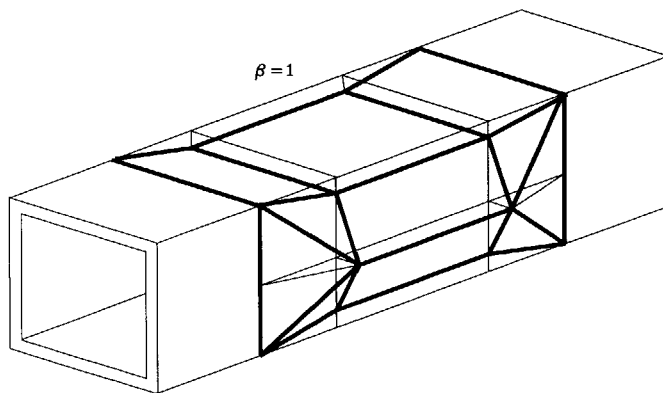
**Figure 5.2  Chord web crippling model (Mouty 1978)**
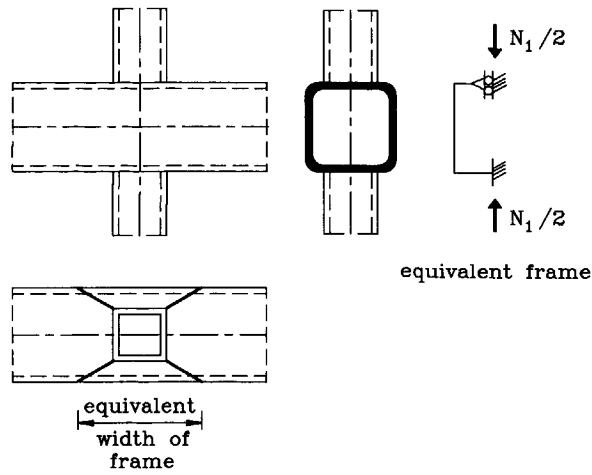
**Figure 5.3  Equivalent frame instability model (Kato 1981)**
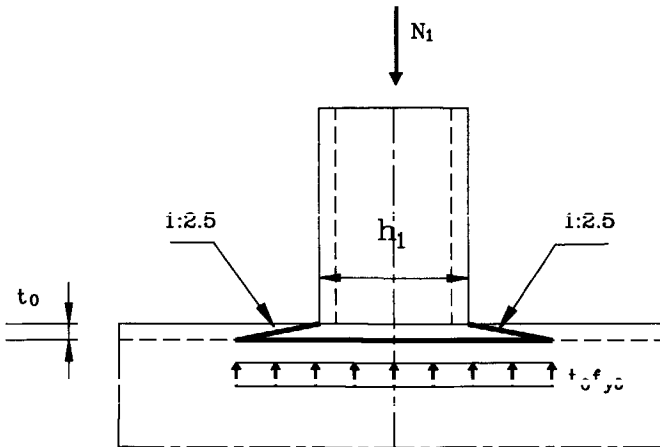


**Figure 5.4  Chord web bearing mechanism  (Wardenier 1982a)**
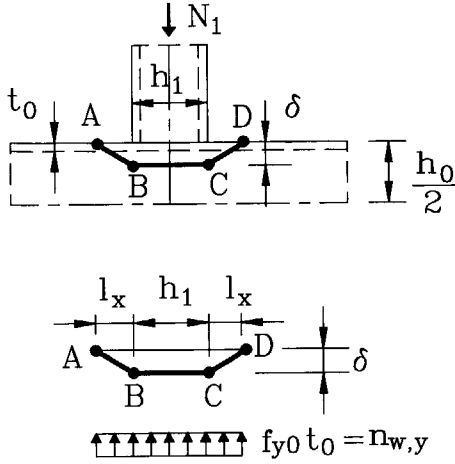
**Figure 5.5 "4-hinge yield line" mechanism (Yu 1996c)**

### 5.1.3.1    Chord web bearing and buckling model

For full width X-joints of RHS, both chord web bearing and buckling should be checked. However, in order to simplify the checking procedure, Wardenier (1982a) combined these two checks into one formula. The design resistance of the joint for the combined check of chord web bearing and buckling has also been used in the CIDECT design guide (Packer 1992a):

$$N_{1,Rd} = 2\kappa(h_1 + 5t_0)f_{y0}/\gamma_M \tag{5.3}$$

Where $\kappa$ can be derived from EC3 buckling curve-a (EC3 1992) which is a function of the slenderness ratio $\lambda$. The ratio $\lambda$ is calculated according to a pin ended strut with a buckling length of $(h_0 - 2t_0)$, thus $\lambda = 2\sqrt{3}\,(h_0/t_0 - 2)$. The partial safety factor for full width X-joints is recommended as $\gamma_M = 1.25$ (Wardenier 1982a). The characteristic strength of the joints can be obtained from equation (5.3) by multiplying the partial safety factor $\gamma_M$:

$$N_{1,k} = 2\kappa(2\gamma\eta + 5)f_{y0}t_0^2 \tag{5.4}$$

It can be understood from equation (5.4) that if the joint fails due to chord web bearing, $\kappa = 1$. However if the joint fails by chord web buckling, then $\kappa < 1$.

### 5.1.3.2    "4-hinge yield line and web buckling" model

As already mentioned, Roberts (1979) used the "4-hinge yield line" model to predict the mechanism collapse load of slender plate girders when subjected to in-plane patch loading. Zoetemeyer (1982) used the "4-hinge yield line" model to determine the failure load of plate

to I-chord connections. Wardenier (1992b) used the same model but with the membrane action of the chord flange included. In this study, the "4-hinge yield line" model is applied to full width X-joints of RHS. The only difference is that there are two webs for X-joints of RHS, but only one for I-chord connections. The "4-hinge yield line" theory can be summarised as follows: at a small load, the flange of the chord behaves as a beam on an elastic foundation consisting of the chord web. Yielding of the chord web initiates with increasing load. With increasing vertical deformation of the flange and extending of the yield region of the web, plastic hinges form in the chord flanges, see Figure 5.5, points A, B, C and D. This failure mechanism is called the "4-hinge yield line" mechanism. Equating the external work to the internal energy dissipation gives:

$$N_1 \delta = 4 b_0 m_p \frac{\delta}{l_x} + 2 n_{w,y} h_1 \delta + 4 \delta n_{w,y} \frac{l_x}{2} \tag{5.5}$$

Where $m_p$ is the plastic bending moment of the flange per unit length,

$$m_p = \frac{t_0^2 \, f_{y0}}{4} \tag{5.6}$$

And $n_{w,y}$ is the reaction force per unit length of one web at yield (two webs for RHS chord),

$$n_{w,y} = f_{y0} \, t_0 \tag{5.7}$$

From equation (5.5):

$$N_1 = 4 \frac{b_0 m_p}{l_x} + 2 n_{w,y} h_1 + 2 n_{w,y} l_x \tag{5.8}$$

In order to find the minimum failure load,

$$\frac{dN_1}{dl_x} = -4 b_0 \frac{m_p}{l_x^2} + 2 n_{w,y} = 0 \tag{5.9}$$

$$l_x = \sqrt{\frac{2 b_0 m_p}{n_{w,y}}} \tag{5.10}$$

Substituting $l_x$ into equation (5.8):

$$N_{1,u} = 4 \sqrt{2 b_0 m_p n_{w,y}} + 2 n_{w,y} h_1 \tag{5.11}$$

In equation (5.11), the yield stress is used for the web reaction force $n_{w,y}$. If web buckling occurs, the web yield stress could be replaced by the web buckling stress. Thus, the web

reaction force at web buckling is:

$$n_{w,b} = \kappa f_{y0} t_0 = \kappa n_{w,y} \qquad (5.12)$$

Where $\kappa$ is calculated according to EC3 (1992) curve-a:

$$\kappa = \frac{1}{\phi + \sqrt{\phi^2 + \overline{\lambda}^2}} \qquad (5.13)$$

$$\phi = 0.5[1 + 0.21(\overline{\lambda} - 0.2) + \overline{\lambda}^2] \qquad (5.14)$$

$$\overline{\lambda} = \frac{\lambda}{\lambda_E} \qquad (5.15)$$

$$\lambda_E = \pi \sqrt{\frac{E}{f_{y0}}} \qquad (5.16)$$

It should be mentioned that the buckling reduction factor in equation (5.12) is different from the $\kappa$ values used by Wardenier (1982a) in equations (5.3) and (5.4) where a pin ended strut with a buckling length of $(h_0 - 2t_0)$ has been used. The chord side wall is assumed as a fix ended strut in this study considering that the rotation of the chord side walls is restrained by the chord corners and the walls of the braces. The slenderness ratio based upon a fix ended strut with a buckling length of $(h_0 - 2t_0)/2$ is:

$$\lambda = \sqrt{3} \left( \frac{h_0}{t_0} - 2 \right) \qquad (5.17)$$

Replacing the yield force $n_{w,y}$ with the buckling force $n_{w,b}$, equation (5.11) becomes:

$$N_{1,u} = 4\sqrt{2b_0 m_p n_{w,b}} + 2n_{w,b} h_1 \qquad (5.18)$$

Equation (5.18) is the ultimate load capacity of the joints for a combined "4-hinge yield line flange failure and web buckling". Substituting equations (5.6), (5.7) and (5.12) into (5.18) gives:

$$N_{1,u} = 4(\sqrt{\kappa\gamma} + \kappa\gamma\eta)f_{y0} t_0^2 \qquad (5.19)$$

For the commonly used joint geometrical parameters, equation (5.19) can be approximated by:

$$N_{1,u} = 4\kappa(\sqrt{\gamma} + \gamma\eta)f_{y0} t_0^2 \qquad (5.20)$$

Comparison between equations (5.19) and (20) is given in Table 5.1.

The membrane action of the chord top face is not included in equations (5.19) and (5.20). The membrane effect is a function of the chord top face deformation, see Appendix V. It can be found in Chapter 6 that the deformation of the chord top face is very small at the ultimate load capacity of the joints. Thus, the influence of the membrane action on the ultimate load is neglectable.

Equation (5.20) will be compared to the FE results in Chapter 6.

**Table 5.1     Comparison between equations (5.19) and (5.20)**

| $2\gamma$ | $h_0/t_0$ | $\kappa$ | equation (5.20)/(5.19) | | |
|---|---|---|---|---|---|
|  |  |  | $\eta=0.5$ | $\eta=1.0$ | $\eta=2.0$ |
| 15 | 15 | 0.98 | 1.00 | 1.00 | 1.00 |
| 15 | 30 | 0.88 | 0.97 | 0.98 | 0.99 |
| 35 | 17.5 | 0.97 | 0.99 | 1.00 | 1.00 |
| 35 | 35 | 0.82 | 0.97 | 0.98 | 0.99 |
| 17.5 | 35 | 0.82 | 0.96 | 0.97 | 0.99 |
| $f_{y0}$=355 N/mm$^2$ | | | | | |

## 5.2 X-JOINTS LOADED WITH IN-PLANE BENDING MOMENTS

### 5.2.1 General description of different failure modes

Similar to axially loaded uniplanar X-joints, following failure modes are described for joints loaded with in-plane bending moments (Wardenier 1982a):

a. Plastification of the chord face.
b. Cracking in the chord (punching shear).
c. Cracking in the brace (effective width).
d. Chord side wall failure.

As no crack elements are modelled in the numerical study, the FE results can not calibrate failure modes b and c. Only failure mode a and d will be discussed in detail.

### 5.2.2 Analytical model for chord face plastification

Similar to axially loaded uniplanar X-joints, failure mode a of uniplanar X-joints loaded with in-plane bending moments can also be analysed by using the yield line theory. The yield line pattern is shown in Figure 5.6 (Wardenier 1982a).
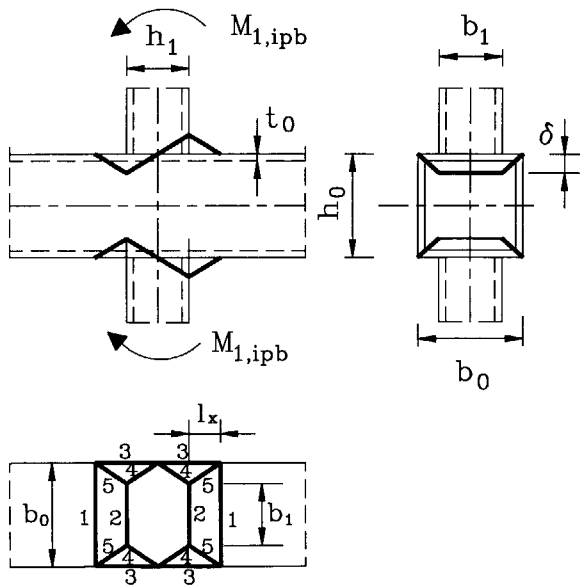


**Figure 5.6  Chord face plastification model**

Neglecting the influence of membrane effects and strain hardening behaviour, the design resistance load of the joints with $\theta=90°$ is (Packer 1992a):

$$M_{1,ipb,Rd}= f_{y0}t_0^2h_1 \left(\frac{2}{\sqrt{1-\beta}}+\frac{h_1/b_0}{1-\beta}+\frac{1}{2h_1/b_0}\right) \qquad (5.21)$$

Rewriting equation (5.21) results in:

$$M_{1,ipb,Rd}=f_{y0}t_0^2h_1\left(\frac{2}{\sqrt{1-\beta}}+\frac{\eta}{1-\beta}+\frac{1}{2\eta}\right) \qquad (5.22)$$

In Chapter 6, equation (5.22) is used as a basis in determining the ultimate moment capacity of uniplanar X-joints loaded with in-plane bending moments.

### 5.2.3  Analytical models for chord web yielding or buckling

#### 5.2.3.1      Chord web bearing model

Similar to axially loaded X-joints, full width X-joints of RHS loaded with in-plane bending moments have been checked with the same chord web bearing model (Wardenier 1982a). The design resistance moment based upon the chord web bearing model has been included in the CIDECT design guide (Packer 1992a):

$$M_{1,ipb,Rd} = 0.5f_{y0}t_0(h_1+5t_0)^2/\gamma_M \qquad (5.23)$$

Where the partial safety factor $\gamma_M=1.25$ (Wardenier 1982a). The characteristic moment strength of the joints according to equation (5.23) can be written as:

$$M_{1,ipb,k}=f_{y0}t_0^2h_1\gamma\eta(1+\frac{5}{2\gamma\eta})^2 \qquad (5.24)$$

Similar to axially loaded uniplanar X-joints, the "4-hinge yield line and web buckling" mechanism is used for uniplanar X-joints loaded with in-plane bending moments.

#### 5.2.3.2      "4-hinge yield line and web buckling" model

For full width X-joints loaded with in-plane bending moments in the braces, the "4-hinge yield line" mechanism is shown in Figure 5.7.
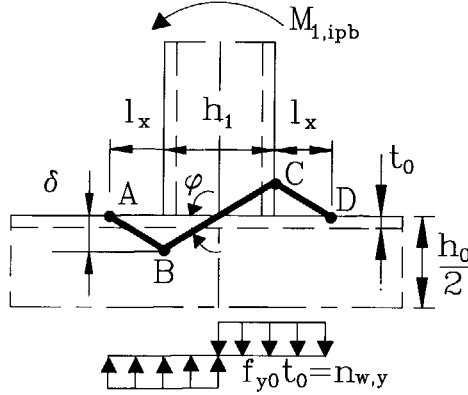
**Figure 5.7 "4-hinge yield line" mechanism (Yu 1996c)**

Equating the external work to the internal energy dissipation:

$$\frac{M_{1,ipb}\delta}{h_1/2} = 4b_0 m_p \frac{\delta}{l_x} + 2b_0 m_p \frac{\delta}{h_1/2} + 4n_{w,y}\delta(\frac{h_1}{4} + \frac{l_x}{2}) \tag{5.25}$$

Where $m_p$ and $n_{w,y}$ can be found in equations (5.6) and (5.7) respectively. From equation (5.25):

$$M_{1,ipb} = (4\frac{b_0 m_p}{l_x} + 4\frac{b_0 m_p}{h_1} + n_{w,y}h_1 + 2n_{w,y}l_x)\frac{h_1}{2} \tag{5.26}$$

In order to find the minimum failure moment,

$$\frac{dM_{1,ipb}}{dl_x} = (2n_{w,y} - 4\frac{b_0 m_p}{l_x^2})\frac{h_1}{2} = 0 \tag{5.27}$$

$$l_x = \sqrt{\frac{2b_0 m_p}{n_{w,y}}} \tag{5.28}$$

Substituting $l_x$, $m_p$ and $n_{w,y}$ into equation (5.26):

$$M_{1,ipb,u} = (2\sqrt{2b_0 m_p n_{w,y}} + \frac{2b_0 m_p}{h_1} + \frac{n_{w,y}h_1}{2})h_1 \tag{5.29}$$

Similar to axially loaded X-joints, the chord web reaction force at yielding $n_{w,y}$ should be

replaced by the reaction force at buckling $n_{w,b}$ if chord web local buckling occurs. In this case, equation (5.29) becomes:

$$M_{1,ipb,u} = (2\sqrt{2b_0 m_p n_{w,b}} + \frac{2b_0 m_p}{h_1} + \frac{n_{w,b} h_1}{2})h_1 \tag{5.30}$$

Substituting equations (5.6), (5.7) and (5.12) into equation (5.30) results in:

$$M_{1,ipb,u} = (2\sqrt{\kappa\gamma} + \kappa\gamma\eta + \frac{1}{2\eta})f_{y0}t_0^2 h_1 \tag{5.31}$$

For the most commonly used joints in rectangular hollow sections, equation (5.31) can be conservatively approximated by:

$$M_{1,ipb,u} = \kappa(2\sqrt{\gamma} + \gamma\eta + \frac{1}{2\eta})f_{y0}t_0^2 h_1 \tag{5.32}$$

Comparison between equations (5.31) and (5.32) is shown in Table 5.2.

**Table 5.2    Comparison between equations (5.31) and (5.32)**

| $2\gamma$ | $h_0/t_0$ | $\kappa$ | equation (5.32)/(5.31) | | |
|:---:|:---:|:---:|:---:|:---:|:---:|
| | | | $\eta=0.5$ | $\eta=1.0$ | $\eta=2.0$ |
| 15 | 15 | 0.98 | 0.99 | 0.99 | 1.00 |
| 15 | 30 | 0.88 | 0.95 | 0.97 | 0.98 |
| 35 | 17.5 | 0.97 | 0.99 | 0.99 | 1.00 |
| 35 | 35 | 0.82 | 0.94 | 0.96 | 0.98 |
| 17.5 | 35 | 0.82 | 0.93 | 0.96 | 0.97 |
| $f_{y0}=355$ N/mm$^2$ | | | | | |

It will be found from the numerical results in Chapter 6 that for full width X-joints loaded with in-plane bending moments, chord side wall buckling failure is only sensitive for joints with large $h_0/t_0$ and $\eta$ values (eg. $h_0/t_0=35$ and $\eta=2.0$). For joints with small $h_0/t_0$ and $\eta$ values, no local buckling of the chord side wall occurs. In this case, the buckling reduction factor is still $\kappa=1$.

The membrane action in the chord flange is not included in the above "4-hinge yield line and web buckling" model. This influence is studied in Appendix V.

Equation (5.32) will be used as a basis for the analyses in Chapter 6.

## 5.3    X-JOINTS LOADED WITH OUT-OF-PLANE BENDING MOMENTS

### 5.3.1    General description of different failure modes

For uniplanar X-joints with brace members subjected to out-of-plane bending moments, one can postulate analogous failure modes to those described for in-plane bending moment loading, which has been done for AWS (1992) and CIDECT (Packer 1992a):

a.    Chord face plastification.
b.    Cracking in chord (punching shear).
c.    Brace effective width.
d.    Chord side wall bearing or buckling.

Failure mode a occurs for joints with small to medium $\beta$ values. While failure modes b, c and d occur for joints with $\beta \approx 1.0$. The "brace effective width" defined in the current design guide is based upon the non-uniform stress distributions in the braces. Furthermore, for full width joints with a large brace depth to thickness ratio (thin-walled sections), brace member may fail by local buckling at the compression side, ie., in the direction along the chord length. However, no such brace local buckling occurs for the geometrical parameters used in Chapter 6.

### 5.3.2    Analytical model for chord face plastification

The yield line pattern for chord face plastification is shown in Figure 5.8.
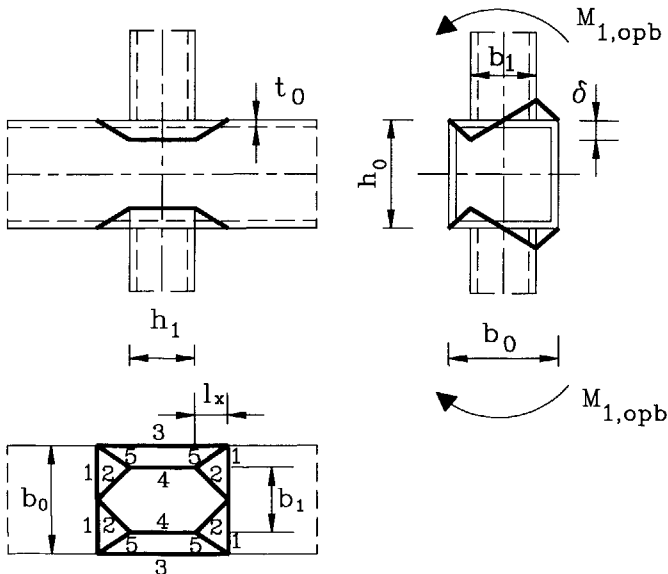


**Figure 5.8  Chord face plastification model (Wardenier 1982a)**

The design resistance moment of the joint has been given in the CIDECT design guide (Packer 1992a):

$$M_{1,opb,Rd} = f_{y0}t_0^2\left(\frac{h_1(1+\beta)}{2(1-\beta)} + \sqrt{\frac{2b_0b_1(1+\beta)}{(1-\beta)}}\right) \tag{5.33}$$

Rewriting equation (5.33):

$$M_{1,opb,Rd} = f_{y0}t_0^2b_1\left(\frac{\eta(1+\beta)}{2\beta(1-\beta)} + \sqrt{\frac{2(1+\beta)}{\beta(1-\beta)}}\right) \tag{5.34}$$

Equation (5.34) is used as the basic formula for the analyses in Chapter 6.

### 5.3.3   Analytical models for chord web yielding or buckling

### 5.3.3.1       Chord web bearing and buckling model

For full width X-joints loaded with out-of-plane bending moments, the chord web bearing model was used by Wardenier (1982a). The design resistance moment according to this model has been given in the CIDECT design guide (Packer 1992a):

$$M_{1,opb,Rd} = f_{y0}t_0(h_1+5t_0)(b_0-t_0)/\gamma_M \tag{5.35}$$

Where $\gamma_M$=1.25 according to Wardenier (1982a). The characteristic moment strength of the joint can be written as:

$$M_{1,opb,k} = \frac{1}{\beta}(2\gamma\eta+5)(1-\frac{1}{2\gamma})f_{y0}t_0^2b_1 \tag{5.36}$$

### 5.3.3.2       "4-hinge yield line and chord web buckling" model

Analogously to X-joints of RHS with brace members subjected to in-plane bending moments, a "4-hinge yield line and web buckling" mechanism is introduced to X-joints of RHS with braces subjected to out-of-plane bending moments, see Figure 5.9.
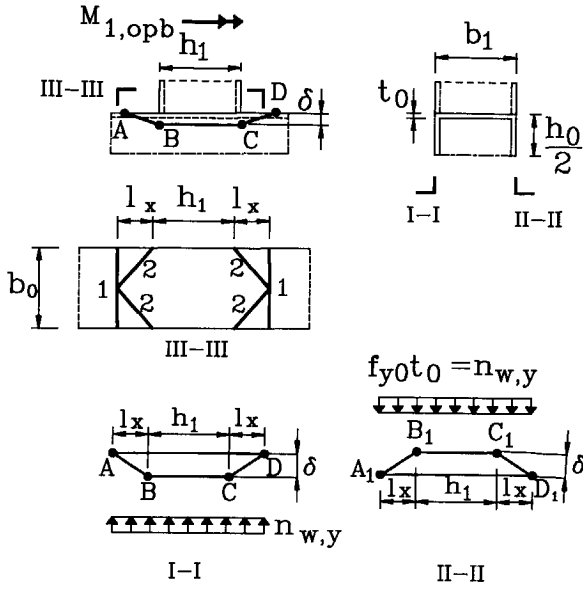
**Figure 5.9 "4-hinge yield line" mechanism (Yu 1996c)**

Equating the external work to the internal energy dissipation:

$$M_{1,opb}\frac{\delta}{b_1/2} = m_p\left(4\frac{\delta}{l_x}\frac{b_0}{2}+4\frac{\delta}{l_2}(\frac{b_0/2}{l_x}+\frac{l_x}{b_0/2})l_2\right)+2n_{w,y}h_1\delta+4n_{w,y}\frac{l_x}{2}\delta \qquad (5.37)$$

Where $m_p$ and $n_{w,y}$ can be found in equations (5.6) and (5.7).

From equation (5.37):

$$M_{1,opb} = \frac{b_1}{2}\left(\frac{4m_pb_0}{l_x}+l_x(\frac{8m_p}{b_0}+2n_{w,y})+2n_{w,y}h_1\right) \qquad (5.38)$$

For the minimum:

$$\frac{dM_{1,opb}}{dl_x} = -\frac{4m_pb_0}{l_x^2}+\frac{8m_p}{b_0}+2n_{w,y}= 0 \qquad (5.39)$$

$$l_x = \sqrt{\frac{2m_pb_0}{\dfrac{4m_p}{b_0}+n_{w,y}}} \qquad (5.40)$$

Substituting equation (5.40) into (5.38):

$$M_{1,opb,u} = b_1\left(2\sqrt{2m_p(4m_p+n_{w,y}b_0)} +n_{w,y}h_1\right) \tag{5.41}$$

Equation (5.41) is the ultimate moment capacity of the joints according to the "4-hinge yield line model" when chord web buckling does not occur. Analogously to axially loaded full width X-joints, the chord web yield force $n_{w,y}$ should be replaced by the chord web buckling force $n_{w,b}$ if buckling occurs:

$$M_{1,opb,u} = b_1\left(2\sqrt{2m_p(4m_p+n_{w,b}b_0)} +n_{w,b}h_1\right) \tag{5.42}$$

Substituting $m_p$ and $n_{w,b}$ into equation (5.42):

$$M_{1,opb,u}=\left(\sqrt{2(1+2\gamma\kappa)} +2\gamma\kappa\eta\right)f_{y0}t_0^2b_1 \tag{5.43}$$

For the commonly used joints of RHS, equation (5.43) can be conservatively approximated by:

$$M_{1,opb,u}=\kappa\left(\sqrt{2(1+2\gamma)} +2\gamma\eta\right)f_{y0}t_0^2b_1 \tag{5.44}$$

Where $\kappa$ is calculated according to EC3 (1992) curve-a for a fixed end strut with a buckling length of $(h_0-2t_0)/2$, or using equations (5.13) to (5.17). The comparison between equations (5.43) and (5.44) is shown in Table 5.3.

**Table 5.3    Comparison between equations (5.43) and (5.44)**

| $2\gamma$ | $h_0/t_0$ | $\kappa$ | equation (5.44)/(5.43) | | |
|:---:|:---:|:---:|:---:|:---:|:---:|
| | | | $\eta=0.5$ | $\eta=1.0$ | $\eta=2.0$ |
| 15 | 15 | 0.98 | 1.00 | 1.00 | 1.00 |
| 15 | 30 | 0.88 | 0.97 | 0.98 | 0.99 |
| 35 | 17.5 | 0.97 | 0.99 | 1.00 | 1.00 |
| 35 | 35 | 0.82 | 0.97 | 0.98 | 0.99 |
| 17.5 | 35 | 0.82 | 0.96 | 0.97 | 0.98 |
| $f_{y0}=355$ N/mm$^2$ | | | | | |

It is shown in Chapter 6 that the rotation at the ultimate moment capacity of the joint is very small for full width X-joints of RHS loaded with out-of-plane bending moments. Thus, the membrane action is neglectable. Equation (5.44) is compared with the numerical results in Chapter 6.

## 5.4    INFLUENCE OF THE CHORD BENDING MOMENTS

For joints in tubular structures, the chord member may be subjected to a bending moment, particularly for rigid-jointed frames. For X-joints loaded with axial forces on the braces and bending moments on the chord, the ultimate load capacity may be reduced due to the existence of the axial stresses on the chord top face caused by the bending moments in the chord, see Figure 5.10. The extent of the reduction of the joint ultimate load capacity depends upon the moment ratios between the moment applied on the chord and the design resistance moment of the chord section. This behaviour has been numerically studied by Yu (1995, 1996d).
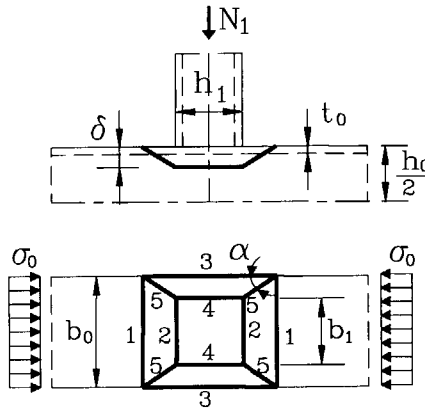


**Figure 5.10   Yield line pattern and bending stresses in the chord**

According to EC3 (1992), the design resistance moment of a section can be determined as follows:

$$M_{pl,Rd} = W_{pl} f_{y0} / \gamma_{M0} \qquad \text{(for class 1 or 2)} \qquad (5.45)$$

Where $M_{pl,Rd}$ is the plastic design resistance moment of the chord cross section; $W_{pl}$ is the plastic section modulus; For class 1, 2 and 3 cross-sections, the partial safety factor $\gamma_{M0} = 1.0$ (EC3 1992).

$$M_{pl,Rd} = W_{el} f_{y0} / \gamma_{M0} \qquad \text{(for class 3)} \qquad (5.46)$$

Where $M_{el,Rd}$ is the elastic design resistance moment of the chord cross section; $W_{el}$ is the elastic section modulus. The moment ratio can be defined as follows:

$$J_m = \begin{cases} M_0/M_{pl,Rd} & \text{(class 1 or 2)} \\ M_0/M_{el,Rd} & \text{(class 3)} \end{cases} \qquad (5.47)$$

In the current design guides, very little information is available for joints subjected to combined axial forces in the brace and bending moment ($M_0$) in the chord. Therefore, the

effect is generally taken into account based upon the effect of the axial loading in the chord.

The analytical model of Zhao (1993a) based upon the yield line theory for T-joints may gave a basic insight into the problem. The yield line pattern can be assumed as shown in Figure 5.10.

Equating the work of the external force to the internal energy of the plastic yield lines:

$$N_1 \delta = \sum m_{pi} l_i \phi_i = \sum M_i \phi_i \qquad (5.48)$$

Where $m_{pi}$ is the plastic moment per unit length of yield line i, $l_i$ is the length of yield line i, $M_i$ is the plastic moment of yield line i and $\phi_i$ is the rotation angle of yield line i.

When the chord is subjected to in-plane bending moments, axial stresses ($\sigma_0$) exist in the chord, see Figure 5.10.

When a yield line is parallel to the axial stresses, eg. lines 3 and 4, the plastic moment of the yield line is:

$$M_i = \frac{1}{4} f_{y0} t_0^2 l_i = m_p l_i \qquad (i = 3 \text{ or } 4) \qquad (5.49)$$

When a yield line is normal to the axial stresses, eg. lines 1 and 2, the reduced plastic moment of a yield line is:

$$M_i = m_p (1 - J_m^2) l_i \qquad (i = 1 \text{ or } 2) \qquad (5.50)$$

When a yield line is inclined to the axial stresses (line 5), different approaches have been used to calculate the plastic moment of the yield line by different researchers, among which were Murray (1984) and Zhao (1993a, 1993b). According to Murray, the plastic moment of the inclined yield line can be calculated with equation (5.50). This recommendation was based upon the omission of the twisting moment on the inclined yield line (Zhao 1993a, 1993b).

The internal energy for each yield line:

$$E_1 = \frac{4 tg\alpha}{1 - \beta} m_p (1 - J_m^2) \delta \qquad (line 1) \qquad (5.51)$$

$$E_2 = \frac{4\beta tg\alpha}{1 - \beta} m_p (1 - J_m^2) \delta \qquad (line 2) \qquad (5.52)$$

$$E_3 = 4(\frac{\eta}{1 - \beta} + ctg\alpha) m_p \delta \qquad (line 3) \qquad (5.53)$$

$$E_4 = \frac{4\eta}{1-\beta} m_p \delta \qquad \text{(line 4)} \qquad (5.54)$$

For yield line 5, according to Murray (1984):

$$E_5 = 4(tg\alpha + ctg\alpha)m_p(1 - J_m^2)\delta \qquad \text{(line 5)} \qquad (5.55)$$

The total internal energy:

$$E_{tot} = \frac{8m_p\delta}{1-\beta}\left(tg\alpha(1 - J_m^2) + (1-\beta)(1 - \frac{J_m^2}{2})ctg\alpha + \eta\right) \qquad (5.56)$$

Equating the external work to the internal energy yields:

$$N_1 = \frac{8m_p}{1-\beta}\left(tg\alpha(1 - J_m^2) + (1-\beta)(1 - \frac{J_m^2}{2})ctg\alpha + \eta\right) \qquad (5.57)$$

From the minimum condition: $\dfrac{dN_1}{d\alpha} = 0$

$$tg\alpha = \sqrt{\frac{(1 - \frac{J_m^2}{2})(1-\beta)}{(1 - J_m^2)}} \qquad (5.58)$$

Substituting equation (5.58) into equation (5.57),

$$\frac{N_{1,u}}{f_{y0}t_0^2} = \frac{2}{1-\beta}\left(\eta + 2\sqrt{(1 - \frac{J_m^2}{2})(1 - J_m^2)(1-\beta)}\right) \qquad (5.59)$$

It can be found that equation (5.59) is identical to equation (5.2) if $J_m = 0$. The interaction formula according to equation (5.59) is:

$$f(J_m) = \frac{N_{1,u}(J_m)}{N_{1,u}(J_m = 0)} = \frac{\eta + 2\sqrt{(1 - \frac{J_m^2}{2})(1 - J_m^2)(1-\beta)}}{\eta + 2\sqrt{1-\beta}} \qquad (5.60)$$

Theoretically speaking, $f(J_m)$ should be equal to zero when $J_m = 1$. However, this is not the case in equation (5.60). The reason is that for joints with $J_m = 1$, failure of the chord section due to chord member bending dominates and the yield line pattern shown in Figure 5.10 is

invalid.

According to Zhao (1993a, 1993b), the plastic moment of the inclined yield line 5 in Figure 5.10 is:

$$M_5 = m_p(1 - J_m^2)(\frac{b_0 - b_1}{2}) \tag{5.61}$$

Similar to the method based on Murray (1984), the internal energy of yield line 5 can be calculated based on Zhao (1993a, 1993b):

$$E_5 = 4m_p(1 - J_m^2)\frac{\delta}{\cos\alpha} \qquad \text{(line 5)} \tag{5.62}$$

The total internal energy:

$$E_{tot} = 4m_p\left((\frac{1+\beta}{1-\beta}tg\alpha + \frac{1}{\cos\alpha})(1 - J_m^2) + ctg\alpha + \frac{2\eta}{1-\beta}\right)\delta \tag{5.63}$$

Equating the external work to the internal energy:

$$N_1 = 4m_p\left((\frac{1+\beta}{1-\beta}tg\alpha + \frac{1}{\cos\alpha})(1 - J_m^2) + ctg\alpha + \frac{2\eta}{1-\beta}\right) \tag{5.64}$$

From the minimum condition $\dfrac{dN_1}{d\alpha} = 0$,

$$(1 - J_m^2)\frac{1+\beta}{1-\beta} - ctg^2\alpha + (1 - J_m^2)\sin\alpha = 0 \tag{5.65}$$

It should be mentioned that there is no direct analytical solution for equation (5.65). Due to the complexity of the equation, an iteration procedure has to be used. For each joint loaded with a specific moment ratio $J_m$, the unknown $\alpha$ value can be numerically determined with equation (5.65). Substituting the moment ratio $J_m$ and the obtained $\alpha$ value to equation (5.64), the failure load of the joint can be determined.

From the above analysis, it can be understood that the reduction of the joint ultimate load capacity is caused by the reduction of the plastic moment of the yield lines when a yield line is not parallel to the axial stresses. Although different methods to calculate the reduction of the plastic moment may lead to slight differences in the results, they still can give an analytical basis for the understanding of the problem.

The interaction relation based upon Murray (1984) and Zhao (1993a) are compared with the numerical results in Chapter 6.

# APPENDIX V MEMBRANE ACTIONS IN FULL WIDTH X-JOINTS

## V-1 MEMBRANE ACTION IN AXIALLY LOADED FULL WIDTH X-JOINTS OF RECTANGULAR HOLLOW SECTIONS

In Chapter 5, the failure load of axially loaded full width X-joints is predicted using the "4-hinge yield line and web buckling" mechanism with the membrane action in the chord top face excluded. It is known that due to the deformation of the chord top face, membrane forces appear in the chord top face which increase the load capacity of the joint. The joint can be simplified as a model with rigid plastic material and fix ended supports as shown in Figure V-1, a similar model as used by Wardenier (1982b) for an I-section chord. The difference is that there are two webs for a rectangular hollow section chord, but only one for an I-section chord.



**Figure V-1** **"4-hinge yield line" mechanism including membrane action of axially loaded full width X-joints**

As shown in Figure V-1, yield hinges at points A, B, C and D occur due to the combined action of a moment M and a membrane force N. The elongations $\Delta l$ due to the membrane force N and the rotations $\phi$ due to the moment M are located at points A, B, C and D. If m and n are represented as the bending moment and membrane force per unit width of the chord top face respectively, the moment M and membrane force N are:

$$M = b_0 m \qquad\qquad (V\text{-}1)$$

$$N = b_0 n \qquad\qquad (V\text{-}2)$$

**The equilibrium conditions:**

According to Figure V-1, the horizontal and vertical reaction forces at point D are:

$$H_D = N\cos\phi \approx N \tag{V-3}$$

$$V_D = \frac{N_1}{2} - n_{w,y}(2l_x + h_1) \tag{V-4}$$

Combined with equations (V-1) to (V-4), the equilibrium equation can be obtained by moment equilibrium at point C of Figure V-1:

$$N_1 = \frac{4b_0 m}{l_x} + \frac{2b_0 n\delta}{l_x} + 2n_w h_1 + 2n_w l_x \tag{V-5}$$

**The yield condition:**

The yield condition for the combined actions of a moment and a axial force in a solid rectangular cross section per unit width is given by:

$$\psi = \frac{m}{m_p} + \left(\frac{n}{n_{w,y}}\right)^2 - 1 = 0 \tag{V-6}$$

Where $m_p$ and $n_{w,y}$ are the plastic bending moment capacity and the axial load capacity per unit width of a plate with rectangular section:

$$m_p = \frac{t_0^2 f_{y0}}{4} \tag{5.6}$$

$$n_{w.v} = t_0 f_{v0} \tag{5.7}$$

**The normality conditions:**

According to the normality rule, the plastic strain rates are:

$$d\phi = \frac{\partial\psi}{\partial m}d\lambda = \frac{1}{m_p}d\lambda \tag{V-7}$$

$$d(\Delta l) = \frac{\partial\psi}{\partial n}d\lambda = \frac{2n}{n_{w,y}^2}d\lambda \tag{V-8}$$

Where $d\lambda$ is a scalar factor.

From equations (5.6), (5.7), (V-7) and (V-8), it can be obtained that

$$\frac{d\phi}{d\Delta l} = \frac{2}{t_0} \frac{n_{w,y}}{n} \tag{V-9}$$

## The kinematic conditions:

According to Figure V-1, the kinematic equations for a small value of $\phi$ and $\Delta l$ are given by:

$$\phi = \frac{\delta}{l_x} \tag{V-10}$$

$$\Delta l = \frac{\delta^2}{4l_x} \tag{V-11}$$

Combine equations (V-10) and (V-11):

$$\frac{d\phi}{d\Delta l} = \frac{d\delta}{l_x} \frac{4l_x}{2\delta \cdot d\delta} = \frac{2}{\delta} \tag{V-12}$$

The relationship between n and $\delta$ can be obtained from equations (V-9) and (V-12):

$$n = \frac{\delta}{t_0} n_{w,y} \tag{V-13}$$

Substitution of (V-13) into equation (V-6) gives the relationship between m and $\delta$:

$$m = (1 - \frac{\delta^2}{t_0^2}) m_p \qquad\qquad (\frac{\delta}{t_0} \leq 1) \tag{V-14}$$

## The minimum failure load:

Substitution of equations (V-13) and (V-14) into (V-5),

$$N_1 = \frac{4b_0 m_p}{l_x}(1 - \frac{\delta^2}{t_0^2}) + \frac{2\delta^2}{t_0 l_x} b_0 n_{w,y} + 2n_{w,y} h_1 + 2n_{w,y} l_x \tag{V-15}$$

In order to find the minimum failure load,

$$\frac{dN_1}{dl_x} = 0 \tag{V-16}$$

Then,

$$l_x = \sqrt{\frac{2b_0 m_p}{n_{w,y}}(1 - \frac{\delta^2}{t_0^2}) + \frac{b_0 \delta^2}{t_0}} \qquad\qquad (V\text{-}17)$$

Substitute $l_x$ in equation (V-15), the ultimate load capacity is:

$$N_{1,u} = 4\sqrt{2b_0 m_p n_{w,y}(1 - \frac{\delta^2}{t_0^2} + \frac{n_{w,y}}{2m_p}\frac{\delta^2}{t_0}) + 2n_{w,y}h_1} \qquad (\frac{\delta}{t_0} \le 1) \qquad (V\text{-}18)$$

Equation (V-18) is the ultimate load capacity of the joint including the membrane action of the chord top face without considering the chord web buckling. The corresponding equation excluding the membrane effect can be found in equation (5.11), Chapter 5:

$$N_{1,u} = 4\sqrt{2b_0 m_p n_{w,y}} + 2n_{w,y}h_1 \qquad\qquad (5.11)$$

Equations (V-18) and (5.11) can be rewritten as:

$$N_{1,u} = 4\left(\sqrt{\gamma(1 + \frac{\delta^2}{t_0^2}) + \eta\gamma}\right) f_{y0} t_0^2 \qquad\qquad (\frac{\delta}{t_0} \le 1) \qquad (V\text{-}19)$$

$$N_{1,u} = 4(\sqrt{\gamma} + \eta\gamma) f_{y0} t_0^2 \qquad\qquad (V\text{-}20)$$

Equations (V-19) and (V-20) are compared in Figure V-2. It is shown that the membrane action is a function of the displacement over chord thickness ratio. According to the numerical results in Chapter 6, for axially loaded full width X-joints of RHS, the deformation at the ultimate load capacity is very small (with a $\delta_u/t_0$ ratio less than 0.32). The marked points in Figure V-2 are corresponding to the $\delta_u/t_0$ ratios in the numerical results. The influence of the membrane action is less than 2%.
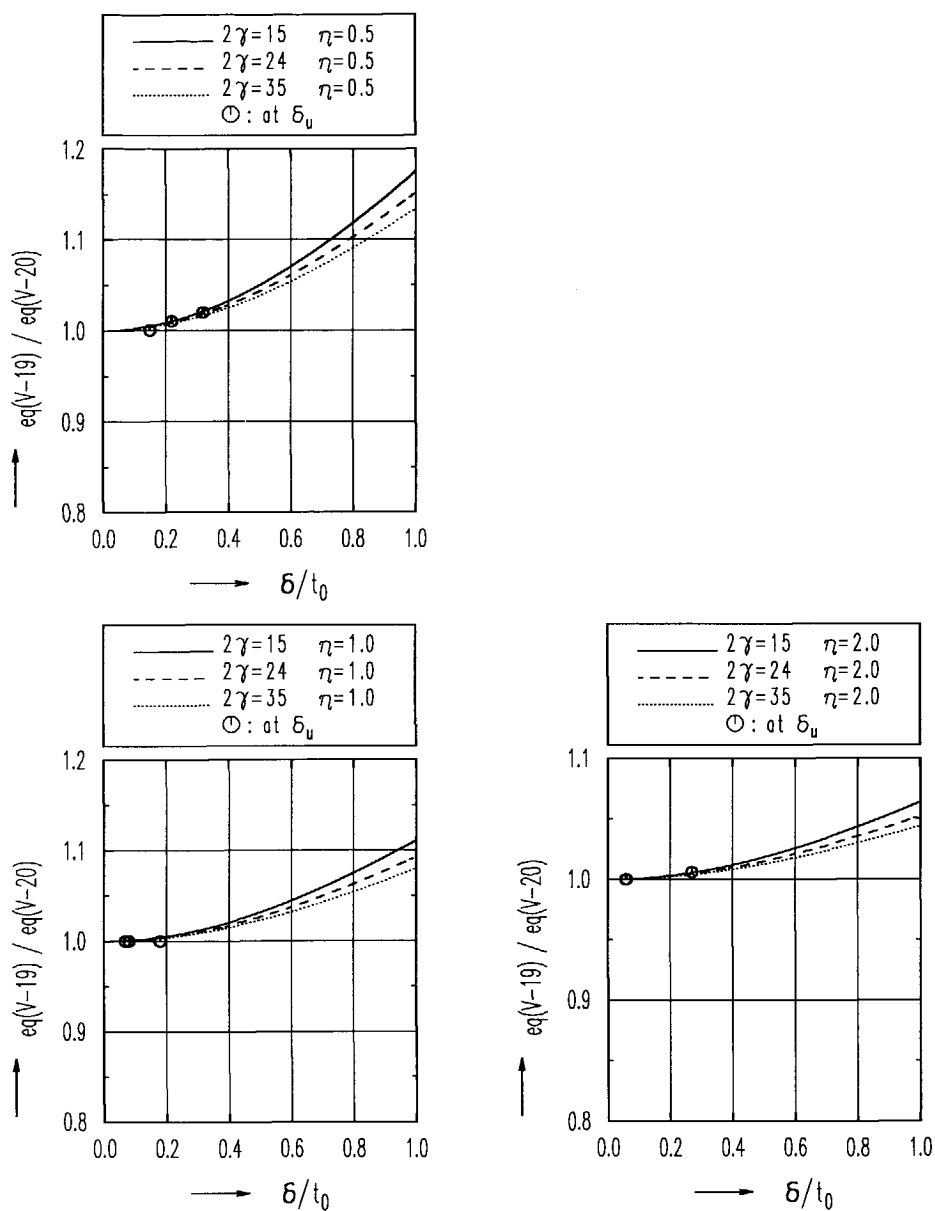
**Figure V-2     Influence of membrane action in axially loaded full width X-joints of RHS**

### V-2 MEMBRANE ACTION IN FULL WIDTH X-JOINTS OF RHS LOADED WITH IN-PLANE BENDING MOMENTS

Similar to the situation for axially loaded full width X-joints, yield hinges will occur due to the combined action of the bending moment M and the membrane force N, see Figure V-3. The yield condition, the kinematic equations and the normality rule are exactly the same as described in Appendix V-1.



**Figure V-3** **"4-hinge yield line" mechanism including membrane action of full width X-joints loaded with in-plane bending moments**

### Moment equilibrium

Moment equilibrium with respect to points A and C:

$$N_D(2l_x+h_1)+2n_{w,y}(l_x+\frac{h_1}{2})^2-2M-M_{1,ipb}=0 \qquad (V-21)$$

$$N_D l_x+2n_{w,y}\frac{l_x^2}{2}-2M-N\cos\phi\delta=0 \qquad (V-22)$$

Where M and N can be found in equations (V-1) and (V-2). For a small $\phi$, $\cos\phi=1$. Combination of equations (V-21) and (V-22) becomes:

$$M_{1,ipb}=\frac{2h_1M+h_1\delta N}{l_x}+n_{w,y}h_1l_x+2M+2N\delta+\frac{h_1^2}{2}n_{w,y} \qquad (V-23)$$

Substitute M, N and equations (V-13) and (V-14) into equation (V-23):

$$M_{1,ipb} = \frac{2b_0 h_1 (1 - \frac{\delta^2}{t_0^2}) m_p + b_0 h_1 \frac{\delta^2}{t_0} n_{w,y}}{l_x} + n_{w,y} h_1 l_x + 2b_0 (1 - \frac{\delta^2}{t_0^2}) m_p + 2b_0 \frac{\delta^2}{t_0} n_{w,y} + \frac{h_1^2}{2} n_{w,y} \quad (V-24)$$

In order to find the minimum failure moment,

$$\frac{dM_{1,ipb}}{l_x} = 0 \quad (V-25)$$

Then,

$$l_x = \sqrt{\frac{2b_0 m_p}{n_{w,y}}(1 - \frac{\delta^2}{t_0^2}) + \frac{b_0 \delta^2}{t_0}} \quad (V-26)$$

Substituting equation (V-26) into (V-24):

$$M_{1,ipb,u} = \left( 2\sqrt{2b_0 m_p n_{w,y}(1 - \frac{\delta^2}{t_0^2} + \frac{n_{w,y}}{2m_p}\frac{\delta^2}{t_0}) + \frac{2b_0 m_p}{h_1}(1 - \frac{\delta^2}{t_0^2}) + \frac{2b_0 n_{w,y}}{h_1}\frac{\delta^2}{t_0} + \frac{n_{w,y} h_1}{2}} \right) h_1 \quad (V-27)$$

Equation (V-27) is the joint ultimate moment capacity based upon the "4-hinge yield line" mechanism with the membrane effect included. It can be rewritten as:

$$M_{1,ipb,u} = \left( 2\sqrt{\gamma(1 + \frac{\delta^2}{t_0^2}) + \eta\gamma + \frac{1}{2\eta}(1 + \frac{\delta^2}{t_0^2}) + \frac{1}{\eta}\frac{\delta^2}{t_0^2}} \right) f_{y0} t_0^2 h_1 \qquad (\frac{\delta}{t_0} \leq 1) \quad (V-28)$$

The corresponding solution neglecting the membrane action can be found in equation (5.29), Chapter 5:

$$M_{1,ipb,u} = \left( 2\sqrt{2b_0 m_p n_{w,y}} + \frac{2b_0 m_p}{h_1} + \frac{n_{w,y} h_1}{2} \right) h_1 \quad (5.29)$$

Equation (5.29) can be rewritten as:

$$M_{1,ipb,u} = (2\sqrt{\gamma} + \gamma\eta + \frac{1}{2\eta})f_{y0}t_0^2 h_1 \qquad\qquad\qquad (V-29)$$

Equations (V-28) and (V-29) are compared in Figure V-4 where the influence of the membrane action is shown. The corresponding $\delta_u/t_0$ values according to the numerical results in Chapter 6 are marked in Figure V-4. The maximum membrane influence is found to be 28% for a joint with low $\eta$ ($\eta$=0.5) and high $2\gamma$ (2=$\gamma$35) values. For joints with other geometrical parameters, the membrane influence is much smaller.
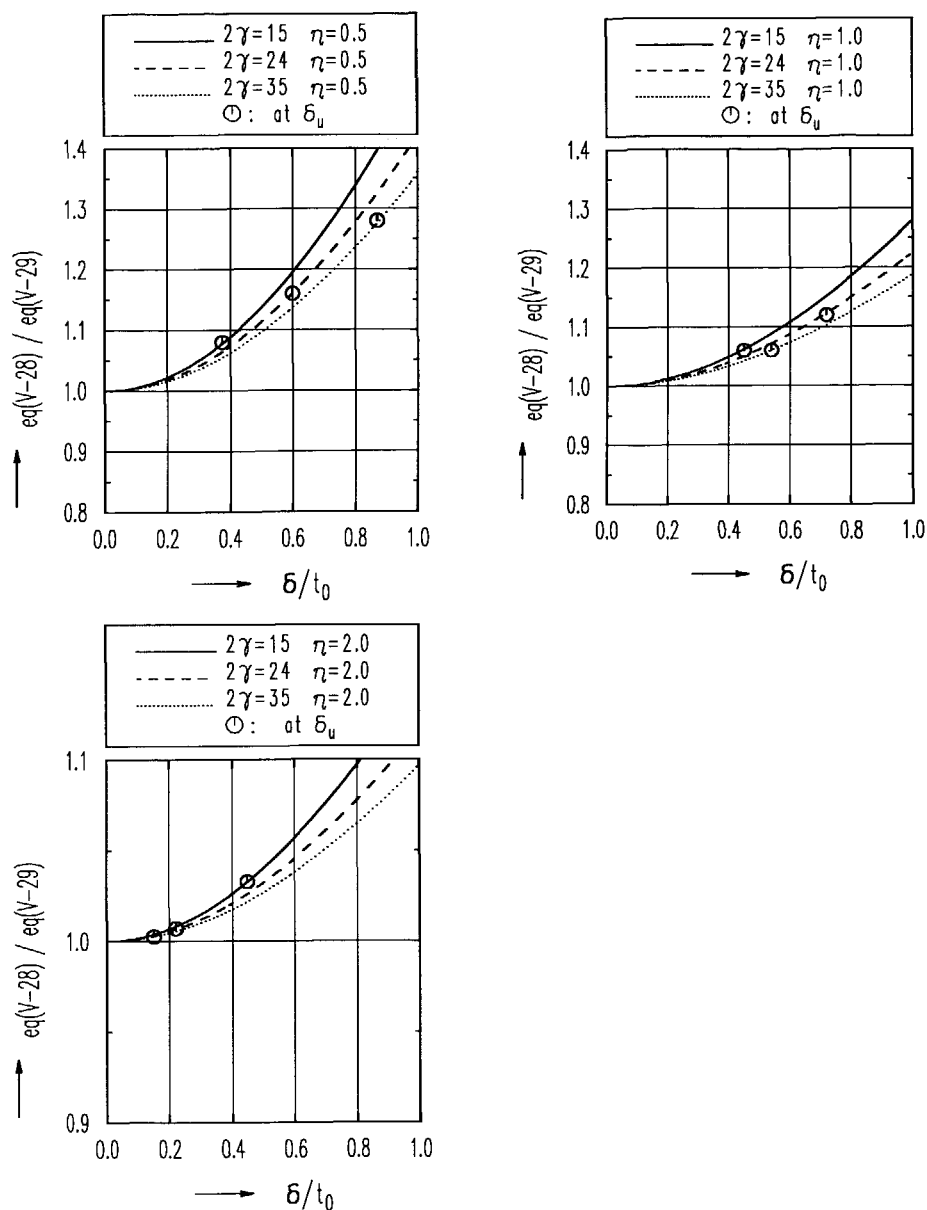
**Figure V-4** **Influence of membrane action in full width X-joints of RHS loaded with in-plane bending moments**

# 6    NUMERICAL STUDY ON UNIPLANAR X-JOINTS

## 6.1    AXIALLY LOADED UNIPLANAR X-JOINTS

### 6.1.1    Introduction

In the 60's to 70's, the investigations on uniplanar RHS joints concentrated on experimental tests and analytical studies. With the increasing interest in the behaviour of multiplanar RHS joints, some additional experimental tests on uniplanar connections have been done in the 80's and the 90's for comparison purposes. Experimental testing is expensive and time consuming. With the development of computer technology in the last decade, there has been a growth in the use of non-linear finite element analyses for simulating joint behaviour. Using nonlinear finite element analysis as a tool in investigating the static behaviour of tubular joints, a large number of parameter studies can be carried out, which makes the analyses much cheaper and faster than experimental tests.

In the current design guides, AWS (1989), CIDECT (Packer 1992a), EC3 (1993b) and IIW (1989), the design resistance formulae for uniplanar RHS joints loaded with axial forces, in-plane bending or out-of-plane bending moments have been established based upon analytical models or experimental results. The existing design formula for chord side wall failure was found to be very conservative compared to the numerical results. A new analytical formula based upon the so-called "4-hinge yield line and web buckling" mechanism is established in Chapter 5 and is checked with the numerical results in this chapter. Numerical verifications of the analytical models for full width joints with $\eta=\beta$ was done by Yu (1996c). Different $\eta$ values are included in this Chapter in order to enlarge the range of validity of the analytical formulae.

Since the study on uniplanar joints loaded with axial forces, in-plane or out-of-plane bending moments is taken as a basis for the further investigation on uniplanar or multiplanar joints subjected to other load cases, numerical investigations on uniplanar X-joints under the above three load cases are firstly carried out.

Because cracking is not simulated in the FE analyses, punching shear and the effective width models cannot be calibrated with the FE results. Thus, this study concentrates on the failure modes of chord top face plastification and chord web yielding or buckling.

### 6.1.2    Research programme

The configuration of an axially loaded uniplanar X-joint is shown in Figure 6.1, while the dimensions and non-dimensional geometrical parameters are shown in Figure 6.2. The joint geometrical parameters are summarised in Table 6.1. Five $\beta$ values ($\beta=0.2, 0.4, 0.6, 0.8, 1.0$) and three $2\gamma$ values ($2\gamma=15, 24$ and $35$) are considered in this parameter study. For each joint with a specific set of $\beta$ and $2\gamma$ values, three $\eta$ values ($\eta=0.5*\beta$, $1.0*\beta$ and $2*\beta$) are included. In total there are 32 finite element analyses. The nominal dimensions and the geometrical parameters of the joints are listed in Table 6.2.
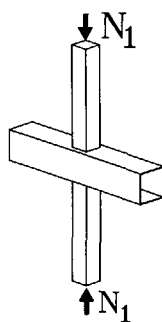
**Figure 6.1   Configuration of an axially loaded X-joint in RHS**



$\alpha = 2l_0/b_0$
$\beta = b_1/b_0$
$2\gamma = b_0/t_0$
$\tau = t_1/t_0$
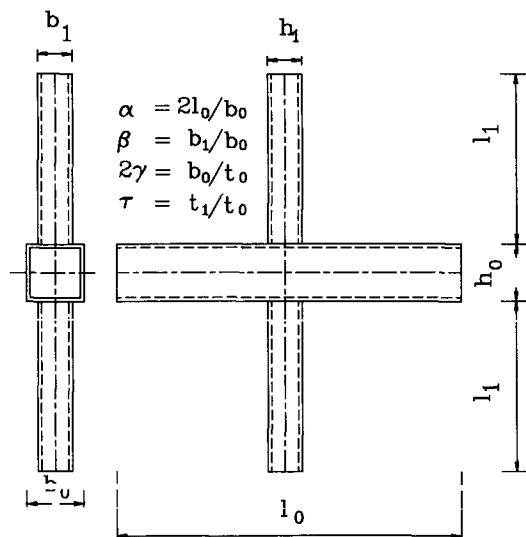
**Figure 6.2      Dimensions and non-dimensional geometrical parameters of an uniplanar X-joint**

**Table 6.1** **Research programme of the numerical parameter study for axially loaded uniplanar X-joints**

| | η | β | | | | |
|---|---|---|---|---|---|---|
| | | 0.2 | 0.4 | 0.6 | 0.8 | 1.0 |
| 2γ=15 | 0.5 β | | | | | x10ae05[*] |
| | 1.0 β | | x1a | x4a | x7a | x10a[*] |
| | 2.0 β | | x1ae2 | x4ae2 | x7ae2 | x10ae2[*] |
| 2γ=24 | 0.5 β | | | x5ae05 | x8ae05 | x11ae05[*] |
| | 1.0 β | | x2a | x5a | x8a | x11a[*] |
| | 2.0 β | | | x5ae2 | x8ae2 | x11ae2[*] |
| 2γ=35 | 0.5 β | | x3ae05 | x6ae05 | x9ae05 | x12ae05[*] |
| | 1.0 β | x13a | x3a | x6a | x9a | x12a[*] |
| | 2.0 β | | x3ae2 | x6ae2 | x9ae2 | x12ae2[*] |
| Notation example: x9ae2 means **X**-joint, No.**9**, under axial load, η=**2.0**\*β. $b_0$=150 mm, $f_{y0}$=355 N/mm$^2$ | | | | | | |

*: Without weld

**Table 6.2** **Nominal dimensions and geometrical parameters for uniplanar X-joints**

| Joint | Nominal dimensions (mm) | | | | | | | Geometrical parameters | | |
|---|---|---|---|---|---|---|---|---|---|---|
| | chord | | | brace | | | | β | 2γ | η |
| | $b_0$ | $t_0$ | $l_0$ | $b_1$ | $h_1$ | $t_1$ | $l_1$ | | | |
| x1a | 150 | 10 | 900 | 60 | 60 | 10 | 300 | 0.4 | 15 | 0.4 |
| x1ae2 | 150 | 10 | 900 | 60 | 120 | 10 | 300 | 0.4 | 15 | 0.8 |
| x2a | 150 | 6.25 | 900 | 60 | 60 | 6.25 | 300 | 0.4 | 24 | 0.4 |
| x3ae05 | 150 | 4.29 | 900 | 60 | 30 | 4.29 | 300 | 0.4 | 35 | 0.2 |
| x3a | 150 | 4.29 | 900 | 60 | 60 | 4.29 | 300 | 0.4 | 35 | 0.4 |
| x3ae2 | 150 | 4.29 | 900 | 60 | 120 | 4.29 | 300 | 0.4 | 35 | 0.8 |
| x4a | 150 | 10 | 900 | 90 | 90 | 10 | 450 | 0.6 | 15 | 0.6 |
| x4ae2 | 150 | 10 | 900 | 90 | 180 | 10 | 450 | 0.6 | 15 | 1.2 |
| x5ae05 | 150 | 6.25 | 900 | 90 | 45 | 6.25 | 450 | 0.6 | 24 | 0.3 |
| x5a | 150 | 6.25 | 900 | 90 | 90 | 6.25 | 450 | 0.6 | 24 | 0.6 |
| x5ae2 | 150 | 6.25 | 900 | 90 | 180 | 6.25 | 450 | 0.6 | 24 | 1.2 |

**Table 6.2     (Continued)**

| Joint | Nominal dimensions (mm) | | | | | | | Geometrical parameters | | |
|-------|-------|-------|-------|-------|-------|-------|-------|-------|-------|-------|
| | chord | | | brace | | | | | | |
| | $b_0$ | $t_0$ | $l_0$ | $b_1$ | $h_1$ | $t_1$ | $l_1$ | $\beta$ | $2\gamma$ | $\eta$ |
| x6ae05 | 150 | 4.29 | 900 | 90 | 45 | 4.29 | 450 | 0.6 | 35 | 0.3 |
| x6a | 150 | 4.29 | 900 | 90 | 90 | 4.29 | 450 | 0.6 | 35 | 0.6 |
| x6ae2 | 150 | 4.29 | 900 | 90 | 180 | 4.29 | 450 | 0.6 | 35 | 1.2 |
| x7a | 150 | 10 | 900 | 120 | 120 | 10 | 600 | 0.8 | 15 | 0.8 |
| x7ae2 | 150 | 10 | 900 | 120 | 240 | 10 | 600 | 0.8 | 15 | 1.6 |
| x8ae05 | 150 | 6.25 | 900 | 120 | 60 | 6.25 | 600 | 0.8 | 24 | 0.4 |
| x8a | 150 | 6.25 | 900 | 120 | 120 | 6.25 | 600 | 0.8 | 24 | 0.8 |
| x8ae2 | 150 | 6.25 | 900 | 120 | 240 | 6.25 | 600 | 0.8 | 24 | 1.6 |
| x9ae05 | 150 | 4.29 | 900 | 120 | 60 | 4.29 | 600 | 0.8 | 35 | 0.4 |
| x9a | 150 | 4.29 | 900 | 120 | 120 | 4.29 | 600 | 0.8 | 35 | 0.8 |
| x9ae2 | 150 | 4.29 | 900 | 120 | 240 | 4.29 | 600 | 0.8 | 35 | 1.6 |
| x13a | 150 | 4.29 | 900 | 30 | 30 | 4.29 | 150 | 0.2 | 35 | 0.2 |
| x10ae05[*] | 150 | 10 | 900 | 150 | 75 | 10 | 750 | 1.0 | 15 | 0.5 |
| x10a[*] | 150 | 10 | 900 | 150 | 150 | 10 | 750 | 1.0 | 15 | 1.0 |
| x10ae2[*] | 150 | 10 | 900 | 150 | 300 | 10 | 750 | 1.0 | 15 | 2.0 |
| x11ae05[*] | 150 | 6.25 | 900 | 150 | 75 | 6.25 | 750 | 1.0 | 24 | 0.5 |
| x11a[*] | 150 | 6.25 | 900 | 150 | 150 | 6.25 | 750 | 1.0 | 24 | 1.0 |
| x11ae2[*] | 150 | 6.25 | 900 | 150 | 300 | 6.25 | 750 | 1.0 | 24 | 2.0 |
| x12ae05[*] | 150 | 4.29 | 900 | 150 | 75 | 4.29 | 750 | 1.0 | 35 | 0.5 |
| x12a[*] | 150 | 4.29 | 900 | 150 | 150 | 4.29 | 750 | 1.0 | 35 | 1.0 |
| x12ae2[*] | 150 | 4.29 | 900 | 150 | 300 | 4.29 | 750 | 1.0 | 35 | 2.0 |

*:      Without weld

### 6.1.3   The finite element analysis

The general considerations with regard to the finite element analyses have been described in Chapter 4. Thus, for further description of the modelling of the welds, the corner radii and the material properties of the chord and the braces etc., see Chapter 4, Section 4.5. Only

specific characteristics are described in this section:

- Considering symmetry of geometry and load, one eighth of a X-joint has been modelled. The origin of the coordinate system is in the center of the chord.

- The boundary conditions are shown in Figure 6.3.

- For joints with β=1.0, no weld is modelled in the direction of the chord length.

- Displacement control is used to apply axial loads on the in-plane braces.

- The thickness of the plate at the ends of the chord is 25 mm.



| BOUNDARY CONDITIONS | | | |
|---|---|---|---|
| Degrees of freedom | Nodes on plane X=0.0 | Nodes on plane Y=0.0 | Nodes on plane Z=0.0 |
| $u_x$ | 0. | free | free |
| $u_y$ | free | 0. | free |
| $u_z$ | free | free | 0. |
| $\Phi_x$ | free | 0. | 0. |
| $\Phi_y$ | 0. | free | 0. |
| $\Phi_z$ | 0. | 0. | free |
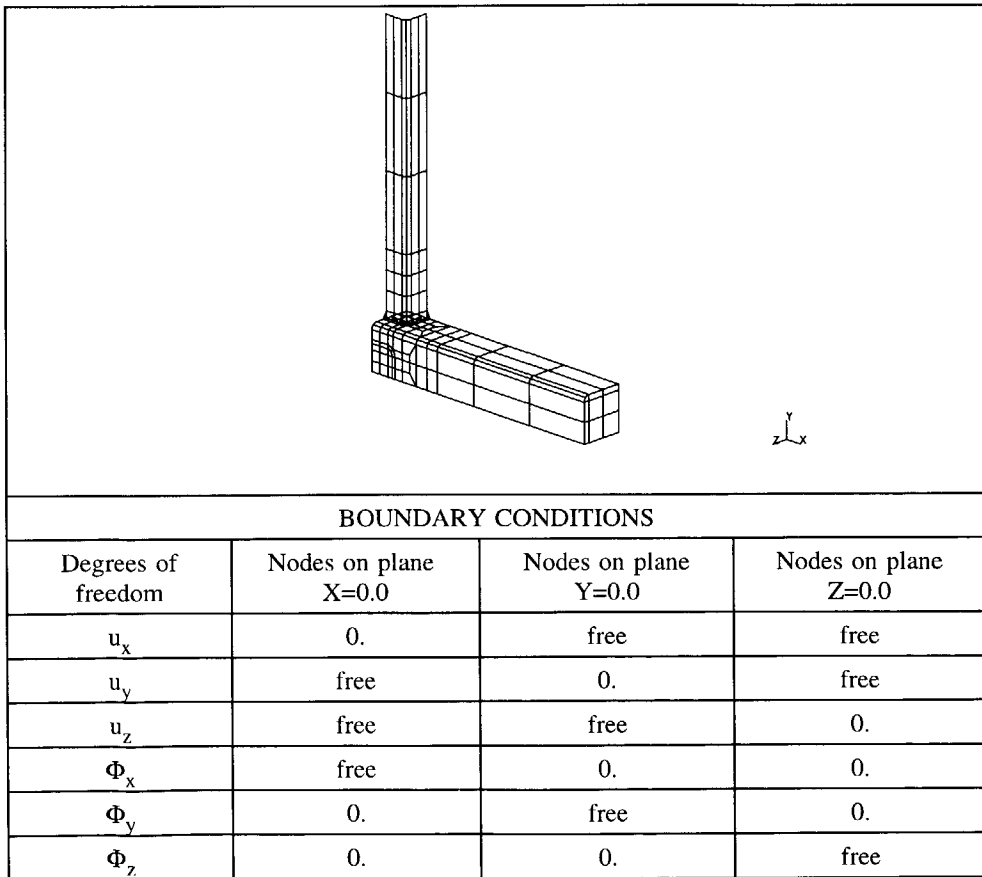
**Figure 6.3**    **Finite element meshes and boundary conditions of axially loaded X-joints**

### 6.1.4   Numerical results and observations

The numerical results are illustrated in three groups of figures:

1)      results for joins made of square hollow sections ($\beta \leq 0.8$), see Figure 6.4.

2)      results for joints made of rectangular hollow sections ($\beta \leq 0.8$), see Figure 6.5.

3)      results for joints made of square and rectangular hollow sections ($\beta = 1.0$), see Figure 6.6.

In Figures 6.4 to 6.6, the ultimate deformation limit ($3\% b_0$) is indicated and the ultimate load capacity of each joint is marked in the (non-dimensional) load vs. chord top face indentation curves.

In Figures 6.4 and 6.5, the non-dimensional load of $N_1/f_{y0}t_0^2$ is used as the vertical axis which is a suitable parameter to represent the chord face plastification failure. However, this parameter cannot physically represents the ultimate load capacity of joints with $\beta = 1.0$. Because for joints with $\beta = 1.0$, chord side wall failure occurs. Thus, the load applied to the braces is given on the vertical axis for joints with $\beta = 1.0$.


Observations from Figure 6.4:

-       For joints with $\beta \leq 0.6$, the non-dimensional loads of the joints are increasing with the increase of the chord top face indentation, due to the membrane action of the chord. Maximum loads are not reached for such joints. The membrane action for joints with smaller $\beta$ values and larger $2\gamma$ values is more pronounced. These curves are typical for the chord top face plastification failure mode.

-       For joints with $\beta = 0.8$, maximum loads are found. The non-dimensional load vs. indentation curves do not abruptly drop down after the maximum.

-       The $2\gamma$ influence observed may partly be caused by the different weld sizes of the joints. Because the weld sizes are related to the thickness of the braces. In the numerical parameter study, the brace thickness is equal to the chord thickness.

Observations from Figure 6.5:

-       For joints with a specific set of $\beta$ and $2\gamma$ values, the results of joints with different $\eta$ values are compared. The influence of the $\eta$ values on the ultimate load capacity of the joints can be clearly seen. Both the joint stiffness and the joint ultimate load capacity are increased with larger $\eta$ values.

Observations from Figure 6.6:

-       For joints with β=1.0, maximum loads are reached. The load vs. indentation curves drop down abruptly after the maximum especially for joints with larger 2γ and larger η values. The deformation at maximum load for these joints is very small. These curves are typical for chord side wall failures. For joints with smaller 2γ and smaller η values, the deformation at maximum load is larger, since web plastification instead of web buckling occurs.

-       The larger the 2γ and η values, the smaller the deformation at maximum load due to chord web buckling.

-       The deformation at maximum load can be substituted into equation (V-19) in Appendix V-1, in order to determine the membrane effect. The corresponding data points are marked in Figure V-2, Appendix V. It can be seen that for these joints the membrane effect in the chord flange is neglectable, due to the small deformation at maximum load.
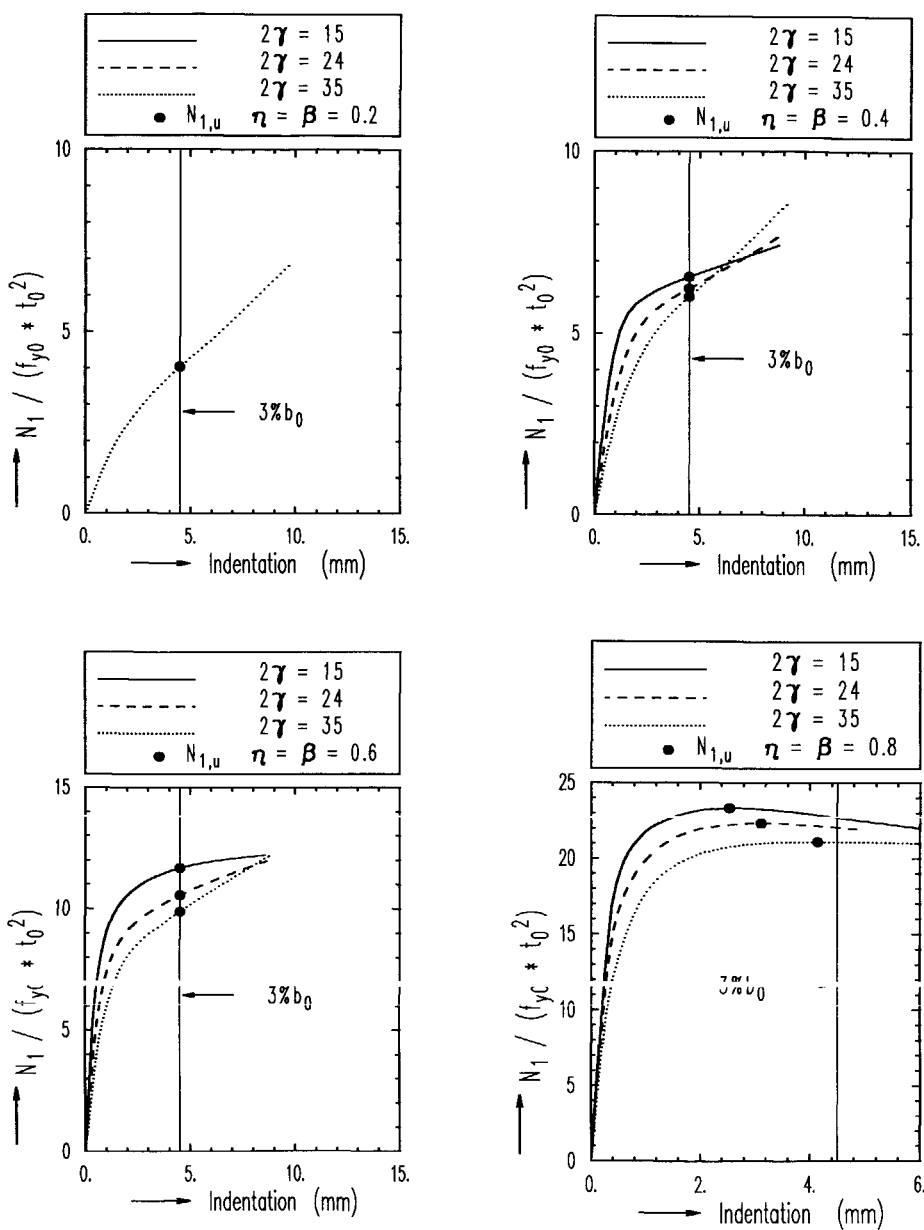
**Figure 6.4** **Numerical results of axially loaded uniplanar X-joints in square hollow sections ($\eta=\beta$)**
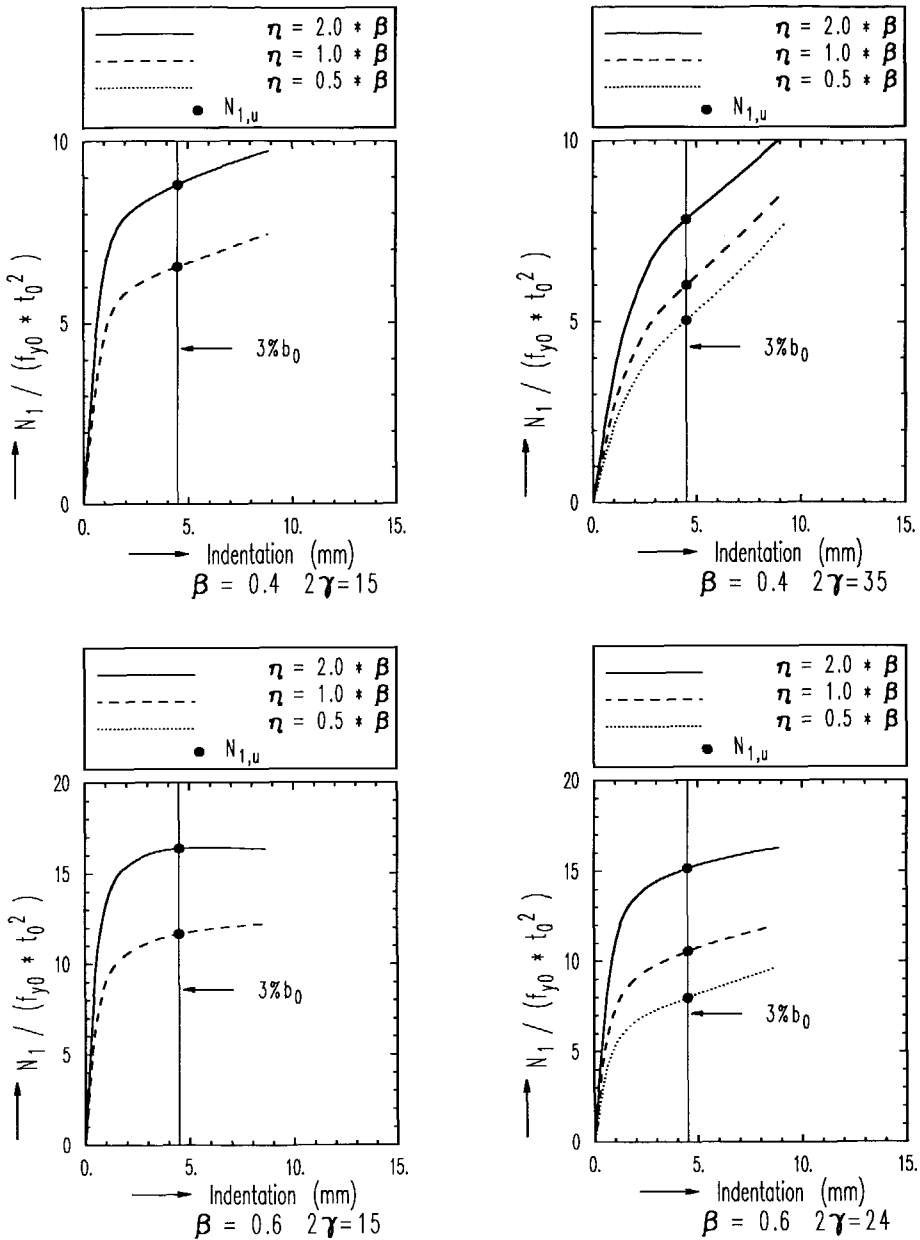
**Figure 6.5** **Numerical results of axially loaded uniplanar X-joints in rectangular hollow sections ($\eta$ influences)**
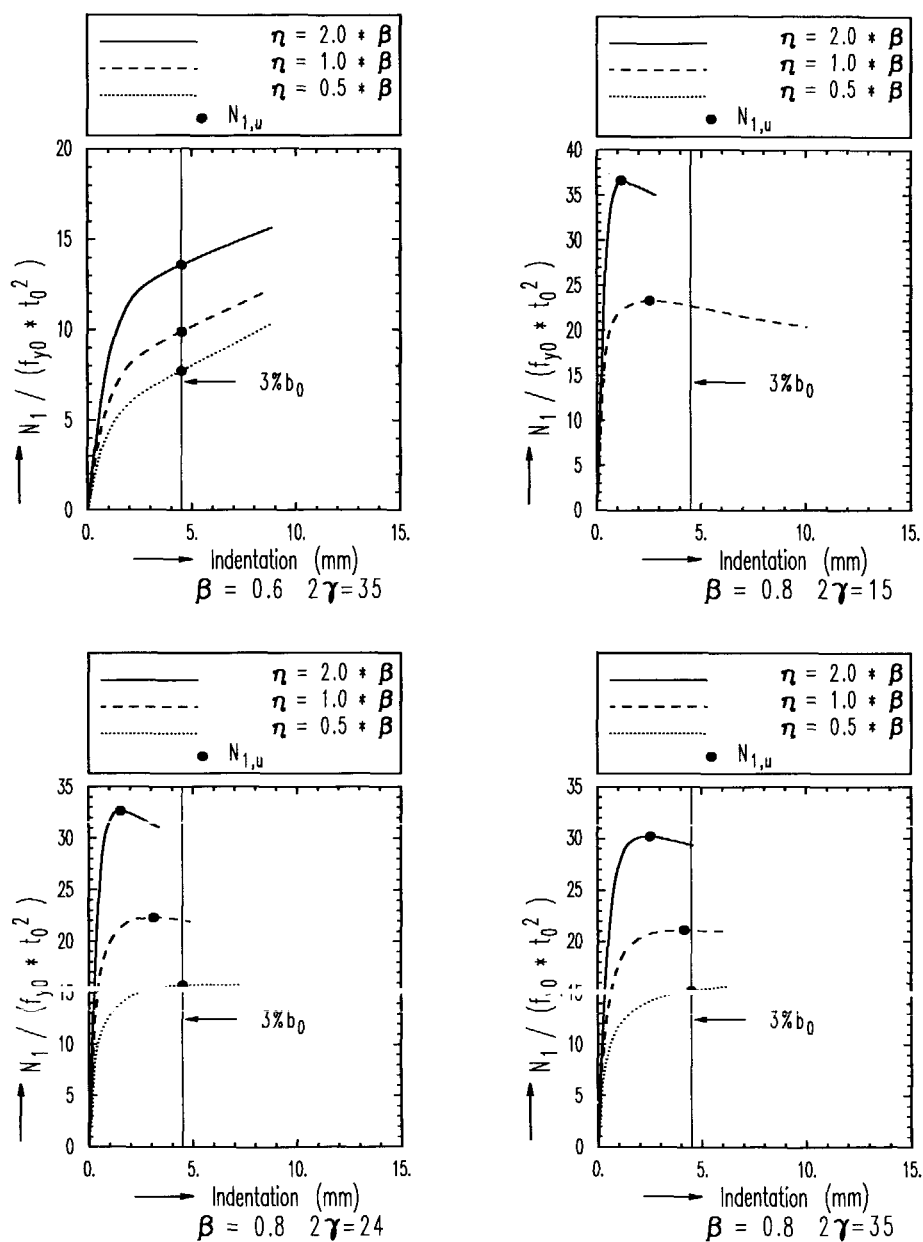
**Figure 6.5**    **Numerical results of axially loaded uniplanar X-joints in rectangular hollow sections ($\eta$ influences continued)**
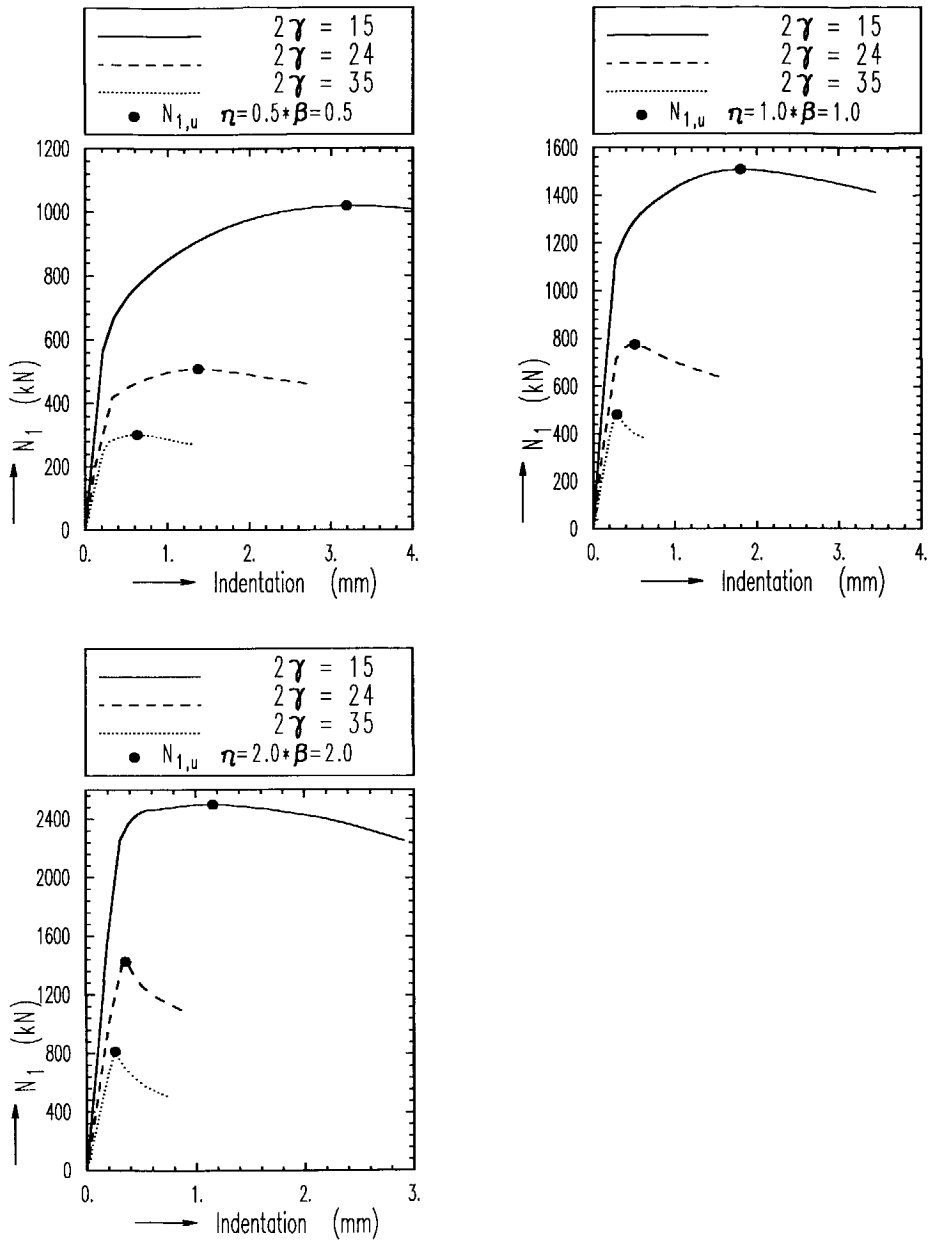
**Figure 6.6** **Numerical results of axially loaded uniplanar X-joints in rectangular hollow sections ($\beta=1.0$)**

The ultimate load capacity for joints with β≤0.8 and for joints with β=1.0 is listed in Tables 6.3 and 6.4 respectively. The ultimate load capacity is determined based upon the procedure described in Chapter 4, Figure 4.20.

**Table 6.3**     **Numerical results of uniplanar X-joints in square and rectangular hollow sections (β≤0.8)**

| Joint | Geometrical parameters | | | Numerical results | |
|---|---|---|---|---|---|
| | β | 2γ | η | $N_{1,u}/(f_{y0}*t_0^2)$ | Criteria |
| x1a | 0.4 | 15 | 0.4 | 6.55 | $\delta_u$ |
| x1ae2 | 0.4 | 15 | 0.8 | 8.80 | $\delta_u$ |
| x2a | 0.4 | 24 | 0.4 | 6.23 | $\delta_u$ |
| x3ae05 | 0.4 | 35 | 0.2 | **5.03** | $\delta_s$ |
| x3a | 0.4 | 35 | 0.4 | **6.00** | $\delta_s$ |
| x3ae2 | 0.4 | 35 | 0.8 | **7.81** | $\delta_s$ |
| x4a | 0.6 | 15 | 0.6 | 11.68 | $\delta_u$ |
| x4ae2 | 0.6 | 15 | 1.2 | 16.39 | $\delta_u$ |
| x5ae05 | 0.6 | 24 | 0.3 | 7.99 | $\delta_u$ |
| x5a | 0.6 | 24 | 0.6 | 10.56 | $\delta_u$ |
| x5ae2 | 0.6 | 24 | 1.2 | 15.15 | $\delta_u$ |
| x6ae05 | 0.6 | 35 | 0.3 | 7.71 | $\delta_u$ |
| x6a | 0.6 | 35 | 0.6 | 9.88 | $\delta_u$ |
| x6ae2 | 0.6 | 3 | 1.2 | 13.58 | $\delta_u$ |
| x7a | 0.8 | 15 | 0.8 | 23.32 | Max. |
| x7ae2 | 0.8 | 15 | 1.6 | 36.60 | Max |
| x8ae05 | 0.8 | 24 | 0.4 | 15.77 | $\delta_u$ |
| x8a | 0.8 | 24 | 0.8 | 22.32 | Max. |
| x8ae2 | 0.8 | 24 | 1.6 | 32.63 | Max. |
| x9ae05 | 0.8 | 35 | 0.4 | 15.25 | $\delta_u$ |
| x9a | 0.8 | 35 | 0.8 | 21.10 | Max. |
| x9ae2 | 0.8 | 35 | 1.6 | 30.22 | Max. |
| x13a | 0.2 | 35 | 0.2 | **4.04** | $\delta_s$ |

Note:   $\delta_u$ = deformation at 3%$b_0$;    $\delta_s$ = deformation at 1%$b_0$.

**Table 6.4    Numerical results of axially loaded full width uniplanar X-joints in square and rectangular hollow sections ($\beta=1.0$)**

| Joint | Geometrical parameters | | | Numerical results | |
|---|---|---|---|---|---|
| | $\beta$ | $2\gamma$ | $\eta$ | $N_{1,u}$ kN | Criteria |
| x10ae05[*] | 1.0 | 15 | 0.5 | 1019 | Max. |
| x10a[*] | 1.0 | 15 | 1.0 | 1507 | Max. |
| x10ae2[*] | 1.0 | 15 | 2.0 | 2498 | Max. |
| x11ae05[*] | 1.0 | 24 | 0.5 | 509 | Max. |
| x11a[*] | 1.0 | 24 | 1.0 | 776 | Max. |
| x11ae2[*] | 1.0 | 24 | 2.0 | 1427 | Max. |
| x12ae05[*] | 1.0 | 35 | 0.5 | 302 | Max. |
| x12a[*] | 1.0 | 35 | 1.0 | 482 | Max. |
| x12ae2[*] | 1.0 | 35 | 2.0 | 816 | Max. |

[*]     Without weld

### 6.1.5  The ultimate load capacity of joints with chord face plastification

For joints with small to medium $\beta$ values, the failure mode is plastification of the chord top faces. The CIDECT formula, equation (5.2), derived from the yield line theory is used as the basis for the analysis.

$$\frac{N_{1,Rd}}{f_{y0}t_0^2} = \frac{2}{1-\beta}(\eta + 2\sqrt{1-\beta}\,)$$

(5.2)

The FE results listed in Table 6.3 are compared with the CIDECT formula, equation (5.2), in Figure 6.7.
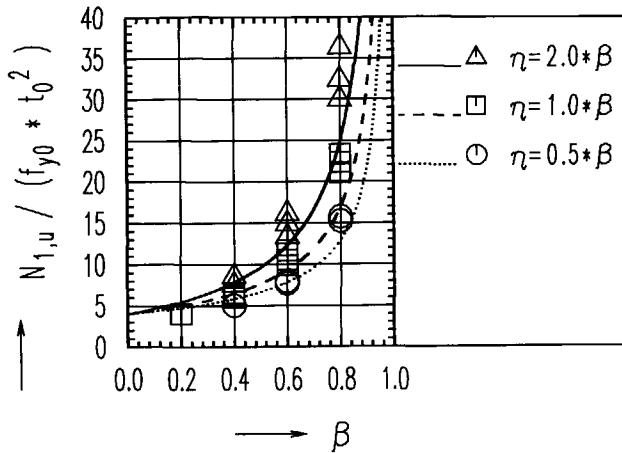


**Figure 6.7  Comparison between the FE results and the CIDECT formula ($\beta \le 0.8$)**

It can be seen that for joints with larger $\beta$ values the CIDECT formula is lower than the FE results and it is higher than the FE results for joints with smaller $\beta$ values. This is mainly caused by the deformation criterion used which is not governing for the higher $\beta$ values. A revision is introduced for the design resistance formula in order to establish the joint ultimate load capacity formula. The revision can be done by using correction constants for $\beta$ and $\eta$. However, the author feels that a separate correction function to the analytical formula gives a better approach:

$$\frac{N_{1,u}}{f_{y0}t_0^2} = \frac{2}{1-\beta}(\eta + 2\sqrt{1-\beta}\,) \cdot f(\beta,\eta)$$

(6.1)

Where

$$f(\beta,\eta) = R_1 + R_2\beta + R_3\eta \tag{6.2}$$

A regression analysis is carried out based upon the numerical results in Table 6.3. The bold data in Table 6.3 is excluded in the regression analysis, because the serviceability criterion is critical for such joints. The regression results are listed in Table 6.5. The formulae for the mean normalised error (the numerical results divided by the formula), the coefficient of variation (CoV) and the correlation coefficient ($R^2$) can be found in equations (4.9) to (4.12), Chapter 4.

**Table 6.5    Regression result of equation (6.2)**

| $R_1$ | $R_2$ | $R_3$ | Mean | Coefficient of variation (CoV) | Correlation coefficient ($R^2$) |
|-------|-------|-------|------|-------------------------------|--------------------------------|
| 0.7 | 0.6 | 0.1 | 1.011 | 0.069 | 0.978 |

Equation (6.1) and the numerical data points are plotted in Figure 6.8.
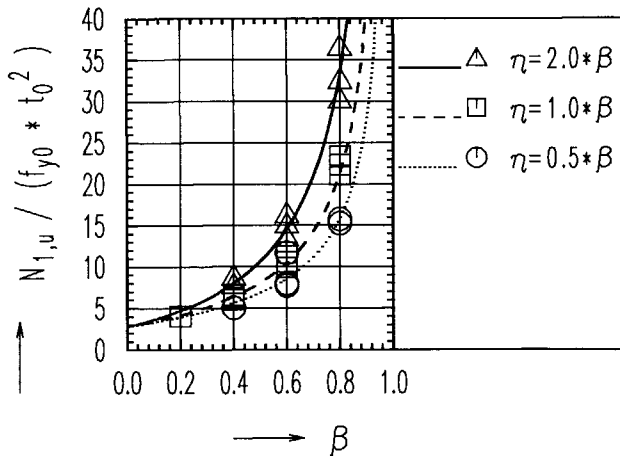


**Figure 6.8  The FE results and the regression formula ($\beta \leq 0.8$)**

### 6.1.6  The ultimate load capacity of joints with chord side wall failure

For all the joints with $\beta=1.0$, a maximum load is reached which is used as the joint ultimate load capacity according to the criterion described in Chapter 4. The joints fail by chord side wall plastification or buckling or in combination with plastification of the chord flanges. The joint ultimate load capacity is outlined in Table 6.4.

**Comparison between the FE results and the CIDECT formula**

Equation (5.4) described in Chapter 5 is the CIDECT characteristic strength of full width joints with chord side wall failure (without the $\gamma_M$ factor of 1.25). In Figure 6.9 and Table 6.6, the ultimate load capacity from the numerical results is compared with equation (5.4).

$$N_{1,k} = 2\kappa(2\gamma\eta + 5)f_{y0}t_0^2 \qquad\qquad (5.4)$$

Where $\kappa$ is derived according to EC3 buckling curve-a (EC3 1992) with a buckling length of $(h_0 - 2t_0)$.

It can be seen that the CIDECT formula is sometimes much lower than the numerical results with a maximum difference of 63% for joint with $2\gamma = 35$ and $\eta = 2\beta$. The $\delta_u$ values in Table 6.6 are the deformations corresponding to the maximum loads in Figure 6.6.
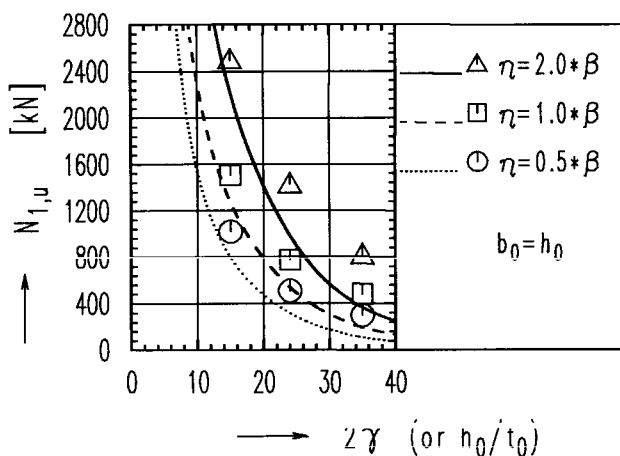


**Figure 6.9**     **Comparison between the FE results and the CIDECT formula ($\beta=1.0$)**

**Table 6.6**     **Comparison between the FE results, the CIDECT formula and the "4-hinge yield line and web buckling" formula**

| Joints | $2\gamma$ | $\delta_u$ mm | eq. 5.20 (1) | CIDECT eq. 5.4 (2) | FE results (3) | $\dfrac{(3)}{(1)}$ | $\dfrac{(3)}{(2)}$ |
|---|---|---|---|---|---|---|---|
| | | | $N_{1,u}$ (kN) | | | Comparisons | |
| x10ae05* | 15 | 3.19 | 903 | 796 | 1019 | 1.130 | 1.284 |
| x10a* | 15 | 1.80 | 1425 | 1274 | 1507 | 1.059 | 1.187 |
| x10ae2* | 15 | 1.16 | 2469 | 2229 | 2498 | 1.013 | 1.124 |
| x11ae05* | 24 | 1.37 | 483 | 314 | 509 | 1.049 | 1.618 |
| x11a* | 24 | 0.51 | 789 | 536 | 776 | 0.978 | 1.446 |
| x11ae2* | 24 | 0.36 | 1402 | 979 | 1427 | 1.013 | 1.455 |
| x12ae05* | 35 | 0.63 | 277 | 111 | 302 | 1.085 | 2.743 |
| x12a* | 35 | 0.29 | 465 | 197 | 482 | 1.033 | 2.463 |
| x12ae2* | 35 | 0.26 | 840 | 369 | 816 | 0.967 | 2.224 |
| Mean | | | | | | 1.036 | 1.727 |
| CoV | | | | | | 0.051 | 0.345 |
| $R^2$ | | | | | | 0.993 | 0.787 |
| $\beta$=1.0        $f_{y0}$=355 N/mm$^2$ | | | | | | | |

**Comparison between the FE results and the "4-hinge yield line and chord web buckling" model**

In Figure 6.10 and Table 6.6, the numerical results are quantitatively compared with the "4-hinge yield line and chord web buckling" model, equation (5.20).

$$N_{1,u} = 4\kappa(\sqrt{\gamma} + \gamma\eta)f_{y0}t_0^2 \qquad\qquad (5.20)$$

It should be mentioned that the values of $\kappa$ in equations (5.4) and (5.20) are different. The first is determined according to a pin ended column with a buckling length of $(h_0-2t_0)$ while the second according to a fix ended column with a buckling length of $(h_0-2t_0)/2$ considering that the chord side walls are restrained by the corners of the chord and the walls of the braces.
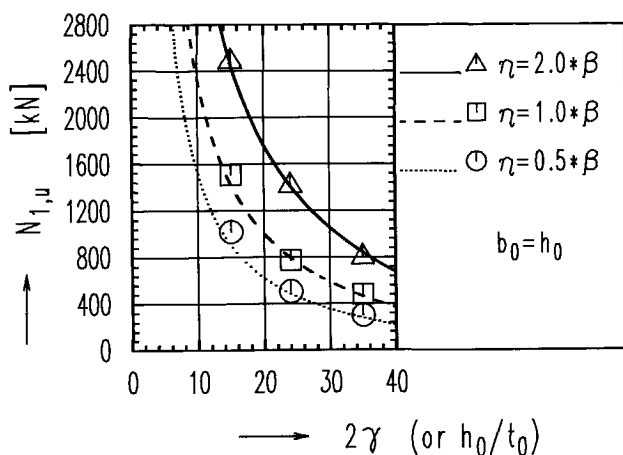
**Figure 6.10    Comparison between the FE results and the "4-hinge yield line and web buckling" model (β=1.0), equation (5.20)**

### 6.1.7    Conclusions

The static behaviour and strength of axially loaded uniplanar X-joints in RHS are numerically investigated. The joint geometrical parameters included are β=0.2, 0.4, 0.8, 1.0; 2γ=15, 24, 35 and η=0.5β, 1.0β and 2.0β. The formulae based upon the analytical model and the CIDECT design guide are compared with the numerical results. The following conclusions can be drawn:

-    For joints with chord face plastification as failure mode, the CIDECT formula is conservative for the ultimate load capacity for joints with large β values and is non-conservative for joints with small β values. Thus, a revision function is introduced for the design resistance formula. The ultimate load capacity formula is recommended as equation (6.1).

-    For full width joints with chord side wall failure, the CIDECT formula is very conservative for joints with high chord wall slenderness. A newly developed formula, equation (5.20) according to the so-called "4-hinge yield line and web buckling" model is recommended with better statistical results compared to the FE results.

## 6.2.    X-JOINTS LOADED WITH IN-PLANE BENDING MOMENTS

### 6.2.1.  Introduction

For uniplanar X-joints loaded with in-plane bending moments, the moment resistance formulae have been given in the CIDECT design guide (Packer 1992a) which were based upon previous research (Wardenier 1982a). For joints with chord top face plastification failure, the moment resistance formula is based upon the yield line theory. For joints with chord side wall failure, it is based upon chord side wall yielding where no chord side wall buckling is considered. From previous work (Yu 1996c), the ultimate moment capacity formula has been derived for full width joints loaded with in-plane bending moments. It has been found that chord web buckling is not critical for full width X-joints under in-plane bending moments  within the range of validity of the geometrical parameters. In this section, more geometrical parameters including different η values are included in order to check the validity of the formula.

Based upon the analytical formulae described in Chapter 5, two sets of ultimate moment capacity formulae are presented in this section: one for chord top face plastification failure and another one for chord side wall failure.

### 6.2.2.  Research programme

The configuration of an uniplanar X-joint loaded with in-plane bending moments is shown in Figure 6.11. The joint geometrical parameters investigated are summarised in Table 6.7. Five $\beta$ values ($\beta$=0.2, 0.4, 0.6, 0.8, 1.0), three $2\gamma$ values ($2\gamma$=15, 24 and 35) and three η values (η=0.5*$\beta$, 1.0*$\beta$ and 2.0*$\beta$) are considered in this parameter study. In total, there are 27 finite element analyses. The nominal dimensions and the material properties of the joints and the weld are the same as the corresponding joints in the previous section.
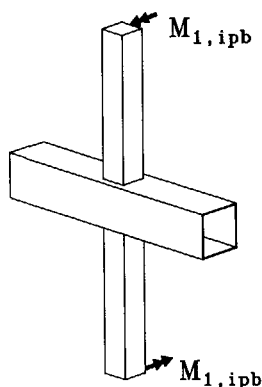


**Figure 6.11    Configuration of an uniplanar X-joint loaded with in-plane bending moments**

**Table 6.7**    **Research programme of uniplanar X-joints loaded with in-plane bending moments**

| | η | β | | | | |
|---|---|---|---|---|---|---|
| | | 0.2 | 0.4 | 0.6 | 0.8 | 1.0 |
| $2\gamma=15$ | 0.5 β | | | | | x10ie05[*] |
| | 1.0 β | | x1i | x4i | x7i | x10i[*] |
| | 2.0 β | | | | | x10ie2[*] |
| $2\gamma=24$ | 0.5 β | | | x5ie05 | x8ie05 | |
| | 1.0 β | | x2i | x5i | x8i | x11i[*] |
| | 2.0 β | | | x5ie2 | x8ie2 | x11ie2[*] |
| $2\gamma=35$ | 0.5 β | | x3ie05 | | x9ie05 | x12ie05[*] |
| | 1.0 β | x13i | x3i | x6i | x9i | x12i[*] |
| | 2.0 β | x13ie2 | x3ie2 | | x9ie2 | x12ie2[*] |
| Notation example: x9ie2 means X-joint, no.**9**, under in-plane bending, $\eta=2.0*\beta$. $b_0=150$ mm, $f_{y0}=355$ N/mm$^2$ | | | | | | |

[*]:    without weld

### 6.2.3.  The finite element analysis

General considerations with regard to the numerical parameter study can be found in Chapter 4. Only some specific aspects are mentioned in this section:

-    Considering symmetry of geometry and load, a quarter of an X-joint has been modelled. The origin of the coordinate system is in the center of the chord.

-    The boundary conditions are shown in Figure 6.12. In order to prevent rigid body motion, an extra restraint in X-direction is added to one node with a coordinate of X=0, Y=$(h_0-t_0)$/2 and Z=0.

-    For joints with β=1.0, no weld along the direction of the chord length has been modelled.

-    The in-plane bending moment can be applied by two opposite axial forces or by shear forces to the brace ends, see Figure 6.13 (a) and (b). The first method results in pure bending moments in the braces. The second method results in bending moments and shear forces in the braces and also axial forces in the chord. Due to the existence of

the axial forces in the chord, the ultimate moment capacity of the joints using the second method is expected to underestimate the actual strength. In this study, the length of the braces is 5 times their width as described in Chapter 4. Comparisons of the two methods are shown in Figure 6.14. It can be seen that for joint with $\beta=0.6$ and $2\gamma=35$, the difference between the two methods is very small. For joint with $\beta=0.4$ and $2\gamma=15$, a larger difference is found. Thus, the first method is used for the parameter study where only pure bending moments are applied on the braces. Using this method, the value of the applied loads are independent of the length of the braces. Load control can only be used in order to achieve an equal value of the two opposite loads even after the elastic stage of the material.



| BOUNDARY CONDITIONS | | | |
|---|---|---|---|
| Degrees of freedom | Node at X=0.0, Y=$(h_0-t_0)/2$, Z=0.0 | Nodes on plane Y=0.0 | Nodes on plane Z=0.0 |
| $u_x$ | 0. | free | free |
| $u_y$ | free | 0. | free |
| $u_z$ | 0. | free | 0. |
| $\Phi_x$ | 0. | 0. | 0. |
| $\Phi_y$ | 0. | free | 0. |
| $\Phi_z$ | free | 0. | free |
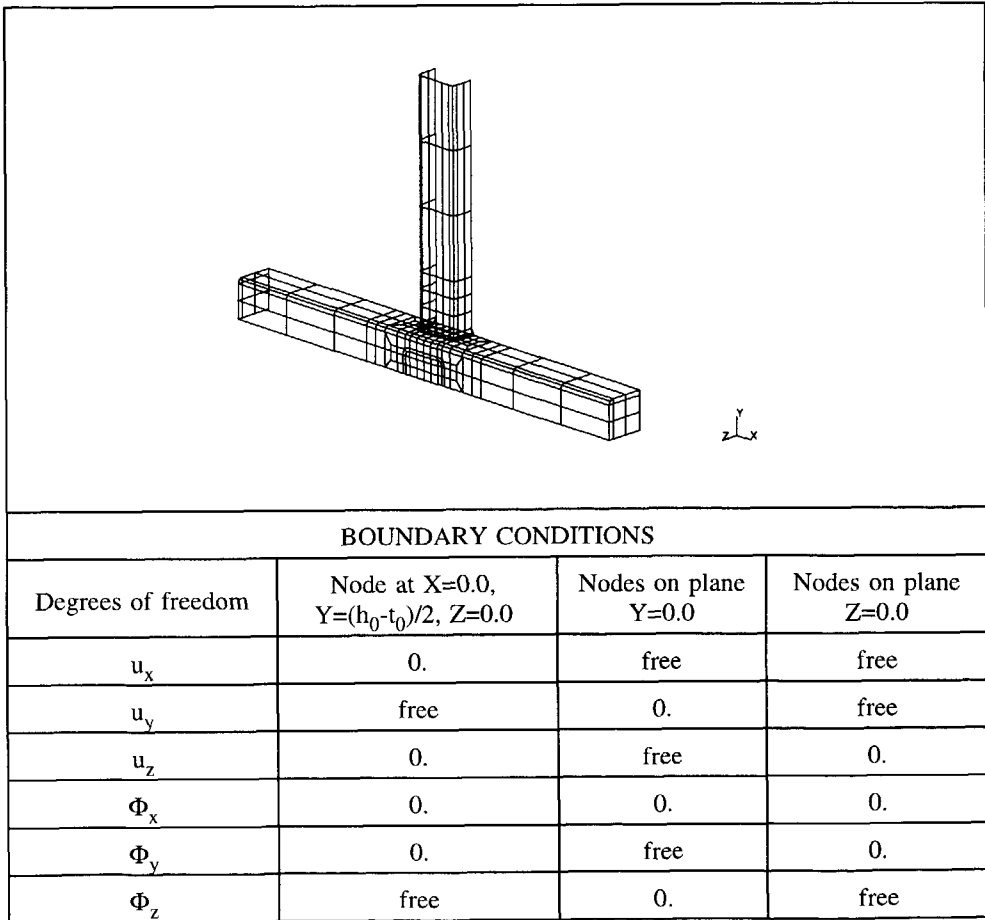
**Figure 6.12** **Finite element meshes and boundary conditions of an uniplanar X-joint loaded with in-plane bending moments**
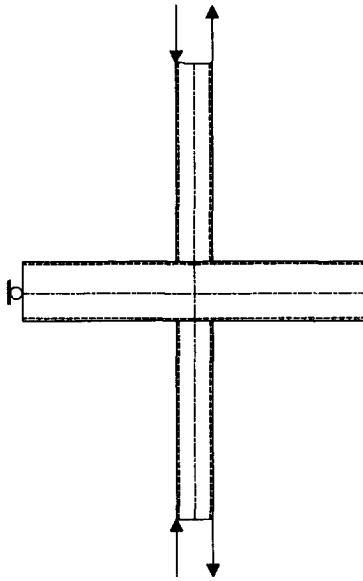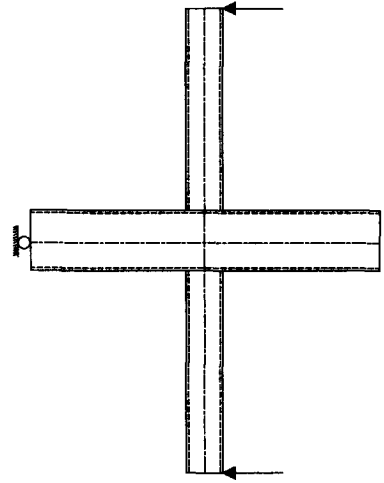
**(a) Pure bending moments**            **(b) Shear forces and bending moments**

**Figure 6.13   Two methods used to apply the in-plane bending moments**
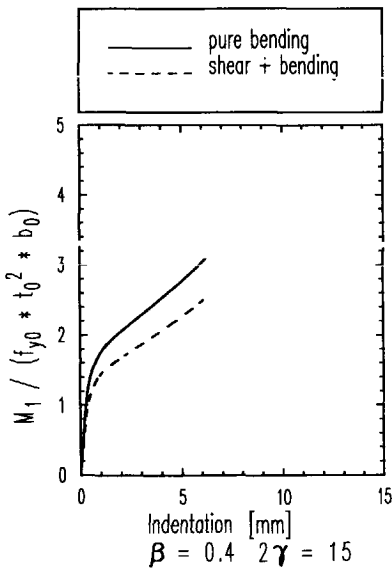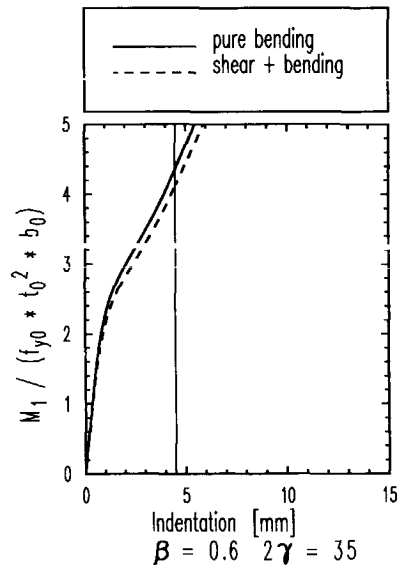


(a)                                                   (b)

**Figure 6.14    Results of the two methods used to apply the in-plane bending moments**

### 6.2.4. Numerical results and observations

Similar to the previous section, the numerical results are illustrated in three groups of figures.

1) joints made of square hollow sections ($\beta \leq 0.8$), Figure 6.15;
2) joints made of rectangular hollow sections ($\beta \leq 0.8$), Figure 6.16;
3) joints made of rectangular hollow sections ($\beta = 1.0$), Figure 6.17.

In Figures 6.15 to 6.17, the horizontal axis gives the chord top face indentation at the intersection of the brace and the chord face. The relationship between the chord face indentation and the rotation of the joint is $\phi = \delta/(h_1/2)$, as shown in Figure 4.21, Chapter 4. For the reason of readability, only the ultimate deformation limit at $3\% b_0$ is indicated; the ultimate rotation limit at $\phi_{0.1}$ is not indicated but only marked if it is critical in Figures 6.15 to 6.17. In Figures 6.15 and 6.16, the non-dimensional moment $M_{1,ipb}/(f_{y0}t_0^2 b_0)$ is used for the vertical axis. In Figure 6.17, the applied moment is used as the vertical axis, because for full width joints, another failure mode occurs.

According to the procedure to determine the ultimate moment capacity described in Chapter 4 (Figure 4.22), the ultimate moment capacity of each joint is obtained and marked in Figures 6.15 to 6.17. The quantitative values are listed in Tables 6.8 and 6.9.

Observations from Figure 6.15 are:

- No maximum moment is reached for joints with $\beta \leq 0.8$. These curves represent the typical failure mode of chord top face plastification.

- For the joins with $\eta = 0.2$ and 0.4, the joint ultimate rotation limit of $\phi_{0.1}$ is critical, namely, the indentation corresponding to $\phi_{0.1}$ is smaller than $3\% b_0$.

- For joints with $\eta = 0.6$ and 0.8, the joint ultimate deformation limit of $3\% b_0$ is critical.

- It seems that there is a small $2\gamma$ influence for joints with the same $\eta$ and $\beta$ values. However, this can be considered as the influence of the weld sizes. Because the brace thickness is taken the same as that of the chord. This results in a larger weld size for joints with a smaller $2\gamma$ value.

Observations from Figure 6.16 are:

- No maximum moment is found. These curves are typical for chord top face plastification. The ultimate moment capacity is determined either by $\phi_{0.1}$ or by $3\% b_0$ whichever is smaller.

- A clear $\eta$ influence is observed.

Observations from Figure 6.17 are:

-   For most of the joints with $\eta \leq 1.0$, no maximum moment is found. Although a maximum is found for the joint with $\eta = 1.0$ and $2\gamma = 35$, the moment vs. indentation curve does not drop down abruptly.

-   For all the joints with $\eta = 2.0$, a maximum is reached except for the joint with $2\gamma = 15$. The deformation at the maximum for the joints with $2\gamma = 24$ or 35 is much smaller than that for the joint with $2\gamma = 15$. Thus, full width uniplanar X-joints loaded with in-plane bending moments are less sensitive to local buckling of the chord side walls if $\eta \leq 1.0$ and $h_0/t_0 \leq 35$. For joints with $\eta = 2.0$ and $h_0/t_0 \geq 24$, local buckling occurs. It should be mentioned that when chord web buckling is considered, the ratio of $h_0/t_0$ should be considered instead of the $2\gamma$ value. Since square hollow section chords are used in the parameter study, these two ratios have the same value here.
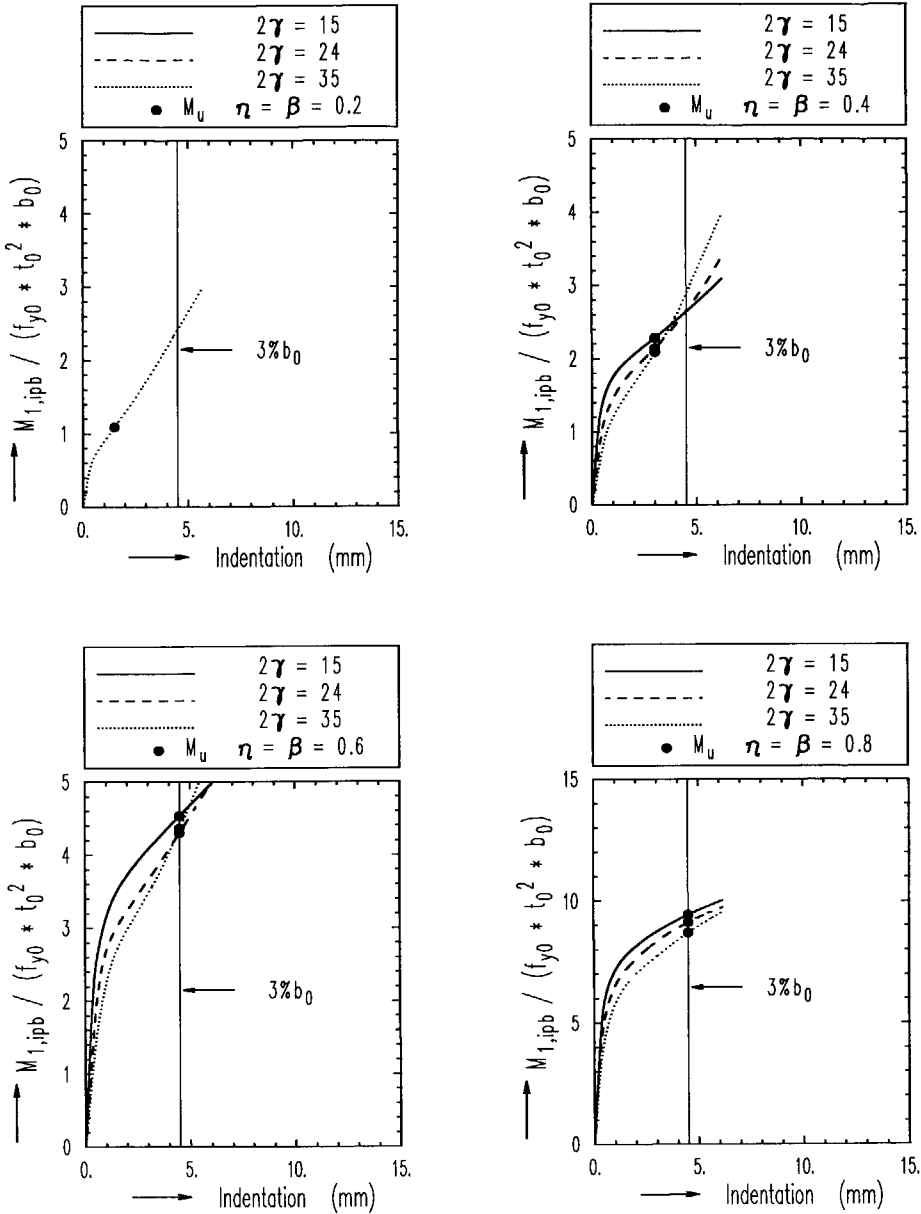
**Figure 6.15** **Numerical results of uniplanar X-joints of square hollow sections loaded with in-plane bending moments ($\eta=\beta$)**
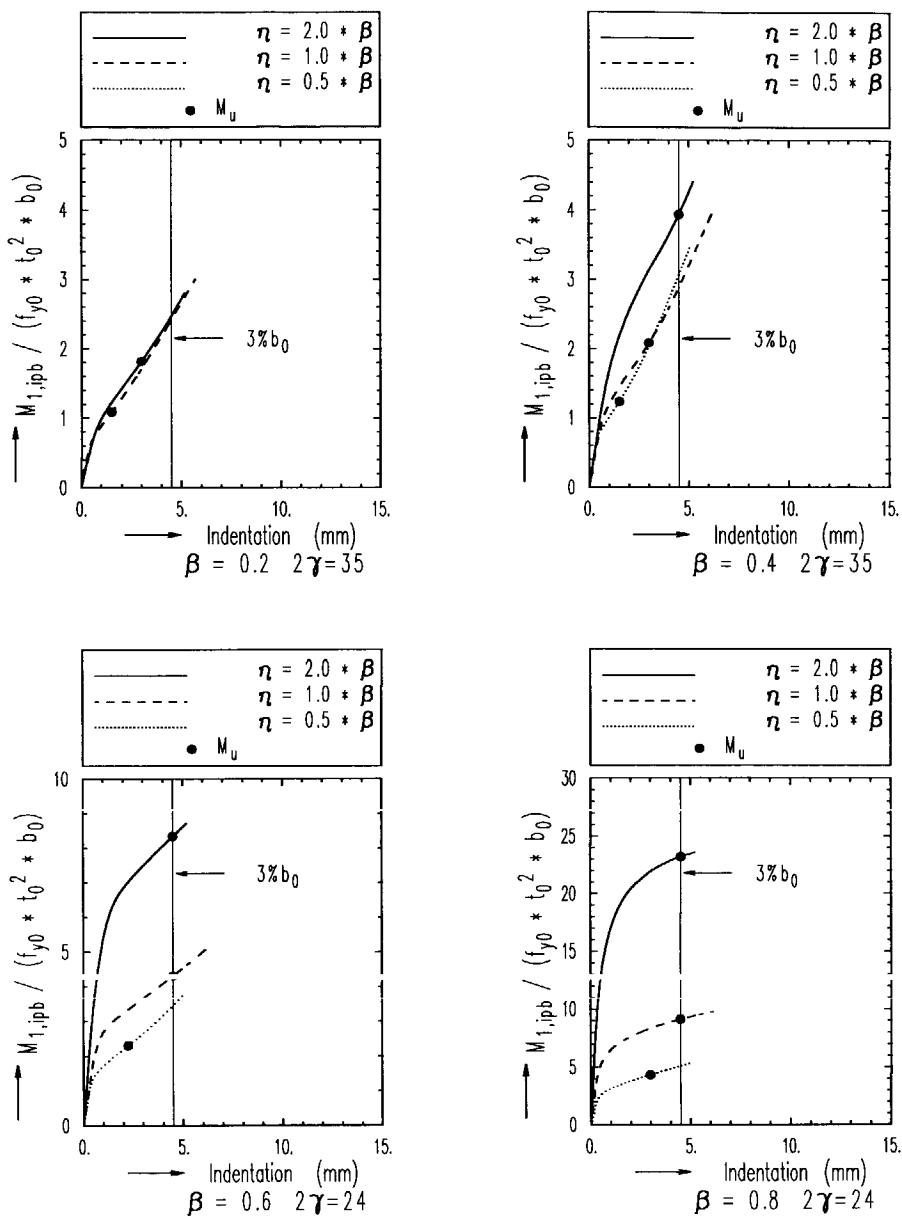
**Figure 6.16    Numerical results of uniplanar X-joints of rectangular hollow sections loaded with in-plane bending moments ($\eta$ influence)**
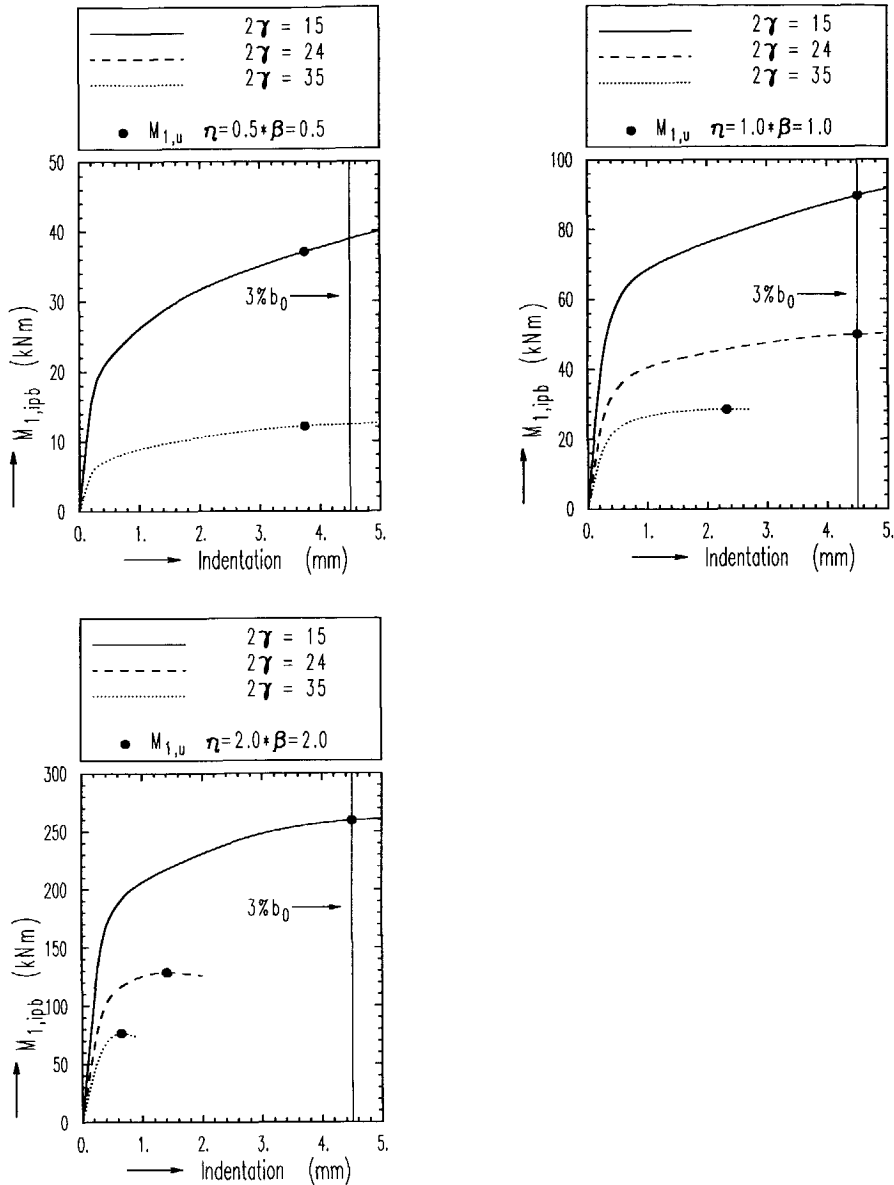
**Figure 6.17** **Numerical results of uniplanar X-joints of rectangular hollow sections loaded with in-plane bending moments ($\beta$=1.0)**

**Table 6.8** Numerical results of uniplanar X-joints loaded with in-plane bending moments ($\beta \leq 0.8$)

| Joints | Geometrical parameters | | | Numerical results | | |
|--------|------|------|------|------------------------------------|-------------|----------|
| | $\beta$ | $2\gamma$ | $\eta$ | $M_{1,ipb,u}/(f_{y0}t_0^2b_0)$ | $\delta_u$ (mm) | Criteria |
| x1i | 0.4 | 15 | 0.4 | 2.28 | 3.00 | $\phi_{0.1}$ |
| x2i | 0.4 | 24 | 0.4 | 2.14 | 3.00 | $\phi_{0.1}$ |
| x3ie05 | 0.4 | 35 | 0.2 | 1.24 | 1.50 | $\phi_{0.1}$ |
| x3i | 0.4 | 35 | 0.4 | 2.08 | 3.00 | $\phi_{0.1}$ |
| x3ie2 | 0.4 | 35 | 0.8 | 3.94 | 4.50 | $3\%b_0$ |
| x4i | 0.6 | 15 | 0.6 | 4.54 | 4.50 | $3\%b_0$ |
| x5ie05 | 0.6 | 24 | 0.3 | 2.31 | 2.25 | $\phi_{0.1}$ |
| x5i | 0.6 | 24 | 0.6 | 4.30 | 4.50 | $3\%b_0$ |
| x5ie2 | 0.6 | 24 | 1.2 | 8.34 | 4.50 | $3\%b_0$ |
| x6ie05 | 0.6 | 35 | 0.3 | 2.15 | 2.25 | $\phi_{0.1}$ |
| x6i | 0.6 | 35 | 0.6 | 4.35 | 4.50 | $3\%b_0$ |
| x6ie2 | 0.6 | 35 | 1.2 | 7.92 | 4.50 | $3\%b_0$ |
| x7i | 0.8 | 15 | 0.8 | 9.44 | 4.50 | $3\%b_0$ |
| x8ie05 | 0.8 | 24 | 0.4 | 4.34 | 3.00 | $\phi_{0.1}$ |
| x8i | 0.8 | 24 | 0.8 | 9.13 | 4.50 | $3\%b_0$ |
| x8ie2 | 0.8 | 24 | 1.6 | 23.20 | 4.50 | $3\%b_0$ |
| x9ie05 | 0.8 | 35 | 0.4 | 4.14 | 3.00 | $\phi_{0.1}$ |
| x9i | 0.8 | 35 | 0.8 | 8.70 | 4.50 | $3\%b_0$ |
| x9ie2 | 0.8 | 35 | 1.6 | 21.70 | 4.50 | $3\%b_0$ |
| x13i | 0.2 | 35 | 0.2 | 1.09 | 1.50 | $\phi_{0.1}$ |
| x13ie2 | 0.2 | 35 | 0.4 | 1.82 | 3.00 | $\phi_{0.1}$ |

**Table 6.9** **Numerical results of uniplanar X-joints loaded with in-plane bending moments ($\beta=1.0$)**

| Joint | Geometrical parameters | | | Numerical results | | |
|---|---|---|---|---|---|---|
| | $\beta$ | $2\gamma$ or $h_0/t_0$ | $\eta$ | $M_{1,ipb,u}$ (kNm) | $\delta_u$ | Criteria |
| x10ie05[*] | 1.00 | 15 | 0.5 | 37.09 | 3.75 | $\phi_{0.1}$ |
| x10ie[*] | 1.00 | 15 | 1.0 | 89.73 | 4.50 | $3\%b_0$ |
| x10ie2[*] | 1.00 | 15 | 2.0 | 259.65 | 4.50 | $3\%b_0$ |
| x11i[*] | 1.00 | 24 | 1.0 | 50.01 | 4.50 | $3\%b_0$ |
| x11ie2[*] | 1.00 | 24 | 2.0 | 128.67 | 1.41 | Max. |
| x12ie05[*] | 1.00 | 35 | 0.5 | 12.21 | 3.75 | $\phi_{0.1}$ |
| x12i[*] | 1.00 | 35 | 1.0 | 28.57 | 2.33 | Max. |
| x12ie2[*] | 1.00 | 35 | 2.0 | 76.48 | 0.65 | Max. |

*: without weld

### 6.2.5.  The ultimate moment capacity of joints with chord face plastification

For joints with chord top face plastification failure, the analytical formula based upon the yield line theory is given by equation (5.22):

$$M_{1,ipb,Rd} = f_{y0} t_0{}^2 h_1 \left( \frac{2}{\sqrt{1-\beta}} + \frac{\eta}{1-\beta} + \frac{1}{2\eta} \right) \qquad (5.22)$$

This formula has been adopted in the CIDECT design guide as the joint design resistance. The FE results are compared with the CIDECT formula in Figure 6.18. It can be seen that the CIDECT formula is a lower bound of the numerical results especially for joints with larger $\beta$ values. A more efficient formula can be derived by introducing a revision function to equation (5.22). Here a similar approach is used as for axially loaded X-joints:

$$M_{1,ipb,u} = f_{y0} t_0{}^2 h_1 \left( \frac{2}{\sqrt{1-\beta}} + \frac{\eta}{1-\beta} + \frac{1}{2\eta} \right) \cdot f(\beta,\eta) \qquad (6.3)$$

Where

$$f(\beta,\eta) = R_1 + R_2 \beta + R_3 \eta \qquad (6.4)$$

$R_1$ to $R_3$ can be determined with a non-linear regression analysis of the numerical results listed in Table 6.8. The statistical results of the regression analysis are listed in Table 6.10. The formulae for the mean normalised error, the coefficient of variation (CoV) and the correlation coefficient ($R^2$) can be found in equations (4.9) to (4.12), Chapter 4. The mean normalised error is based upon the FE result divided by equation (6.3).

**Table 6.10    Regression results for chord top face yielding**

| $\tilde{R}_1$ | $\tilde{R}_2$ | $\tilde{R}_3$ | Mean normalised error | Coefficient of variation CoV | Correlation coefficient $R^2$ |
|---|---|---|---|---|---|
| 1.00 | 0.6 | -0.25 | 1.028 | 0.056 | 0.977 |

The FE data points and equation (6.3) are plotted in Figure 6.19.
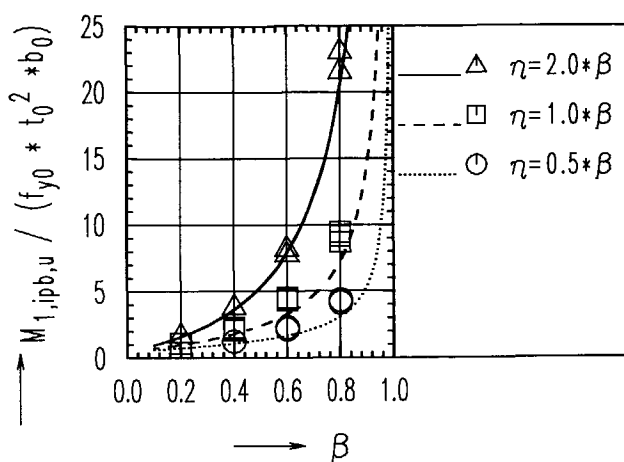
**Figure 6.18** Comparison between the FE results and the CIDECT formula ($\beta \leq 0.8$)
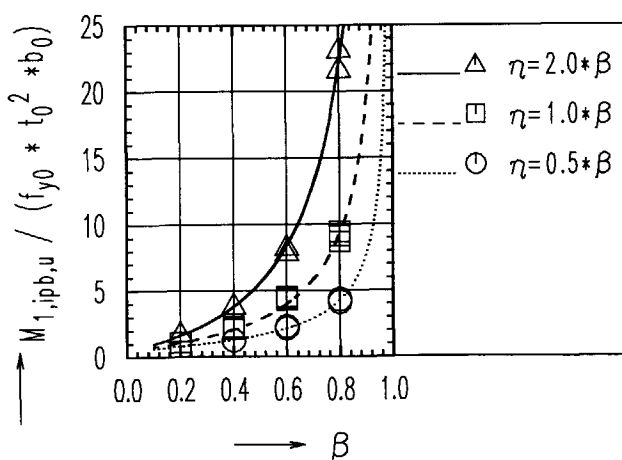


**Figure 6.19** The FE results and the ultimate moment capacity formula ($\beta \leq 0.8$)

## 6.2.6. The ultimate moment capacity of joints with chord side wall failure

### Comparison with the CIDECT formula

In Chapter 5, the CIDECT formula is rewritten in the characteristic form as equation (5.24):

$$M_{1,ipb,k} = f_{y0}t_0^2 h_1 \ \gamma\eta(1+\frac{5}{2\gamma\eta})^2 \qquad (5.24)$$

In equation (5.24), the local buckling effect is not considered although it occurs for joints with $\eta=2.0$ and larger $h_0/t_0$ values. A comparison between the FE results and equation (5.24) is shown in Figure 6.20 and Table 6.11. The $\delta_u$ values in Table 6.11 are corresponding to the ultimate moment capacity of the joints. The maximum difference between the FE results and the CIDECT formula is 42%. The CIDECT formula is a lower bound for the FE results except for the result of the joint with $\eta=2.0$ and $2\gamma=35$.
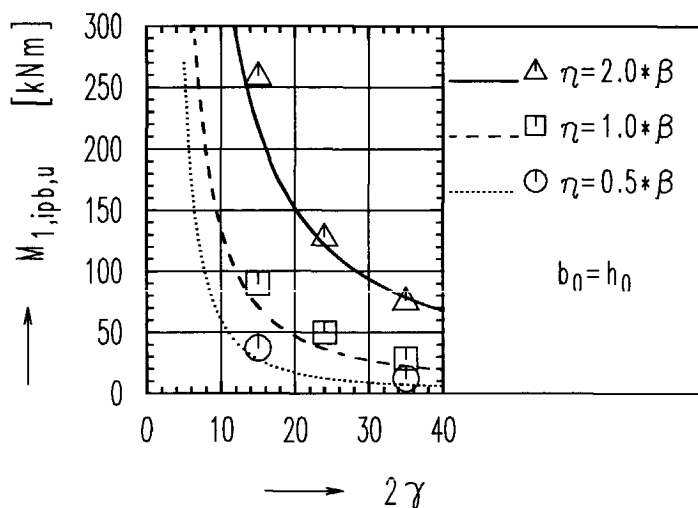


**Figure 6.20    Comparison between the FE results and the CIDECT formula ($\beta$=1.0)**

**Table 6.11** Comparisons between the FE results, the CIDECT formula and the "4-hinge yield line and web buckling" formula

| Joints | $2\gamma$ or $h_0/t_0$ | $\eta$ | $\delta_u$ mm | $\kappa$ | $M_{1,ipb,u}$ (kNm) | | | Comparisons | |
|---|---|---|---|---|---|---|---|---|---|
| | | | | | eq. 5.32 (1) | CIDECT eq. 5.24 (2) | FE results (3) | $\dfrac{(3)}{(1)}$ | $\dfrac{(3)}{(2)}$ |
| x10ie05[*] | 15 | 0.5 | 3.75 | 1.00 | 27.24 | 27.73 | 37.09 | 1.362 | 1.337 |
| x10i[*] | 15 | 1.0 | 4.50 | 1.00 | 71.78 | 71.00 | 89.73 | 1.250 | 1.264 |
| x10ie2[*] | 15 | 2.0 | 4.50 | 0.98 | 216.35 | 217.44 | 259.65 | 1.202 | 1.194 |
| x11i[*] | 24 | 1.0 | 4.50 | 1.00 | 40.42 | 36.44 | 50.01 | 1.237 | 1.372 |
| x11ie2[*] | 24 | 2.0 | 1.41 | 0.92 | 119.33 | 121.73 | 128.67 | 1.073 | 1.057 |
| x12ie05[*] | 35 | 0.5 | 3.75 | 1.00 | 8.88 | 7.08 | 12.21 | 1.376 | 1.724 |
| x12i[*] | 35 | 1.0 | 2.33 | 1.00 | 25.84 | 22.38 | 28.63 | 1.109 | 1.279 |
| x12ie2[*] | 35 | 2.0 | 1.12 | 0.82 | 70.11 | 78.68 | 76.64 | 1.088 | 0.974 |
| Mean | | | | | | | | 1.212 | 1.275 |
| CoV | | | | | | | | 0.097 | 0.178 |
| $R^2$ | | | | | | | | 0.950 | 0.951 |
| $\beta=1.0$     $f_{y0}=355$ N/mm$^2$ | | | | | | | | | |

[*]: Without weld

**Comparison with the "4-hinge yield line and web buckling" model**

Equation (5.32) is the analytical formula deduced using the "4-hinge yield line and chord web buckling" model developed in Chapter 5:

$$M_{1,ipb,u} = \kappa(2\sqrt{\gamma} + \gamma\eta + \frac{1}{2\eta})f_{y0}t_0^2h_1 \qquad (5.32)$$

In equation (5.32), a buckling reduction factor is included. As observed from the FE results, no local buckling occurs for $\eta \leq 1.0$. Although a maximum moment is reached for joint with $\eta=1.0$ and $2\gamma=35$, the moment-indentation curve does not abruptly drop down after the maximum which means that some plastification is developed. In this case, the buckling reduction factor in equation (5.32) is taken as $\kappa=1.0$. However, for joints with $\eta=2.0$, $2\gamma=24$

and 35, local buckling occurs. In such cases, the buckling reduction factor is calculated according to EC3 (1992) buckling curve-a for a fix ended strut of buckling length $(h_0-2t_0)/2$. For simplicity, the same formula for the buckling reduction factor can be used for joints with $\eta=2.0$ and $h_0/t_0=15$, because it is almost 1.00 (0.98). For $1<\eta<2$, a linear interpolation between $\eta=1.0$ and 2.0 is needed to determine the buckling reduction factor. Thus, the buckling reduction factor is defined as follows:

$$\kappa = \begin{cases} 1 & (\eta \leq 1.0) \\ \dfrac{1}{\phi+\sqrt{\phi^2+\overline{\lambda}^2}} & (\eta = 2.0) \\ 1+(\eta-1)(\dfrac{1}{\phi+\sqrt{\phi^2+\overline{\lambda}^2}}-1) & (1.0<\eta<2.0) \end{cases} \qquad (6.5)$$

Where $\phi$ and $\overline{\lambda}$ can be determined according to equations (5.14) to (5.17).

In Figure 6.21, the FE results are compared with equation (5.32) based upon the "4-hinge yield line and web buckling" model. The quantitative comparisons between the FE results and equation (5.32) are listed in Table 6.11. A better coefficient of variation (CoV) based upon the "4-hinge yield line and web buckling" model is found compared to that based upon the CIDECT formula, although the mean values and the correlation coefficients based upon the two formulae are very close to each other. The maximum difference between the formulae based upon the "4-hinge yield line and web buckling" model and the FE result is 27%. The large difference is caused by the neglecting of the membrane effects. For joints where the ultimate moment capacity is determined at an indentation of 3%$b_0$ or a rotation of $\phi_{0.1}$, the membrane effect is relatively larger. While for joints with a maximum moment, the indentation at the maximum is much smaller which results in a neglectable membrane effect. In order to examine the membrane effect, the indentation at the ultimate moment capacity of each joint is substituted into equation (V-28). The corresponding data points are marked in Figure V-4. Taking joint x12ie05[*] as an example, the ultimate moment capacity from the FE result is determined at a rotation of $\phi_{0.1}$ (δ=3.75 mm), the corresponding membrane effect at the ultimate moment capacity is 28%. While for joint x12ie2[*] where a maximum is reached, the membrane effect at the ultimate moment capacity is only 0.3%.
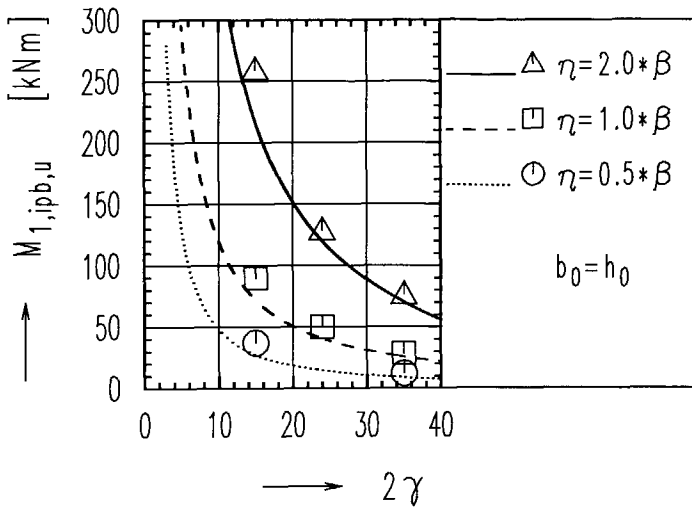
**Figure 6.21** **Comparison between the FE results and the "4-hinge yield line and chord web buckling" model ($\beta$=1.0)**

### 6.2.7. Conclusions

- For joints with chord top face plastification, the CIDECT formula is a lower bound for the numerical results. A more efficient ultimate moment capacity formula, equation (6.3), is recommended with introduction of a revision to the CIDECT formula.

- For full width joints, chord side wall buckling is more sensitive for joints with larger $\eta$ and larger $h_0/t_0$ values. In the CIDECT formula, no local buckling effect is considered, although chord side wall buckling occurs for joints with $\eta$=2.0. In the formula based upon the "4-hinge yield line and web buckling" model, this effect is included, equations (5.32) and (6.5).

## 6.3. X-JOINTS LOADED WITH OUT-OF-PLANE BENDING MOMENTS

### 6.3.1. Introduction

As described in Chapter 5, the out-of-plane bending moments on uniplanar X-joints mainly cause chord top face plastification, chord cracking or chord face plastification in combination with chord side wall yielding or buckling. Similar to the previous sections, brace failure is excluded by choosing the thickness of the braces equal to that of the chord. Cracking is not simulated in this thesis. Thus, only the failure modes of chord top face plastification and a combination of chord top face yielding and chord side wall buckling are examined in this numerical study. Based upon the numerical results and the analytical formulae, two sets of ultimate moment capacity formulae are considered.

### 6.3.2. Research programme

Configuration of an uniplanar X-joint loaded with out-of-plane bending moments is shown in Figure 6.22. The joint geometrical parameters are summarised in Table 6.12. The corresponding nominal dimensions and the material properties of the joints and the weld are the same as those of the corresponding joints in the previous sections. In total, there are 27 FE analyses.
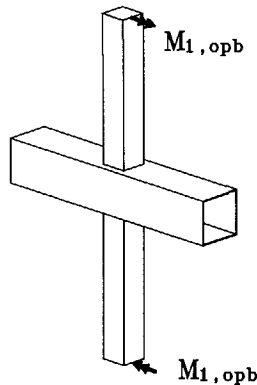


**Figure 6.22    Configuration of an X-joint loaded with out-of-plane bending moments**

**Table 6.12    Research programme of uniplanar X-joints loaded with out-of-plane bending moments**

|  | $\eta$ | $\beta$ | | | | |
|---|---|---|---|---|---|---|
|  |  | 0.2 | 0.4 | 0.6 | 0.8 | 1.0 |
| $2\gamma=15$ | 0.5 $\beta$ |  |  |  |  | x10oe052[*] |
|  | 1.0 $\beta$ |  | x1o | x4o | x7o | x10o[*] |
|  | 2.0 $\beta$ |  |  |  |  | x10oe2[*] |
| $2\gamma=24$ | 0.5 $\beta$ |  |  | x5oe05 | x8oe05 |  |
|  | 1.0 $\beta$ |  | x2o | x5o | x8o | x11o[*] |
|  | 2.0 $\beta$ |  |  | x5oe2 | x8oe2 | x11oe2[*] |
| $2\gamma=35$ | 0.5 $\beta$ |  | x3oe05 |  | x9oe05 | x12oe052[*] |
|  | 1.0 $\beta$ | x13o | x3o | x6o | x9o | x12o[*] |
|  | 2.0 $\beta$ | x13oe2 | x3oe2 |  | x9oe2 | x12oe2[*] |

Notation example: x9oe2 means **X**-joint, No.9, under out-of-plane bending, $\eta=2.0*\beta$.

$b_0=150$ mm, $f_{y0}=355$ N/mm$^2$

[*]:    without weld

### 6.3.3.  The finite element analysis

The general considerations with regarding to the numerical analyses are described in Chapter 4, Section 4.5. Only the exceptions are given here:

- Considering symmetry of geometry and load, a quarter of an X-joint has been modelled. The boundary conditions used for the FE analysis are shown in Figure 6.23. In order to prevent rigid body motion, an extra restraint in Z-direction is added to one node at the chord with a coordinate of X=0, Y=$(h_0-t_0)/2$, Z=0.

- Similar to the joints loaded with in-plane bending moments, two methods can be used to apply the out-of-plane bending moments. The out-of-plane bending moments can be applied by two opposite axial forces or by shear forces at the ends of the braces, see Figure 6.24 (a) and (b). Figure 6.24 (a) results in pure bending moments in the braces and (b) results in shear forces and bending moments in the braces. Method (a) is used in order to apply pure bending moments in the braces. Load control is used in order to get an equal value of the two opposite loads after the elastic stage of the material.

| Degrees of freedom | Node at X=0.0, $Y=(h_0-t_0)/2$, Z=0.0 | Nodes on plane X=0.0 | Nodes on plane Y=0.0 |
|---|---|---|---|
| BOUNDARY CONDITIONS | | | |
| $u_x$ | 0. | 0. | free |
| $u_y$ | free | free | 0. |
| $u_z$ | 0. | free | free |
| $\Phi_x$ | free | free | 0. |
| $\Phi_y$ | 0. | 0. | free |
| $\Phi_z$ | 0. | 0. | 0. |
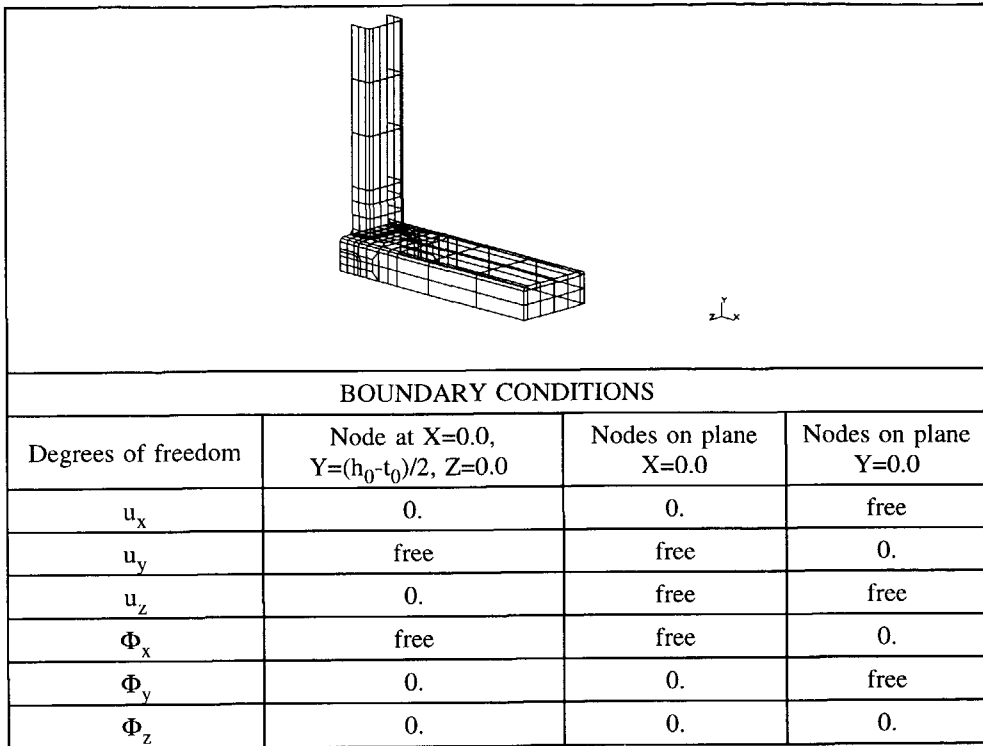
**Figure 6.23    FE meshes and boundary conditions of an X-joint loaded with out-of-plane bending moments**
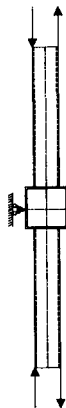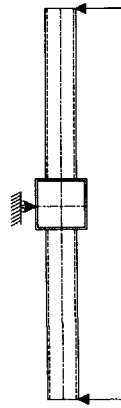


**(a)  Pure bending moments**            **(b) Shear forces and bending moments**

**Figure 6.24    Two methods used to apply the out-of-plane bending moments**

### 6.3.4. Numerical results and observations

Similar to the previous two sections, the numerical results are plotted in three groups of figures:

1)      joints made of square hollow sections ($\beta \leq 0.8$), Figure 6.25;
2)      joints made of rectangular hollow sections ($\beta \leq 0.8$), Figure 6.26;
3)      joints made of rectangular hollow sections ($\beta = 1.0$), Figure 6.27.

In Figures 6.25 and 6.26, the non-dimensional moment of $M_{1,opb}/(f_{y0}t_0^2 b_0)$ is used. In order to make the vertical axis non-dimensional, $b_0$ is introduced which is fixed at 150 mm in the numerical study. Furthermore, the ultimate moment capacity is linear with $f_{y0}t_0^2$.

In Figure 6.27, the out-of-plane bending moment is used on the vertical axis. Because for full width joints, a different failure mode occurs, the ultimate moment capacity is not linear to $t_0^2$ any more.

Observations from Figure 6.25:

-       For joints with $\beta \leq 0.6$, no maximum moment is reached. The non-dimensional moment is increasing with increasing indentation. These curves are typical for a chord top face plastification failure. As shown in the figure, the governing ultimate moment capacity does not always occur at the $3\%b_0$ indentation. For joints with $\beta \leq 0.4$, the joint rotation of $\phi_{0.1}$ ($\phi = 0.5 * b_1/\delta$) is critical, see the marked points at an indentation smaller than $3\%b_0$.
-       For joints with $\beta = 0.8$, $2\gamma = 15$ and 24, a maximum moment is reached. However, the non-dimensional moment-indentation curves do not abruptly drop down and plastification is developed in the joints.
-       There is a small $2\gamma$ influence mainly caused by the weld sizes, similar to Sections 6.1 and 6.2.

Observations from Figure 6.26:

-       A clear $\eta$ influence is observed.
-       For joints with $\beta \leq 0.6$ and $\beta = 0.8$, $\eta = 0.5$, the non-dimensional moment vs. indentation curves are typical for a chord top face plastification failure. For joints with $\beta = 0.8$ and $\eta = 1.0 * \beta$ or $2.0 * \beta$, a maximum moment is reached. The curves do not drop down abruptly after the maximum.

Observations from Figure 6.27:

-       For joints with $\beta = 1.0$, a maximum moment capacity is reached. Similar to the behaviour of axially loaded joints, the moment vs. indentation curves drop down abruptly after the maximum moment is reached especially for joints with large $h_0/t_0$ values. The indentation at the maximum moment is very small for joints with large $h_0/t_0$ values. These curves are typical for a chord side wall buckling failure. For joints with $2\gamma = 15$, plastification of the chord top face and the chord side walls is developed.

The numerically determined (non-dimensional) ultimate moment capacity of the joints with $\beta \leq 0.8$ and $\beta = 1.0$ is listed in Tables 6.13 and 6.14 respectively.
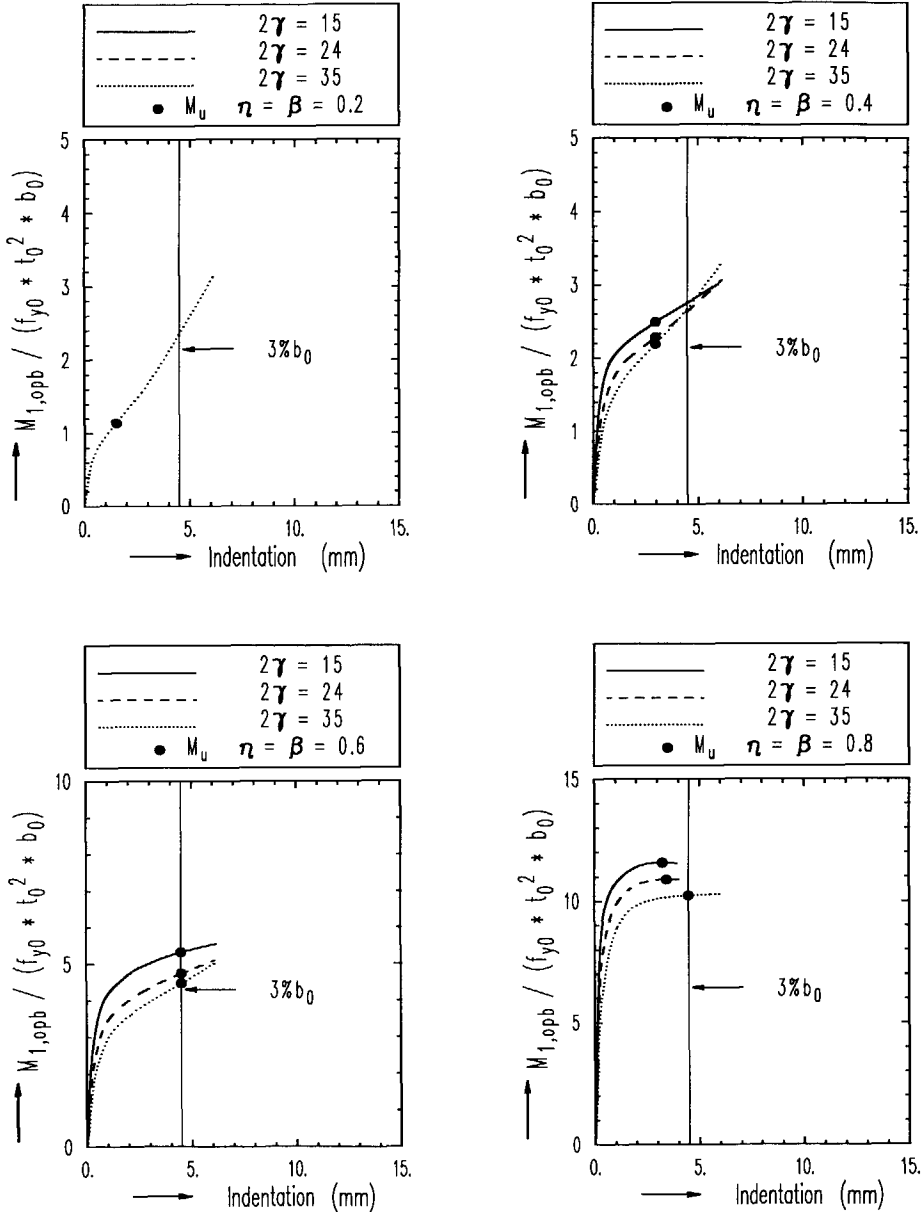


**Figure 6.25**     **Numerical results of uniplanar X-joints in square hollow sections loaded with out-of-plane bending moments ($\eta = \beta$)**
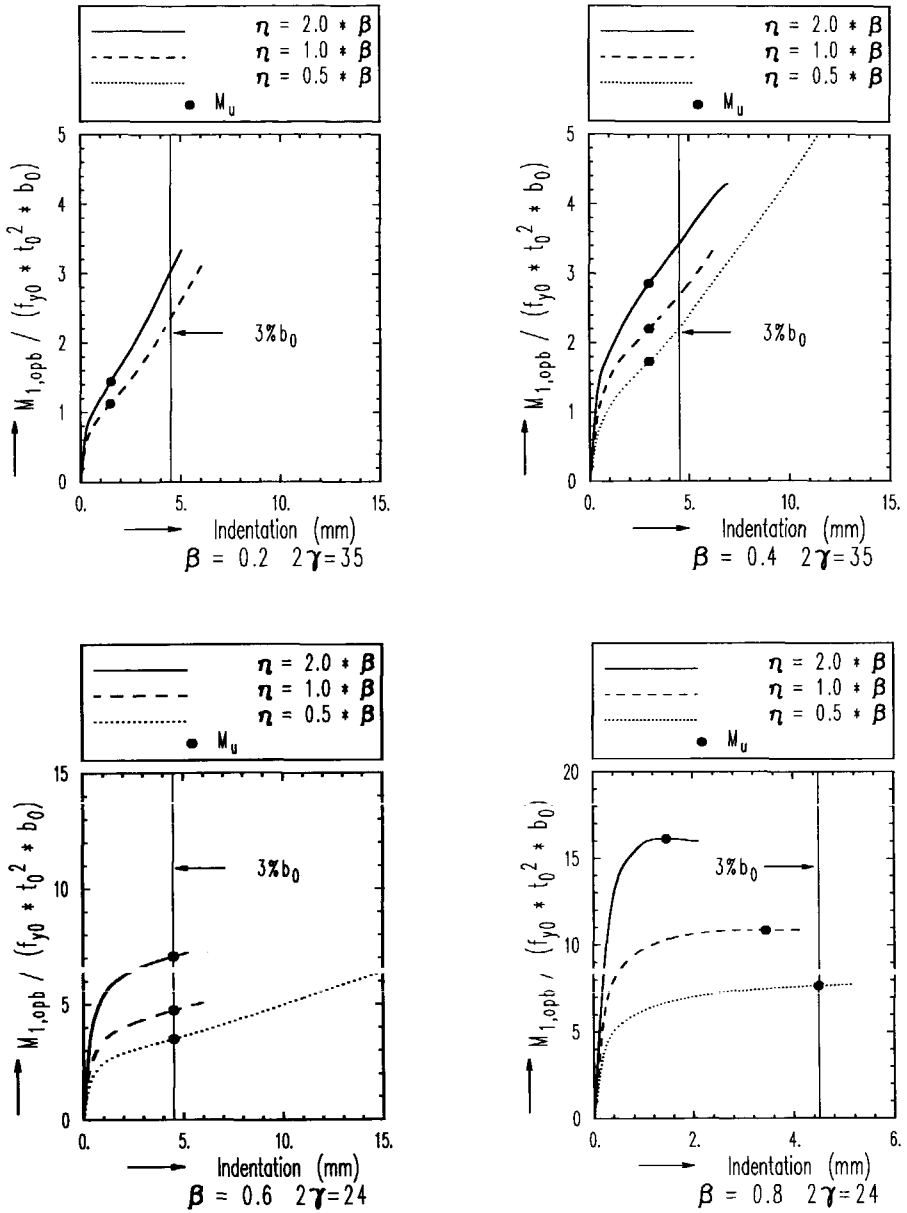
**Figure 6.26**  **Numerical results of uniplanar X-joints in rectangular hollow sections loaded with out-of-plane bending moments ($\eta$ influence)**
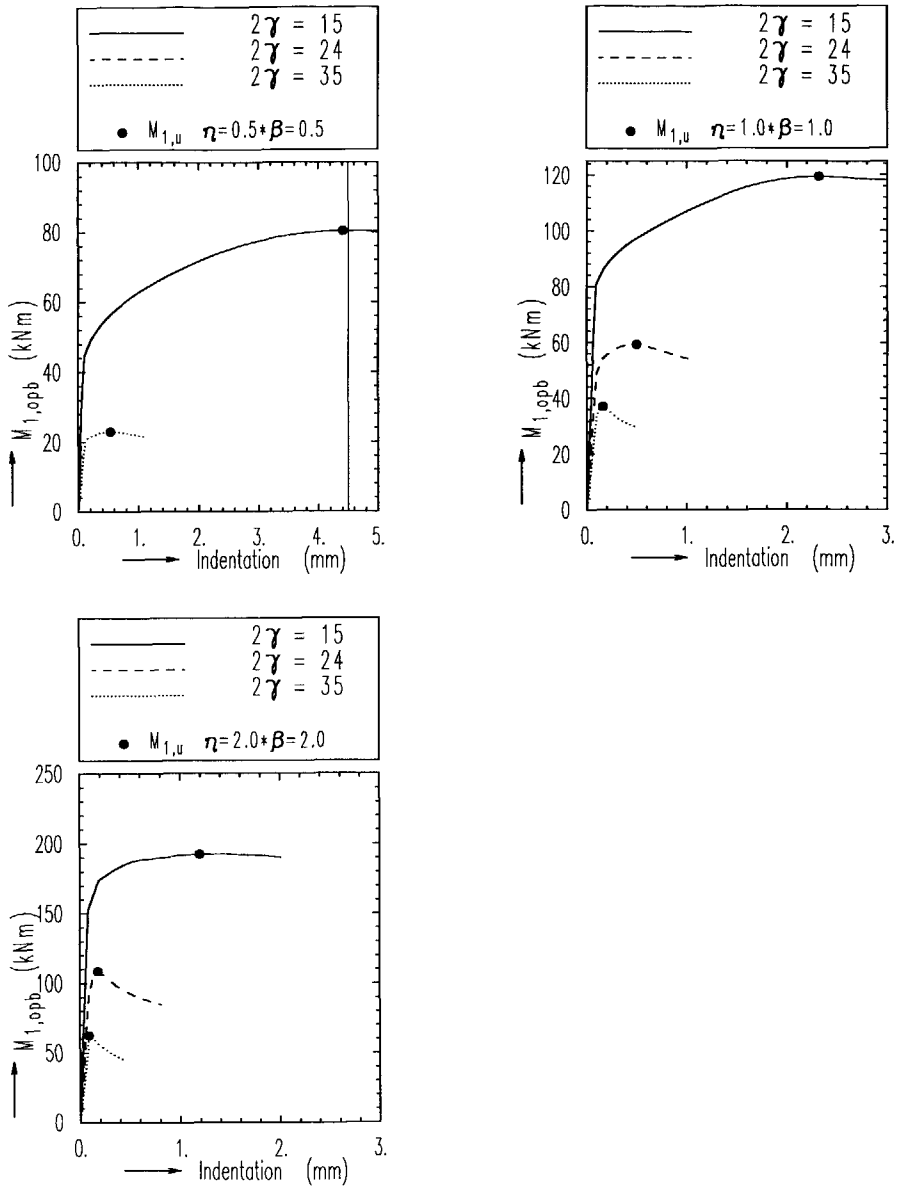
**Figure 6.27** **Numerical results of uniplanar X-joints in rectangular hollow sections loaded with out-of-plane bending moments ($\beta=1$)**

**Table 6.13** **Numerical results of uniplanar X-joints loaded with out-of-plane bending moments ($\beta \leq 0.8$)**

| Joints | Geometrical parameters | | | Numerical results | | |
|--------|------|------|------|-------------------------------|-----------------|----------|
|        | $\beta$ | $2\gamma$ | $\eta$ | $M_{1,opb,u}/(f_{y0}t_0^2 b_0)$ | $\delta_u$ (mm) | Criteria |
| x1o    | 0.4 | 15 | 0.4 | 2.50  | 3.00 | $\phi_{0.1}$ |
| x2o    | 0.4 | 24 | 0.4 | 2.29  | 3.00 | $\phi_{0.1}$ |
| x3oe05 | 0.4 | 35 | 0.2 | 1.72  | 3.00 | $\phi_{0.1}$ |
| x3o    | 0.4 | 35 | 0.4 | 2.20  | 3.00 | $\phi_{0.1}$ |
| x3oe2  | 0.4 | 35 | 0.8 | 2.85  | 3.00 | $\phi_{0.1}$ |
| x4o    | 0.6 | 15 | 0.6 | 5.32  | 4.50 | $3\%b_0$ |
| x5oe05 | 0.6 | 24 | 0.3 | 3.50  | 4.50 | $3\%b_0$ |
| x5o    | 0.6 | 24 | 0.6 | 4.74  | 4.50 | $3\%b_0$ |
| x5oe2  | 0.6 | 24 | 1.2 | 7.07  | 4.50 | $3\%b_0$ |
| x6oe05 | 0.6 | 35 | 0.3 | 3.44  | 4.50 | $3\%b_0$ |
| x6o    | 0.6 | 35 | 0.6 | 4.47  | 4.50 | $3\%b_0$ |
| x6oe2  | 0.6 | 35 | 1.2 | 6.25  | 4.50 | $3\%b_0$ |
| x7o    | 0.8 | 15 | 0.8 | 11.57 | 3.26 | Max. |
| x8oe05 | 0.8 | 24 | 0.4 | 7.66  | 4.50 | $3\%b_0$ |
| x8o    | 0.8 | 24 | 0.8 | 10.87 | 3.45 | Max. |
| x8oe2  | 0.8 | 24 | 1.6 | 16.13 | 1.47 | Max. |
| x9oe05 | 0.8 | 35 | 0.4 | 7.29  | 4.50 | $3\%b_0$ |
| x9o    | 0.8 | 35 | 0.8 | 10.22 | 4.50 | $3\%b_0$ |
| x9oe2  | 0.8 | 35 | 1.6 | 14.92 | 2.24 | Max. |
| x13o   | 0.2 | 35 | 0.2 | 1.14  | 1.50 | $\phi_{0.1}$ |
| x13oe2 | 0.2 | 35 | 0.4 | 1.45  | 1.50 | $\phi_{0.1}$ |

**Table 6.14** **Numerical results of uniplanar X-joints loaded with out-of-plane bending moments ($\beta=1.0$)**

| Joint | Geometrical parameters | | | Numerical results | | | |
|---|---|---|---|---|---|---|---|
| | $\beta$ | $2\gamma$ | $\eta$ | $M_{1,opb,u}/(f_{y0}t_0^2b_0)$ | $M_{1,opb,u}$ (kNm) | $\delta_u$ | Criteria |
| x10oe05* | 1.00 | 15 | 0.5 | 15.10 | 80.41 | 4.40 | Max. |
| x10oe* | 1.00 | 15 | 1.0 | 22.43 | 119.44 | 2.32 | Max. |
| x10oe2* | 1.00 | 15 | 2.0 | 36.15 | 192.50 | 1.19 | Max. |
| x11o* | 1.00 | 24 | 1.0 | 28.54 | 59.37 | 0.50 | Max. |
| x11oe2* | 1.00 | 24 | 2.0 | 52.23 | 108.64 | 0.18 | Max. |
| x12oe05* | 1.00 | 35 | 0.5 | 23.51 | 23.04 | 0.54 | Max. |
| x12o* | 1.00 | 35 | 1.0 | 37.98 | 37.22 | 0.16 | Max. |
| x12oe2* | 1.00 | 35 | 2.0 | 64.02 | 62.74 | 0.09 | Max. |

*: without weld

### 6.3.5. The ultimate moment capacity of joints with chord face plastification

For the joints with a chord top face plastification failure, the analytical formula based upon the yield line theory is given in equation (5.34):

$$M_{1,opb,Rd} = f_{y0}t_0^2b_1\left(\frac{\eta(1+\beta)}{2\beta(1-\beta)} + \sqrt{\frac{2(1+\beta)}{\beta(1-\beta)}}\right) \tag{5.34}$$

Equation (5.34) has also been used as the design resistance moment in the CIDECT design guide.

Comparison between the numerical results in Table 6.13 and the CIDECT design formula, equation (5.34) is shown in Figure 6.28. It can be seen that the CIDECT formula is sometimes very conservative compared to the FE results. A more efficient ultimate moment capacity formula can be obtained by introducing a revision to equation (5.34), similar as discussed for axially loaded joints, see Section 6.1:

$$M_{1,opb,u} = f_{y0} t_0^2 b_1 \left( \frac{\eta(1+\beta)}{2\beta(1-\beta)} + \sqrt{\frac{2(1+\beta)}{\beta(1-\beta)}} \right) f(\beta,\eta) \tag{6.6}$$

The revision function is defined as follows:

$$f(\beta,\eta) = R_1 + R_2*\beta + R_3*\eta \tag{6.7}$$

The values of $R_1$ to $R_3$ can be determined using non-linear regression analysis of the numerical results. The regression results are listed in Table 6.15. The formulae for the mean value, the coefficient of variation (CoV) and the correlation coefficient ($R^2$) can be found in equations (4.9) to (4.12), Chapter 4. The mean normalised error is based upon the FE result divided by equation (6.6).

**Table 6.15    Regression result for chord top face yielding**

| $R_1$ | $R_2$ | $R_3$ | Mean normalised error | Coefficient of variation (CoV) | Correlation coefficient ($R^2$) |
|-------|-------|-------|------------------------|--------------------------------|----------------------------------|
| 1.0 | 0.5 | 0.0 | 1.046 | 0.087 | 0.964 |

The FE results and equation (6.6), obtained after the regression analysis, are compared in Figure 6.29.
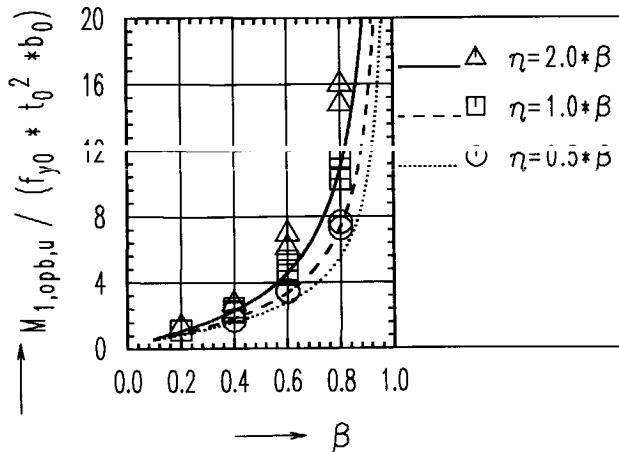


**Figure 6.28    Comparison between the FE results and the CIDECT formula ($\beta \leq 0.8$)**
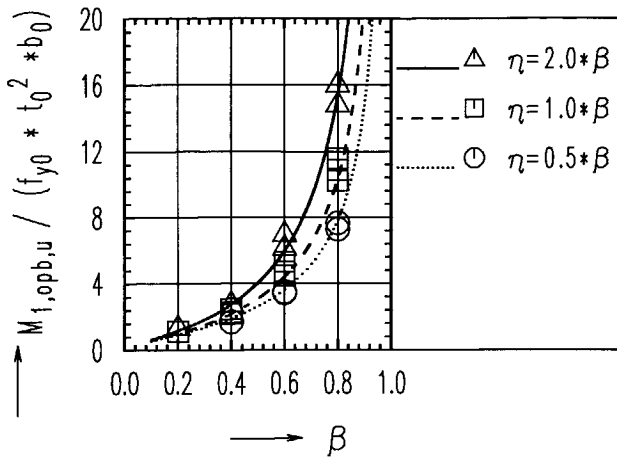
**Figure 6.29  The FE results and the ultimate moment capacity formula** ($\beta \leq 0.8$)

### 6.3.6.  The ultimate moment capacity of joints with chord web yielding or buckling

For all the joints with $\beta=1.0$, a maximum moment capacity is reached as shown in Figure 6.27. The failure mode for such joints is very similar to that for axially loaded joints.

**Comparison with the CIDECT formula**

In order to compare the FE results with the CIDECT formula, the CIDECT design formula has to be written in characteristic form (i.e., without the $\gamma_M$ factor of 1.25) as described in Chapter 5:

$$M_{1,opb,k} = \frac{1}{\beta}(2\gamma\eta+5)(1-\frac{1}{2\gamma})f_{y0}t_0^2b_1 \qquad (5.36)$$

The comparison between the FE results and equation (5.36) is shown in Figure 6.30. It can be seen that the CIDECT formula without the $\gamma_M$ factor of 1.25 is unsafe for joint with $2\gamma=35$ and $\eta=2.0$. Because full width joints with larger $2\gamma$ (actually $h_0/t_0$) and larger $\eta$ values are more sensitive for local buckling of the chord side wall. However, this has not been included in the CIDECT formula. A quantitative comparison between the FE results and the CIDECT formula is listed in Table 6.16. The $\delta_u$ values in Table 6.16 are the indentations corresponding to the maximum moment.
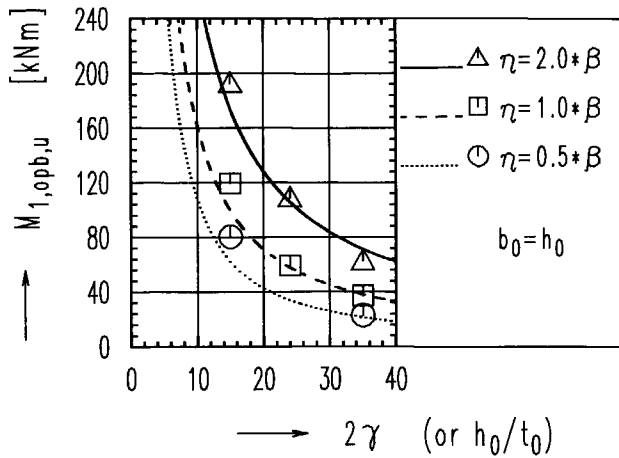
**Figure 6.30 Comparison between the FE results and the CIDECT formula ($\beta$=1.0)**

**Table 6.16**     **Comparisons between the FE results, the CIDECT formula and the "4-hinge yield line and web buckling" formula ($\beta$=1.0)**

| Joints | $2\gamma$ | $\eta$ | $\delta_u$ mm | $\kappa$ | $M_{1,opb,u}$ (kNm) eq. 5.44 (1) | CIDECT eq. 5.36 (2) | FE results (3) | $\dfrac{(3)}{(1)}$ | $\dfrac{(3)}{(1)}$ |
|---|---|---|---|---|---|---|---|---|---|
| x10oe05[*] | 15 | 0.5 | 4.40 | 0.98 | 68.64 | 62.13 | 80.41 | 1.173 | 0.77 |
| x10o[*] | 15 | 1.0 | 2.32 | 0.98 | 107.79 | 99.40 | 119.44 | 1.109 | 0.83 |
| x10oe2[*] | 15 | 2.0 | 1.19 | 0.98 | 186.06 | 173.95 | 192.50 | 1.036 | 0.90 |
| x11o[*] | 24 | 1.0 | 0.30 | 0.92 | 59.47 | 57.81 | 59.37 | 0.993 | 0.97 |
| x11oe2[*] | 24 | 2.0 | 0.18 | 0.92 | 105.40 | 105.65 | 108.64 | 1.026 | 0.97 |
| x12oe05[*] | 35 | 0.5 | 0.54 | 0.82 | 20.88 | 21.42 | 23.04 | 1.098 | 0.93 |
| x12o[*] | 35 | 1.0 | 0.16 | 0.82 | 34.95 | 38.08 | 37.22 | 1.060 | 1.02 |
| x12oe2[*] | 35 | 2.0 | 0.09 | 0.82 | 63.07 | 71.40 | 62.74 | 0.990 | 1.14 |
| Mean | | | | | | | | 1.061 | 1.074 |
| CoV | | | | | | | | 0.060 | 0.120 |
| $R^2$ | | | | | | | | 0.987 | 0.957 |
| $\beta$=1.0    $f_{y0}$=355 N/mm$^2$ | | | | | | | | | |

[*]: Without weld

**Comparison with the '4-hinge yield line and chord web buckling" model**

In Chapter 5, equation (5.44) is derived based upon the "4-hinge yield line and chord web buckling" model:

$$M_{1,opb,u} = \kappa\left(\sqrt{2(1+2\gamma)} + 2\gamma\eta\right)f_{y0}t_0^2 b_1 \tag{5.44}$$

In this formula, a buckling reduction factor $\kappa$ is introduced. The $\kappa$ value can be determined according to equations (5.13) to (5.17), Chapter 5.

The FE results are compared with equation (5.44) in Figure 6.31 and Table 6.16. It can be seen that there is a good agreement between the FE results and the "4-hinge yield line and chord web buckling" model. From Table 6.16, it can be seen that the larger the $2\gamma$ value (actually $h_0/t_0$), the smaller the deformation $\delta_u$ at maximum load, due to chord side wall buckling.
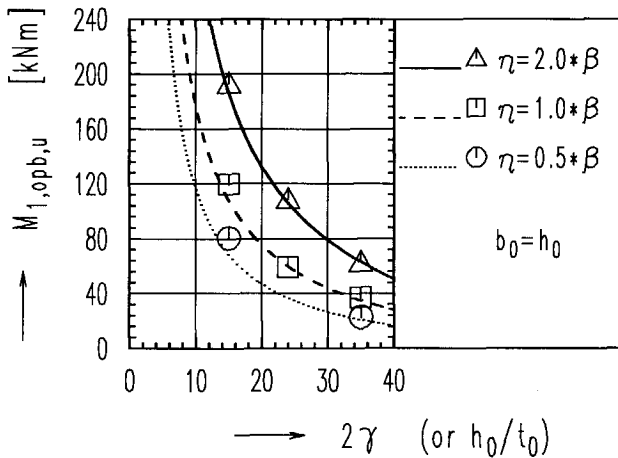


**Figure 6.31** **Comparison between the FE results and the "4-hinge yield line and web buckling" model ($\beta=1.0$)**

### 6.3.7. Conclusions

-   For joints with a chord top face plastification failure, the CIDECT formula based upon the yield line theory is conservative compared to the FE results. The ultimate moment capacity formula is derived by introducing a revision function equation (6.7) to the CIDECT formula.

-   For full width joints with a chord side wall failure, the CIDECT formula without the

$\gamma_M$ factor of 1.25 is unsafe for joint with $2\gamma=35$ and $\eta=2.0$ compared to the numerical results. The ultimate moment capacity formula equation (5.44) based upon the "4-hinge yield line and web buckling" model is calibrated well with the numerical results.

## 6.4  INFLUENCE OF THE CHORD AXIAL PRELOADING ON THE ULTIMATE LOAD CAPACITY OF X-JOINTS

### 6.4.1  Introduction

In Chapter 5, it has been analytically described that the joint ultimate load capacity is reduced by the existence of the axial stresses in the chord due to the reduction of the plastic moment of the yield lines when the axial stresses are inclined or normal to the yield lines. The axial stresses can be caused by axial forces or bending moments in the chord of an X-joint or bending moments in the chord of a T-joint. The influence of the chord bending moments on the ultimate load capacity of a T-joint and an X-joint has been numerically investigated (Yu 1995, 1996d). The same interaction formula between the joint ultimate load capacity and the chord bending moments has been recommended for both T- and X-joints when the moment resistance of the chord section was determined according to section classes 1, 2 or 3 (EC3 1992). According to the experimental results of K- and T-joints (Wardenier 1974, 1976 and Barentse 1976), the axial compression stresses in the chord reduce the joint strength, while the axial tensile stresses in the chord increase the joint strength due to the membrane action. In this section, only the influence of the compressive preloading in the chord is studied numerically. Configuration of an X-joint is shown in Figure 6.32 where the joint is loaded with axial forces in the braces and axial preloading in the chord.
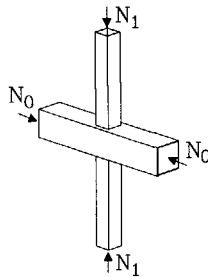


**Figure 6.32**   **Configuration of an X-joint loaded with axial forces in the braces and axial compressive preloading in the chord**

According to EC3 (1992), the design compression resistance for different classes of cross-sections can be determined as follows:

For class 1, 2 or 3 cross-sections:

$$N_{0,Rd} = A f_{y0} / \gamma_{M0} \tag{6.8}$$

For class 4 cross-sections:

$$N_{0,Rd} = A_{eff} f_{y0} / \gamma_{M1} \tag{6.9}$$

Where A is the area of the chord cross-section; $A_{eff}$ is the effective area of the cross-section; $N_{0,Rd}$ is the axial resistance of the chord; $f_{y0}$ is the yield stress of the chord; $\gamma_{M0}=1$ and $\gamma_{M1}=1.1$ according to EC3. In this study, section class 4 is excluded.

The ratio of the axial preloading in the chord is defined by the following equation:

$$n = \frac{N_0}{N_{0,Rd}} = \frac{\sigma_0}{f_{y0}} \tag{6.10}$$

Where $\sigma_0$ is the axial stress in the chord corresponding to $N_0$. Theoretically speaking, if the axial preloading in the chord is equal to the design compression resistance of the cross-section, the ultimate load capacity of the joint is reduced to zero. Different axial preloading ratios are used in the numerical parameter study in order to establish the interaction relation between the ratio of the axial preloading and the ultimate load capacity of the joint.

### 6.4.2   Research programme

The numerical parameter study consists of X-joints loaded with axial forces on the braces and axial compressive preloading on the chord. The joint geometrical parameters are summarised in Table 6.17. For each joint with a specific set of geometrical parameters, four axial preloading ratios are included with n=0, 0.4, 0.6 and 0.8 respectively. In total, 48 joints have been analysed. Obviously, for n=0, the joints are the same as in Section 6.1. For joints with $2\gamma=15$ and 24, the chord cross sections are class 1, while for joints with $2\gamma=35$, the chord cross sections are class 3. The nominal geometrical dimensions and the material properties of the joints and the weld are the same as in Section 6.1. The only difference is the load case.

**Table 6.17   Research programme for X-joints loaded with axial forces in the braces and axial preloading in the chord**

| $2\gamma$ | $\beta$ | | | |
|---|---|---|---|---|
| | 0.4 | 0.6 | 0.8 | 1.0 |
| 15 | x1a | x4a | x7a | x10a[*] |
| 24 | x2a | x5a | x8a | x11a[*] |
| 35 | x3a | x6a | x9a | x12a[*] |
| n=0, 0.4, 0.6, 0.8;    $f_{y0}=355$ N/mm$^2$ | | | | |

[*]: Without weld.

### 6.4.3 The FE analysis

The numerical model is the same as used in Section 6.1. The axial compressive forces are pre-loaded at the ends of the chord with one load step. After that, the axial forces on the braces are applied by displacement control. Considering symmetry of load and geometry, 1/8 of a joint is analysed. The material properties and boundary conditions are also the same as used in Section 6.1.

### 6.4.4 The numerical results

The numerical results of the joints with different geometrical parameters are shown in Figure 6.33. For each joint with the same $\beta$ and $2\gamma$ values, 4 axial preloading ratios are included with n=0, 0.4, 0.6 and 0.8 respectively. The chord top face indentation at the ultimate deformation limit of $3\%b_0$ is indicated in the figures. The ultimate load capacity of a joint is defined as the maximum from the load versus indentation curves if it is reached before the ultimate deformation limit. Otherwise it is taken as the load at $3\%b_0$ indentation. The non-dimensional ultimate load capacity of each joint is listed in Table 6.18.

According to the numerical results of the load vs. indentation curves in Figure 6.33, three failure modes can be distinguished, namely, failure dominated by chord top face plastification, failure dominated by chord prestressing or failure dominated by chord web buckling. The word "dominated" is used because the joints fail actually as the result of an interaction of the forces applied on the braces and those on the chord.

The first failure mode occurs for joints with small to medium $\beta$ values and small axial preloading ratios. The load capacity for such joints is increasing with the increase of chord top face indentation. A maximum load is not reached for such joints. In such cases, there is a clear influence of the chord axial preloading on the ultimate load capacity. As a general tendency, with the increase of the axial preloading ratio, the ultimate load capacity of the joint decreases.

The second failure mode occurs for joints with small to medium $\beta$ values, large $2\gamma$ values and high axial preloading ratios. This failure mode can be identified from the load vs. indentation curves where the load decreases abruptly after the maximum load is reached. The ultimate load capacity of such joints is reduced considerably due to the large reduction of the membrane effects by the compressive preloading in the chord.

The third failure mode occurs for joints with $\beta=1.0$. The load vs. indentation curves of the joints with chord axial preloading are similar to those of the joints without axial preloading. Thus, similar failure modes occur for joints with or without chord axial preloading. The influence of the chord preloading is very small for such joints.

From the above observations, it can be concluded that the influence of axial preloading in the chord depends upon the modes of failure and the modes of failure depend upon the joint geometrical parameters and the axial preloading ratios. The most significant influence of the chord axial preloading is found for joints dominated by a failure of chord prestressing. While the influence of the axial preloading for joints dominated by a failure of chord web buckling is very small.
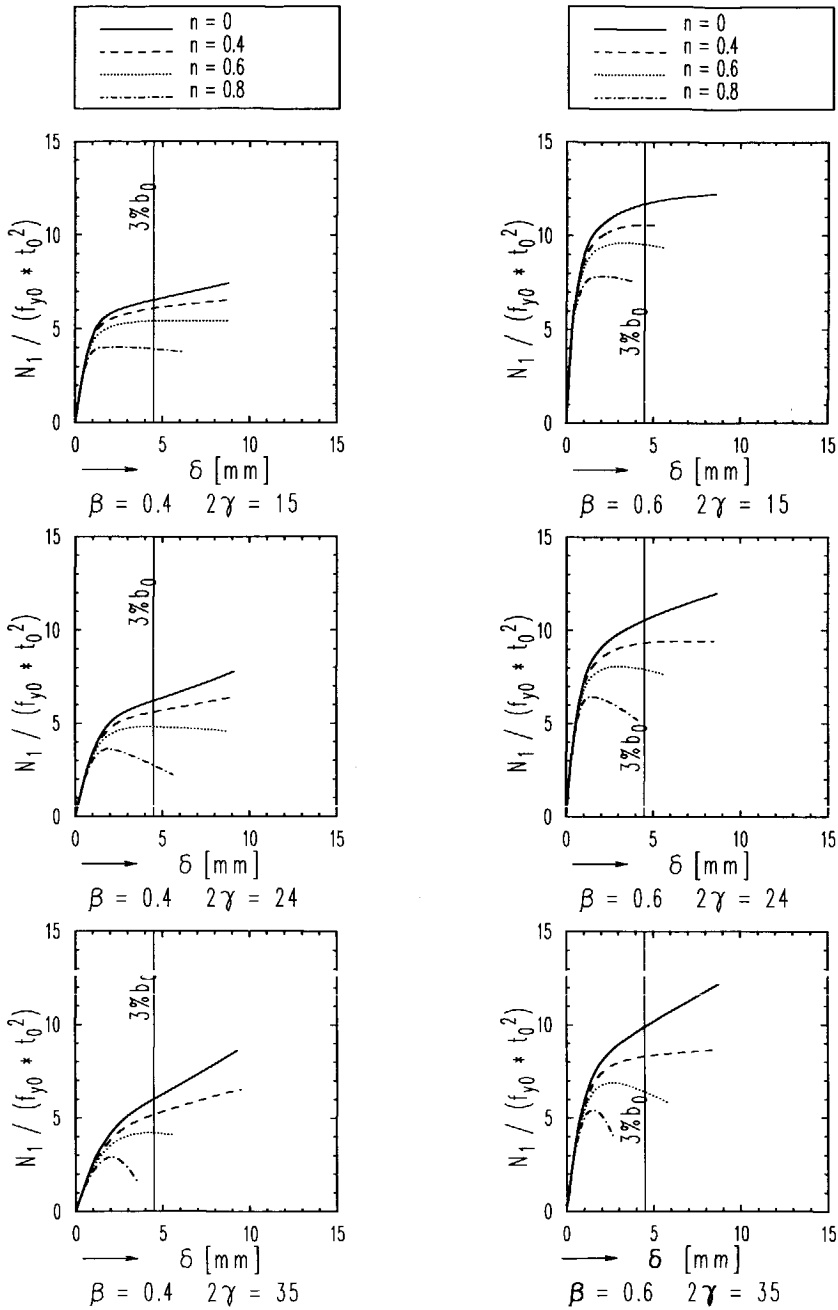
**Figure 6.33**　　　　**Numerical results of axially loaded X-joints with chord axial preloading**
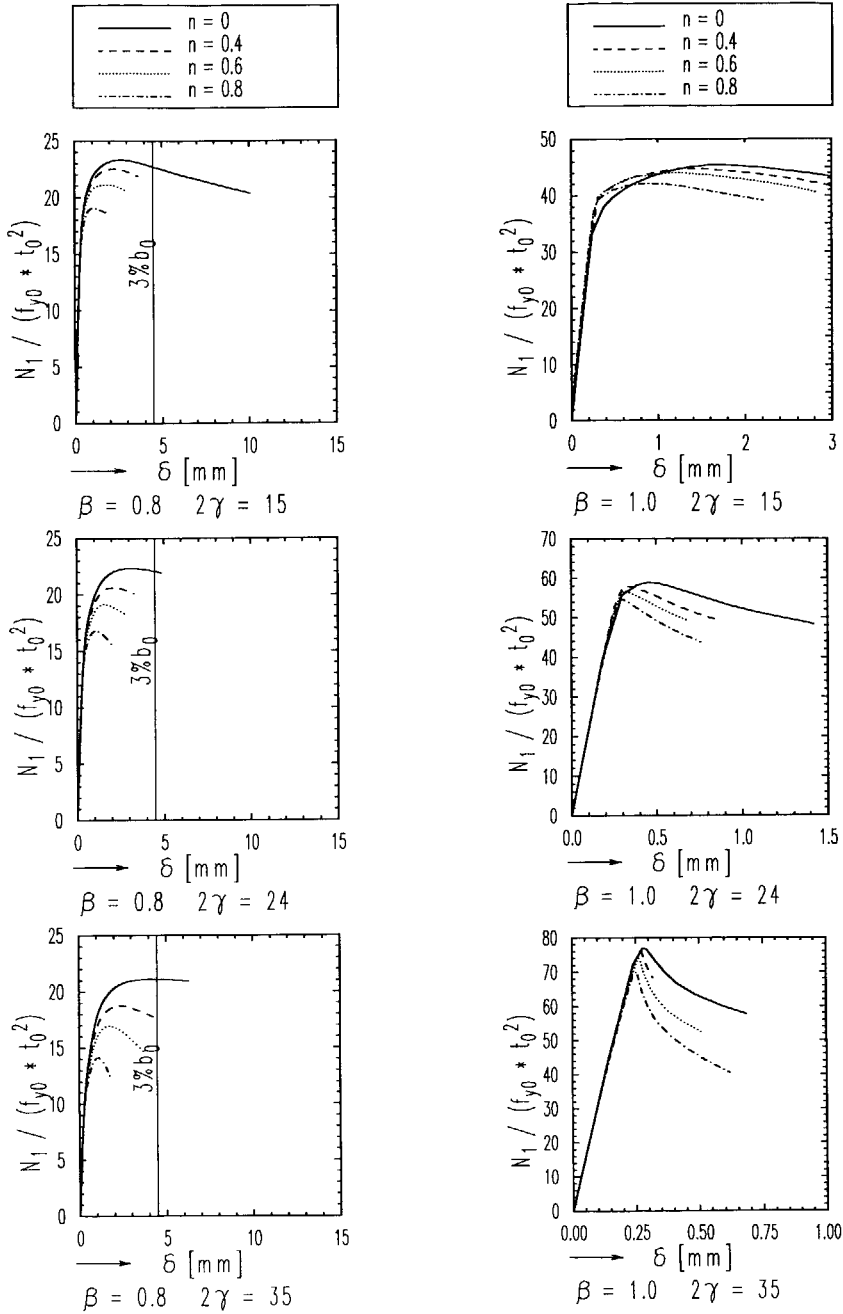
**Figure 6.33** (continued)

**Table 6.18**          **Numerical results of axially loaded X-joints with different chord axial preloading ratios**

|         | β   | 2γ  | $N_{1,u}(n)/(f_{y0}t_0^2)$ | | | |
|---------|-----|-----|-------|--------|--------|--------|
|         |     |     | n=0   | n=0.4  | n=0.6  | n=0.8  |
| x1a     | 0.4 | 15  | 6.55  | 6.10   | 5.41   | 4.04   |
| x2a     | 0.4 | 24  | 6.23  | 5.62   | 4.83   | 3.64   |
| x3a     | 0.4 | 35  | 6.00  | 5.18   | 4.21   | 2.90   |
| x4a     | 0.6 | 15  | 11.68 | 10.56  | 9.60   | 7.84   |
| x5a     | 0.6 | 24  | 10.56 | 9.35   | 8.07   | 6.45   |
| x6a     | 0.6 | 35  | 9.88  | 8.32   | 6.90   | 5.47   |
| x7a     | 0.8 | 15  | 23.32 | 22.50  | 21.10  | 19.03  |
| x8a     | 0.8 | 24  | 22.32 | 20.61  | 19.15  | 16.78  |
| x9a     | 0.8 | 35  | 21.10 | 18.80  | 16.99  | 14.15  |
| x10a[*] | 1.0 | 15  | 45.37 | 44.71  | 43.99  | 42.04  |
| x11a[*] | 1.0 | 24  | 58.89 | 57.90  | 56.75  | 54.60  |
| x12a[*] | 1.0 | 35  | 76.81 | 76.23  | 74.10  | 70.27  |

[*]: Without weld.

### 6.4.5   The interaction formula between the joint ultimate load capacity and the chord axial preloading

The reduction function of the joint ultimate load capacity due to the axial preloading in the chord is defined as:

$$f(n) = \frac{N_{1,u}(n)}{N_{1,u}(n=0)} \tag{6.11}$$

Where $N_{1,u}(n)$ is the joint ultimate load capacity with axial preloading ratio n and $N_{1,u}(n=0)$ is that with axial preloading ratio n=0, i.e., an X-joint loaded only with axial forces on the braces. Based upon this definition, the interaction data points of $\{f(n),n\}$ can be obtained from Table 6.18 which are used for the regression analysis for the determination of the interaction formula.

The interaction contours between the normalised ultimate load capacity and the axial preloading ratio are shown in Figure 6.34 for four β values.
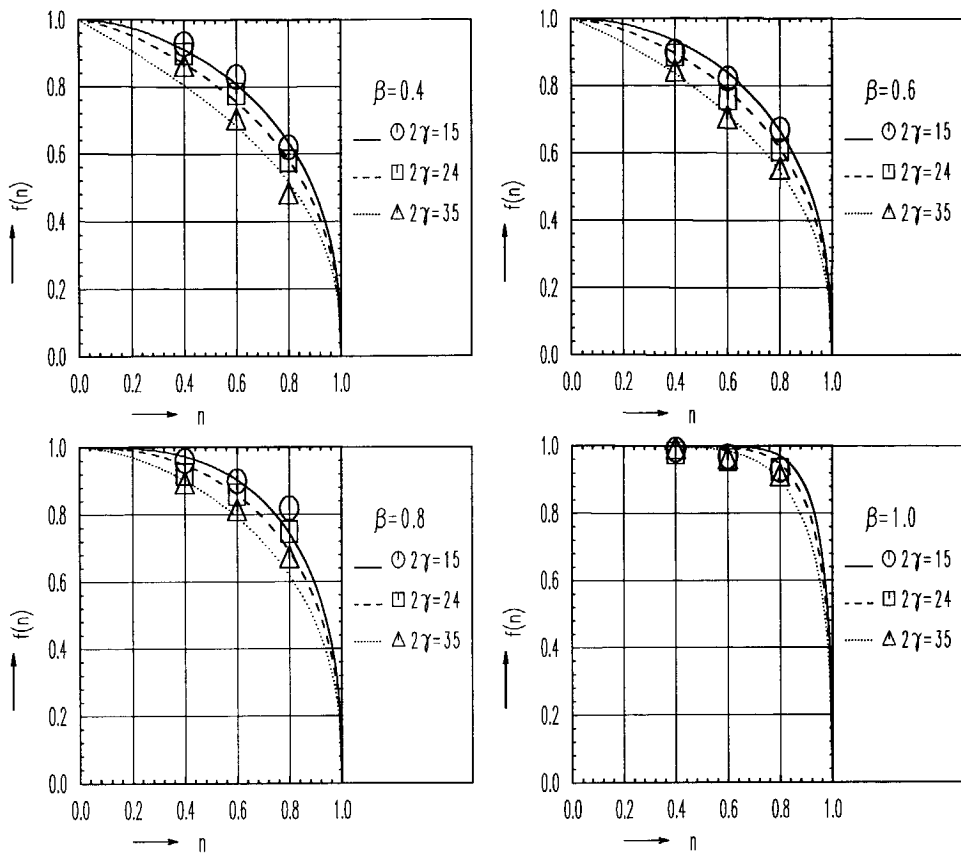
**Figure 6.34**    **Interaction contours from the numerical results of X-joints loaded with chord axial preloading**

For each β value, three 2γ values are included. Following general tendency can be found from Figure 6.34:

- The influence of the chord axial preloading is decreasing with increasing β values. For β=1.0, the influence of the axial preloading is very small.

- The influence of the axial preloading is increasing with increasing 2γ values. Namely, the joint ultimate load capacity is decreasing with decreasing chord wall thickness for a joint with the same β value and the same axial preloading ratio. Especially for joints with 2γ=35, the reduction of the joint ultimate load capacity is significant. However, if only the data points for joints with 2γ=15 and 24 are considered, there is only a slight 2γ influence which is the same tendency as observed in previous investigations for the influence of chord bending moments on the ultimate load capacity of T- and X-joints (Yu 1995 and 1996c). In the previous study for chord bending, the 2γ

influence on the reduction of the joint ultimate load capacity was neglected but the design resistance moment of the chord section was calculated according to section classes (class 1 for joints with $2\gamma=15$ and 24 and class 3 for joints with $2\gamma=35$, $f_{y0}=355$ N/mm$^2$). For section class 1, the plastic bending moment of the section was used while for section class 3, the elastic bending moment of the section was used. Thus, the influence for joints with $2\gamma=35$ would be larger if the plastic moment of such sections was used as design resistance moment instead of the elastic moment of the section. This influence is further discussed in Section 6.5.

Theoretically speaking, if n=0, then f(n)=1.0, while if n=1, then f(n)=0. Based upon these considerations and the general tendency observed, i.e., the influence of n is large for small $\beta$ and large $2\gamma$ values, the following interaction formula is used:

$$f(n) = \left(1 - n^{f(\beta,\gamma)}\right)^{R_1} \tag{6.12}$$

Where

$$f(\beta,\gamma) = \frac{2}{(1 + R_2\gamma^{R_3})(1 - R_4\beta^{R_5})} \tag{6.13}$$

n and f(n) are defined in equations (6.10) and (6.11).

A nonlinear regression analysis is carried out using the FE results in Table 6.18. The regression results are listed in Table 6.19.

**Table 6.19  Regression results of equations (6.12) and (6.13)**

| $R_1$ | $R_2$ | $R_3$ | $R_4$ | $R_5$ | Mean normalised error | Coefficient of Variation (CoV) | Correlation coefficient ($R^2$) |
|-------|-------|-------|-------|-------|-----------------------|--------------------------------|----------------------------------|
| 0.4 | 0.004 | 2 | 0.85 | 3 | 1.002 | 0.035 | 0.959 |

A reasonable correlation coefficient and a very low coefficient of variation is found in Table 6.19. It is shown in Section 6.5 that equations (6.12) and (6.13) can also be used for both T-joints and X-joints loaded with axial forces on the braces and bending moments on the chord if the design resistance moment of the chord section is calculated according to its plastic moment only.

### 6.4.6 Comparison with the CIDECT formula

In the CIDECT design guide (Packer 1992a), a reduction function given by Wardenier (1982a) has been used to determine the influence of the chord axial preloading:

$$f(n) = 1.3 - \frac{0.4}{\beta} n \qquad (6.14)$$

Where n can be found in equation (6.10).

A comparison between equation (6.12) and (6.14) is shown in Figure 6.35. It can be seen that, compared to the numerical results for X-joints, the CIDECT formula is on the unsafe side except for X-joints with small β values.
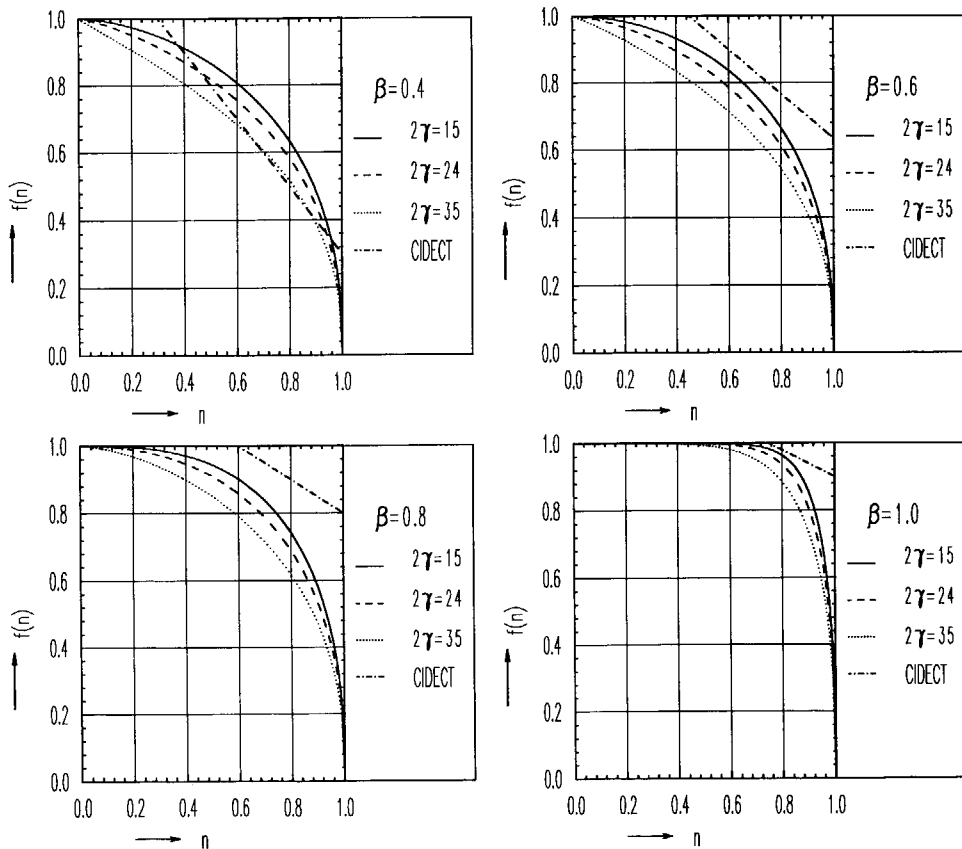


**Figure 6.35**  **Comparison between the FE results and the CIDECT formula**

### 6.4.7   Conclusions

This section deals with the investigation into the influence of the chord axial preloading on the joint ultimate load capacity. This influence depends upon the modes of failure and the modes of failure depend upon both joint geometrical parameters and chord preloading ratios. For joints with small to medium $\beta$ values, large $2\gamma$ values and high axial preloading ratios, failure of the joint is dominated by the preloading. In such a case, the joint ultimate load capacity is reduced considerably due to the preloading, because the membrane effects are largely reduced by the preloading. The smallest preloading effect is found for joints with $\beta=1.0$. For joints with other $\beta$ and $2\gamma$ values, the preloading effect is between the two extreme cases. A reduction formula equation (6.12) based upon the numerical results is derived.

## 6.5 INFLUENCE OF THE CHORD BENDING MOMENTS ON THE ULTIMATE LOAD CAPACITY OF X-JOINTS

### 6.5.1 Introduction

This section deals with the numerical analysis of the ultimate load capacity of X-joints loaded with axial forces in the braces and bending moments in the chord, as shown in Figure 6.36. In Section 6.4, the influence of the chord axial preloading on the ultimate load capacity of an X-joint has been numerically investigated. It has been found that the reduction of the joint ultimate load capacity is not only a function of the preloading ratios and the $\beta$ values but also a function of the $2\gamma$ values. For joints with $2\gamma=15$ and $2\gamma=24$, the reduction of the joint ultimate load capacity due to the axial preloading is rather similar, while for joints with $2\gamma=35$, the reduction of the joint ultimate load capacity is more pronounced, see Figure 6.34, in Section 6.4.

However, according to the previous investigations into the influence of the chord bending moments on the ultimate load capacity of a T- and an X-joint (Yu 1995, 1996d), it was shown that the reduction of the joint ultimate load capacity is a function of the moment ratios and the $\beta$ values and the influence of the $2\gamma$ values was omitted. This conclusion was based upon the fact that the design resistance moment was determined according to section classes (EC3 1992). For section classes 1 and 2, the plastic moment capacity was used as the design resistance moment of the chord section. While for section class 3, the elastic moment capacity was used. If only the plastic moment capacity of the chord is used as the design resistance moment or if only the elastic moment capacity of the chord is used as the design resistance moment independent of the section classes, the reduction function will be different. In this section, the above three methods are used as a comparison.
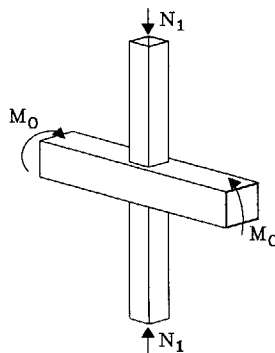


**Figure 6.36 X-joint loaded with axial forces and bending moments**

**6.5.2   Research programme**

The numerical research programme is given in Table 6.20 which consists of X-joints loaded with axial forces on the braces and in-plane bending moments on the chord. The joint geometrical parameters are $\beta$=0.4, 0.6, 0.8, 1.0 and $2\gamma$=15, 24, 35 respectively. For each joint with a specific set of geometrical parameters, four moment ratios are included with $J_m$=0, 0.4, 0.6 and 0.8 respectively, where the moment ratio is defined in Chapter 5 according to EC3 (1992):

$$J_m = \begin{cases} M_0/M_{pl,Rd} & \text{(class 1 or 2)} \\ M_0/M_{el,Rd} & \text{(class 3)} \end{cases} \tag{5.47}$$

Where $M_{pl,Rd}$ is the design plastic resistance moment of the chord cross-section and $M_{el,Rd}$ is the design elastic resistance moment of the chord cross-section, see equations (5.45) and (5.46). For joints with $2\gamma$=15 and 24, the chord cross-sections are class 1, while for joints with $2\gamma$=35, the chord cross-sections are class 3 in the present study. For class 1, 2 or 3 cross-sections, the partial safety factor $\gamma_{M0}$=1.0 (EC3 1992).

$$M_{pl,Rd} = W_{pl} f_{y0}/\gamma_{M0} \qquad \text{(class 1 or 2)} \tag{5.45}$$

$$M_{el,Rd} = W_{el} f_{y0}/\gamma_{M0} \qquad \text{(class 3)} \tag{5.46}$$

**Table 6.20   Research programme for X-joints loaded with axial forces in the braces and bending moments in the chord**

| Section classes | $2\gamma$ | $\beta$ | | | |
|---|---|---|---|---|---|
| | | 0.4 | 0.6 | 0.8 | 1.0 |
| 1 | 15 | x1a | x4a | x7a | x10a[*] |
| 1 | 24 | x2a | x5a | x8a | x11a[*] |
| 3 | 35 | x3a | x6a | x9a | x12a[*] |
| According to EC3: $J_m$=0, 0.4, 0.6, 0.8 | | | | $f_{y0}$=355 N/mm$^2$ | |

[*]: Without weld.

If the design resistance moment of the chord cross-section is calculated only according to its plastic moment capacity or only to its elastic moment capacity, the values of the moment ratio in Table 6.20 are changed according to the shape factor of the chord cross-section which is given as follows for a square hollow section:

$$\alpha_s = \frac{W_{pl}}{W_{el}} = \frac{\frac{1}{4}\left(b_0^3 - (b_0 - 2t_0)^3\right)}{\frac{1}{6b_0}\left(b_0^4 - (b_0 - 2t_0)^4\right)} = \frac{3\left(1 - (1 - \frac{2}{2\gamma})^3\right)}{2\left(1 - (1 - \frac{2}{2\gamma})^4\right)}$$
(6.15)

The values of the shape factor for the joints with $2\gamma=15$, 24 and 35 are 1.2, 1.17 and 1.16 respectively.

In Table 6.21, the moment ratios based upon only the plastic or only the elastic moment capacity of the chord-section are compared with those based upon EC3.

**Table 6.21    Moment ratios based upon three methods**

| Based upon | $2\gamma$ | Moment ratios | | |
|---|---|---|---|---|
| EC3 | 15 | 0.4 | 0.6 | 0.8 |
| | 24 | 0.4 | 0.6 | 0.8 |
| | 35 | 0.4 | 0.6 | 0.8 |
| Only $M_{pl.Rd}$ | 15 | 0.4 | 0.6 | 0.8 |
| | 24 | 0.4 | 0.6 | 0.8 |
| | 35 | 0.35 | 0.52 | 0.69 |
| Only $M_{el.Rd}$ | 15 | 0.48 | 0.72 | 0.96 |
| | 24 | 0.47 | 0.71 | 0.94 |
| | 35 | 0.4 | 0.6 | 0.8 |
| $f_{y0}=355$ N/mm$^2$ | | | | |

The dimensions and the material properties of the joints and the weld are exactly the same as those in Section 6.1. The only difference is the load case.

### 6.5.3   The FE analysis

The general considerations for the numerical models are described in Chapter 4. The chord bending moments are pre-loaded in one step by applying opposite axial forces on the top and the bottom faces of the chord ends. After the chord bending moments are pre-loaded to a prescribed moment ratio, the axial forces on the braces are applied by displacement control considering its efficiency in convergency. Considering symmetry of load and geometry, a quarter of a joint is analysed.

### 6.5.4   The numerical results and observations

Figure 6.37 shows the non-dimensional load versus chord top face indentation curves for the joints with different geometrical parameters. For each set of $\beta$ and $2\gamma$ values, 4 moment ratios are included. The chord top face indentation at $3\%b_0$ is indicated in the figures. It can be seen from Figure 6.37 that the joint ultimate load capacity is decreased with the increase of the moment ratio. For joints with $\beta=1.0$, the influence of the moment ratio on the joint ultimate load capacity is smaller than that for joints with other $\beta$ ratios. The non-dimensional ultimate load capacity of the joints based upon the procedure in Chapter 4 is listed in Table 6.22.

**Table 6.22    Numerical results of axially loaded X-joints with different moment ratios**

| Section classes | Joints | $N_{1,u}(J_m)/(f_{y0}t_0^2)$ | | | |
|---|---|---|---|---|---|
| | | $J_m=0$ | $J_m=0.4$ | $J_m=0.6$ | $J_m=0.8$ |
| 1 | x1a | 6.55 | 5.95 | 5.24 | 3.85 |
| 1 | x2a | 6.23 | 5.52 | 4.80 | 3.63 |
| 3 | x3a | 6.00 | 5.31 | 4.69 | 3.73 |
| 1 | x4a | 11.68 | 10.72 | 9.66 | 7.75 |
| 1 | x5a | 10.56 | 9.46 | 8.40 | 6.86 |
| 3 | x6a | 9.88 | 8.79 | 7.86 | 6.50 |
| 1 | x7a | 23.32 | 22.48 | 21.05 | 18.32 |
| 1 | x8a | 22.32 | 21.28 | 20.10 | 17.66 |
| 3 | x9a | 21.10 | 19.80 | 18.83 | 17.38 |
| 1 | x10a[*] | 45.37 | 44.78 | 44.21 | 42.02 |
| 1 | x11a[*] | 58.89 | 58.18 | 56.67 | 51.92 |
| 3 | x12a[*] | 76.81 | 75.30 | 73.92 | 71.71 |
| The moment ratios are based upon EC3 | | | | | |

[*]: Without weld
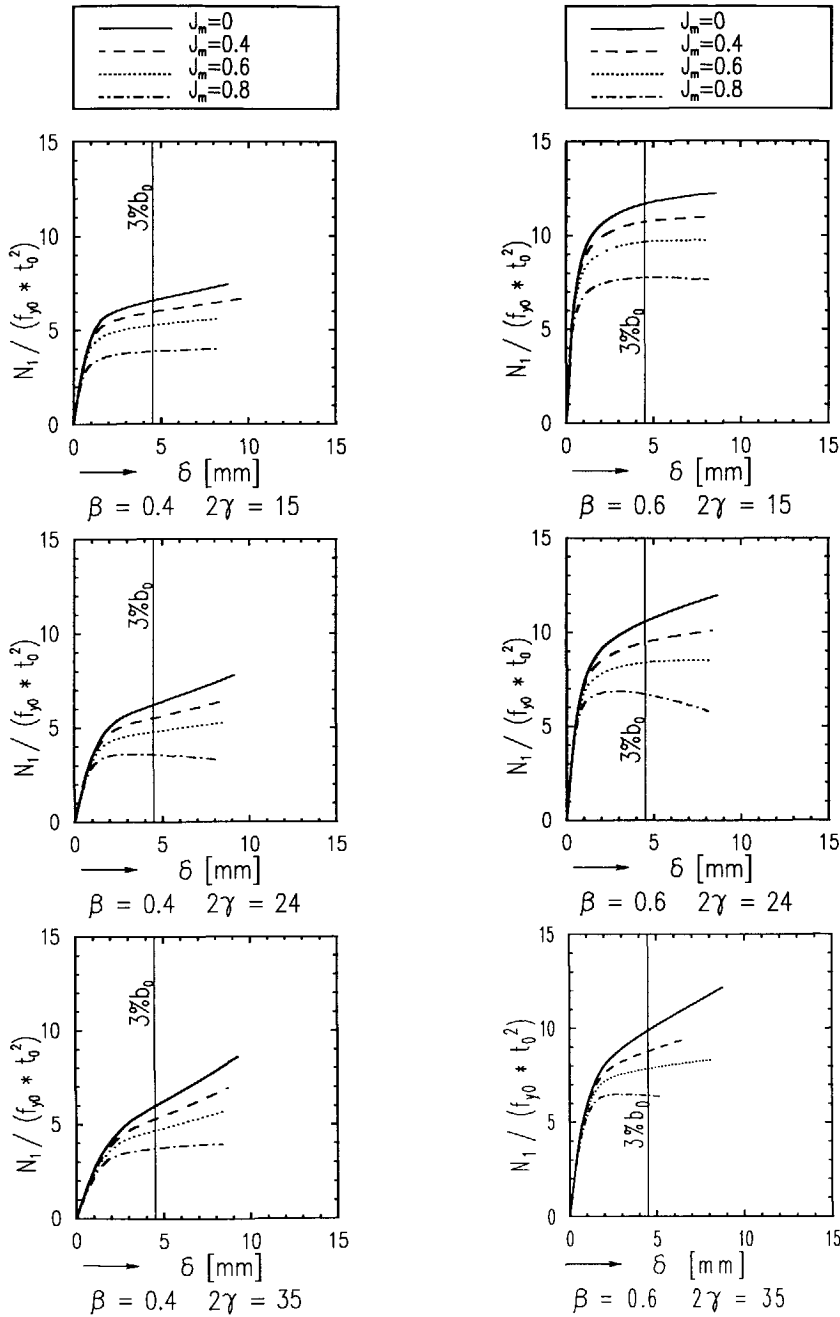
**Figure 6.37  Numerical results of axially loaded X-joints with different moment ratios**
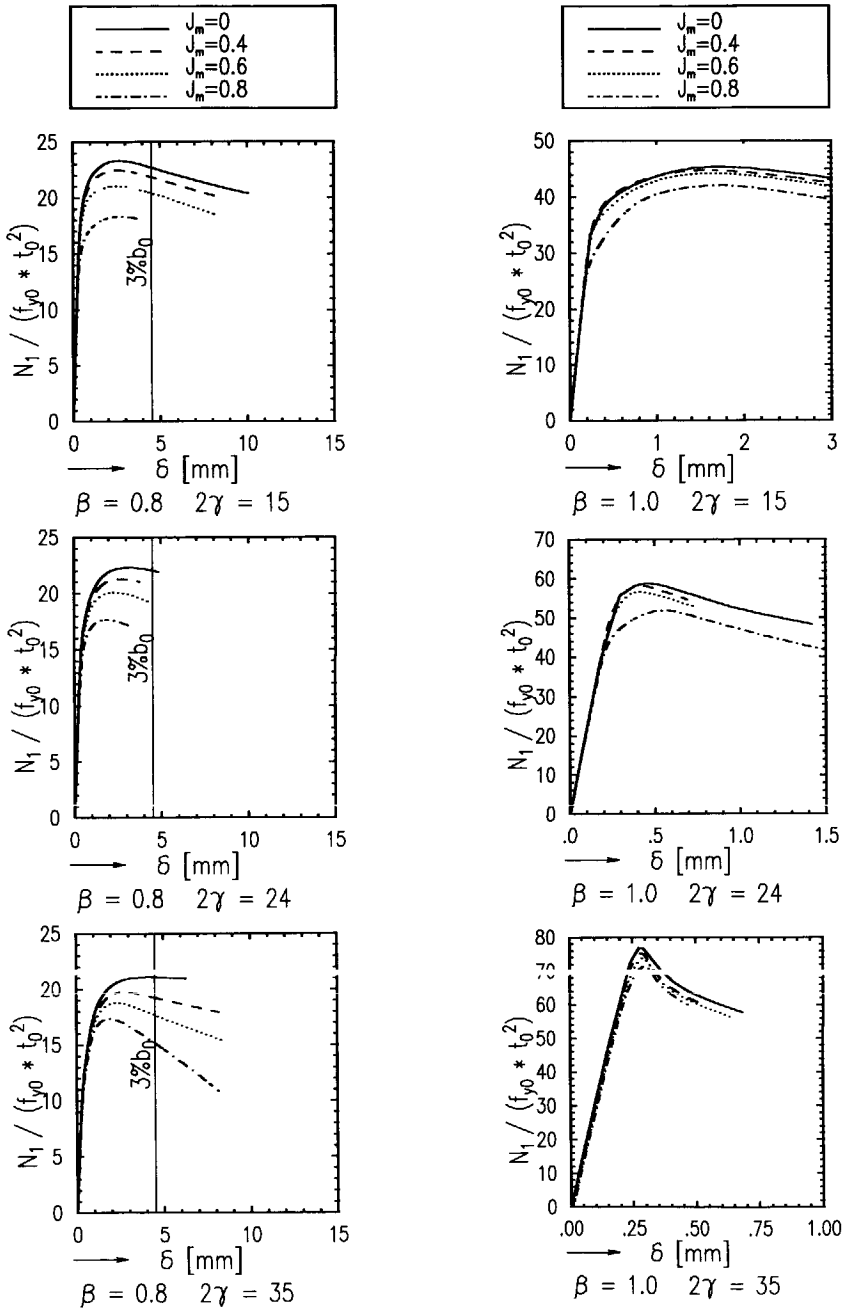
**Figure 6.37    (continued)**

## 6.5.5   The interaction formula based upon EC3

### 6.5.5.1        The numerical interaction formula

The reduction function of the joint ultimate load capacity is defined as:

$$f(J_m) = \frac{N_{1,u}(J_m)}{N_{1,u}(J_m = 0)} \tag{6.16}$$

Where $N_{1,u}(J_m)$ is the joint ultimate load capacity with a moment ratio $J_m$ and $N_{1,u}(J_m = 0)$ is that with a moment ratio $J_m = 0$. It is obvious that $N_{1,u}(J_m = 0)$ is equal to the ultimate load capacity of X-joints loaded only with axial forces on the braces. The data points of $\{f(m), J_m\}$ obtained from Table 6.22 are illustrated in Figure 6.38.

From Figure 6.38, it can be seen that there is a clear $\beta$ influence on the interaction contours between the dimensionless ultimate load capacity and the bending moment ratio. The larger the $\beta$ values, the higher the interaction curves. This means that the larger the $\beta$ values, the less the influence of the bending moment on the ultimate load capacity of the joint. This tendency is the same as for T-joints, see Chapter 7.

For X-joints with $\beta = 1$ and $J_m < 1$, the reduction function $f(J_m)$ is smaller than 1, as shown in Figure 6.38. It is expected that the same interaction formula can be used for both T- and X-joints due to the similarity of the problem. Considering that no numerical data points for T-joints with $\beta = 1$ and $J_m < 1$ are available, the numerical results of X-joints with $\beta = 1$ and $J_m < 1$ will be used for the determination of the interaction formula for both T- and X-joints. Theoretically speaking, if $J_m = 0$, then $f(J_m) = 1$, while if $J_m = 1$, then $f(J_m) = 0$. Thus, an interaction formula is assumed to have the above characteristics based upon the equation recommended for T-joints (Yu 1995):

$$f(J_m) = \sqrt[3]{1 - J_m^{f(\beta)}} \tag{6.17}$$

Where

$$f(\beta) = \frac{1}{1 - R_1 \beta^{R_2}} \tag{6.18}$$

$J_m$ and $f(J_m)$ can be found in equations (5.47) and (6.16), or (7.28) for T-joints. The nonlinear regression analysis is carried out including the FE results of both T- and X-joints. The FE results of T-joints can be found in Table 7.3, Chapter 7. The regression results are listed in Table 6.23.

**Table 6.23  Regression results of equation (6.17) based upon EC3**

| $R_1$ | $R_2$ | Correlation coefficient $R^2$ | Mean normalised error | Coefficient of Variation |
|-------|-------|-------------------------------|-----------------------|--------------------------|
| 0.85  | 1.6   | 0.965                         | 0.995                 | 0.039                    |

A reasonable correlation coefficient and a very low coefficient of variation are obtained as shown in Table 6.23. Thus, equation (6.17) can be used for both T- and X-joints with all β values and moment ratios if the design resistance moment of the chord section is determined according to EC3. A comparison between equation (6.17) and the FE results of X-joints is plotted in Figure 6.38.
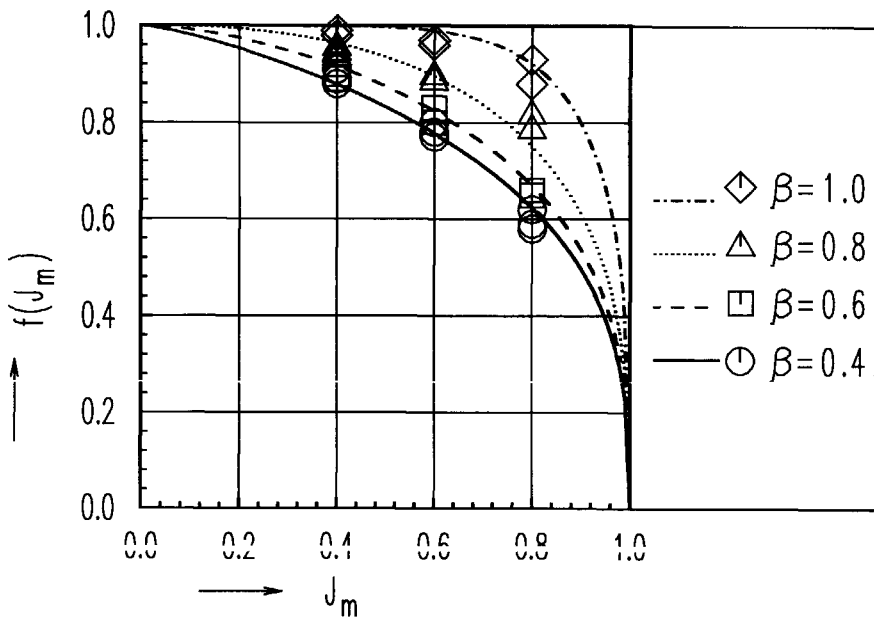


**Figure 6.38  Interaction contours of the FE results of X-joints based upon EC3**

**6.5.5.2      Comparison with the analytical solutions based upon the yield line theory**

The analytical solutions based upon the yield line theory have been described in Section 5.4. The reduction of the joint ultimate load capacity is caused by the reduction of the plastic moment capacity of a yield line when the yield line is normal or inclined to the axial stresses. Although different methods to calculate the reduction of the plastic moment capacity may lead to slightly different results, they still give an analytical basis for the understanding of the problem. The methods of Murray (1984) and Zhao (1993a, 1993b) have been used in

calculating the reduced plastic moment capacity of an inclined yield line.

**Comparison with the analytical solution based upon Murray**

The interaction formulae deduced based on Murray is (see Chapter 5):

$$f(J_m) = \frac{N_{1,u}(J_m)}{N_{1,u}(J_m=0)} = \frac{\eta+2\sqrt{(1-\frac{J_m^2}{2})(1-J_m^2)(1-\beta)}}{\eta+2\sqrt{1-\beta}} \tag{5.60}$$

In Table 6.24, a set of $f(J_m)$ values according to equation (5.60) is outlined and compared with equation (6.17) based upon the FE results. It can be seen that the difference between the analytical results based upon Murray and those of equation (6.17) based upon the FE results is within 4%.

**Table 6.24    Comparison between equation (6.17) and the analytical results based on Murray**

|  | $f(J_m)_{Murray}$ | | | $f(J_m)_{Murray}$/eq(6.17) | | |
|---|---|---|---|---|---|---|
| $J_m$ | 0.4 | 0.6 | 0.8 | 0.4 | 0.6 | 0.8 |
| $\beta=0.4$ | 0.90 | 0.78 | 0.60 | 1.02 | 1.00 | 0.96 |
| $\beta=0.6$ | 0.92 | 0.81 | 0.66 | 1.00 | 0.99 | 0.99 |
| $\beta=0.8$ | 0.94 | 0.85 | 0.73 | 0.98 | 0.96 | 0.97 |

**Comparison with the analytical solution based upon Zhao**

The interaction relationship based upon Zhao in Chapter 5 is as follows:

$$N_1 = 4m_p\left((\frac{1+\beta}{1-\beta}tg\alpha+\frac{1}{\cos\alpha})(1-J_m^2)+ctg\alpha+\frac{2\eta}{1-\beta}\right) \tag{5.64}$$

Where $\alpha$ can be determined by the following equation:

$$(1-J_m^2)\frac{1+\beta}{1-\beta}-ctg^2\alpha+(1-J_m^2)\sin\alpha=0 \tag{5.65}$$

Substituting the obtained $\alpha$ value from equation (5.65) into equation (5.64), the failure load of the joint can be determined. With this method, a set of interaction data points $\{f(J_m),J_m\}$

is obtained and compared with equation (6.17) in Table 6.25. It can be seen that the difference between the results based on Zhao (1993a, 1993b) and the FE results of equation (6.17) is within 7%.

Thus, equation (6.17) agrees reasonably well with the analytical results. Based upon the numerical analyses, equation (6.17) can be recommended as the reduction formula for chord bending moments if the design resistance moment of the chord cross-section is determined based upon EC3. This formula can be used for both X- and T-joints.

**Table 6.25    Comparison between equation (6.17) and the analytical results based upon Zhao**

|                | $f(J_m)_{Zhao}$ | | | $f(J_m)_{Zhao}/eq(6.17)$ | | |
|----------------|-----|-----|-----|-----|-----|-----|
| $J_m$          | 0.4 | 0.6 | 0.8 | 0.4 | 0.6 | 0.8 |
| $\beta=0.4$    | 0.92 | 0.82 | 0.66 | 1.05 | 1.05 | 1.06 |
| $\beta=0.6$    | 0.94 | 0.86 | 0.72 | 1.02 | 1.05 | 1.07 |
| $\beta=0.8$    | 0.96 | 0.90 | 0.80 | 1.00 | 1.01 | 1.07 |

### 6.5.6    The interaction formula based upon the plastic moment capacity only

Different methods to determine the design resistance moment of the chord cross-section result in different moment ratios as shown in Table 6.21. If the moment ratios are determined based upon the plastic moment capacity for all section classes, a $2\gamma$ influence is observed. It is expected that a similar interaction formula can be used for joints with chord bending moments and for joints with chord axial preloading if $M_{pl,Rd}$ is used, since the stress distributions of the chord top face are similar in the two cases. Based upon this idea, all the numerical data points for T- and X-joints under chord bending moments and X-joints under chord axial preloading are used for the regression analyses. The numerical data can be found in Table 7.3, Chapter 7 and Tables 6.18 and 6.22 in this chapter. The form of the interaction formula is assumed similar to equation (6.12):

$$f(J_m) = \left(1 - \left(\frac{M_0}{M_{pl,Rd}}\right) f(\beta,\gamma)\right)^{R_1} \tag{6.19}$$

Where

$$f(\beta,\gamma) = \frac{2}{(1+R_2\gamma^{R_3})(1-R_4\beta^{R_5})} \tag{6.20}$$

The regression results are listed in Table 6.26. A reasonable correlation coefficient and a very low coefficient of variation are obtained. Comparison between Table 6.26 and Table 6.19 shows that the regression formula, equation (6.19) is the same as equation (6.12) in Section 6.4 with only slightly different statistical values.

Comparison between equation (6.19) and the numerical results of T- and X-joints with chord bending moments and X-joints with chord axial preloading is plotted in Figure 6.39.

**Table 6.26** **Regression results of equations (6.19) and (6.20) for T- and X-joints with chord bending and X-joints with chord axial preloading (based upon the plastic moment capacity)**

| $R_1$ | $R_2$ | $R_3$ | $R_4$ | $R_5$ | Mean | Coefficient of variation COV | Correlation coefficient $R^2$ |
|-------|-------|-------|-------|-------|------|------------------------------|-------------------------------|
| 0.4 | 0.004 | 2 | 0.85 | 3 | 1.011 | 0.041 | 0.950 |

Although the above analysis shows that the reduction formula for joints with chord bending moments agrees well with that for joints with chord axial preloading, the approach of $M_{pl,Rd}$ is invalid if there is not enough rotation capacity of the chord cross-section, since the strains in the chord top face based upon $M_{pl,Rd}$ are much higher than those based upon $N_{0,Rd}$. For joints with chord bending moments, using $M_{el,Rd}$ instead of $M_{pl,Rd}$ would give similar strains in the chord top face as for joints with chord axial preloading.
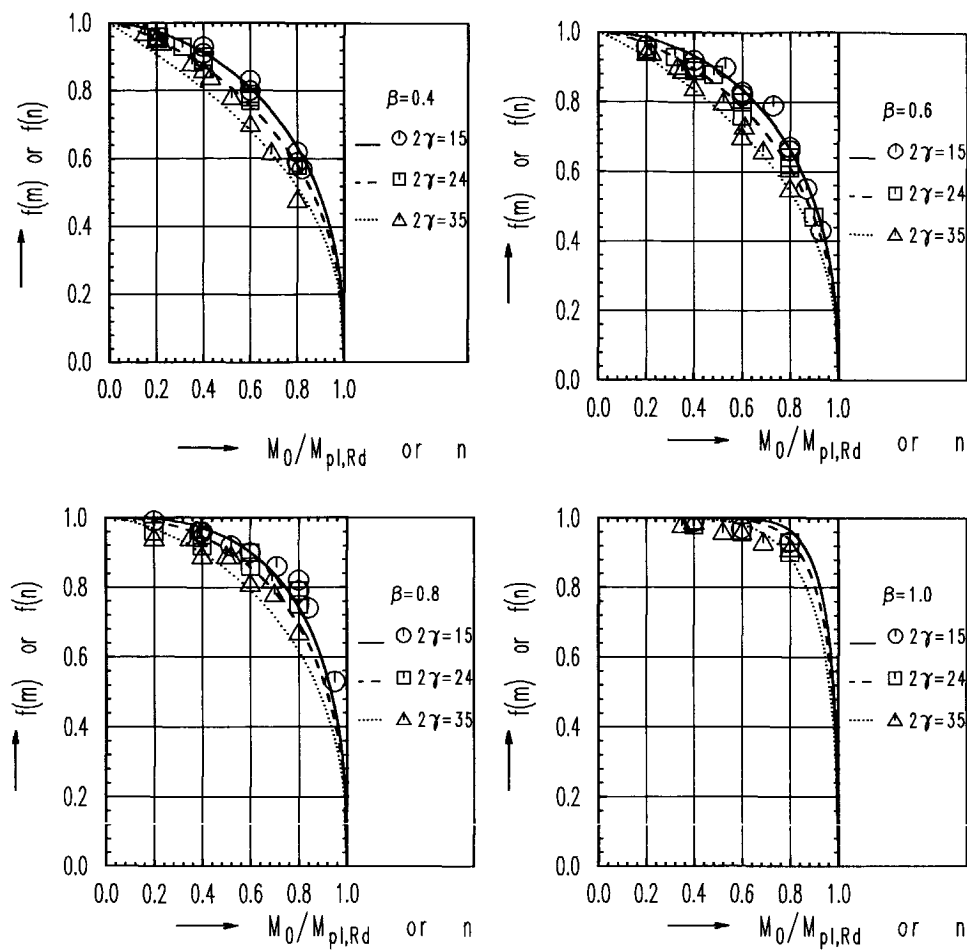
**Figure 6.39**   **Interaction contours for X- and T-joints with chord bending and X-joints with chord axial preloading (based upon the plastic moment capacity)**

### 6.5.7 The interaction formula based upon the elastic moment capacity only

The moment ratios based upon the elastic moment capacity of the chord cross-section are listed in Table 6.21. The numerical results based upon $M_{el,Rd}$ are illustrated in Figure 6.40.
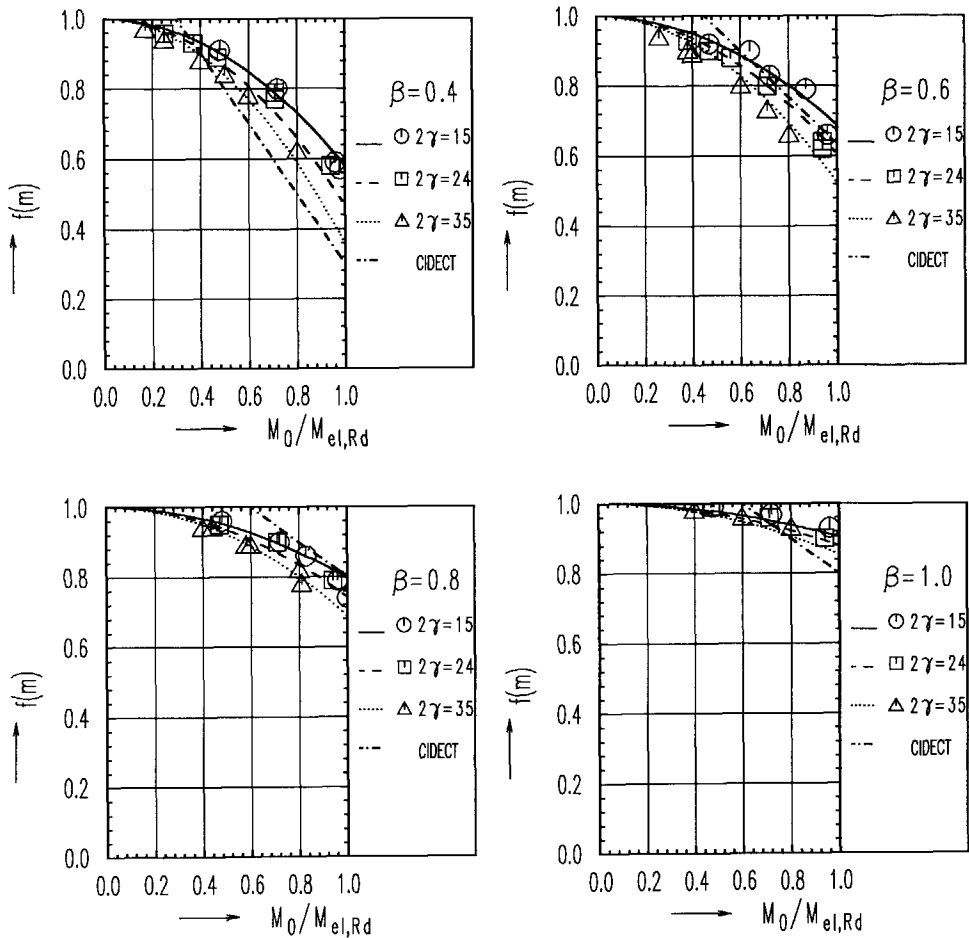


**Figure 6.40** Interaction contours for X- and T-joints with chord bending (based upon the elastic moment capacity)

Based upon Figure 6.40, the reduction function is given as follows:

$$f(J_m) = 1 - R_1(1-R_2\beta) \gamma^{R3} \left(\frac{M_0}{M_{el,Rd}}\right)^{R_4}$$  (6.21)

The regression results are listed in Table 6.27.

**Table 6.27**    **Regression results of equation (6.21) for T- and X-joints with chord bending moments (based upon the elastic moment capacity)**

| $R_1$ | $R_2$ | $R_3$ | $R_4$ | Mean normalised error | Coefficient of variation (CoV) | Correlation coefficient ($R^2$) |
|-------|-------|-------|-------|----------------------|-------------------------------|--------------------------------|
| 0.23  | 0.85  | 0.5   | 2     | 1.000                | 0.032                         | 0.959                          |

The reduction function for joints with chord bending moments based upon the elastic moments is not the same as that for joints with axial preloading due to the different stress distributions. The CIDECT formula of equation (6.14) is plotted in Figure 6.40 as a comparison.

### 6.5.8   Conclusions

The influence of chord bending moments on the joint ultimate load capacity is determined in three ways which leads to three sets of interaction formulae.

If the design resistance moment of the chord is determined based upon EC3 (section classes), interaction formula (6.17) is recommended which agrees reasonably well with the analytical solutions. Equation (6.17) can be used for both T- and X-joints with bending moments on the chord.

If the design resistance moment of the chord is determined based upon the plastic moment capacity for all section classes, equation (6.19) is recommended which can be used for both T- and X-joints with chord bending moments and X-joints with chord axial preloading (checked for $f_{y0} \leq 355$ N/mm$^2$).

If the design resistance moment of the chord is determined based upon the elastic moment capacity, equation (6.21) is recommended which is valid for T- and X-joints with chord bending moments only.

# 7    NUMERICAL STUDY ON UNIPLANAR T-JOINTS

## 7.1    AXIALLY LOADED T-JOINTS INCLUDING CHORD BENDING MOMENT

### 7.1.1    Introduction

For a T-joint, the axial load applied to the brace will be balanced by the end supports of the chord which will cause global bending moments and shear forces in the chord member. The extent of the chord bending and shear effects depends upon the joint parameters such as the width ratio between the brace and the chord ($\beta$), the width to thickness ratio of the chord ($2\gamma$) and the chord length to width ratio ($\alpha/2$). This bending moment will reduce the ultimate load capacity of the joint for a concentrated load applied to the brace as described in Chapters 5 and 6. Very little information is available for this effect in the existing design recommendations. In order to separate the influence of the bending moment from the axial load, compensating bending moments can be applied to the chord ends in such a way that the chord moment at the intersection between the brace and the chord remains zero. It is envisaged that by separating the effects of chord bending from those of the brace concentrated load, failure of uniplanar T-joints can be described in a clearer manner. As a result, the normalized load-moment contour can offer a clear insight into the influence of the chord moment. This method has been adopted for joints of square hollow sections (Yu 1995) where the resistance moment of the chord have been based upon the section classes (EC3 1992).

Similar to Section 6.5, Chapter 6, three approaches are used to determine the resistance moment of the chord cross-section (based upon EC3, based upon the plastic moment capacity only or based upon the elastic moment capacity only) which results in three reduction functions for T-joints with chord bending moments. It is expected that the chord bending moments on T- and X-joints will have a similar influence on the joint ultimate load capacity. As a result, identical interaction formulae could be used for both T- and X-joints.

The study presented covers failure due to plastification of the chord face or chord walls. Punching shear and brace effective width failure are not included in the numerical analyses.

### 7.1.2    The resistance moment of the chord member

### 7.1.2.1    Based upon EC3

**Classifications of cross-sections**

The design of members and the method of analysis are influenced by the cross-sectional dimensions. EC3 (1992) and the CIDECT design guide (Rondal 1992) specify width-to-thickness ratios to classify the cross-sections as Classes 1, 2, 3 and 4. The cross-section classes in this research programme with $f_{y0}=355$ N/mm$^2$ are class 1 ($2\gamma=15$ and 24) and class 3 ($2\gamma=35$).

For class 1 cross-sections, full plasticity is developed in the cross-section with full rotation capacity.

For cross-section class 2, full plasticity is developed in the cross-section with restricted rotation capacity.

The ultimate resistance moment of class 1 and 2 sections should be determined according to plastic design. Thus, it is equal to the design plastic resistance moment.

For class 3 cross-sections, the ultimate limit state is reached by yielding of the extreme fibres of the cross-section. Thus, the ultimate resistance moment is equal to the design elastic resistance moment.

For class 4 cross-sections, the stress at the extreme fibres of the cross-section is less than the yield stress. The ultimate moment resistance is governed by local buckling and occurs at a value less than the design elastic resistance moment.

### Class 1 and 2 cross-sections

According to EC3 (1992), the effect of shear may be neglected if the shear load does not exceed 50% of the shear resistance of the section. Thus, the design plastic resistance moment including the shear reduction in the web of a rectangular hollow section can be written as:

$$M_{Sd} \leq M_{V,Rd} = M_{f,Rd} + M_{w,Rd} \cdot \xi = M_{f,Rd} + (1-\rho)M_{w,Rd} = M_{pl,Rd} - \rho M_{w,Rd} \tag{7.1}$$

$$\xi = 1 - \rho \tag{7.2}$$

For a square hollow section,

$$\frac{M_{w,Rd}}{M_{pl,Rd}} = \frac{0.5 t_0 (b_0 - t_0)^2 f_{y0}}{0.5 t_0 (b_0 - t_0)^2 f_{y0} + (b_0 - t_0)^2 t_0 f_{y0}} = \frac{1}{3} \tag{7.3}$$

Thus, the right side of equation (7.1) can be rewritten as:

$$M_{V,Rd} = M_{pl,Rd}(1 - \frac{1}{3}\rho) \tag{7.4}$$

Where,

$$M_{pl,Rd} = \frac{3}{2}(b_0 - t_0)^2 t_0 f_{y0}/\gamma_{M0} \tag{7.5}$$

$\gamma_{M0} = 1$ for class 1, 2 and 3 sections according to EC3. For the clearness of reading, $\gamma_{M0}$ will not be included in the formulae.

If the shear design value exceeds 50% of the design plastic shear resistance, then the effect of the shear should be taken into account, thus,

$$\rho = (2\frac{V_{Sd}}{V_{pl,Rd}} - 1)^2 \tag{7.6}$$

Where,

$$V_{pl,Rd} = 2(b_0 - t_0)t_0\frac{f_{y0}}{\sqrt{3}} \tag{7.7}$$

$$V_{Sd} = \frac{N_1}{2} \tag{7.8}$$

When the plastic bending moment capacity of the chord is reached, $N_1 = N_{V,Rd}$ or $M_{Sd} = M_{V,Rd}$ by definition. The relationship between $M_{V,Rd}$ and $N_{V,Rd}$ is given as follows:

$$M_{V,Rd} = \frac{N_{V,Rd}(l_0 - b_1)}{4} = \frac{N_{V,Rd}b_0(\frac{\alpha}{2} - \beta)}{4} \tag{7.9}$$

Substituting equation (7.6), (7.8) and (7.9) into (7.4) gives the following equation:

$$\frac{N_{V,Rd}^2}{V_{pl,Rd}^2} + N_{V,Rd}\left(\frac{3b_0(\alpha/2 - \beta)}{4M_{pl,Rd}} - \frac{2}{V_{pl,Rd}}\right) - 2 = 0 \tag{7.10}$$

Substituting equation (7.5) and (7.7) into (7.10) yields:

$$\left(\frac{N_{V,Rd}}{t_0^2 f_{y0}}\right)^2 \frac{\sqrt{3}}{2(2\gamma - 1)} - \frac{N_{V,Rd}}{t_0^2 f_{y0}}\left(\frac{2\gamma(\alpha/2 - \beta)}{\sqrt{3}(2\gamma - 1)} - 2\right) - \frac{4(2\gamma - 1)}{\sqrt{3}} = 0 \tag{7.11}$$

From equation (7.11), the axial load applied to the brace $N_{V,Rd}$ is given as follows when $M_{Sd} = M_{V,Rd}$:

$$\frac{N_{V,Rd}}{f_{y0}t_0^2} = \frac{(2\gamma - 1)}{\sqrt{3}}(-C_1 + \sqrt{C_1^2 + 8}\ ) \tag{7.12}$$

Where

$$C_1 = \frac{\frac{\alpha}{2} - \beta}{\sqrt{3}(1 - \frac{1}{2\gamma})} - 2 \qquad (7.13)$$

It should be mentioned that equations (7.9) and (7.12) are valid for the case that the shear force is larger than half of the design plastic shear resistance of the section.

For $V_{Sd} < 0.5V_{pl,Rd}$, the moment resistance of the cross-section is not reduced by the shear, thus

$$\rho = 0 \qquad (7.14)$$

$$M_{V,Rd} = M_{pl,Rd} \qquad (7.15)$$

### Class 3 cross-section

Analogously to equation (7.1) which is valid for section classes 1 and 2, the formula for section class 3 can be deduced considering that the design elastic resistance moment with shear reduction is:

$$M_{Sd} \leq M_{V,e,Rd} = M_{e,Rd} - \rho M_{w,e,Rd} \qquad (7.16)$$

Where

$$M_{w,e,Rd} = \frac{t_0(b_0 - t_0)^2 f_{y0}}{3} = \frac{b_0^3 f_{y0}}{3 \cdot 2\gamma}(1 - \frac{1}{2\gamma})^2 = \frac{b_0^3 f_{y0}}{3} C_2 \qquad (7.17)$$

$$C_2 = \frac{(1 - \frac{1}{2\gamma})^2}{2\gamma} \qquad (7.18)$$

$$M_{e,Rd} = \frac{b_0^4 - (b_0 - 2t_0)^2}{6b_0} f_{y0} = \frac{b_0^3 f_{y0}}{6}\left(1 - (1 - \frac{2}{2\gamma})^4\right) = \frac{b_0^3 f_{y0}}{6} C_3 \qquad (7.19)$$

$$C_3 = 1 - (1 - \frac{2}{2\gamma})^4 \tag{7.20}$$

When the design elastic resistance moment of the chord is reached, $N_1 = N_{V,e,Rd}$ or $M_{Sd} = M_{V,e,Rd}$ by definition. For a chord with a square hollow section, $M_{V,e,Rd}$ is given as follows:

$$M_{V,e,Rd} = \frac{N_{V,e,Rd} b_0 (\frac{\alpha}{2} - \beta)}{4} \tag{7.21}$$

Substituting equations (7.6) to (7.8) and (7.17) to (7.21) into (7.16), the axial load applied to the brace when design elastic resistance moment is reached is:

$$\frac{N_{V,e,Rd}}{t_0 f_{y0}^2} = \frac{2\gamma - 1}{\sqrt{3}} \left( -C_4 + \sqrt{C_4^2 - 4(1 - C_5)} \right) \tag{7.22}$$

$$C_4 = \frac{\sqrt{3} (\frac{\alpha}{2} - \beta)}{2(1 - \frac{1}{2\gamma})} - 2 \tag{7.23}$$

$$C_5 = \frac{C_3}{2C_2} \tag{7.24}$$

Equations (7.21) and (7.22) are valid for the case when the shear design load is larger than half of the design plastic shear resistance. Otherwise, the following formula applies:

$$M_{V,e,Rd} = M_{e,Rd} = \frac{b_0^3 f_y C_3}{6} \tag{7.25}$$

### 7.1.2.2 Based upon the plastic moment capacity only

Similar to Section 6.5, Chapter 6, if the design resistance moment of the chord section is determined based upon its plastic moment capacity, equation (7.9) or equation (7.15) should be used for the shear design load larger or smaller than 50% of the design plastic shear resistance respectively, independent of the section classes.

### 7.1.2.3 Based upon the elastic moment capacity only

If the design resistance moment of the chord section is based upon its elastic moment capacity, equation (7.21) or (7.25) should be used for the shear design load larger or smaller than 50% of the design plastic shear resistance respectively, independent of the section classes.

## 7.1.3 Research programme

The research programme for the numerical study is shown in Tables 7.1 and 7.2. Table 7.1 gives the joints including chord overall bending and Table 7.2 gives the joints excluding the chord bending moment at the intersection between the brace and the chord. Both the chord and the brace are made of square hollow sections. The width of the chord is fixed at 150 mm. The joint parameters of the numerical models are $\beta$=0.4, 0.6, 0.8, 1.0 and $2\gamma$=15, 24 and 35 respectively. For each joint with the same $\beta$ and $2\gamma$ values, several $\alpha$ values have been included for the investigation. It should be mentioned that for smaller $\beta$ values ($\beta$=0.4 and 0.6), the chord bending effect is relatively small if the value of $\alpha$ is smaller than 12. However, for larger $\beta$ values ($\beta$=0.8, 1.0), the chord bending effect is already quite large for a small $\alpha$ value ($\alpha$=9). That is why different ranges of $\alpha$ values are used in the parameter study depending upon the $\beta$ values of the joint, see Table 7.1. Actually, the effect of overall chord bending and chord shear depends upon the $\alpha$ values for a specified set of $\beta$ and $2\gamma$ values. For smaller $\alpha$ values, the bending effect is smaller. However, too small $\alpha$ values may cause an influence of the boundary conditions.

Figure 7.1 shows the configuration of a typical uniplanar T-joint including chord bending moment.
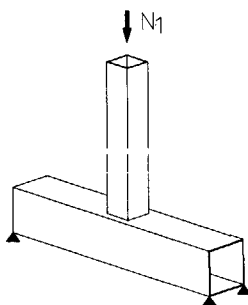


**Figure 7.1    Uniplanar T-joint including chord bending moment**

**Table 7.1    Uniplanar T-joints including chord bending**

| 2γ | β | Including overall bending | | | | | |
|---|---|---|---|---|---|---|---|
| | | α | | | | | |
| | | 6 | 9 | 12 | 18 | 30 | 40 |
| 15 | 0.4 | | | | | | t7-4 |
| | 0.6 | | | t8-2 | t8-3 | t8-5 | |
| | 0.8 | | t5-a | t5-2 | t5-3 | | t5-4 |
| | 1.0 | t101 | t10a | t102 | t103 | | |
| 24 | 0.4 | | | t1-2 | t1-3 | | t1-4 |
| | 0.6 | | | t3-2 | t3-3 | | t3-4 |
| | 1.0 | t111 | t11a | t112 | t113 | | |
| 35 | 0.4 | | | t2-2 | t2-3 | | t2-4 |
| | 0.6 | | | t4-2 | t4-3 | | t4-4 |
| | 0.8 | | t6-a | t6-2 | t6-3 | | |
| | 1.0 | t121 | t12a | t122 | t123 | | |

**Table 7.2    Uniplanar T-joints Excluding Chord Bending**

| 2γ | β | Excluding overall bending |
|---|---|---|
| | | α=12 |
| 15 | 0.4 | t7-2-m |
| | 0.6 | t8-2-m |
| | 0.8 | t5-2-m |
| | 1.0 | t102-m |
| 24 | 0.4 | t1-2-m |
| | 0.6 | t3-2-m |
| | 1.0 | t112-m |
| 35 | 0.4 | t2-2-m |
| | 0.6 | t4-2-m |
| | 0.8 | t6-2-m |
| | 1.0 | t122-m |

For the analysis excluding the effect of chord bending, compensating bending moments are applied at the ends of the chord to make sure that the moment in the chord at the intersection

between the chord and the brace is equal to 0. At each load step, the bending moments are applied as a result of two counter direction axial forces acting at the top and bottom flanges of the chord respectively, see Figure 7.2.
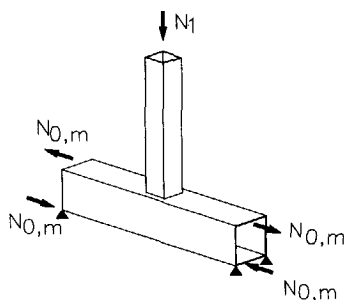


**Figure 7.2    Uniplanar T-joint excluding chord bending moment at the intersection between brace and chord**

For square hollow sections, the relationship can be approximately written as:

$$M_0 = \frac{N_1(l_0 - b_1)}{4} = \frac{N_1 b_0(\frac{\alpha}{2} - \beta)}{4} = N_{0,m} b_0 \tag{7.26}$$

Thus, the $N_{0,m}$ value is proportional to the axial load $N_1$ on the brace at each load step:

$$\frac{N_{0,m}}{N_1} = \frac{(\frac{\alpha}{2} - \beta)}{4} \tag{7.27}$$

### 7.1.4   The FE analysis

This numerical investigation has been carried out before the extensive numerical parameter studies in Chapters 6, 8, 9 and other sections in this chapter. Thus, the material properties of the chord and the brace have been used as those from experiments (Davies 1992b). The measured engineering stress-strain curves have been translated into true stress-true strain curves, see Figure 4.9, Chapter 4. The weld has not been modelled in this study. Considering symmetry in geometry and loading, a quarter of a T-joint has been used for the numerical study, see Figure 7.3.
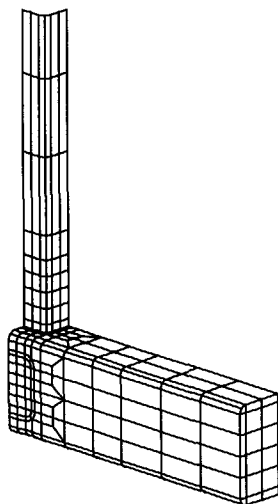
**Figure 7.3  Element meshes of 1/4 geometry of a T-joint**

Load control can only be used in order to apply compensation bending moments at the chord ends. At each load step, two pairs of counter-directional axial loads $N_{0,m}$ are applied proportionally to $N_1$ based upon equation (7.27).

From experience, special care should be taken for the boundary conditions. The elements at the end of the brace should be made very stiff in order to apply the load uniformly. The elements at the chord end should be stronger in order to prevent chord end failure when the compensating bending moments are applied. Especially for joints with large $\beta$ and small $2\gamma$ values, the chord end always yields first if it is not strengthened. The reason is that for joints with large $\beta$ and small $2\gamma$ values, the ultimate load applied to the brace is high, thus large compensating bending moments should be applied. Using post-processing technique, all of the results have been checked in order to make sure that no failure at the chord end occurs. It should be mentioned that strengthening the chord end elements with high yield strength may cause another problem which is the influence of the boundary conditions. In order to avoid this, the chord length should be long enough. In this study, an $\alpha$ value of 12 is chosen for all the joints when compensating bending moments are applied.

## 7.1.5  Results of T-joints including and excluding the influence of overall chord bending

Figure 7.4 shows the non-dimensional load versus indentation curves for joints with different geometry parameters. For each set of $\beta$ and $2\gamma$ values, several $\alpha$ values of the joints are included. The results of the joints with compensated chord bending moment (indicated with "-m") are plotted in solid lines. It can be seen that the ultimate load capacity of joints with overall chord bending is reduced in general compared to that of joints with compensating

bending moments. The greater the $\alpha$ value, the larger the reduction.
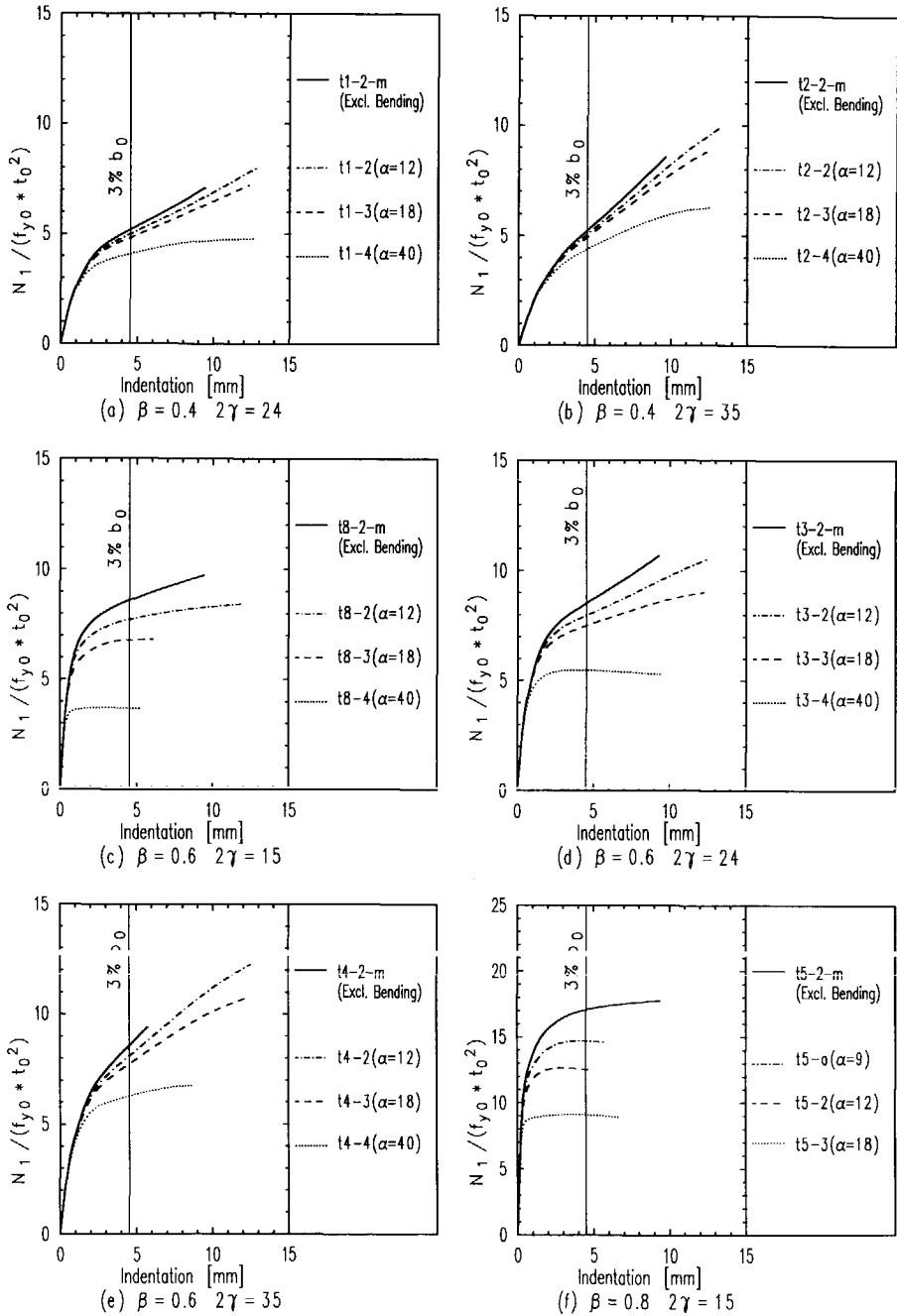


**Figure 7.4   Influence of the chord bending**
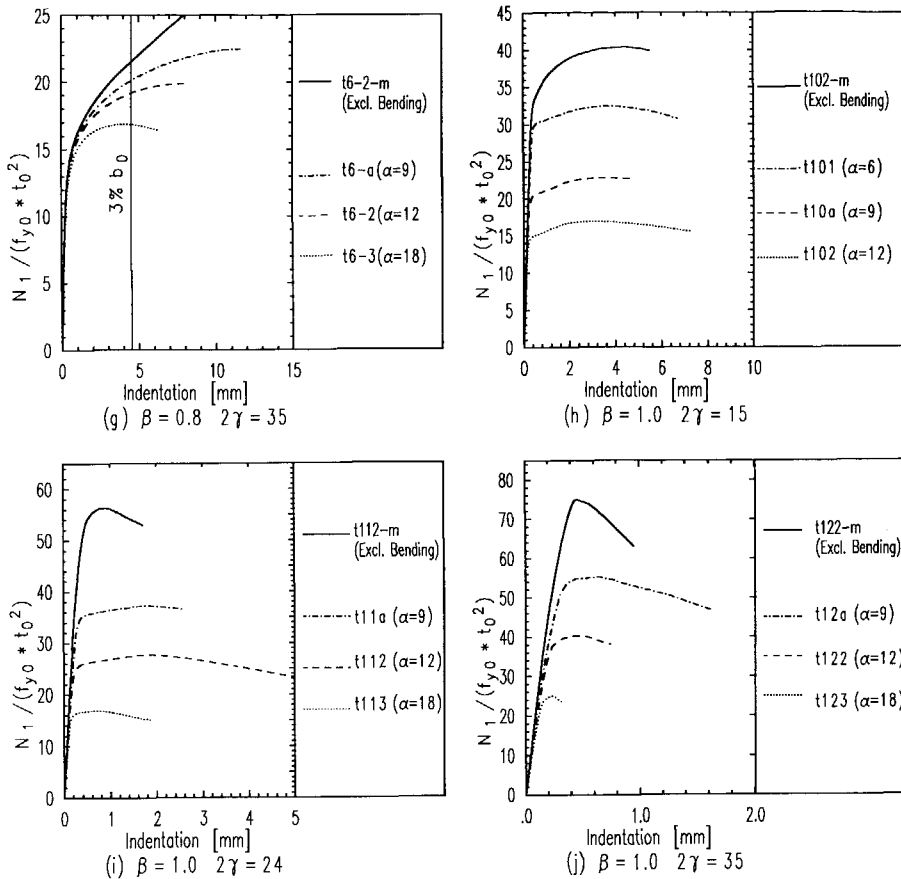
**Figure 7.4  Influence of the chord bending (continued)**

## 7.1.6  Interaction contours between local failure and failure due to chord overall bending

### 7.1.6.1  Based upon EC3

From the typical non-dimensional load versus indentation curves in Figure 7.4, the ultimate load capacity for joints including the chord bending moment and the ultimate load for joints excluding the chord bending moment can be obtained and listed in Table 7.3. The second one is taken as the normalising ultimate load capacity of the joint.

**Table 7.3** **Numerical results of T-joints including and excluding chord bending moments**

| Joints including chord bending | | | | | Corresponding joints excluding chord bending | | Interaction relationship | |
|---|---|---|---|---|---|---|---|---|
| Joints | $\beta$ | $2\gamma$ | $\alpha$ | $\dfrac{N_{1,u}(J_m)}{f_{y0}t_0^2}$ | Joints | $\dfrac{N_{1,u}(J_m=0)}{f_{y0}t_0^2}$ | $J_m$ | $\dfrac{N_{1,u}(J_m)}{N_{1,u}(J_m=0)}$ |
| t1-2 | 0.4 | 24 | 12 | 4.97 | t1-2-m | 5.18 | 0.21 | 0.96 |
| t1-3 | 0.4 | 24 | 18 | 4.81 | t1-2-m | 5.18 | 0.31 | 0.93 |
| t1-4 | 0.4 | 24 | 40 | 4.08 | t1-2-m | 5.18 | 0.60 | 0.79 |
| t2-2 | 0.4 | 35 | 12 | 5.07 | t2-2-m | 5.25 | 0.17 | 0.97 |
| t2-3 | 0.4 | 35 | 18 | 4.94 | t2-2-m | 5.25 | 0.25 | 0.94 |
| t2-4 | 0.4 | 35 | 40 | 4.40 | t2-2-m | 5.25 | 0.50 | 0.84 |
| t3-2 | 0.6 | 24 | 12 | 7.95 | t3-2-m | 8.52 | 0.32 | 0.93 |
| t3-3 | 0.6 | 24 | 18 | 7.49 | t3-2-m | 8.52 | 0.48 | 0.88 |
| t3-4 | 0.6 | 24 | 40 | 5.46 | t3-2-m | 8.52 | 0.80 | 0.64 |
| t3-5 | 0.6 | 24 | 60 | 4.03 | t3-2-m | 8.52 | 0.90 | 0.47 |
| t4-2 | 0.6 | 35 | 12 | 8.10 | t4-2-m | 8.58 | 0.26 | 0.94 |
| t4-3 | 0.6 | 35 | 18 | 7.74 | t4-2-m | 8.58 | 0.38 | 0.92 |
| t4-4 | 0.6 | 35 | 40 | 6.29 | t4-2-m | 8.58 | 0.71 | 0.73 |
| t5-a | 0.8 | 15 | 9 | 14.70 | t5-2-m | 17.07 | 0.71 | 0.86 |
| t5-2 | 0.8 | 15 | 12 | 12.63 | t5-2-m | 17.07 | 0.84 | 0.74 |
| t5-3 | 0.8 | 15 | 18 | 9.11 | t5-2-m | 17.07 | 0.95 | 0.53 |
| t6-a | 0.8 | 35 | 9 | 20.15 | t6-2-m | 21.55 | 0.44 | 0.94 |
| t6-2 | 0.8 | 35 | 12 | 19.21 | t6-2-m | 21.55 | 0.58 | 0.89 |
| t6-3 | 0.8 | 35 | 18 | 16.90 | t6-2-m | 21.55 | 0.81 | 0.78 |
| t7-4 | 0.4 | 14 | 40 | 3.28 | t7-2-m | 5.73 | 0.82 | 0.57 |
| t8-2 | 0.6 | 15 | 12 | 7.72 | t8-2-m | 8.59 | 0.53 | 0.90 |
| t8-3 | 0.6 | 15 | 18 | 6.79 | t8-2-m | 8.59 | 0.73 | 0.79 |
| t8-4 | 0.6 | 15 | 40 | 3.69 | t8-2-m | 8.59 | 0.91 | 0.43 |
| t8-5 | 0.6 | 15 | 30 | 4.75 | t8-2-m | 8.59 | 0.87 | 0.55 |

$f_{y0}$=420 N/mm$^2$, $f_{y1}$=430 N/mm$^2$, $b_0$=150 mm, $\tau$=1

$J_m$ according to EC3

**Table 7.3** **(continued)**

| Joints including chord bending | | | | | Corresponding joints excluding chord bending | | Interaction relationship | |
|---|---|---|---|---|---|---|---|---|
| Joints | $\beta$ | $2\gamma$ | $\alpha$ | $\dfrac{N_{1,u}(J_m)}{f_{y0}t_0^2}$ | Joints | $\dfrac{N_{1,u}(J_m=0)}{f_{y0}t_0^2}$ | $J_m$ | $\dfrac{N_{1,u}(J_m)}{N_{1,u}(J_m=0)}$ |
| t101 | 1.00 | 15 | 6 | 32.46 | t102-m | 40.36 | 1.09 | 0.80 |
| t10a | 1.00 | 15 | 9 | 22.81 | t102-m | 40.36 | 1.06 | 0.57 |
| t102 | 1.00 | 15 | 12 | 16.92 | t102-m | 40.36 | 1.08 | 0.42 |
| t103 | 1.00 | 15 | 18 | 10.40 | t102-m | 40.36 | 1.06 | 0.26 |
| t111 | 1.00 | 24 | 6 | 51.62 | t112-m | 56.36 | 1.04 | 0.92 |
| t11a | 1.00 | 24 | 9 | 37.11 | t112-m | 56.36 | 1.03 | 0.66 |
| t112 | 1.00 | 24 | 12 | 27.58 | t112-m | 56.36 | 1.04 | 0.49 |
| t113 | 1.00 | 24 | 18 | 16.92 | t112-m | 56.36 | 1.02 | 0.30 |
| t121 | 1.00 | 35 | 6 | 73.89 | t122-m | 75.15 | 1.04 | 0.98 |
| t12a | 1.00 | 35 | 9 | 55.46 | t122-m | 75.15 | 1.15 | 0.74 |
| t122 | 1.00 | 35 | 12 | 40.39 | t122-m | 75.15 | 1.18 | 0.54 |
| t123 | 1.00 | 35 | 18 | 25.12 | t122-m | 75.15 | 1.17 | 0.33 |

$f_{y0}=419.7 \text{ N/mm}^2$, $f_{y1}=430 \text{ N/mm}^2$, $b_0=150 \text{ mm}$, $\tau=1$

$J_m$ according to EC3

The moment ratio for T-joints should be determined as follows:

$$J_m = \begin{cases} M_0/M_{v,Rd} & \text{(class 1 or 2)} \\ M_0/M_{v,e,Rd} & \text{(class 3)} \end{cases} \tag{7.28}$$

Where the bending moment on the chord at the ultimate load capacity is:

$$M_0 = \frac{N_{1,u}(J_m)b_1(\frac{\alpha}{2}-\beta)}{4} \tag{7.29}$$

The normalising $M_{V,Rd}$ or $M_{V,c,Rd}$ can be determined according to the section classes and the percentage of the shear force to the ultimate shear resistance. Thus, for class 1 and 2 sections, $M_{V,Rd}$ is calculated according to equation (7.9) or (7.15) respectively for shear loads larger or smaller than 50% of the shear resistance. Similarly, $M_{V,e,Rd}$ is calculated according to equation (7.21) or (7.25) for class 3 sections.

The interaction data points for T-joints are shown in Figure 7.5.
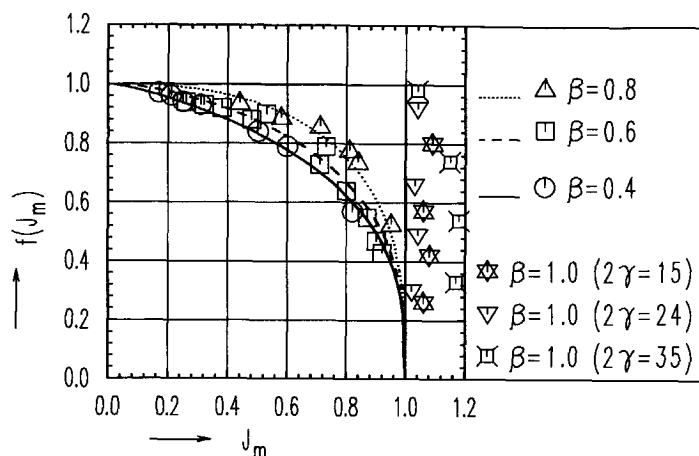


**Figure 7.5  The interaction contour of the numerical results**

Figure 7.5 shows that there is a clear $\beta$ influence in the interaction relationship between the axial load and the bending moment. The larger the $\beta$ values, the higher the interaction curves. It should be mentioned that for $\beta=1.0$, all the moment ratios exceed 1.0 according to the FE results due to the strain hardening effects. For an extremely small $\alpha$ value ($\alpha$ smaller than 6), the moment ratio could be smaller than 1. However, this will led to a boundary influence on the ultimate load capacity as mentioned before. For a T-joint with a moment ratio larger than or equal to 1.0, it means physically that a chord bending failure is critical instead of a joint failure. In this case, the failure load can be easily determined by the resistance moment of the chord section.

As described in Chapter 6, the interaction relationship can be specified by using curve fitting techniques with the numerical results of both T- and X-joints. Finally, the same interaction formula for both T- and X-joints is obtained in equation (6.17) for $J_m \le 1.0$. This formula is plotted in Figure 7.5.

$$f(J_m) = \left(1 - J_m^{\frac{1}{1-0.85\beta^{1.6}}}\right)^{\frac{1}{3}} \tag{6.17}$$

Where $J_m$ is given in equation (7.28) for T-joints instead of equation (5.47) for X-joints.

### 7.1.6.2    Based upon the plastic moment capacity only

If the resistance moment of the chord section is determined based upon its plastic moment capacity independent of the section classes, a $2\gamma$ influence is found in the interaction contours as described in Chapter 6. In such a case, the interaction formula for T-joints is the same as equation (6.19). The only difference is that $M_{pl,Rd}$ in equation (6.19) for X-joints should be replaced by $M_{V,Rd}$ for T-joints:

$$f(J_m) = \left( 1 - (\frac{M_0}{M_{V,Rd}})^{\frac{2}{(1+0.004\gamma^2)(1-0.85\beta^3)}} \right)^{0.4} \qquad (7.30)$$

The design plastic resistance moment ($M_{V,Rd}$) can be determined from equation (7.9) or (7.15) depending upon the shear force.

### 7.1.6.3    Based upon the elastic moment capacity only

If the resistance moment of the chord section is determined based upon its elastic moment capacity for all the joints, the same equation as (6.21) can be used. The only difference is that $M_{el,Rd}$ should be replaced by $M_{V,e,Rd}$ for T-joints:

$$f(J_m) = 1 - 0.23(1-0.85\beta)\sqrt{\gamma} \ (\frac{M_0}{M_{V,e,Rd}})^2 \qquad (7.31)$$

The design elastic resistance moment ($M_{V,e,Rd}$) can be determined from equation (7.21) or (7.25) depending upon the shear force.

### 7.1.7   Conclusions

A parameter study on T-joints in square hollow sections subjected to axial loads and chord bending moments has been carried out. The geometry parameters varied in the study are:

-    The width ratio between the brace and the chord $\beta$;
-    The width to thickness ratio of the chord $2\gamma$;
-    The chord length to width ratio $\alpha/2$.

Each joint has been analysed twice, i.e. including and excluding the effects of chord bending moments at the intersection between the brace and the chord. The following conclusions can be drawn:

-    By separating the effect of the chord bending moment from that of the concentrated load, failure of uniplanar T-joints can be described in a clear manner.

-    Three sets of interaction formulae between axial load and the global bending moment have been derived numerically where the resistance moment of the chord is based

upon EC3 (1992), based upon the plastic moment capacity only or based upon the elastic moment capacity only respectively. These formulae can be used for both T- and X-joints.

- For $\beta=1.0$ and $M_0/M_{V,Rd}\geq1.0$, failure of a T-joint is governed by the resistance moment of the chord section or by the brace effective width criteria. The last criterion has not been checked numerically.

## 7.2 AXIALLY LOADED T-JOINTS EXCLUDING CHORD BENDING MOMENT

### 7.2.1 Introduction

In Section 7.1, the influence of the chord bending moment of an axially loaded T-joint has been numerically investigated and reduction functions $f(J_m)$ due to chord bending moment have been established. Because $f(J_m)=N_{1,u}(J_m)/N_{1,u}(J_m=0)$, the normalising term of $N_{1,u}(J_m=0)$ should be known in order to determine the ultimate load capacity of an axially loaded T-joint including chord bending moment. This normalising term $N_{1,u}(J_m=0)$ is defined as the ultimate load capacity of axially loaded T-joints excluding chord bending moment at the intersection between the chord and the brace ($J_m=0$). The numerical analysis for joints with $J_m=0$ has been done in Section 7.1. The geometrical parameters and the FE results can be found in Tables 7.2 and 7.3. By excluding the chord bending moment, local failure of a T-joint can be expressed in a clear manner. For axially loaded T-joints excluding chord bending moment, it is expected that failure modes should be similar to those of axially loaded X-joints. In this section, some additional numerical analyses for X-joints have been done. According to the numerical results, it is shown that identical ultimate load capacity formulae can be used for both X- and T-joints if the bending moment in the chord is excluded.

### 7.2.2 Comparison between the results of axially loaded T-joints excluding chord bending moment and those of axially loaded X-joints

The welds are not included for the investigated T-joints in Section 7.1, while butt welds are included for X-joints with $\beta=0.4$, 0.6 and 0.8 in Section 6.1, Chapter 6. Therefore, a direct comparison between the results of axially loaded T-joints excluding chord bending and those of axially loaded X-joints is not possible. In order to solve this problem, some additional analyses are carried out for the joints in Section 6.1 with the weld excluded, see Table 7.4. The joints in Table 7.4 are corresponding to those in Table 6.1. The only difference is that the welds are excluded in the numerical model. For example, joint x2a* in Table 7.4 is the same as joint x2a in Table 6.1 with the exception that no weld is included for joint x2a*. In Figure 7.6, the numerical results of the X-joints in Table 7.4 are compared with those of the corresponding T-joints in Table 7.2. The quantitative comparisons between the results of T- and X-joints are listed in Table 7.5. It can be seen that the difference is neglectable.

**Table 7.4    Extra study of axially loaded X-joints with the welds excluded**

| | $\beta$ | | | |
|---|---|---|---|---|
| | 0.4 | 0.6 | 0.8 | 1.0 |
| $2\gamma=15$ | | x4a* | x7a* | |
| $2\gamma=24$ | x2a* | x5a* | | x11a* |
| $2\gamma=35$ | | x6a* | | |
| $\alpha=12$, $f_{y0}=355$ N/mm$^2$ | | | | |
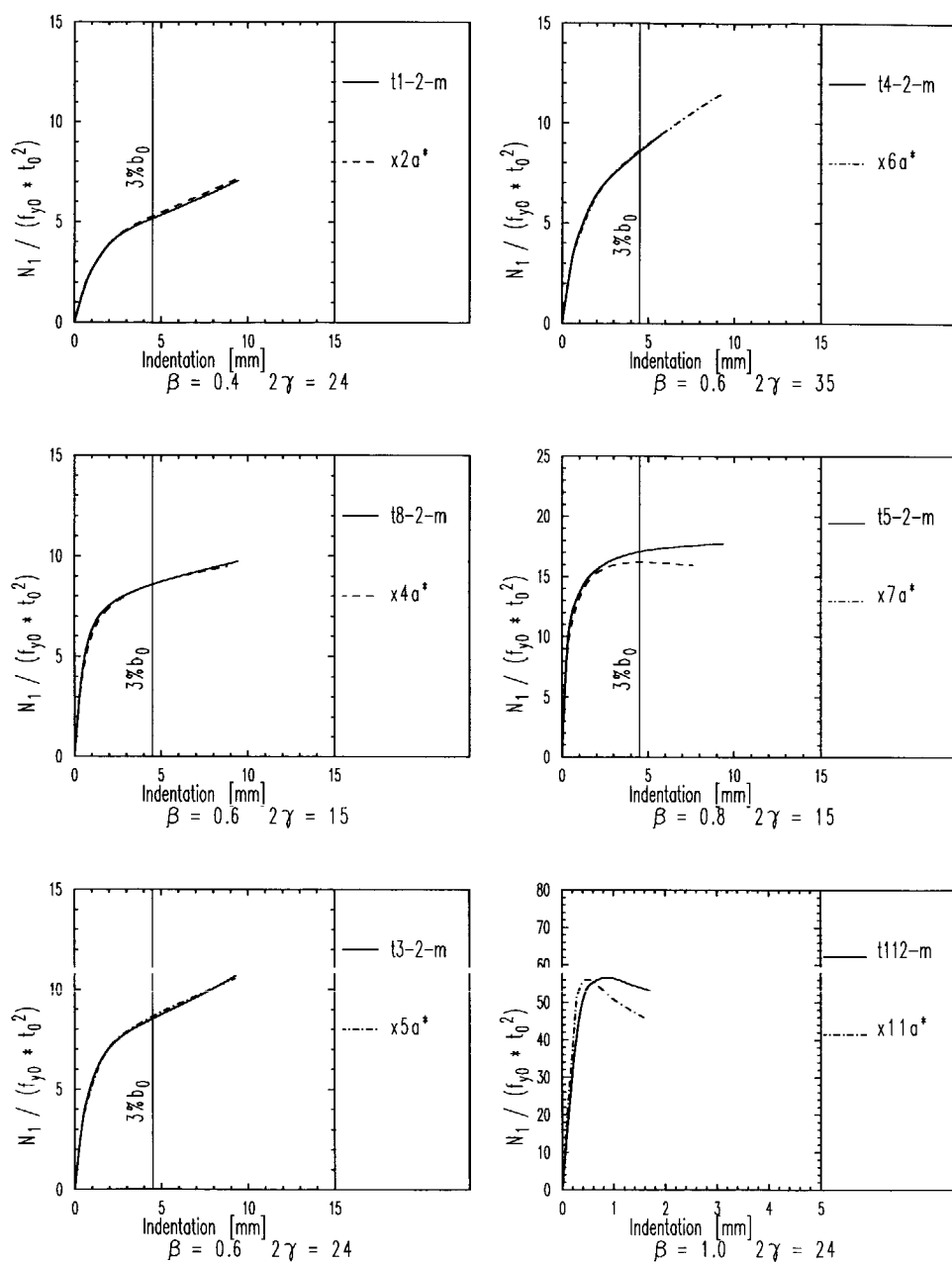
**Figure 7.6**     **Comparison between the results of axially loaded T-joints excluding chord bending and those of axially loaded X-joints**

**Table 7.5    Comparison between the results of axially loaded T-joints excluding chord bending and those of axially loaded X-joints**

| Parameters | | T-joints | | X-joints | | (1)/(2) |
|---|---|---|---|---|---|---|
| | | | (1) | Name | (2) | |
| $\beta$ | $2\gamma$ | Name | $N_{1,u}/(f_{y0}t_0^2)$ | | $N_{1,u}/(f_{y0}t_0^2)$ | |
| 0.4 | 24 | t1-2-m | 5.18 | x2a[*] | 5.29 | 0.98 |
| 0.6 | 15 | t8-2-m | 8.59 | x4a[*] | 8.59 | 1.00 |
| 0.6 | 24 | t3-2-m | 8.52 | x5a[*] | 8.64 | 0.99 |
| 0.6 | 35 | t4-2-m | 8.58 | x6a[*] | 8.62 | 1.00 |
| 0.8 | 15 | t5-2-m | 17.07 | x7a[*] | 16.20 | 1.05 |
| 1.0 | 24 | t112-m | 56.36 | x11a[*] | 55.96 | 1.01 |
| $\alpha=12$ | | | | | | |

[*]: Without weld.

Note:  1)    for T-joints, $f_{y0}$=419.7 N/mm$^2$; for X-joints, $f_{y0}$=355 N/mm$^2$.
       2)    for both T- and X-joints, weld is excluded.


### 7.2.3    Conclusions

By excluding the chord bending moment at the intersection between the chord and the brace, the joint behaviour of an axially loaded T-joint is similar to that of an axially loaded X-joint for the same joint geometrical parameters. The difference between the ultimate load capacity of an axially loaded T-joint excluding chord bending and that of an axially loaded X-joint is neglectable. Therefore, the ultimate load capacity formulae equation (6.1) and (5.20) for axially loaded X-joints can also be used for axially loaded T-joints excluding chord bending moment. Together with the interaction formulae in Section 7.1, a complete set of formulae for axially loaded T-joints including and excluding chord bending moments is established.

## 7.3   UNIPLANAR T-JOINTS LOADED WITH IN-PLANE BENDING MOMENTS

### 7.3.1   Introduction

Similar to X-joints loaded with in-plane bending moments, failure modes of T-joints loaded with in-plane bending moment can be classified as a): chord face plastification; b): chord punching shear; c): brace cracking (effective width) on the tension side or brace buckling on the compression side; d): chord side wall yielding or buckling. Besides, chord shear failure may occur for T-joints loaded with in-plane bending moment. This failure mode is actually a member failure instead of a joint failure. The shear force and the moment distributions along the chord length are shown in Figure 7.7.
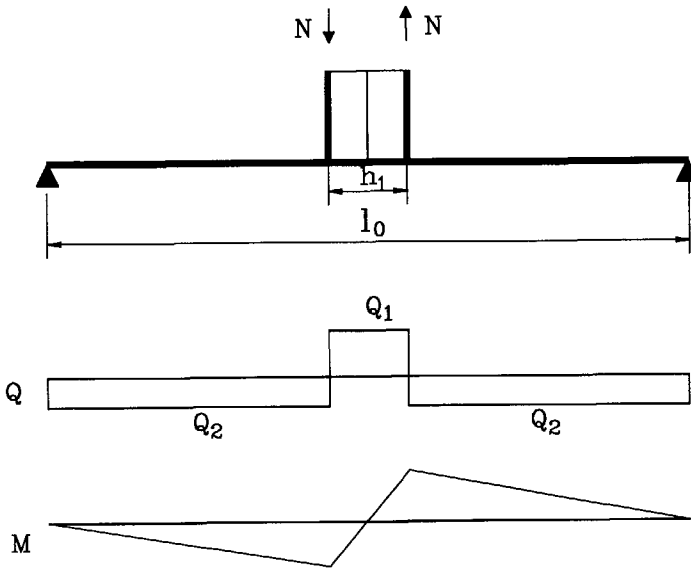


**Figure 7.7    Shear force and moment distributions in the chord of a T-joint loaded with in-plane bending moment**

The shear forces shown in Figure 7.7 are:

$$Q_1 = N(1 - \frac{h_1}{l_0}) \tag{7.32}$$

$$Q_2 = \frac{Nh_1}{l_0} \tag{7.33}$$

Shear failure can be easily checked with the following formula:

$$Q_2 \leq V_{pl,Rd} = 2(h_0 - t_0)t_0 \frac{f_{y0}}{\sqrt{3}}$$  (7.34)

The chord bending moment at the intersection between the chord and the brace is:

$$M = \frac{Nh_1}{2}(1 - \frac{h_1}{l_0}) = \frac{M_{1,ipb}}{2}(1 - \frac{h_1}{l_0})$$  (7.35)

It can be seen that the bending moment in the chord is generally smaller than half of the bending moment applied on the brace $M_{1,ipb}$. Generally, failure due to the bending moment in the chord is not critical. Compared to axially loaded T-joints, the influence of the chord bending moment on the joint ultimate moment capacity is relatively small.

As no cracking is modelled, only failure modes a) and d) are studied in the numerical study.

### 7.3.2          Research programme

The configuration of an uniplanar T-joint loaded with an in-plane bending moment is shown in Figure 7.8. The research programme for the numerical parameter study is summarised in Table 7.6. The dimensions and the material properties of the joints and the weld are the same as those of the corresponding X-joints in Section 6.2, Chapter 6.
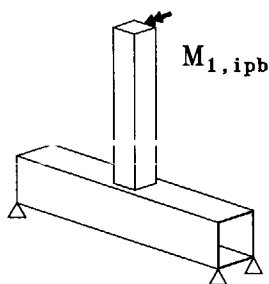


**Figure 7.8      Configuration of a T-joint loaded with an in-plane bending moment**

**Table 7.6      Research programme of T-joints loaded with in-plane bending moments**

| | η | β | | | |
|---|---|---|---|---|---|
| | | 0.4 | 0.6 | 0.8 | 1.0 |
| 2γ=15 | 0.5 β | | | | t10ie05[*] |
| | 1.0 β | t1i | t4i | t7i | t10i[*] |
| | 2.0 β | | | | t10ie2[*] |
| 2γ=24 | 0.5 β | | t5ie05 | | |
| | 1.0 β | t2i | t5i | t8i | |
| | 2.0 β | | t5ie2 | t8ie2 | t11ie2[*] |
| 2γ=35 | 0.5 β | t3ie05 | | | t12ie05[*] |
| | 1.0 β | t3i | t6i | t9i | t12i[*] |
| | 2.0 β | t3ie2 | | | t12ie2[*] |

*:      without weld

### 7.3.3        The FE analysis

The general considerations of the FE analysis are described in Chapter 4. Because of symmetry in geometry and loading, half of a T-joint is modelled. The finite element meshes for each corresponding joint are the same as in Section 6.2, Chapter 6, where a quarter of a joint is modelled. For the application of the in-plane bending moment, load control has been used in order to apply pure bending moment on the brace, see Figure 6.13. Due to the differences in symmetry and support conditions for T-joints, the boundary conditions in this section are different from those for X-joints in Section 6.2. The finite element meshes and the boundary conditions for a T-joint are shown in Figure 7.9. The origin of the coordinate system is in the center of the chord.
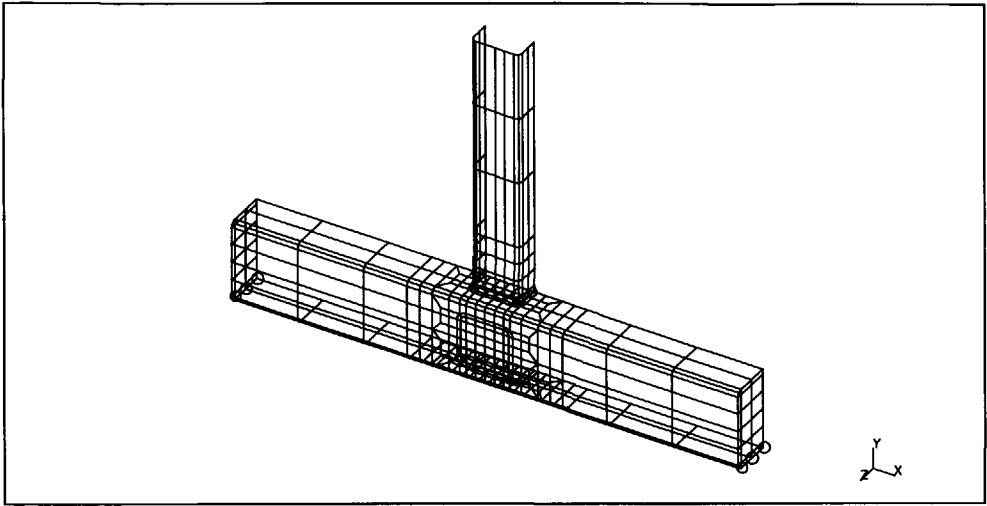
| BOUNDARY CONDITIONS | | | |
|---|---|---|---|
| Degrees of freedom | Node at X=0.0, Y=$(h_0-t_0)/2$, Z=0.0 | Nodes on plane Z=0.0 | Nodes at supports |
| $u_x$ | 0. | free | free |
| $u_y$ | free | free | 0. |
| $u_z$ | 0. | 0. | free |
| $\Phi_x$ | 0. | 0. | free |
| $\Phi_y$ | 0. | 0. | free |
| $\Phi_z$ | free | free | free |

**Figure 7.9    FE meshes of a T-joint loaded with in-plane bending moment**

### 7.3.4      The numerical results and observations

The numerical results are illustrated in three groups of figures:

1)    joints made of square hollow sections ($\beta \leq 0.8$), Figure 7.10;
2)    joints made of rectangular hollow sections ($\beta \leq 0.8$), Figure 7.11;
3)    joints made of rectangular hollow sections ($\beta = 1.0$), Figure 7.12.

In the three figures, the ultimate moment capacity of the joint is marked and the ultimate deformation limit of 3%$b_0$ is indicated. The procedure to determine the ultimate moment capacity of the joint can be found in Chapter 4.

Observations from Figure 7.10 are:

- For joints with $\beta=0.4$, the ultimate moment capacity marked in the figure is determined at the rotation limit of $\phi_{0.1}$ where the corresponding indentation is smaller than the ultimate deformation limit ($3\%b_0$).

- For joints with $\beta=0.6$ and 0.8, the ultimate moment capacity is determined at $3\%b_0$.

- The joint behaviour is the same as that of the corresponding X-joints loaded with in-plane bending moments (Figure 6.15). The non-dimensional moment is increasing with the increase of the chord top face indentation. Failure of the joint is due to plastification of the chord face.

Observations from Figure 7.11 are:

- The moment vs. indentation curves are very similar to those of the corresponding X-joints loaded with in-plane bending moments (Figure 6.16). The $\eta$ influence can be clearly seen. The non-dimensional moment vs. indentation curves are typical for the failure of chord top face plastification where the moment is increasing with the increase of indentation.

Observations from Figure 7.12 are:

- For joints with $\eta=0.5$ and 1.0, the moment vs. indentation curves are similar to those of X-joints loaded with in-plane bending moments (Figure 6.17). No maximum moment is found except for the joint with $\eta=1.0$ and $2\gamma=35$.

- For the joint with $\eta=2.0$ and $2\gamma=24$, a maximum is not reached in Figure 7.12, while there is a maximum for the corresponding curve of X-joint (Figure 6.17). Thus, full width uniplanar T-joints are less sensitive for chord side wall buckling than the corresponding uniplanar X-joints loaded with in-plane bending moments. A maximum is found for the joint with $\eta=2.0$ and $2\gamma=35$ in Figure 7.12.

The ultimate moment capacity and the corresponding indentation of each joint are quantitatively listed in Tables 7.7 and 7.8 which will be compared with the results of the X-joints loaded with in-plane bending moments.
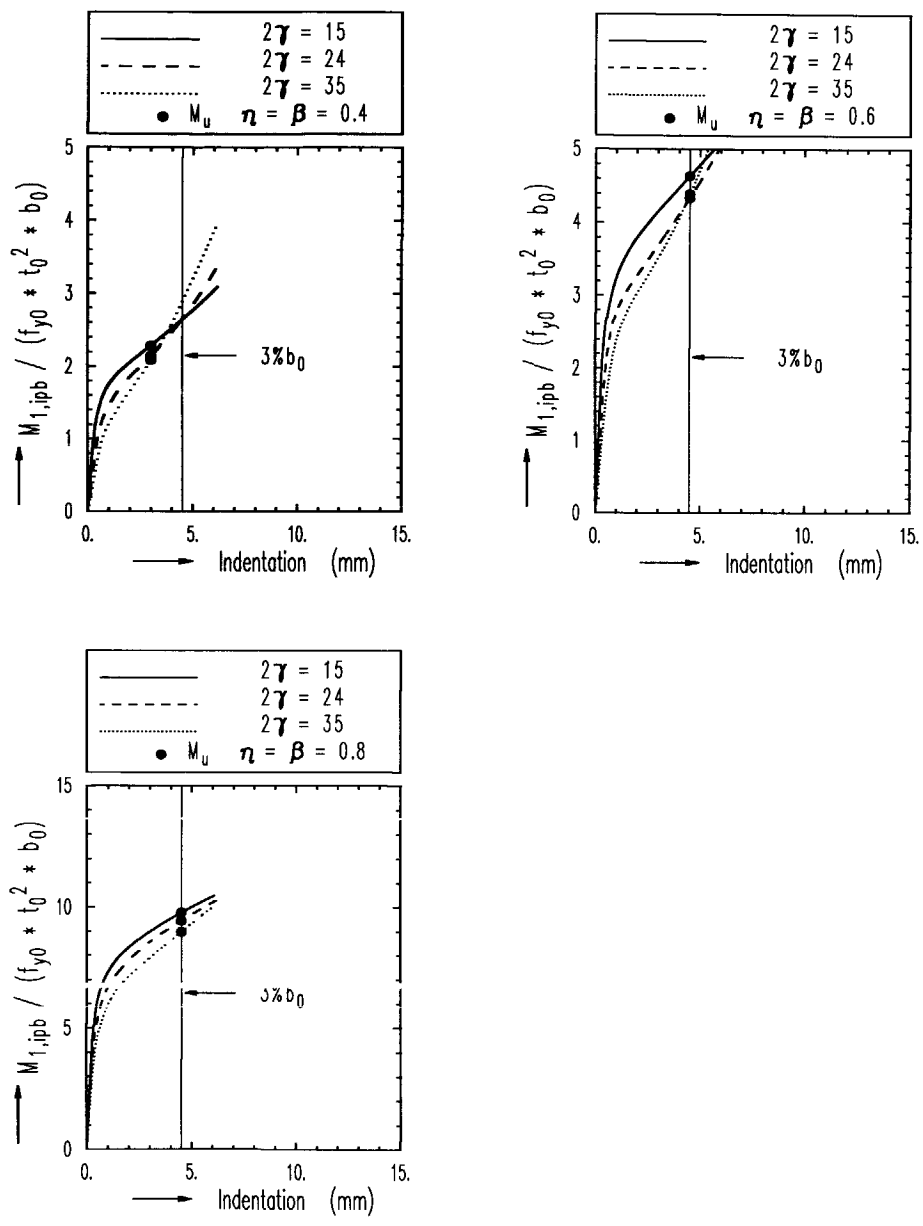
**Figure 7.10**  **Numerical results of T-joints in square hollow sections loaded with in-plane bending moment ($\eta=\beta$)**
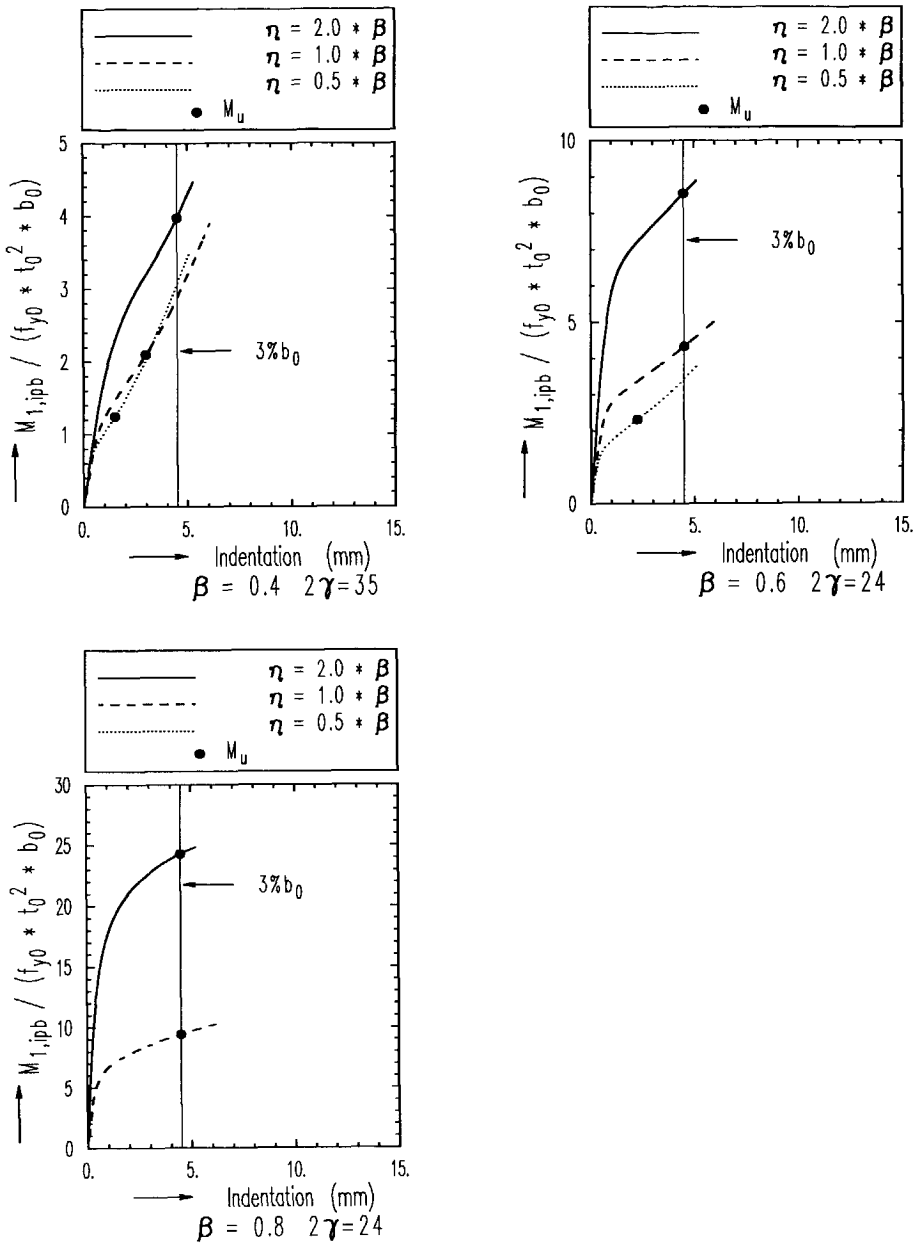
**Figure 7.11** **Numerical results of T-joints in rectangular hollow sections loaded with in-plane bending moment ($\eta$ influence)**
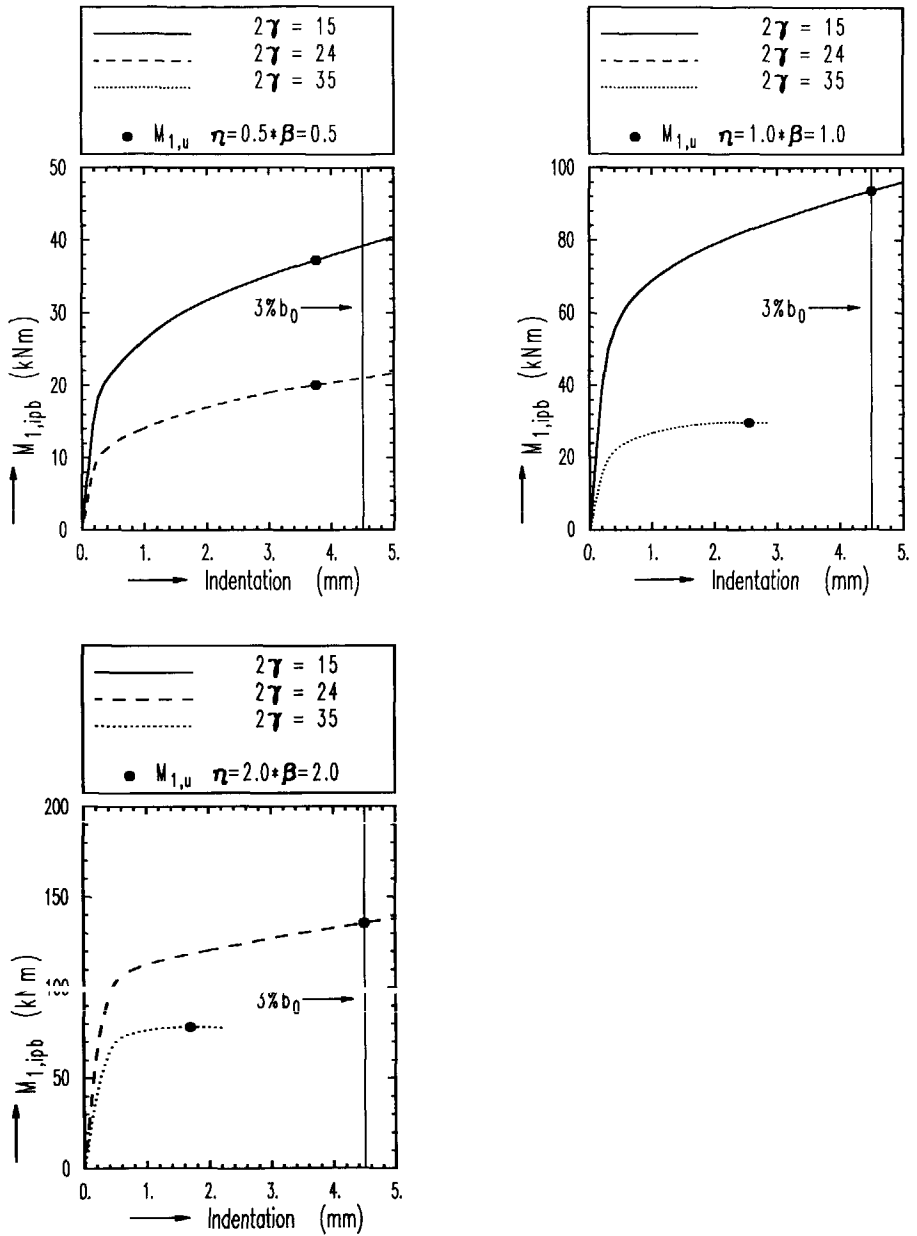
**Figure 7.12** **Numerical results of uniplanar T-joints of rectangular hollow sections loaded with in-plane bending moment ($\beta=1.0$)**

**Table 7.7** **FE results of T-joints loaded with in-plane bending moment (β≤0.8)**

| Joints | Geometrical parameters | | | Numerical results | | |
|--------|----|------|-----|----|----|----|
| | β | 2γ | η | $M_{1,ipb,u}/(f_{y0}t_0{}^2b_0)$ | $\delta_u$ (mm) | Criteria |
| t1i | 0.4 | 15 | 0.4 | 2.30 | 3.00 | $\phi_{0.1}$ |
| t2i | 0.4 | 24 | 0.4 | 2.15 | 3.00 | $\phi_{0.1}$ |
| t3ie05 | 0.4 | 35 | 0.2 | 1.25 | 1.50 | $\phi_{0.1}$ |
| t3i | 0.4 | 35 | 0.4 | 2.10 | 3.00 | $\phi_{0.1}$ |
| t3ie2 | 0.4 | 35 | 0.8 | 3.98 | 4.50 | $3\%b_0$ |
| t4i | 0.6 | 15 | 0.6 | 4.63 | 4.50 | $3\%b_0$ |
| t5ie05 | 0.6 | 24 | 0.3 | 2.32 | 2.25 | $\phi_{0.1}$ |
| t5i | 0.6 | 24 | 0.6 | 4.33 | 4.50 | $3\%b_0$ |
| t5ie2 | 0.6 | 24 | 1.2 | 8.54 | 4.50 | $3\%b_0$ |
| t6i | 0.6 | 35 | 0.6 | 4.38 | 4.50 | $3\%b_0$ |
| t7i | 0.8 | 15 | 0.8 | 9.77 | 4.50 | $3\%b_0$ |
| t8i | 0.8 | 24 | 0.8 | 9.42 | 4.50 | $3\%b_0$ |
| t8ie2 | 0.8 | 24 | 1.6 | 24.30 | 4.50 | $3\%b_0$ |
| t9i | 0.8 | 35 | 0.8 | 8.96 | 4.50 | $3\%b_0$ |

**Table 7.8** **FE results of T-joints loaded with in-plane bending moment (β=1.0)**

| Joint | Geometrical parameters | | | Numerical results | | |
|-------|----|------|-----|----|----|----|
| | β | 2γ | η | $M_{1,ipb,u}$ (kNm) | $\delta_u$ (mm) | Criteria |
| t10ie05[*] | 1.00 | 15 | 0.5 | 37.28 | 3.75 | $\phi_{0.1}$ |
| t10i[*] | 1.00 | 15 | 1.0 | 93.71 | 4.50 | $3\%b_0$ |
| t10ie2[*] | 1.00 | 15 | 2.0 | 228.29 | 4.50 | $3\%b_0$ |
| t11ie05[*] | 1.00 | 24 | 0.5 | 20.08 | 3.75 | $\phi_{0.1}$ |
| t11ie2[*] | 1.00 | 24 | 2.0 | 135.53 | 4.50 | $3\%b_0$ |
| t12i[*] | 1.00 | 35 | 1.0 | 29.74 | 2.56 | Max. |
| t12ie2[*] | 1.00 | 35 | 2.0 | 78.09 | 1.69 | Max. |

[*]: without weld

### 7.3.5          Comparison with the results of X-joints loaded with in-plane bending moments

In Figure 7.13, the ultimate moment capacity listed in Tables 7.7 and 7.8 are compared to the corresponding results of X-joints loaded with in-plane bending moments listed in Tables 6.8 and 6.9. It can be seen that the difference is within 5%. Thus, the ultimate moment capacity formulae recommended for X-joints in Section 6.2 can be used for T-joints.
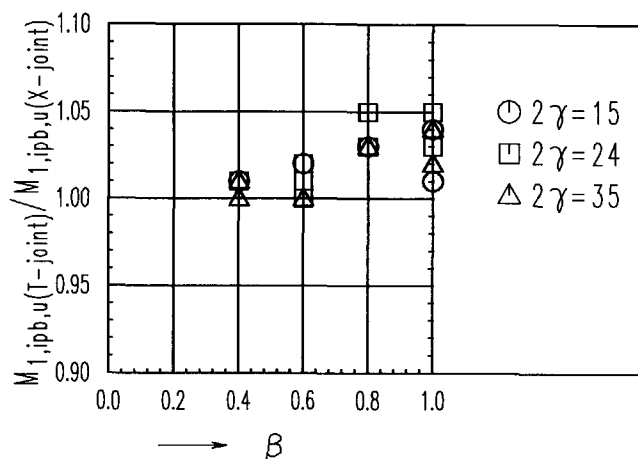


**Figure 7.13    Comparison between the results of T- and X-joints**

### 7.3.6          Conclusions

The static behaviour of uniplanar T-joints loaded with in-plane bending moments has been investigated in this section. The joint geometrical parameters include $\beta$=0.4, 0.6, 0.8 and 1.0; $2\gamma$=15, 24 and 35; $\eta$=0.5*$\beta$, 1.0*$\beta$ and 2.0*$\beta$ respectively. It is concluded that:

-       The joint behaviour of uniplanar T-joints loaded with in-plane bending moments is very similar to that of the corresponding uniplanar X-joints except that chord side wall buckling is less sensitive for T-joints than for X-joints.

-       For the joint geometrical parameters used, the difference in ultimate moment capacity between T- and X-joints is within 5%. Thus, the formulae recommended for X-joints can be used for T-joints.

## 7.4 UNIPLANAR T-JOINTS LOADED WITH OUT-OF-PLANE BENDING MOMENTS

### 7.4.1 Introduction

For uniplanar T-joints loaded with out-of-plane bending moment, the behaviour of the joints with small to medium $\beta$ values is similar to that of uniplanar X-joints. Whereas the behaviour of full width T-joints is totally different from that of X-joints. A full width T-joint loaded with out-of-plane bending moment is actually a box girder under restrained rotation. The theory about rotation and distortion of box girders can be found in Terrington (1970), Li (1987) and Nakai (1988) etc. Unfortunately, these references only deal with the elastic behaviour of the material. No direct theoretical solution can be found for the present work when plastification occurs in the joints. Nevertheless, these books are helpful for the understanding of the problems such as the distribution of the torsional shear stresses, the warping stresses, and the transverse bending stresses and the distortion behaviour etc. In the CIDEC design guide (Packer 1992a), the failure mechanism of full width T-joints is considered as effective width of the brace or the bearing strength of the chord side walls. For full width T- and X-joints, identical design resistance formulae are recommended except that when chord side wall failure occurs a higher $\gamma_M$ factor is used for X-joints. This consideration was based upon an assumption that the distortion failure of the chord section is not dominating. However, if no diaphragm stiffening is used, distortion failure of the chord section occurs. In this section, both numerical and analytical studies on this failure mode are carried out and a formula for the ultimate moment capacity is recommended which is valid for T-joints with different $\alpha$ values. The analytical model used in this section is based upon the failure mechanism recommended by Niemi (1986). For T-joints with small to medium $\beta$ values, a numerical study is carried out and it is expected that the same ultimate moment capacity formula can be used as for X-joints.

### 7.4.2 Research programme

The configuration of a T-joint loaded with out-of-plane bending moment is shown in Figure 7.14. The research programme is summarised in Table 7.9.
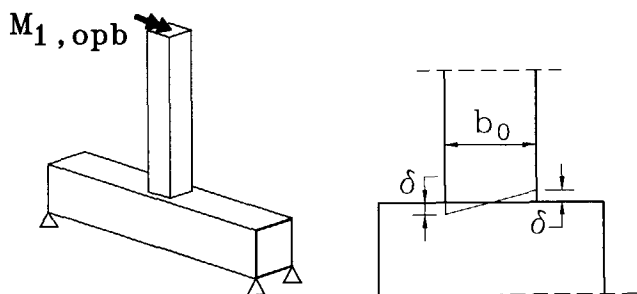


**Figure 7.14    Configuration of a T-joint loaded with out-of-plane bending moment**

**Table 7.9**     **Research programme for T-joints loaded with out-of-plane bending moment**

|            | β      |        |        |        |        |        |        |        |        |
|------------|--------|--------|--------|--------|--------|--------|--------|--------|--------|
|            | 0.4    | 0.6    | 0.8    | 1.0    |        |        |        |        |        |
| 2γ=15      | t1o    | t4o    | t7o    | t10o1  | t10o2  | t10o3  | t10o4  | t10o5  | t10o6  |
| 2γ=24      | t2o    | t5o    | t8o    | t11o1  | t11o2  | t11o3  | t11o4  | t11o5  | t11o6  |
| 2γ=35      | t3o    | t6o    | t9o    | t12o1  | t12o2  | t12o3  | t12o4  | t12o5  | t12o6  |
| α          | 12     |        |        | 6      | 9      | 12     | 18     | 24     | 40     |

In this section, only joints with square hollow sections are included. The depth of the chord is fixed at 150 mm. For joints with β≤0.8, the dimensions and the material properties of the chord, the braces and the weld are the same as used in Section 7.2. For joints with β=1.0, the dimensions of the joints are the same as in the previous section except that the chord length ratio varies with α=6, 9, 12, 18, 24 and 40. The weld along the chord length for joints with β=1.0 is not included. The thickness of the plates on the chord ends is 25 mm as used in the previous sections.

### 7.4.3     The FE analysis

The general considerations for the FE analysis are described in Chapter 4. Only the specific aspects for this section are described as follows:

-     The finite element meshes of the joints are the same as used in the previous section with a different plane of symmetry and different boundary conditions, see Figure 7.15. In order to prevent rigid body motion, an extra restraint in Z-direction is added to one node of the chord with a coordinate of X=0, Y=$(h_0-t_0)/2$, Z=0. The origin of the coordinate system is in the centre of the chord.

-     Similar to X-joints loaded with out-of-plane bending moments, the out-of-plane bending moment for T-joints is applied by two opposite axial forces at the end of the brace in order to exert pure bending moment. Load control is used.

-     The end of the chord is vertically supported as shown in Figure 7.15.

| BOUNDARY CONDITIONS | | | |
|---|---|---|---|
| Degrees of freedom | Node at (X=0.0, Y=$(h_0-t_0)/2$, Z=0.0) | Nodes on plane X=0.0 | Nodes at support |
| $u_x$ | 0. | 0. | free |
| $u_y$ | free | free | 0. |
| $u_z$ | 0. | free | free |
| $\Phi_x$ | free | free | free |
| $\Phi_y$ | 0. | 0. | free |
| $\Phi_z$ | 0. | 0. | free |
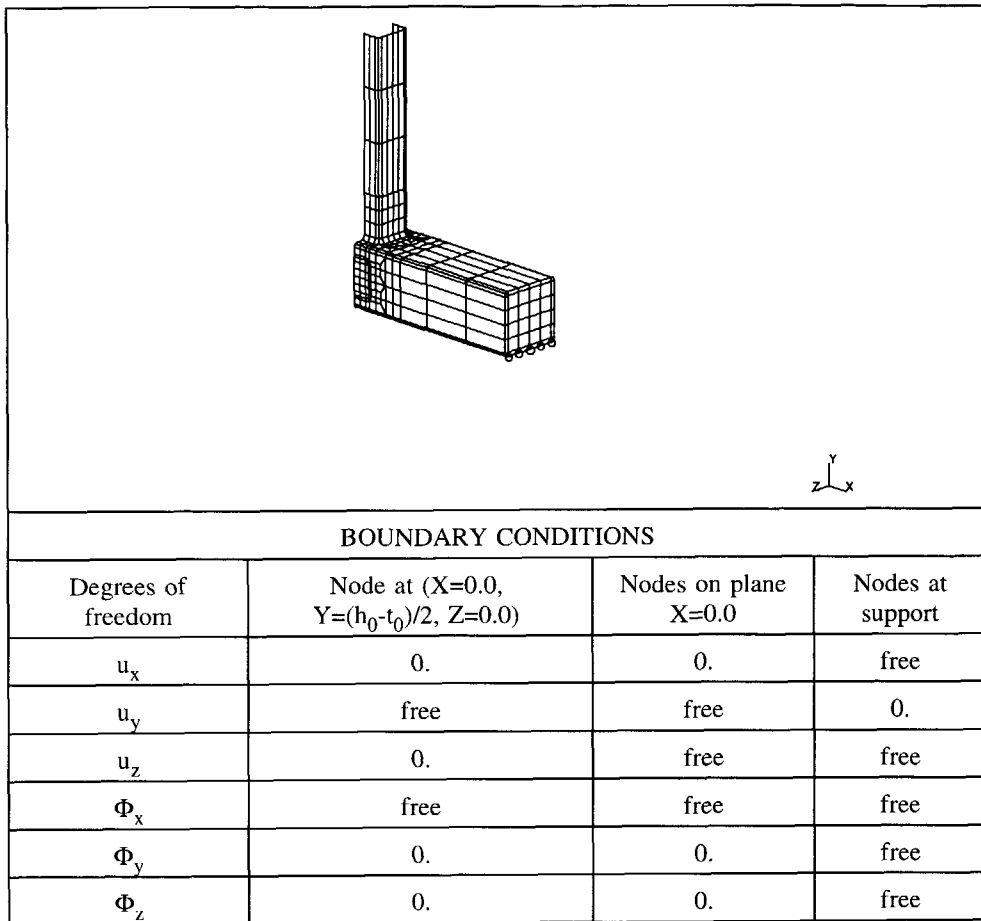
**Figure 7.15   FE meshes and boundary conditions of a T-joint loaded with out-of-plane bending moment**

### 7.4.4    The numerical results

The non-dimensional moment vs. indentation curves for joints with $\beta$=0.4, 0.6 and 0.8 are shown in Figure 7.16. For joints with $\beta$=1.0, the moment vs. displacement curves are shown in Figure 7.17.

In Figure 7.16, the X-axis is the indentation ($\delta$) of the chord top face in the compression side of the brace, see Figure 7.14. The Y-axis is the non-dimensional moment which is the same as used for X-joints. The non-dimensional moment vs. indentation curves are similar to those of X-joints as expected. Because for T-joints with small to medium $\beta$ values, large plastic indentation of the chord top face is governing which is the same as for X-joints. The ultimate

moment capacity for T-joints will be compared with that of X-joints in this section. It can be seen that there is hardly difference between the two.

In Figure 7.17, the displacement due to distortion is given on the X-axis. The displacement due to distortion is measured as the relative vertical displacement of points $P_1$ and $P_2$ as shown in Figure 7.18. The behaviour of T-joints is totally different from that of X-joints because distortion failure of the chord section is dominating. It can be seen that the stiffness and the ultimate moment capacity of the joints is influenced by the $2\gamma$ and the $\alpha$ values. The larger the $\alpha$ value, the lower the stiffness of the joint. The influence of the $\alpha$ value on the ultimate moment capacity is clear until $\alpha$ reaches a critical value which depends upon the $2\gamma$ values. However, if $\alpha$ is equal to or larger than a critical value, the ultimate moment capacity becomes constant. For example, for joint with $2\gamma=15$, the $\alpha$ influence upon the ultimate moment capacity is clear for $\alpha \leq 9$; while there is hardly any $\alpha$ influence for $\alpha$ between 12 and 40. The critical $\alpha$ value for joint with $2\gamma=15$ is about 12. For joints with $2\gamma=24$ and 35, the critical $\alpha$ value is higher than 12. The physical meaning of the critical $\alpha$ value will be further explained based upon a failure mechanism caused by distortion.

The same procedure is used for the determination of the ultimate moment capacity of the joints as described in Chapter 4. The quantitative values of the ultimate moment capacity from the FE results are listed in Table 7.10.
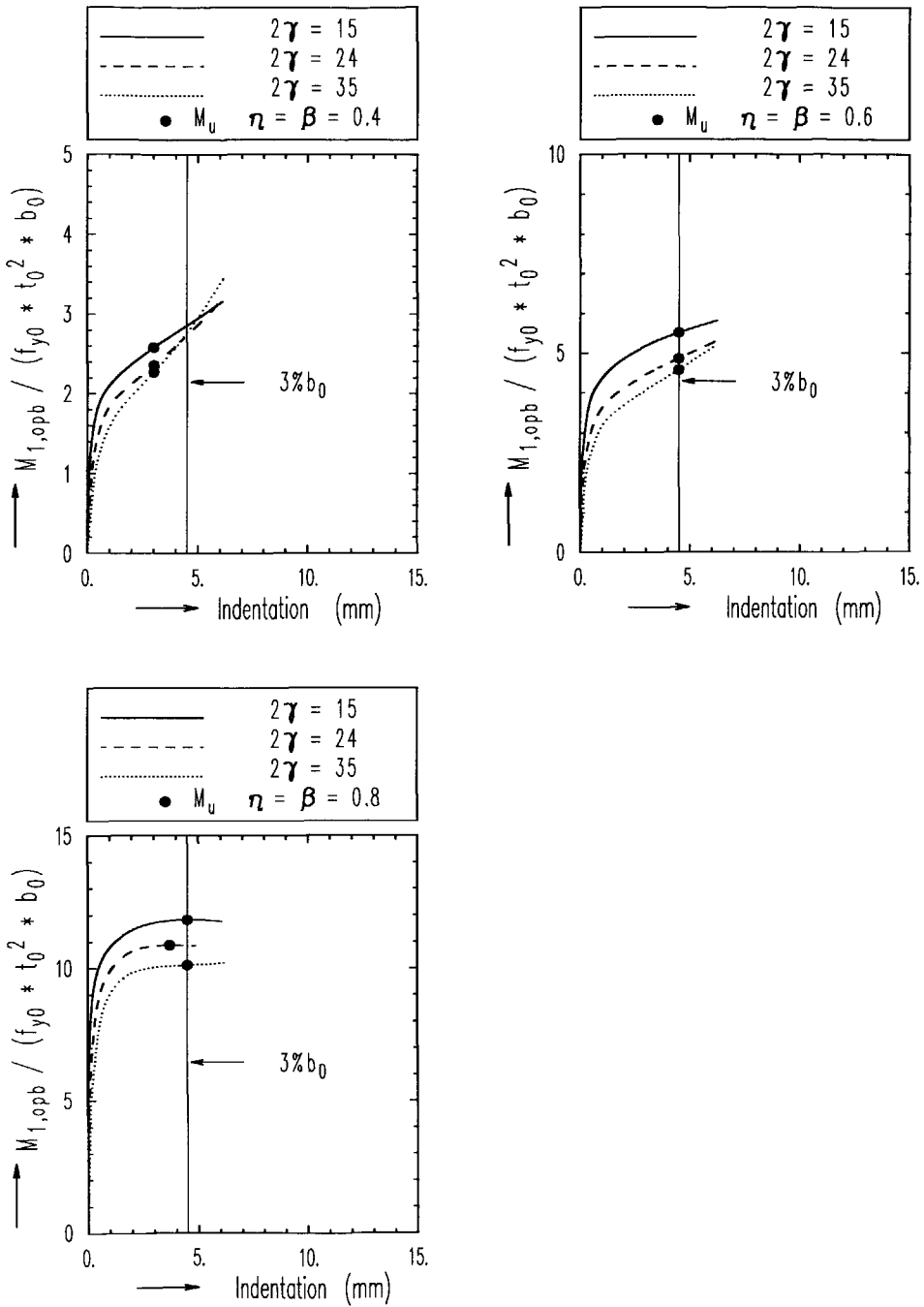
**Figure 7.16** **FE results of T-joints loaded with out-of-plane bending moment ($\beta \leq 0.8$)**
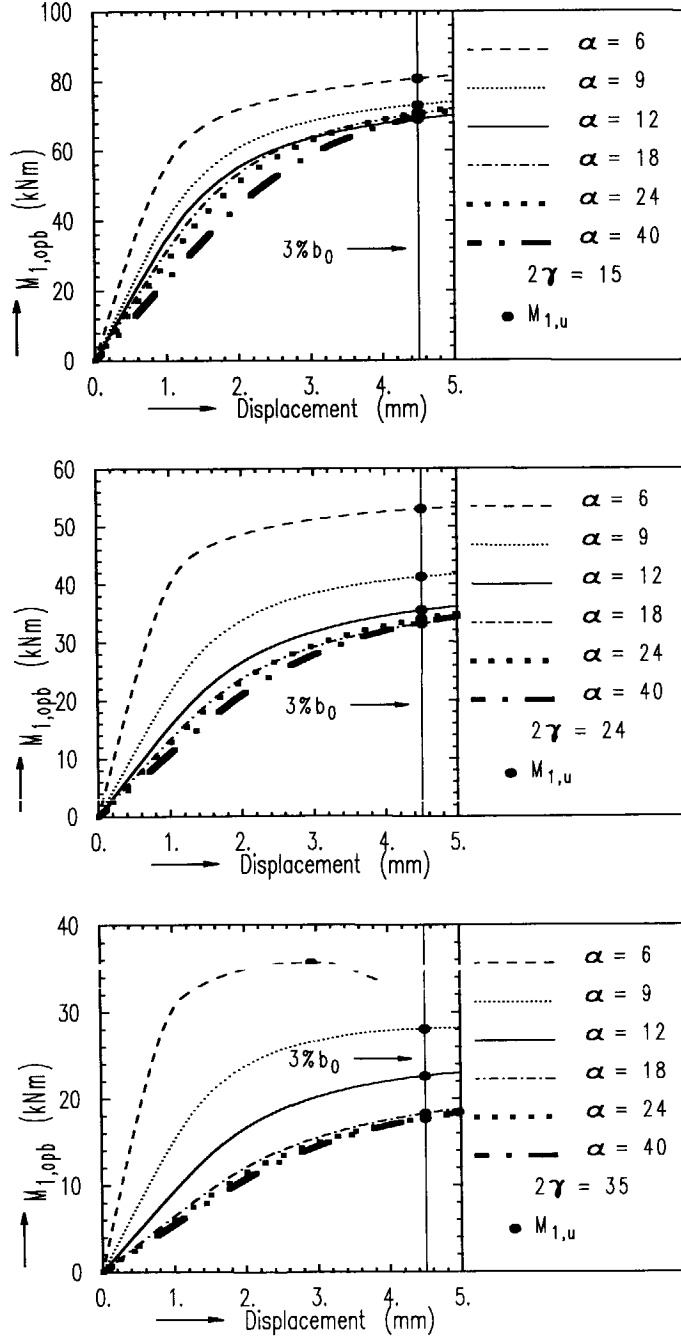
**Figure 7.17    FE results of T-joints loaded with out-of-plane bending moment ($\beta$=1.0)**
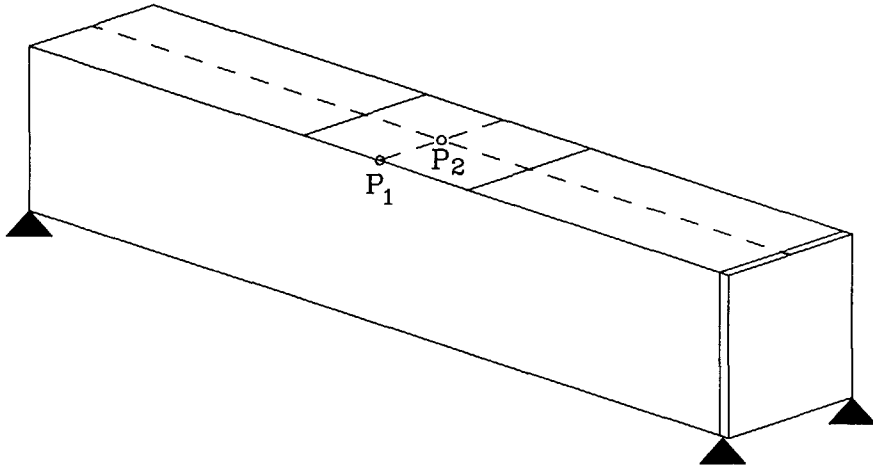
**Figure 7.18   Measured points for the displacement due to distortion**

**Table 7.10    Numerical results of T-joints loaded with out-of-plane bending moment**

| Joint | Geometrical parameters | | | Numerical results | | | |
|---|---|---|---|---|---|---|---|
| | $\beta$ | $2\gamma$ | $\alpha$ | $M_{1,opb,u}/(f_{y0}t_0^2b_0)$ | $M_{1,opb,u}$ (kNm) | $\delta_u$ (mm) | Criteria |
| t1o | 0.4 | 15 | 12 | 2.58 | 13.74 | 3.0 | $\phi_{0.1}$ |
| t2o | 0.4 | 24 | 12 | 2.36 | 12.57 | 3.0 | $\phi_{0.1}$ |
| t3o | 0.4 | 35 | 12 | 2.27 | 12.09 | 3.0 | $\phi_{0.1}$ |
| t4o | 0.6 | 15 | 12 | 5.51 | 11.46 | 4.5 | $3\%b_0$ |
| t5o | 0.6 | 24 | 12 | 4.86 | 10.11 | 4.5 | $3\%b_0$ |
| t6o | 0.6 | 35 | 12 | 4.58 | 9.53 | 4.5 | $3\%b_0$ |
| t7o | 0.8 | 15 | 12 | 11.82 | 11.58 | 4.5 | $3\%b_0$ |
| t8o | 0.8 | 24 | 12 | 10.87 | 10.65 | 3.5 | Max. |
| t9o | 0.8 | 35 | 12 | 10.11 | 9.91 | 4.5 | $3\%b_0$ |
| t10o1 | 1.00 | 15 | 6 | 15.15 | 80.67 | 4.5 | $3\%b_0$ |
| t10o2 | 1.00 | 15 | 9 | 13.71 | 73.01 | 4.5 | $3\%b_0$ |
| t10o3 | 1.00 | 15 | 12 | 12.97 | 69.05 | 4.5 | $3\%b_0$ |
| t10o4 | 1.00 | 15 | 18 | 13.25 | 70.56 | 4.5 | $3\%b_0$ |
| t10o5 | 1.00 | 15 | 24 | 13.29 | 70.77 | 4.5 | $3\%b_0$ |
| t10o6 | 1.00 | 15 | 40 | 13.08 | 69.64 | 4.5 | $3\%b_0$ |
| t11o1 | 1.00 | 24 | 6 | 25.43 | 52.91 | 4.5 | $3\%b_0$ |
| t11o2 | 1.00 | 24 | 9 | 19.80 | 41.48 | 4.5 | $3\%b_0$ |
| t11o3 | 1.00 | 24 | 12 | 17.04 | 35.44 | 4.5 | $3\%b_0$ |
| t11o4 | 1.00 | 24 | 18 | 15.95 | 33.14 | 4.5 | $3\%b_0$ |
| t11o5 | 1.00 | 24 | 24 | 16.31 | 33.92 | 4.5 | $3\%b_0$ |
| t11o6 | 1.00 | 24 | 40 | 16.01 | 33.30 | 4.5 | $3\%b_0$ |
| t12o1 | 1.00 | 35 | 6 | 36.37 | 35.65 | 2.9 | Max. |
| t12o2 | 1.00 | 35 | 9 | 28.64 | 28.07 | 4.5 | $3\%b_0$ |
| t12o3 | 1.00 | 35 | 12 | 23.07 | 22.01 | 4.5 | $3\%b_0$ |
| t12o4 | 1.00 | 35 | 18 | 18.62 | 18.25 | 4.5 | $3\%b_0$ |
| t12o5 | 1.00 | 35 | 24 | 18.05 | 17.69 | 4.5 | $3\%b_0$ |
| t12o6 | 1.00 | 35 | 40 | 18.12 | 17.75 | 4.5 | $3\%b_0$ |

**7.4.5        The ultimate moment capacity for chord top face plastification**

A comparison between the ultimate moment capacity of T- and X-joints is given in Table 7.11 for joints with $\beta$ values of 0.4 to 0.8. It can be seen that the difference is within 4%. This result is expected. Because for both T- and X-joints, failure occurs due to large local plastic indentation of the chord top faces. Thus, the ultimate moment capacity formula recommended for T-joints is the same as for X-joints.

**Table 7.11      Comparison between the FE results of T- and X-joints**

| Joint | Geometrical parameters | | | Numerical results | | |
|---|---|---|---|---|---|---|
| | $\beta$ | $2\gamma$ | $\alpha$ | $M_{1,opb,u}$ (kNm) (T-joints) | $M_{1,opb,u}$ (kNm) (X-joints) | $\dfrac{M_{1,opb,u}(\text{T-joint})}{M_{1,opb,u}(\text{X-joint})}$ |
| t1o | 0.4 | 15 | 12 | 13.74 | 13.31 | 1.03 |
| t2o | 0.4 | 24 | 12 | 12.57 | 12.19 | 1.03 |
| t3o | 0.4 | 35 | 12 | 12.09 | 11.72 | 1.03 |
| t4o | 0.6 | 15 | 12 | 11.46 | 11.07 | 1.04 |
| t5o | 0.6 | 24 | 12 | 10.11 | 9.86 | 1.03 |
| t6o | 0.6 | 35 | 12 | 9.53 | 9.3 | 1.02 |
| t7o | 0.8 | 15 | 12 | 11.58 | 11.34 | 1.02 |
| t8o | 0.8 | 24 | 12 | 10.65 | 10.65 | 1.00 |
| t9o | 0.8 | 35 | 12 | 9.91 | 10.02 | 0.99 |

**7.4.6        The ultimate moment capacity for chord distortion failure**

**The failure mechanism**

When a full width T-joint is subjected to out-of-plane bending moment, the external loading of the joint can be divided into a force system of pure torsional loading and distortional loading as shown in Figure 7.19. The latter is in equilibrium within the cross-section and results in **warping stresses** in the four walls of the chord and large **stresses due to transverse bending moments** in the four corners of the chord.

$$M_{1,opb} = N\,b_0$$

External forces $\Rightarrow$ Torsion $+$ Distortion
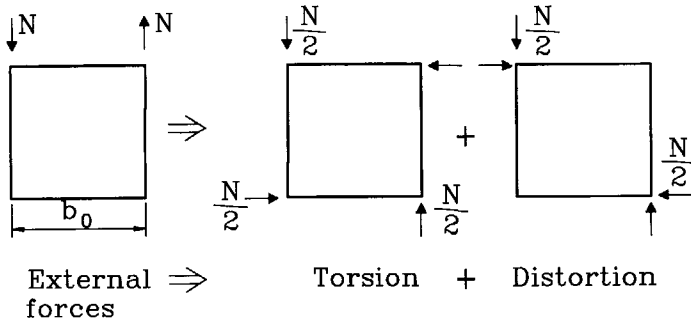
**Figure 7.19  Dividing the external forces into a force system of torsion and distortion**

The distribution of the warping stresses in sections I-I and II-II is shown in Figure 7.20 when plastification occurs, where $k_0$ is the reduction factor due to torsion which will be discussed later on. The distribution of the transverse bending moments in the chord cross section is shown in Figure 7.21.
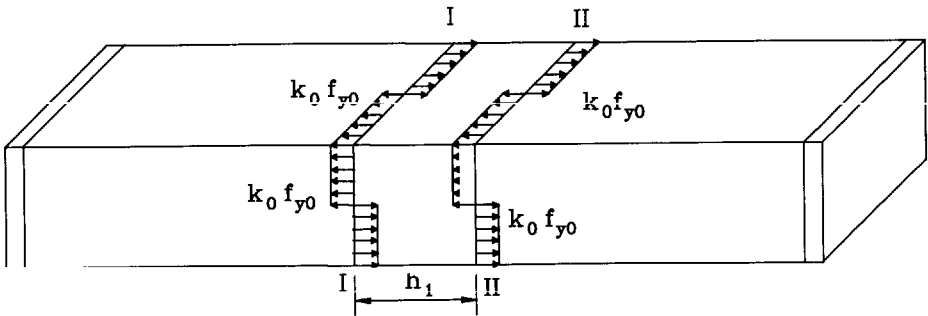


**Figure 7.20  Warping stresses in the middle of the chord sections**
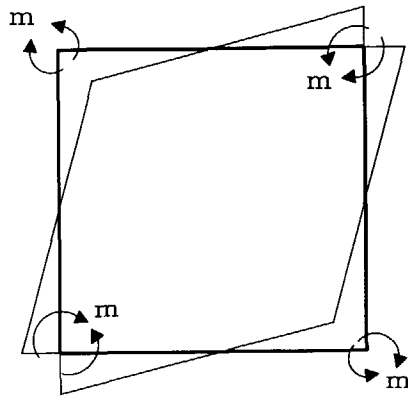
Transverse bending moment

**Figure 7.21 Distribution of the transverse bending moments**

The transverse bending moments at the four corners are always higher than those at other area of a cross section. Thus, yielding of the four corners of the chord occurs. As the external load increases, yielding of the four corners extends along the length of the chord.

According to the FE post-processing result of joint t12o6, the Von Mises stress distribution is shown in Figure 7.22. The yield strength is 355 N/mm$^2$. In Figure 7.22, the development of the chord plastification and the stress pattern can be clearly seen. Yielding in the four corners of the chord is caused by the transverse bending moments. Yielding in the four walls of the chord is caused by the warping stresses.
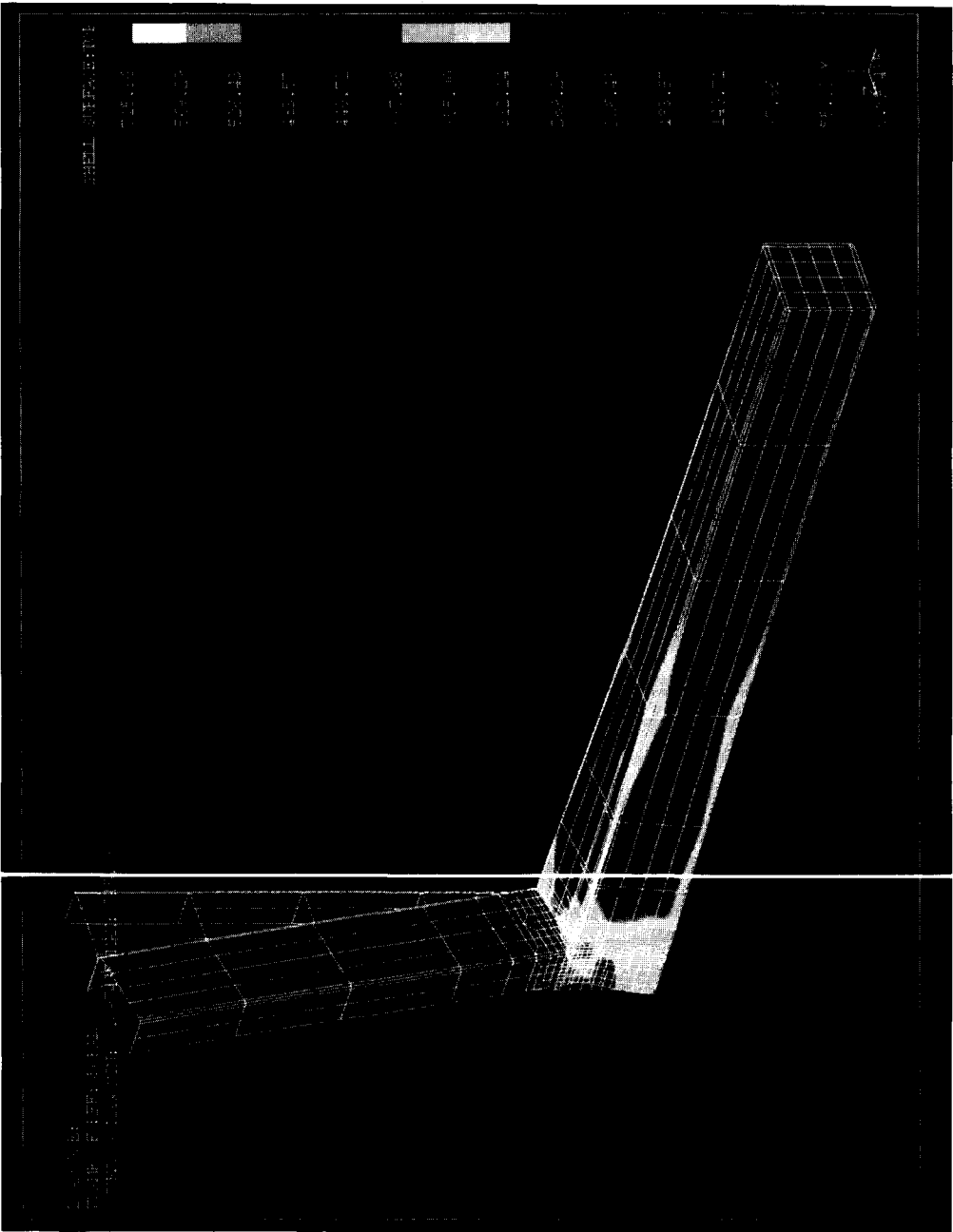
**Figure 7.22    Distribution of the Von Mises stresses for joint with** $\alpha$=40, $\beta$=$\eta$=1.0, 2$\gamma$=35

Based upon the stress distribution observed and the plastic model used by Niemi (1986), a failure mechanism for such joints is assumed as follows:

(1)    If the distortion angle of each side wall of the chord is $\phi_0$ from cross sections I-I to II-II (see Figure 7.23), it follows that all side walls are forced to rotate the same amount but in different directions. Suppose that the distortion decreases linearly to zero at a distance x.

(2)    Yield lines 1 and 2
       When a box girder is subjected to distortion, **warping stresses** exist in the cross section which are parallel to the length of the chord, see Figure 7.20. Due to the existence of the warping stresses, plastic yield lines (lines 1 and 2) appear in cross sections I-I and II-II, see Figure 7.23.

(3)    Longitudinal yield lines at the four corners (lines 3 and 4):
       When a box girder is subjected to distortion, the distribution of the **transverse bending moments** is shown in Figure 7.21. The transverse bending moments at the four corners are always higher than those at other area of a cross section. Thus, longitudinal yield lines (lines 3 and 4) will appear at the four corners. Because each side wall rotates an angle of $\phi_0$, each corner rotates $2\phi_0$ at the middle area of the chord length between cross sections I-I and II-II. The rotation angle of each corner decreases from $2\phi_0$ to zero at a distance of x according to assumption (1).

(4)    In fact, the above yield line model is not a real plastic mechanism. Elastic deformations still exist from section III-III to the end of the chord. The contribution of the reserved elastic energy dissipation is omitted here. Thus, the ultimate moment capacity obtained based upon the assumed model is considered as a lower bound solution.
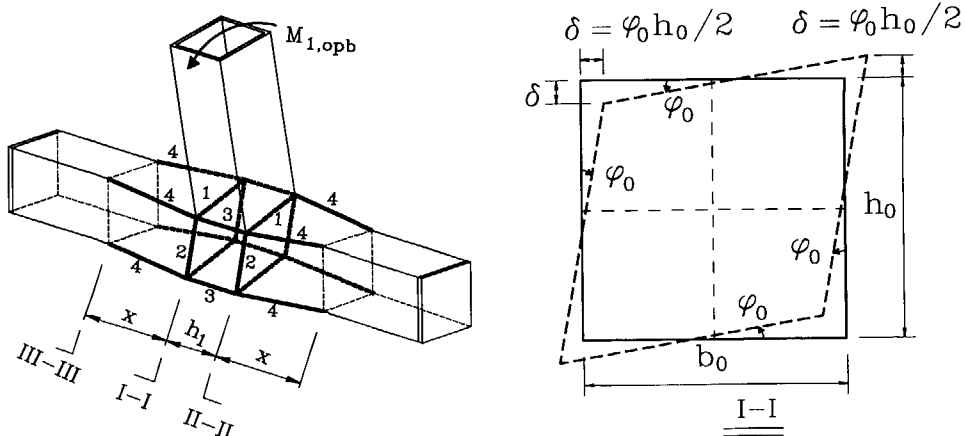


**Figure 7.23    Yield lines of a full width T-joint loaded with out-of-plane bending moment**

**The failure moment**

The general formula of the internal energy is:

$$W_i = \sum m_{pi} \phi_i l_i \tag{7.36}$$

Where $m_{pi}$ is the plastic moment per unit length of yield line i, $\phi_i$ is the rotation angle of yield line i and $l_i$ is the length of yield line i. The calculation of the plastic moment and the rotation angle of each yield line is listed in Table 7.12.

**Table 7.12  The plastic moments and rotation angles of the yield lines**

| Yield lines | No. of yield lines | $m_{pi}$ | $\phi_i$ | $l_i$ |
|:---:|:---:|:---:|:---:|:---:|
| 1 | 4 | $k_0 f_{y0} b_0^2/4$ | $\phi_0 h_0/(2x)$ | t |
| 2 | 4 | $k_0 f_{y0} h_0^2/4$ | $\phi_0 b_0/(2x)$ | t |
| 3 | 4 | $k_0 f_{y0} t_0^2/4$ | $2\phi_0$ | $h_1$ |
| 4 | 8 | $k_0 f_y t_0^2/4$ | $\phi_0$ | x |

$k_0$:    reduction factor for the warping stress taking torsional shear stresses into account, it will be deduced later on in this section.

Equating the internal energy dissipation into the external work gives:

$$W_i = 4 f_{y0} t_0^2 k_0 \phi_0 (\frac{b_0 h_0}{4t_0} \frac{b_0 + h_0}{2x} + \frac{h_1}{2} + \frac{x}{2}) = M_{1,opb} \phi_0 \tag{7.37}$$

Differentiating with respect to x gives the value of x for the minimum solution:

$$x = b_0 \sqrt{\frac{h_0}{4t_0}(1 + \frac{h_0}{b_0})} \tag{7.38}$$

Substituting equation (7.38) into equation (7.37) yields:

$$M_{1,opb,u} = 2 f_{y0} t_0^2 b_0 k_0 \left( 2\sqrt{\frac{\gamma}{2} \frac{h_0}{b_0}(1 + \frac{h_0}{b_0})} + \eta \right) \tag{7.39}$$

It should be mentioned that the minimum chord length should not be less than $(2x+h_1)$ in order to form the mechanism shown in Figure 7.23. If the chord length is longer than $(2x+h_1)$, the ultimate moment capacity $M_{1,opb,u}$ can be determined from equations (7.39). In other words, if the chord length is equal to or longer than a critical chord length $(2x+h_1)$, the ultimate moment capacity of the joints is independent of the chord length. This tendency is verified by the numerical results in Figure 7.17. Similar to the definition of $\alpha$, a critical $\alpha_x$ corresponding to the critical value of $x$ can be defined as follows:

$$\alpha_x = \frac{2(2x+h_1)}{b_0} = 2\left(2\sqrt{\frac{h_0}{4t_0}(1+\frac{h_0}{b_0})} + \eta\right) \tag{7.40}$$

Thus, if $\alpha \geq \alpha_x$, $M_{1,opb,u}$ is determined from equation (7.39).

### The determination of $k_0$

The reduction factor $k_0$ is still unknown. If the out-of-plane bending moment $M_{1,opb}$ is applied to the brace (see Figure 7.23), the torsional moment in the chord is:

$$M_t = \frac{M_{1,opb}}{2} \tag{7.41}$$

The plastic torsion capacity of a box girder for pure torsion is:

$$M_{tp} = \frac{2}{\sqrt{3}} f_{y0} b_0 h_0 t_0 \tag{7.42}$$

According to the Von Mises criteria, the axial warping stress capacity is reduced to

$$\sigma = f_{y0} \sqrt{1-(\frac{M_t}{M_{tp}})^2} \tag{7.43}$$

Hence, the reduction factor $k_0$ due to torsion is:

$$k_0 = \sqrt{1-(\frac{M_t}{M_{tp}})^2} \tag{7.44}$$

The value of $k_0$ can be determined according to equations (7.39), (7.41) to (7.44) using an iteration procedure. For a range of most commonly used geometrical parameters, the $k_0$ value and the corresponding non-dimensional ultimate moment capacity are calculated according

to this procedure and are given in Table 7.13.

**Table 7.13**    **The value of the reduction factor $k_0$ and the ultimate moment capacity based upon an iteration procedure**

|          | $h_0/b_0$ | $2\gamma=15$ | | $2\gamma=24$ | | $2\gamma=35$ | |
|----------|-----------|--------------|----------------------------------------|--------------|----------------------------------------|--------------|----------------------------------------|
|          |           | $k_0$ | $\dfrac{M_{1,opb,u}}{f_{y0}t_0^2 b_0}$ | $k_0$ | $\dfrac{M_{1,opb,u}}{f_{y0}t_0^2 b_0}$ | $k_0$ | $\dfrac{M_{1,opb,u}}{f_{y0}t_0^2 b_0}$ |
| $\eta=0.5$ | 1.0 | 0.95 | 11.30 | 0.97 | 14.35 | 0.98 | 17.32 |
|          | 2.0 | 0.96 | 19.19 | 0.98 | 24.39 | 0.98 | 29.48 |
| $\eta=1.0$ | 1.0 | 0.94 | 12.13 | 0.96 | 15.25 | 0.97 | 18.25 |
|          | 2.0 | 0.96 | 20.07 | 0.97 | 25.31 | 0.98 | 30.43 |
| $\eta=2.0$ | 1.0 | 0.92 | 13.73 | 0.95 | 17.00 | 0.97 | 20.08 |
|          | 2.0 | 0.95 | 21.81 | 0.97 | 27.15 | 0.98 | 32.32 |

This calculation method including reduction factor $k_0$ is not practical for a design recommendation, because an iteration procedure has to be carried out. For simplicity, it is recommended that $k_0=1.0$ is taken without too much loss of accuracy.

**The ultimate moment capacity of full width T-joints with square hollow sections**

**Joints with $\alpha \geq \alpha_x$**

For full width T-joints with square hollow sections, equations (7.38), (7.39) and (7.40) can be approximately written as follows by taking $k_0=1.0$, $h_0=b_0$ and $h_1=b_1=b_0$:

$$x = b_0\sqrt{\gamma} \tag{7.45}$$

$$M_{1,opb,u} = 2f_{y0}t_0^2 b_0 (2\sqrt{\gamma} +1) \qquad (\alpha \geq \alpha_x) \tag{7.46}$$

$$\alpha_x = 2(2\sqrt{\gamma} +1) \tag{7.47}$$

Equation (7.46) is independent of the $\alpha$ values for $\alpha \geq \alpha_x$.

In Figure 7.24, equation (7.46) is compared with the numerical results of full width T-joints with $\alpha \geq \alpha_x$. The statistical results are given in Table 7.14.

**Table 7.14    The statistical results of equation (7.46)**

| Mean | Coefficient of variation (CoV) | $R^2$ |
|------|-------------------------------|-------|
| 1.003 | 0.023 | 0.972 |

### Joints with different $\alpha$ values

For full width T-joints with $\alpha$ smaller than the critical value $\alpha_x$, the ultimate moment capacity is a function of the $\alpha$ and the $2\gamma$ values. Combining with equation (7.46), a general ultimate moment capacity formula for joints with all $\alpha$ values is assumed as follows:

$$M_{1,opb,u} = 2f_{y0}t_0^2 b_0(2\sqrt{\gamma} + 1) \cdot f(\alpha) \tag{7.48}$$

Where

$$f(\alpha) = (\frac{\alpha_x}{\alpha})^{R_1 2\gamma} \geq 1.0 \tag{7.49}$$

The ultimate moment capacity obtained from the FE results is plotted in Figure 7.24. Regression analysis is carried out for the data points with $\beta = 1.0$ and $\alpha < \alpha_x$. The regression results are listed in Table 7.15. Equation (7.48) is plotted in Figure 7.24.

**Table 7.15    Regression results of equations (7.48) and (7.49)**

| $R_1$ | Mean | Coefficient of variation CoV | $R^2$ |
|-------|------|------------------------------|-------|
| 0.015 | 1.012 | 0.005 | 0.967 |
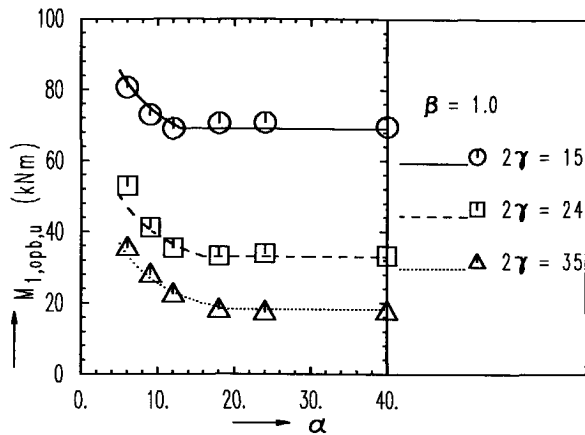
**Figure 7.24    The ultimate moment capacity of full width T-joints loaded with out-of-plane bending moment**

### 7.4.7        Conclusions

-    For T-joints with small to medium $\beta$ values, the same ultimate moment capacity formula can be used as that for X-joints, because the failure mechanism is the same.

-    For full width T-joints subjected to out-of-plane bending moment, failure of the joints is dominated by distortion of the chord section. The ultimate moment capacity of the joints is constant if the chord length is equal to or longer than a critical length. If the chord length is shorter than the critical length, the ultimate moment capacity is higher. A general formula which is valid for joints with all $\alpha$ values based upon the analytical model and the FE numerical results is recommended.

-    The chord side wall bearing formula in the CIDECT design guide for full width T-joints loaded with out-of-plane bending moment is restricted to joints for which distortion failure is prevented.

# 8    NUMERICAL STUDY ON MULTIPLANAR XX-JOINTS

## 8.1    XX-JOINTS LOADED WITH AXIAL FORCES ON BOTH IN-PLANE AND OUT-OF-PLANE BRACES

### 8.1.1    Introduction

In the current design recommendations, the multiplanar effects for multiplanar joints of rectangular hollow sections (RHS) are not included or only indicative influence factors are given. For example, in the CIDECT design guide (Packer 1992a), it is indicated that if the ratio between the axial loads applied to the out-of-plane braces and those applied to the in-plane braces is negative, the design resistance of the multiplanar joint will be reduced by 10% compared to that of their uniplanar counterparts. This multiplanar effect is only roughly considered, since sufficient evidence was not available. However the ultimate load capacity of multiplanar joints is obviously influenced by the magnitude of the load ratios and the geometrical parameters. The lack of information about the static strength of multiplanar joints has lead to a steady increase in research effort in recent years. In 1988, an ECSC funded project was undertaken which included both experimental and numerical investigations on uniplanar T- and X-joints and multiplanar TX-, XX- and KK-joints of RHS etc. (Davies 1992a and 1992b, de Koning 1992, Liu 1993, Yeomans 1993, Yu 1993a, 1993b and Crockett 1994). As a part of this research work, the numerical models for uniplanar X-joints, T-joints and multiplanar TX-joints, XX-joints of RHS under different loading conditions were calibrated against the experimental results. A suitable numerical model has been recommended, described in Chapter 4 which makes it possible to continue with numerical parameter studies.

This section presents the results of the investigation on the static strength and behaviour of multiplanar XX-joints loaded with multiplanar axial forces. The ultimate load capacity of the multiplanar joints are determined by using the following strategy: based on the ultimate load capacity of uniplanar X-joints recommended in Chapter 6, the multiplanar geometrical stiffening effect is determined for multiplanar XX-joints with load ratio $J_{AA}=N_2/N_1=0$; based upon the ultimate load capacity of multiplanar XX-joints with load ratio $J_{AA}=0$, the multiplanar load effects are determined for multiplanar XX-joints with different load ratios $J_{AA}$. Base upon these results, a general formula for multiplanar XX-joints loaded with axial forces is determined.

### 8.1.2    Research programme

The configuration of a multiplanar XX-joint loaded with axial forces on both in-plane and out-of-plane braces is shown in Figure 8.1, while the non-dimensional geometrical parameters are shown in Figure 8.2.
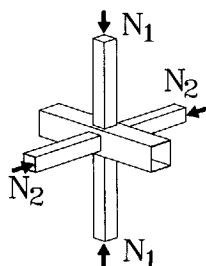
**Figure 8.1  Configuration of a multiplanar XX-joint loaded with axial forces**



$$\alpha = 2l_0/b_0$$
$$\beta = b_1/b_0$$
$$2\gamma = b_0/t_0$$
$$\tau = t_1/t_0$$
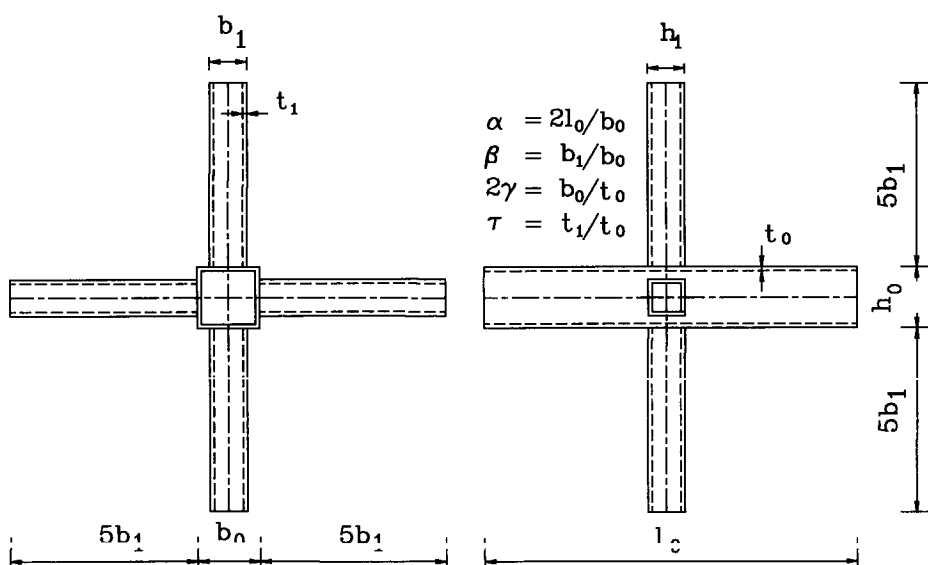
**Figure 8.2  Non-dimensional parameters of a multiplanar XX-joint**

The research programme consists of 13 multiplanar joints. The corresponding uniplanar joints analysed in Chapter 6 are also included for comparison. The joint dimensions and non-dimensional geometrical parameters are summarised in Table 8.1. Five $\beta$ ratios and three $2\gamma$ ratios are considered. For each multiplanar joint with a specific set of $\beta$ and $2\gamma$ values, five load ratios (i.e. the ratio between the loads on the out-of-plane and the in-plane braces) are included with $J_{AA}=N_2/N_1=-1$, -0.5, 0, 0.5 and 1.0. Similar to uniplanar joints, no weld is modelled in the direction along the chord length for joints with $\beta=1.0$. While for joints with other $\beta$ values, butt welds are used. The weld dimensions and the material properties of the joints are the same as used in Chapter 4, Section 4.5.1.

**Table 8.1  Research program for axially loaded XX-joints**

| Uniplanar joints | Multiplanar joints | Nominal dimensions | | Geometrical parameters | |
|---|---|---|---|---|---|
| | | chord | brace | | |
| | | $b_0 x t_0$ mm | $b_1 x t_1$ mm | $\beta$ | $2\gamma$ |
| x1a | xx1aa | 150x10 | 60x10 | 0.4 | 15 |
| x2a | xx2aa | 150x6.25 | 60x6.25 | 0.4 | 24 |
| x3a | xx3aa | 150x4.29 | 60x4.29 | 0.4 | 35 |
| x4a | xx4aa | 150x10 | 90x10 | 0.6 | 15 |
| x5a | xx5aa | 150x6.25 | 90x6.25 | 0.6 | 24 |
| x6a | xx6aa | 150x4.29 | 90x4.29 | 0.6 | 35 |
| x7a | xx7aa | 150x10 | 120x10 | 0.8 | 15 |
| x8a | xx8aa | 150x6.25 | 120x6.25 | 0.8 | 24 |
| x9a | xx9aa | 150x4.29 | 120x4.29 | 0.8 | 35 |
| x10a[*] | xx10aa[*] | 150x10 | 150x10 | 1.0 | 15 |
| x11a[*] | xx11aa[*] | 150x6.25 | 150x6.25 | 1.0 | 24 |
| x12a[*] | xx12aa[*] | 150x4.29 | 150x4.29 | 1.0 | 35 |
| x13a | xx13aa | 150x4.29 | 30x4.29 | 0.2 | 35 |
| $f_{y0}$=355 N/mm$^2$    $l_0$=900 mm    $b_2$=$b_1$=$h_1$    $t_2$=$t_1$ | | | | | |

*: Without weld

### 8.1.3  The FE analysis

General considerations for the FE analysis have been described in Chapter 4, Section 4.5.1. The specific aspects considered in this section are as follows:

-   Considering symmetry in load and geometry, one eighth of a joint has been modelled. The FE meshes and the boundary conditions used for the joints are shown in Figure 8.3. The origin of the coordinate system is in the centre of the chord.

-   For the load cases with load ratios of 0.0 and 1.0, the loads have been applied by displacement control considering its efficiency in convergency. For other load ratios, the loads have been applied by load control in order to maintain a constant load ratio between the loads on the out-of-plane and the in-plane braces even after the elastic stage of the material. In other words, the loads on the out-of-plane braces are

proportional to those on the in-plane braces at each load step.

| BOUNDARY CONDITIONS | | | |
|---|---|---|---|
| Degrees of freedom | Nodes on plane X=0.0 | Nodes on plane Y=0.0 | Nodes on plane Z=0.0 |
| $u_x$ | 0. | free | free |
| $u_y$ | free | 0. | free |
| $u_z$ | free | free | 0. |
| $\Phi_x$ | free | 0. | 0. |
| $\Phi_y$ | 0. | free | 0. |
| $\Phi_z$ | 0. | 0. | free |

**Figure 8.3**    **FE meshes and boundary conditions of an axially loaded multiplanar XX-joint**

### 8.1.4 Numerical results and observations

For each joint with a specific set of $\beta$ and $2\gamma$ values, the results of multiplanar XX-joints with five load ratios and the results of their corresponding uniplanar X-joints are shown in Figure 8.4. The non-dimension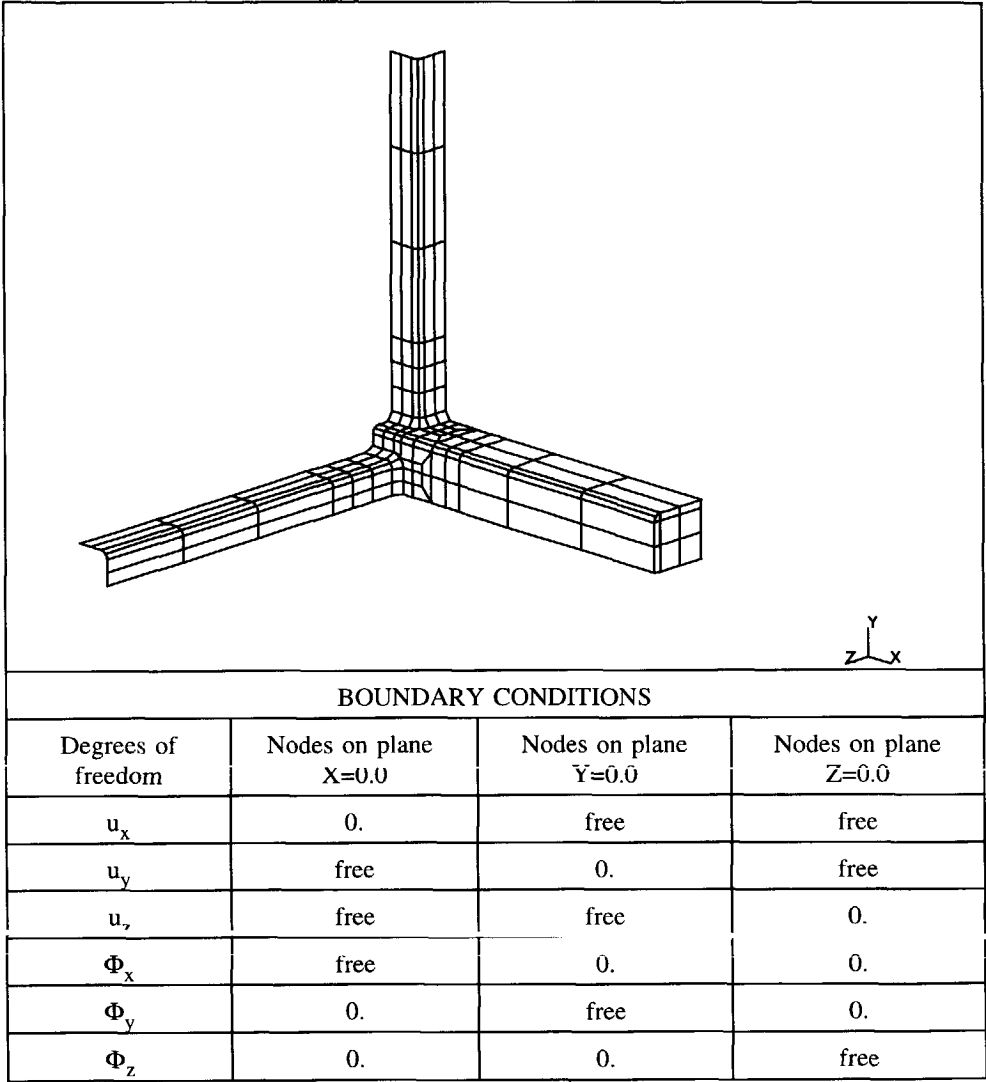al axial load on the in-plane braces $N_1/f_{y,0}t^2$ has been plotted against the indentation of the chord top face where the in-plane brace is connected. The ultimate load capacity determined according to the procedure of Figure 4.20, Chapter 4 is listed in Table 8.2. The finite element analyses of some joints could not be continued up to the deformation limit, due to convergency problems caused by the very high stiffness of the connections which are marked in the figures.

For a few cases, the ratio between the ultimate load capacity and the serviceability load capacity is larger than 1.5 ($N_{1,u}/N_s \geq 1.5$). Those results (bold in Table 8.2) are not included in the regression analyses.

### The multiplanar geometrical stiffening effects

For joints with $\beta \leq 0.6$, almost no increase in ultimate load capacity is observed for multiplanar XX-joints with the out-of-plane braces unloaded ($N_2=0$ or $J_{AA}=0$), compared to the corresponding uniplanar X-joints. However, for joints with $\beta=0.8$ and $\beta=1$, there is an obvious increase in ultimate load capacity due to the existence of the out-of-plane braces. This is logical, because for uniplanar joints with small $\beta$ values, joints fail by chord top face plastification. Thus, the stiffening of the chord side walls with the out-of-plane braces has almost no influence on chord top face failure. However, for uniplanar joints with large $\beta$ values, chord side wall failure or a combination of chord side wall and chord top face failure occurs. With the existence of the out-of-plane braces, the chord side walls are strengthened. The quantitative values of the multiplanar geometrical stiffening effects are listed in Table 8.3.

For joints with $\beta=0.8$, the braces and the weld toes are already connected to the corners of the RHS chord, especially for joint with $2\gamma=15$ ($\tau=1$), the weld toe is very close to the chord side wall. Thus, the geometrical stiffening effect for a joint with $2\gamma=15$ is stronger than that for joints with $2\gamma=24$ or $2\gamma=35$ due to the weld, see Table 8.3.

For joints with $\beta=1$ and $2\gamma=15$ or 24, no maximum load is reached for multiplanar joints with the out-of-plane braces unloaded. The ultimate load capacity for such joints is taken as the load at the ultimate deformation limit of $3\%b_0$, while the ultimate load capacity for the uniplanar joints is the maximum load. Due to the use of the deformation limit, the multiplanar geometrical stiffening effects are stronger for joints with smaller $2\gamma$ values than those for joints with larger $2\gamma$ values, see Figure 8.4 with $\beta=1.0$.
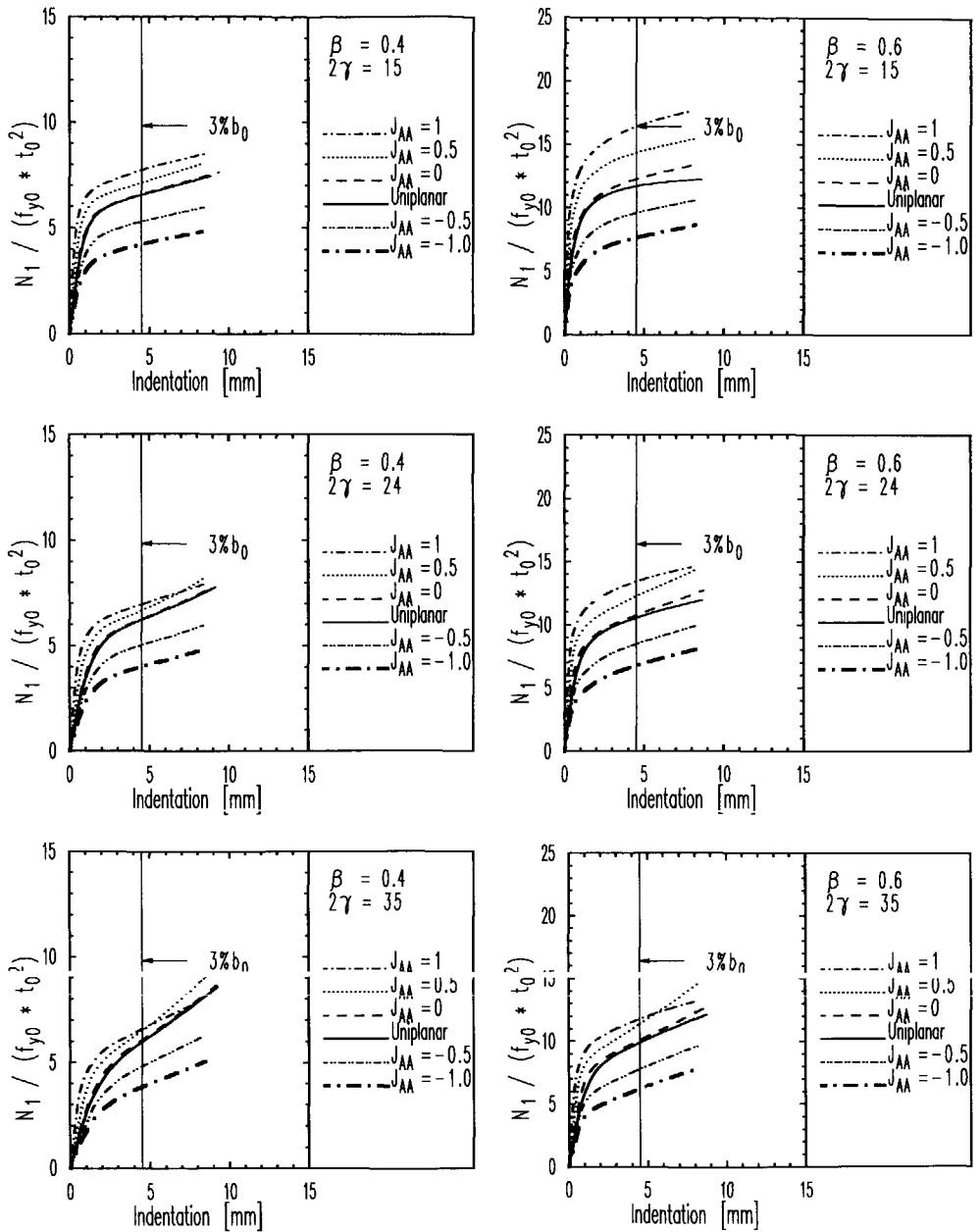
**Figure 8.4  Numerical results of axially loaded X- and XX-joints**
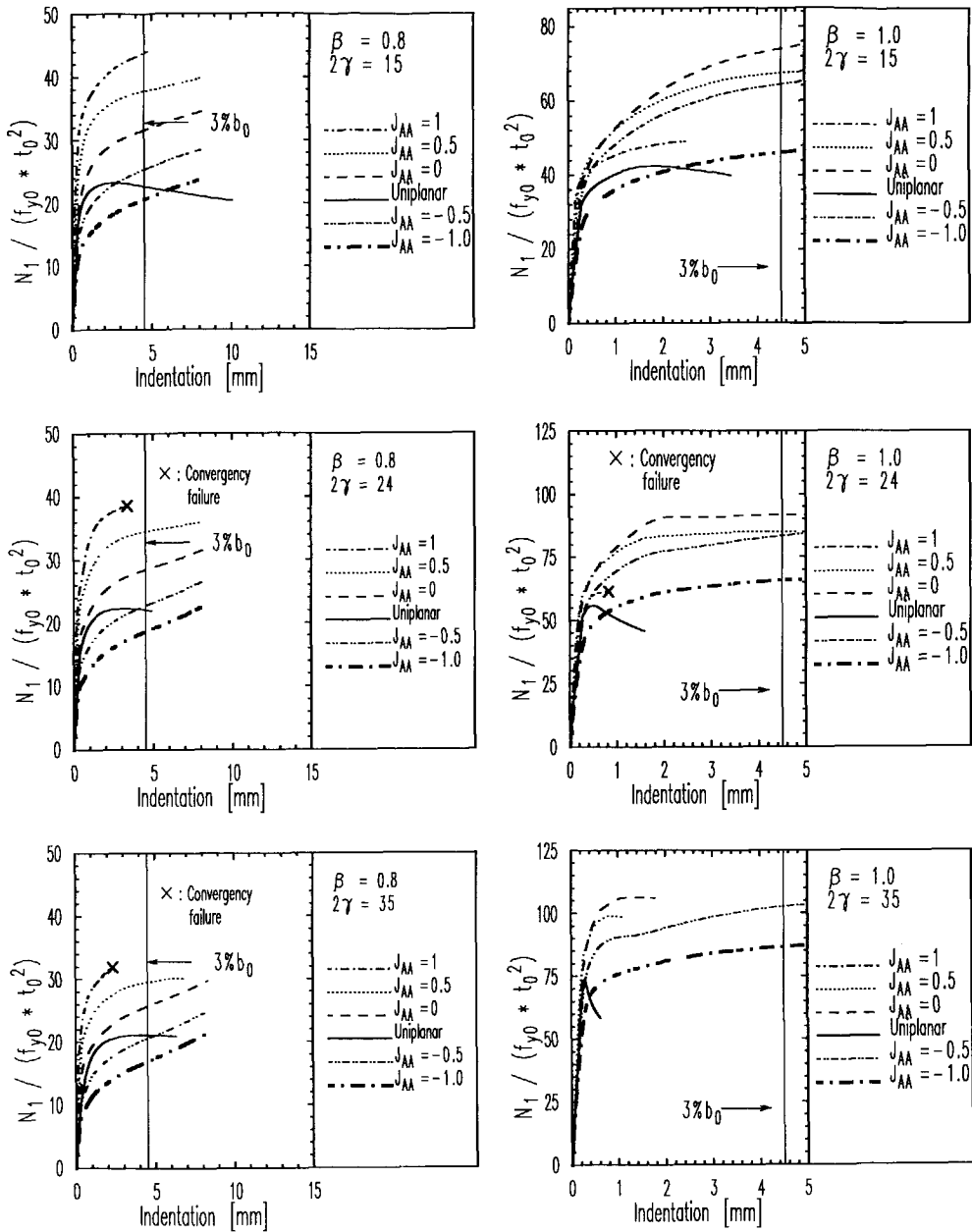
**Figure 8.4** **(continued)**

**Table 8.2 Numerical results of axially loaded X- and XX-joints**

| Uniplanar | | Multiplanar | | | | | |
|---|---|---|---|---|---|---|---|
| Joint | $\dfrac{N_{1,u}}{f_{y0}t_0^2}$ | Joint | $\dfrac{N_{1,u}(J_{AA})}{f_{y0}t_0^2}$ | | | | |
| | | | $J_{AA}=-1$ | $J_{AA}=-0.5$ | $J_{AA}=0$ | $J_{AA}=0.5$ | $J_{AA}=1.0$ |
| x1a | 6.55 | xx1aa | 4.21 | 5.28 | 6.58 | 7.12 | 7.72 |
| x2a | 6.23 | xx2aa | 3.98 | 5.01 | 6.26 | 6.65 | 6.95 |
| x3a | 6.00 | xx3aa | **3.85** | **4.84** | **6.08** | 6.53 | 6.61 |
| x4a | 11.68 | xx4aa | 7.63 | 9.57 | 12.23 | 14.32 | 16.39 |
| x5a | 10.56 | xx5aa | 6.77 | 8.47 | 10.76 | 12.27 | 13.42 |
| x6a | 9.88 | xx6aa | 6.20 | 7.77 | 10.09 | 11.38 | 11.78 |
| x7a | 23.32 | xx7aa | 20.65 | 25.37 | 31.57 | 37.78 | 43.85 |
| x8a | 22.32 | xx8aa | 18.63 | 22.76 | 28.43 | 34.48 | - |
| x9a | 21.10 | xx9aa | 16.91 | 20.56 | 25.69 | 29.53 | - |
| x10a[*] | 42.46 | xx10aa[*] | 46.07 | 64.46 | 74.10 | 67.51 | 49.10 |
| x11a[*] | 55.96 | xx11aa[*] | 65.74 | 83.37 | 90.92 | 85.09 | - |
| x12a[*] | 73.77 | xx12aa[*] | 86.53 | 102.6 | 106.5 | 98.95 | - |
| x13a | 4.04 | xx13aa | **2.74** | **3.36** | **4.06** | **4.32** | 4.48 |

[*]: Without weld

**Table 8.3** **Multiplanar geometrical stiffening effects for axially loaded XX-joints**

| Uniplanar joints | | Multiplanar joints $(J_{AA}=0)$ | | Geometrical parameters | | Multiplanar geometrical effects |
|---|---|---|---|---|---|---|
| No. | $\dfrac{N_{1,u}}{f_{y0}t_0^2}$ | No. | $\dfrac{N_{1,u}(J_{AA}=0)}{f_{y0}t_0^2}$ | $\beta$ | $2\gamma$ | $\dfrac{N_{1,u}(J_{AA}=0)}{N_{1,u}}$ |
| x1a | 6.55 | xx1aa | 6.58 | 0.4 | 15 | 1.00 |
| x2a | 6.23 | xx2aa | 6.26 | 0.4 | 24 | 1.00 |
| x3a | 6.00 | xx3aa | 6.08 | 0.4 | 35 | 1.01 |
| x4a | 11.68 | xx4aa | 12.23 | 0.6 | 15 | 1.05 |
| x5a | 10.56 | xx5aa | 10.76 | 0.6 | 24 | 1.02 |
| x6a | 9.88 | xx6aa | 10.09 | 0.6 | 35 | 1.02 |
| x7a | 23.32 | xx7aa | 31.57 | 0.8 | 15 | 1.35 |
| x8a | 22.33 | xx8aa | 28.43 | 0.8 | 24 | 1.27 |
| x9a | 21.10 | xx9aa | 25.69 | 0.8 | 35 | 1.22 |
| x10a[*] | 42.46 | xx10aa[*] | 74.10 | 1.0 | 15 | 1.75 |
| x11a[*] | 55.96 | xx11aa[*] | 90.92 | 1.0 | 24 | 1.62 |
| x12a[*] | 73.77 | xx12aa[*] | 106.5 | 1.0 | 35 | 1.44 |
| x13a | 4.04 | xx13aa | 4.06 | 0.2 | 35 | 1.00 |

[*]: Without weld

**The multiplanar load effects**

For joints with $\beta \leq 0.8$, the ultimate load capacity increases if the load ratio $J_{AA}$ is positive (i.e. both loaded in compression), see Figure 8.4. The larger the load ratio, the higher the ultimate load capacity of the joint. The ultimate load capacity decreases considerably if the load ratio $J_{AA}$ is negative (i.e. tension on the out-of-plane braces and compression on the in-plane braces). The multiplanar load effects are quantitatively listed in Table 8.4.

For joints with $\beta=1$, the ultimate load capacity of the joints loaded with $J_{AA} \neq 0$ is lower than that of the joints loaded with $J_{AA}=0$. The larger the absolute value of the load ratio $J_{AA}$, the lower the ultimate load capacity of the joints.

**Table 8.4  Multiplanar load effects for axially loaded XX-joints**

| Joints | β | 2γ | $\dfrac{N_{1,u}(J_{AA})}{N_{1,u}(J_{AA}=0)}$ | | | | |
|---|---|---|---|---|---|---|---|
| | | | $J_{AA}=-1.0$ | $J_{AA}=-0.5$ | $J_{AA}=0$ | $J_{AA}=0.5$ | $J_{AA}=1.0$ |
| xx1aa | 0.4 | 15 | 0.64 | 0.80 | 1.00 | 1.08 | 1.17 |
| xx2aa | 0.4 | 24 | 0.64 | 0.80 | 1.00 | 1.06 | 1.11 |
| xx3aa | 0.4 | 35 | 0.63 | 0.80 | 1.00 | 1.07 | 1.09 |
| xx4aa | 0.6 | 15 | 0.62 | 0.78 | 1.00 | 1.17 | 1.34 |
| xx5aa | 0.6 | 24 | 0.63 | 0.79 | 1.00 | 1.14 | 1.25 |
| xx6aa | 0.6 | 35 | 0.61 | 0.77 | 1.00 | 1.13 | 1.17 |
| xx7aa | 0.8 | 15 | 0.65 | 0.80 | 1.00 | 1.20 | 1.39 |
| xx8aa | 0.8 | 24 | 0.66 | 0.80 | 1.00 | 1.21 | - |
| xx9aa | 0.8 | 35 | 0.66 | 0.80 | 1.00 | 1.15 | - |
| xx10aa[*] | 1.0 | 15 | 0.62 | 0.87 | 1.00 | 0.91 | 0.66 |
| xx11aa[*] | 1.0 | 24 | 0.72 | 0.92 | 1.00 | 0.94 | - |
| xx12aa[*] | 1.0 | 35 | 0.81 | 0.96 | 1.00 | 0.93 | - |
| xx13aa | 0.2 | 35 | 0.67 | 0.83 | 1.00 | 1.07 | 1.10 |

[*]: Without weld

### 8.1.5    The ultimate load capacity of axially loaded multiplanar XX-joints

The ultimate load capacity formulae of multiplanar XX-joints can be built up with the following general formulae:

$$N_{1,u}(J_{AA}=0) = c_m \cdot N_{1,u} \tag{8.1}$$

$$N_{1,u}(J_{AA}) = f(J_{AA}) \cdot N_{1,u}(J_{AA}=0) \tag{8.2}$$

Where $N_{1,u}$ is the ultimate load capacity of uniplanar X-joints;
$c_m$ is a factor considering the multiplanar geometrical stiffening effects;
$N_{1,u}(J_{AA}=0)$ is the ultimate load capacity of multiplanar XX-joints with a load ratio $J_{AA}=0$;
$N_{1,u}(J_{AA})$ is the ultimate load capacity of multiplanar XX-joints with a load ratio $J_{AA}$;
$f(J_{AA})$ is a function for the multiplanar load effects.

## The factor for the multiplanar geometrical stiffening effects

As shown in Figure 8.5, the multiplanar geometrical stiffening effects are very small for joints with $\beta \leq 0.6$. For joints with $\beta \geq 0.8$, the multiplanar geometrical stiffening effects are much stronger, since side wall buckling is avoided for multiplanar joints especially for joints with $\beta = 1.0$. For joints with $\beta = 0.8$, there is a $2\gamma$ influence on the geometrical stiffening effect. Actually, the influence is caused by the weld effects as mentioned before, because for joints with $\beta = 0.8$, the braces are intersected with the chord corners. In the parameter study, the thickness of the braces is taken the same as that of the chord. thus, for joints with smaller $2\gamma$ values, the weld size is larger. The weld toes are very close to the chord side walls. Thus, larger multiplanar geometrical stiffening effects are found for joints with smaller $2\gamma$ values. For joints with $\beta = 1$, the $2\gamma$ influence is influenced by the use of the ultimate deformation limit which becomes critical for multiplanar joints whereas a maximum appears for uniplanar joints. Based on the above considerations, the following equation is recommended as a lower bound:

$$c_m = 1 + 0.4\beta^4 \tag{8.3}$$

Equation (8.3) is plotted in Figure 8.5.
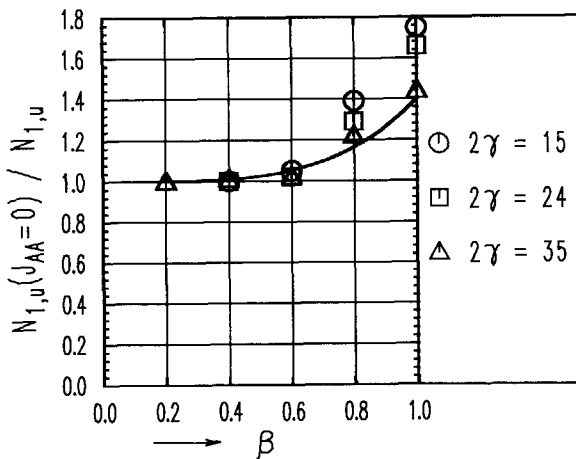


**Figure 8.5  The multiplanar geometrical stiffening effects of axially loaded XX-joints**

## The function for the multiplanar load effects

For joints with $\beta \leq 0.8$ and loaded with negative or zero load ratios, the numerical data points are plotted in Figure 8.6. It can be seen that the ultimate load capacity of the joints is reduced linearly with the load ratios and is almost independent of the $\beta$ and $2\gamma$ values. Following

regression formula for joints with $\beta \leq 0.8$ and load ratio $J_{AA} \leq 0$ has been obtained:

$$f(J_{AA}) = 1 + 0.37 * J_{AA} \qquad (J_{AA} \leq 0) \qquad\qquad (8.4)$$

The regression results are listed in Table 8.5. Equation (8.4) is plotted in Figure 8.6.
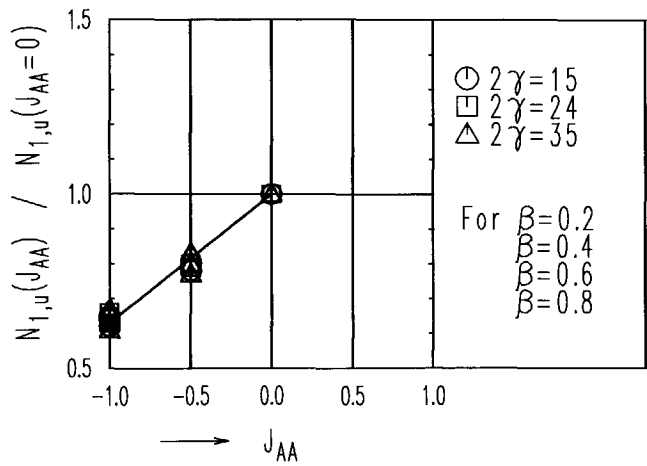


**Figure 8.6  The multiplanar load effects of axially loaded XX-joints with $\beta \leq 0.8$ ($J_{AA} \leq 0$)**

**Table 8.5  Regression results of equation (8.4)**

| $R_1$ | Mean normalised error | Coefficient of variation CoV | Correlation coefficient $R^2$ |
|---|---|---|---|
| 0.37 | 0.997 | 0.026 | 0.985 |

For joints with $\beta \leq 0.8$ and loaded with positive load ratios, the numerical data points are plotted in Figure 8.7. The multiplanar load effects depend not only on the load ratios but also on the $\beta$ and $2\gamma$ values. The multiplanar load effects are stronger for joints with larger $\beta$ and smaller $2\gamma$ values. Following regression formula has been obtained for joints with $J_{AA} \geq 0$:

$$f(J_{AA}) = 1 + J_{AA}(R_1 + \frac{R_2}{2\gamma}\beta + R_3\beta^2) \qquad (J_{AA} \geq 0) \qquad\qquad (8.5)$$

The regression results are listed in Table 8.6. Equation (8.5) is plotted in Figure 8.7.

**Table 8.6 Regression results of equation (8.5)**

| $R_1$ | $R_2$ | $R_3$ | Mean normalised error | Coefficient of variation CoV | Correlation coefficient $R^2$ |
|-------|-------|-------|-----------------------|------------------------------|-------------------------------|
| 0.03 | 4 | 0.3 | 1.000 | 0.018 | 0.960 |
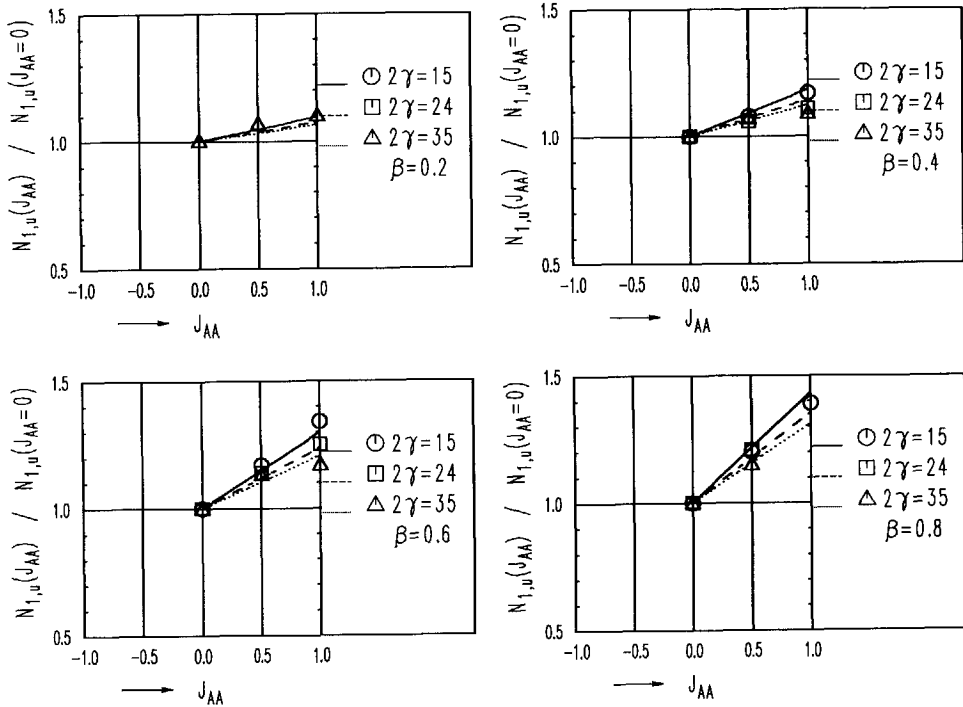


**Figure 8.7 The multiplanar load effects of axially loaded XX-joints ($J_{AA} \geq 0$)**

For joints with $\beta=1$, as mentioned before, the ultimate load capacity of joints loaded with $J_{AA} \neq 0$ is smaller than that for joints loaded with $J_{AA}=0$. The following function for the multiplanar load effects has been obtained after a regression analysis:

$$f(J_{AA}) = 1 - \frac{3}{\gamma} J_{AA}{}^2 \qquad (\beta = 1) \tag{8.6}$$

Equation (8.6) is illustrated in Figure 8.8.
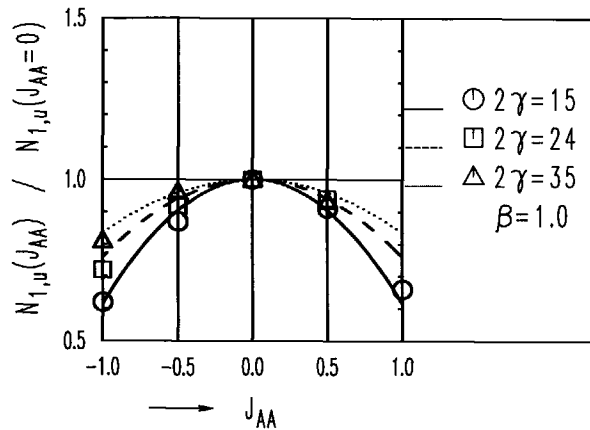
**Figure 8.8  The multiplanar load effects of axially loaded XX-joints ($\beta$=1)**

Although equations (8.4) and (8.5) have been checked for $\beta \leq 0.8$, $\beta = 0.85$ is taken as limitation for the validity, because similar joint behaviour is expected for joints with $\beta = 0.8$ and $\beta = 0.85$. For joints with $0.85 \leq \beta \leq 1.0$, a linear interpolation is needed between equations (8.4) and (8.6) or (8.5) and (8.6).

### 8.1.6   Comparison with analytical formulae

When the axial forces on the in-plane and the out-of-plane braces act in the same sense, Davies (1991a) concluded that there is no increase in joint strength, based upon a ring model. When the forces on the in-plane and the out-of-plane braces are in the opposite senses, two formulae were deduced by him, based upon a ring model and a yield line model respectively.

**The ring model of Davies ($J_{AA} \leq 0$)**

For XX-joints in square hollow sections, the interaction between the axial loads on the two planes of the braces is given by:

$$N_1(J_{AA}) - N_2 = \frac{8m_p}{1-\beta} \cdot (\frac{L}{b_0}) \tag{8.7}$$

Where L is the effective length of the "ring" model. If the out-of-plane braces are unloaded, i.e. $N_2 = 0$ or $J_{AA} = 0$, then equation (8.7) at the ultimate load becomes:

$$N_{1,u}(J_{AA} = 0) = \frac{8m_p}{1-\beta} \cdot (\frac{L}{b_0}) \tag{8.8}$$

Introducing equation (8.8) into equation (8.7) and considering $J_{AA} = N_2/N_1$, then

$$N_{1,u}(J_{AA}) - J_{AA} \cdot N_{1,u}(J_{AA}) = N_{1,u}(J_{AA}=0) \tag{8.9}$$

From equation (8.9), it can be obtained that:

$$f(J_{AA}) = \frac{N_{1,u}(J_{AA})}{N_{1,u}(J_{AA}=0)} = \frac{1}{1-J_{AA}} \tag{8.10}$$

### The yield line model of Davies ($J_{AA} \leq 0$)

For XX-joints in square hollow sections, the interaction formula based upon the yield line model of Davies (1991a) was given as follows:

$$N_1(J_{AA}) - N_2 = \frac{2f_{y0}t_0^2}{1-\beta}\left(\beta + 2\sqrt{2(1-\beta)}\right) \tag{8.11}$$

Based upon equation (8.11), an identical formula as equation (8.10) can be deduced.

Equation (8.4) from the numerical results and equation (8.10) derived from the ring model or the yield line model are compared in Figure 8.9. It can be seen that the multiplanar load effects according to the formula of Davies are stronger than those according to the finite element analysis.
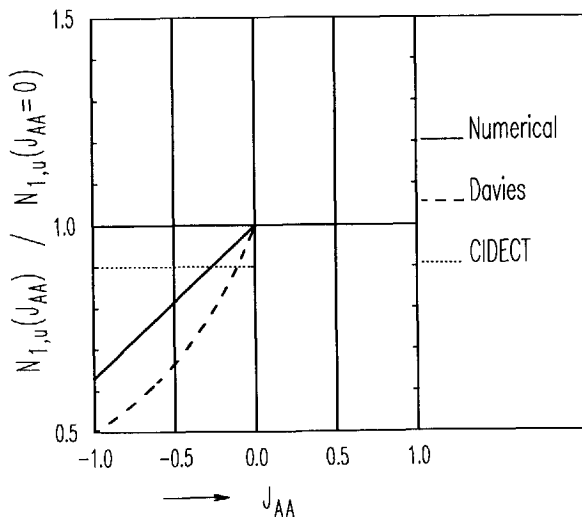
**Figure 8.9** **Comparisons between the numerical results, the model of Davies and the CIDECT formula**

### 8.1.7    Comparison with the CIDECT design guidance

In the CIDECT design guide (Packer 1992a), it is simply recommended that a correction factor of 0.9 for multiplanar joints be applied to the design resistance of uniplanar joints to account for the combined multiplanar geometrical and load effects. From Figure 8.9, it can be seen that the CIDECT formula is unsafe for joints with a small $\beta$ and loaded with larger negative load ratios.

### 8.1.8    Conclusions

A numerical parameter study has been carried out for axially loaded multiplanar XX-joints. The joint geometrical parameters are $\beta$=0.2, 0.4, 0.6, 0.8, 1.0 and $2\gamma$=15, 24 and 35. For each joint with a specific set of $\beta$ and $2\gamma$ values, five load ratios $J_{AA}$=-1, -0.5, 0, 0.5 and 1 are included. Conclusions can be drawn as follows:

-   The ultimate load capacity formula of multiplanar joints with the out-of-plane braces unloaded can be established based upon that of the uniplanar joints multiplied by a multiplanar geometrical stiffening factor $c_m$.

-   The ultimate load capacity formula of multiplanar joints with different load ratios can be derived based upon that of the multiplanar joints with the out-of-plane braces unloaded multiplied by a function for the multiplanar load effects $f(J_{AA})$.

-   The multiplanar geometrical stiffening effect is very small for XX-joints with $\beta \leq 0.6$. While the ultimate load capacity is increased clearly for XX-joints with $\beta \geq 0.8$, compared to that of the uniplanar joints.

-   The ultimate load capacity of the multiplanar joints is increased with the increase of the load ratios for joints with $\beta \leq 0.8$. For joints with $\beta$=1.0, the ultimate load capacity is decreased if the out-of-plane braces are either tension or compression loaded compared to that for unloaded out-of-plane braces.

-   The CIDECT formula is unsafe for joints with small $\beta$ values and loaded with large negative load ratios.

-   A set of ultimate load capacity formulae, equations (8.1) to (8.6) is recommended.

## 8.2 XX-JOINTS LOADED WITH IN-PLANE BENDING MOMENTS ON THE IN-PLANE AND THE OUT-OF-PLANE BRACES

### 8.2.1 Introduction

Although the multiplanar loading effect on the design resistance of axially loaded XX-joints in RHS is roughly considered in the CIDECT design guides, there is little information available about the static behaviour of multiplanar XX-joints in RHS when both the in-plane and the out-of-plane braces are loaded with in-plane bending moments. Van der Vegte (1995) has made numerical investigations for such joints but in circular hollow sections. The joint ultimate moment capacity is determined using the same strategy as in Section 8.1 by separately investigating the multiplanar geometrical stiffening effects based upon the corresponding uniplanar joints and the multiplanar load effects based upon the multiplanar joints when the out-of-plane braces are unloaded.

### 8.2.2 Research programme

The configuration of a multiplanar XX-joint loaded with in-plane bending moments on both in-plane and out-of-plane braces is shown in Figure 8.10.
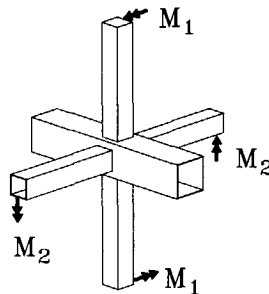


**Figure 8.10 Multiplanar XX-joints loaded with in-plane bending moments**

The research programme consists of 13 multiplanar joints. The joint dimensions and non-dimensional geometrical parameters are summarised in Table 8.7. The joints analysed in this section are exactly the same as those in the previous section. However, different load cases are applied. For each multiplanar joint with a specific set of $\beta$ and $2\gamma$ values, five moment ratios between the moments on the out-of-plane and the in-plane braces are included with $J_{II}=M_2/M_1=-1$, -0.5, 0, 0.5 and 1.0. If two perpendicular chord faces are all pushed in at the same side, the moment ratio is defined as positive. If one chord face is pushed in and another pulled out at the same side, the moment ratio is defined as negative. Thus, Figure 8.10 represents a positive moment ratio.

**Table 8.7**          **Research program for XX-joints loaded with in-plane bending moments**

| Uniplanar joints | Multiplanar joints | Nominal dimensions | | Geometrical parameters | |
|---|---|---|---|---|---|
| | | chord | brace | | |
| | | $b_0xt_0$ mm | $b_1xt_1$ mm | $\beta$ | $2\gamma$ |
| x1i | xx1ii | 150x10 | 60x10 | 0.4 | 15 |
| x2i | xx2ii | 150x6.25 | 60x6.25 | 0.4 | 24 |
| x3i | xx3ii | 150x4.29 | 60x4.29 | 0.4 | 35 |
| x4i | xx4ii | 150x10 | 90x10 | 0.6 | 15 |
| x5i | xx5ii | 150x6.25 | 90x6.25 | 0.6 | 24 |
| x6i | xx6ii | 150x4.29 | 90x4.29 | 0.6 | 35 |
| x7i | xx7ii | 150x10 | 120x10 | 0.8 | 15 |
| x8i | xx8ii | 150x6.25 | 120x6.25 | 0.8 | 24 |
| x9i | xx9ii | 150x4.29 | 120x4.29 | 0.8 | 35 |
| x10i[*] | xx10ii[*] | 150x10 | 150x10 | 1.0 | 15 |
| x11i[*] | xx11ii[*] | 150x6.25 | 150x6.25 | 1.0 | 24 |
| x12i[*] | xx12ii[*] | 150x4.29 | 150x4.29 | 1.0 | 35 |
| x13i | xx13ii | 150x4.29 | 30x4.29 | 0.2 | 35 |
| $f_{y0}$=355 N/mm$^2$     $l_0$=900 mm     $b_2$=$b_1$=$h_1$     $t_2$=$t_1$ | | | | | |
| $M_2/M_1$=-1.0, -0.5, 0.0, 0.5, 1.0 | | | | | |

*: Without weld

### 8.2.3    The FE analysis

General considerations of the numerical modelling have been described in Chapter 4. The specific aspects considered in this section are as follows:

-       A quarter of a joint is modelled considering symmetry of loads and geometry. The boundary conditions and the finite element meshes are shown in Figure 8.11. In order to prevent rigid body motion, one node (with a coordinate of X=0, Y=$(h_0-t_0)/2$ and Z=0) is restrained in X-direction: $u_x$=0.

- Similar to uniplanar X-joints loaded with in-plane bending moments, pure bending moments are applied to the braces by load control. The in-plane bending moments applied to the out-of-plane braces are proportional to those to the in-plane braces.



| BOUNDARY CONDITIONS | | | |
|---|---|---|---|
| Degrees of freedom | Node at (X=0.0, Y=(h$_0$-t$_0$)/2 and Z=0.0) | Nodes on plane Y=0.0 | Nodes on plane Z=0.0 |
| u$_x$ | 0. | free | free |
| u$_y$ | free | 0. | free |
| u$_z$ | 0. | free | 0. |
| $\Phi_x$ | 0. | 0. | 0. |
| $\Phi_y$ | 0. | free | 0. |
| $\Phi_z$ | free | 0. | free |
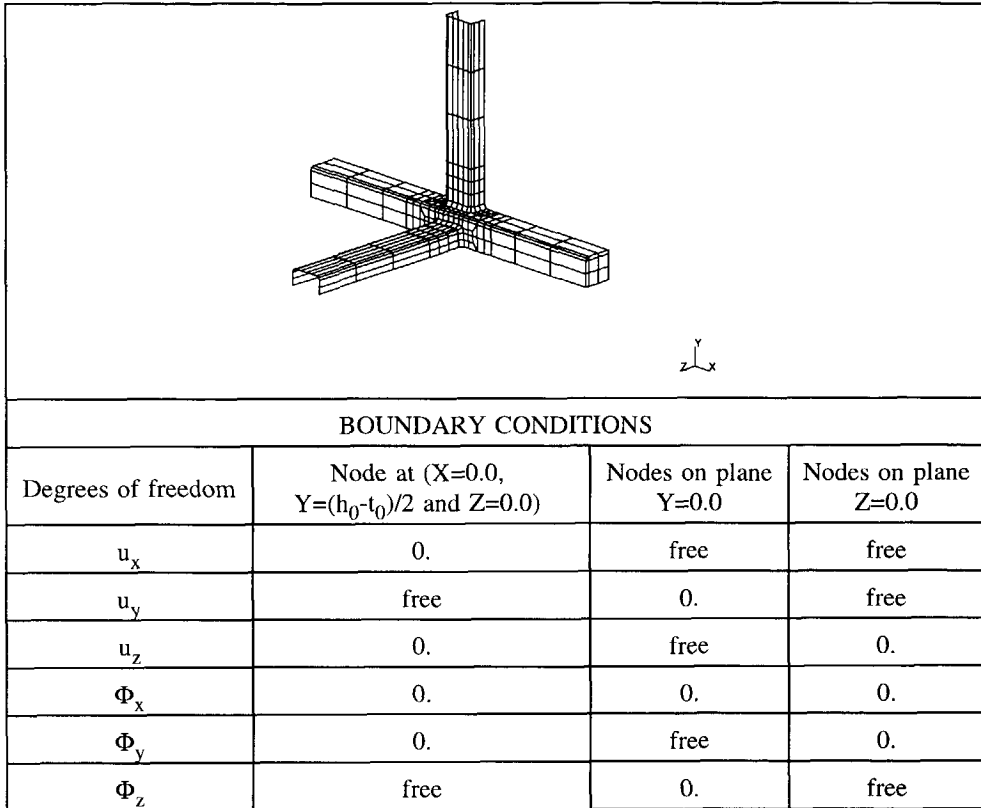
**Figure 8.11**   **FE meshes and boundary conditions of a multiplanar XX-joint loaded with in-plane bending moments**

### 8.2.4   Numerical results and observations

The non-dimensional moment vs. chord top face indentation curves for multiplanar XX-joints are illustrated in Figure 8.12. The corresponding uniplanar joints are also included. The "indentation" in Figure 8.12 represents the chord top face "push-in" at the compression side where the in-plane brace and the chord top intersect, see Figure 4.21, Chapter 4. The ultimate deformation limit of 3%b$_0$ and the ultimate rotation limit of $\phi$=0.1 are indicated in the figure. The ultimate moment capacity of both uniplanar and multiplanar joints loaded with in-plane bending moments is determined according to the procedure of Figure 4.22, Chapter 4 and is listed in Table 8.8. In most cases, the ratio between the ultimate moment capacity and the moment at the serviceability deformation limit is smaller than 1.5. In such cases, the serviceability deformation is not critical. Only in a few cases, the ratio between the ultimate

moment capacity and the moment at the serviceability deformation limit of $1\%b_0$ is larger than $1.5$ $(M_{1,u}/M_s \geq 1.5)$. Those results (bold in Table 8.8) are not used in the regression analyses.
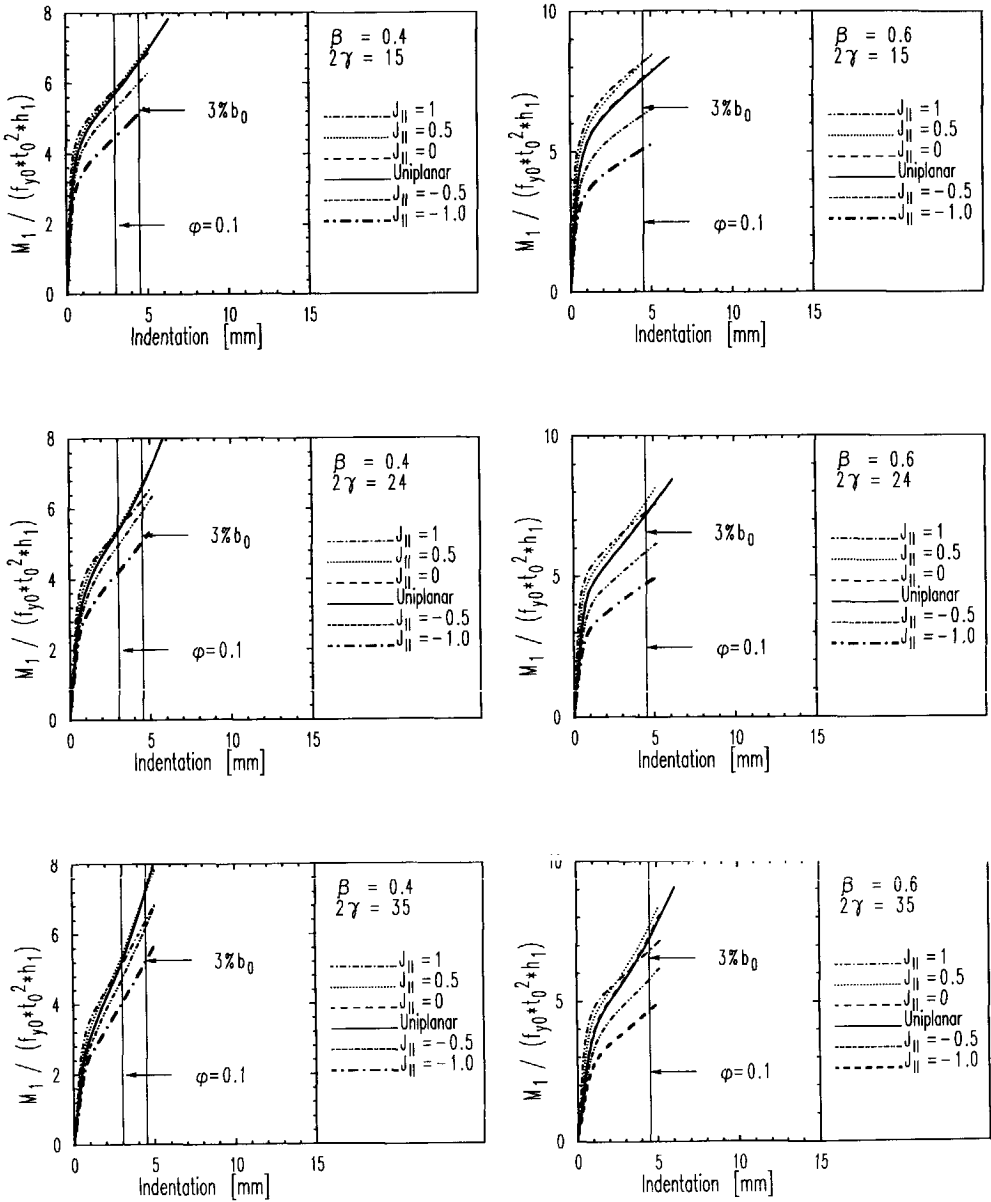


**Figure 8.12    Numerical results of XX-joints loaded with in-plane bending moments**
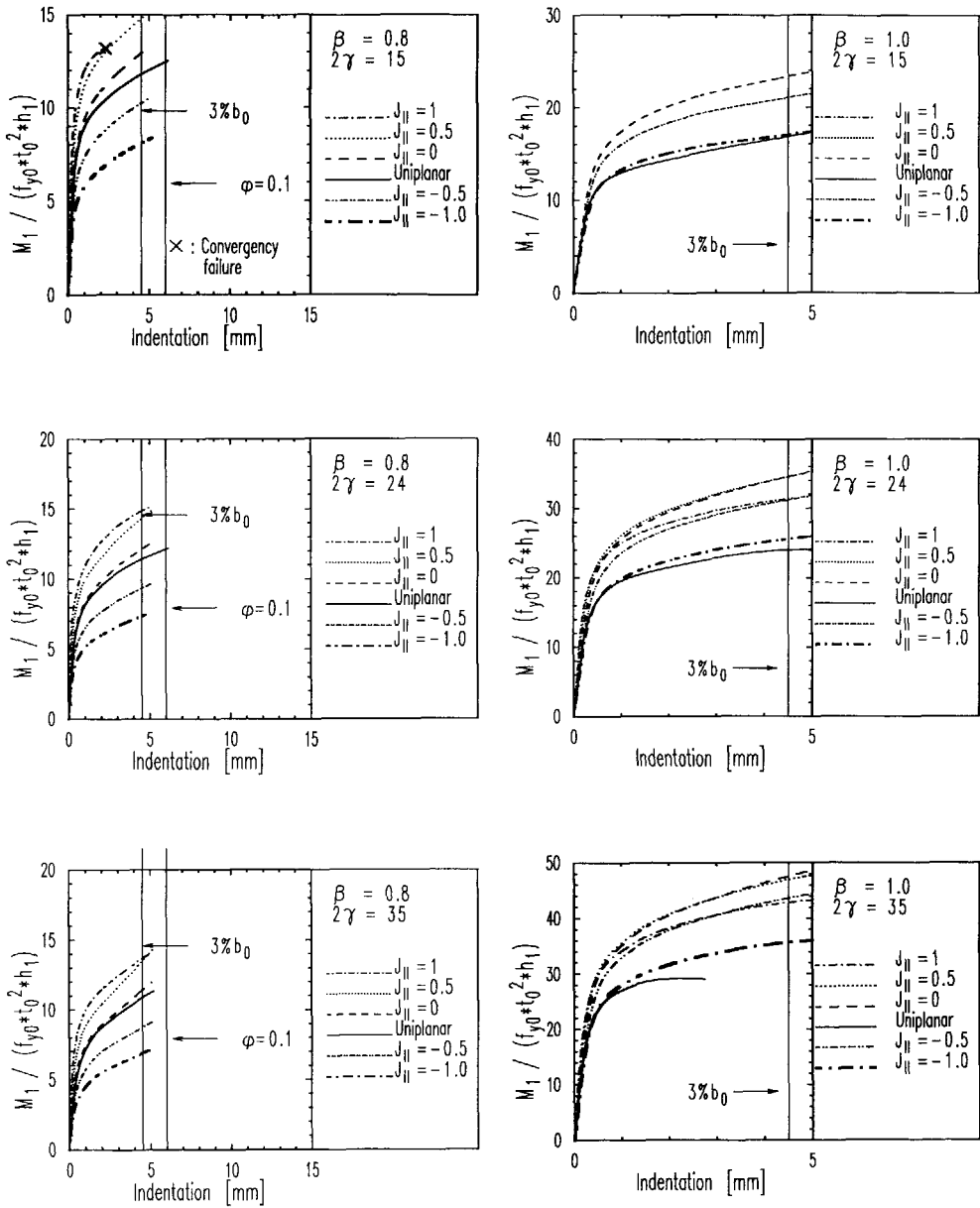
**Figure 8.12    (Continued)**

**Table 8.8    Numerical results of XX-joints loaded with in-plane bending moments**

| Uniplanar | | Multiplanar | | | | | |
|---|---|---|---|---|---|---|---|
| Joint | $\dfrac{M_{1,ipb,u}}{f_{yo}t_0^2 h_1}$ | Joint | $\dfrac{M_{1,ipb,u}(J_{II})}{f_{yo}t_0^2 h_1}$ | | | | |
| | | | $J_{II}$=-1 | $J_{II}$=-0.5 | $J_{II}$=0 | $J_{II}$=0.5 | $J_{II}$=1.0 |
| x1i | 5.71 | xx1ii | 4.49 | 5.30 | 5.72 | 5.82 | 5.84 |
| x2i | 5.35 | xx2ii | 4.20 | 4.95 | 5.36 | 5.46 | 5.39 |
| x3i | 5.21 | xx3ii | 4.05 | 4.72 | 5.22 | 5.37 | 5.14 |
| x4i | 7.56 | xx4ii | 5.08 | 6.30 | 7.61 | 8.13 | 8.17 |
| x5i | 7.17 | xx5ii | 4.74 | 5.86 | 7.20 | 7.62 | 7.27 |
| x6i | **7.25** | xx6ii | 4.68 | 5.78 | **7.34** | **7.71** | 6.81 |
| x7i | 11.80 | xx7ii | 8.09 | 10.24 | 12.94 | 14.78 | - |
| x8i | 11.40 | xx8ii | 7.35 | 9.34 | 12.12 | 14.33 | 14.87 |
| x9i | 10.87 | xx9ii | 6.88 | 8.73 | 11.41 | 13.48 | 13.68 |
| x10i[*] | 16.85 | xx10ii[*] | 17.05 | 21.08 | 23.38 | - | - |
| x11i[*] | 24.04 | xx11ii[*] | 25.63 | 31.28 | 34.62 | 34.62 | 31.47 |
| x12i[*] | 29.21 | xx12ii[*] | 35.66 | 43.66 | 47.58 | 46.99 | 42.97 |
| x13i | 5.43 | xx13ii | 4.94 | 5.27 | 5.44 | 5.59 | 5.71 |

[*]: Without weld

## The multiplanar geometrical stiffening effects

In Figure 8.12, for each multiplanar joint with a specific set of joint geometrical parameters, five moment ratios are included. The corresponding uniplanar joints are indicated for comparison. Comparing the ultimate moment capacity of multiplanar joints with the out-of-plane braces unloaded ($J_{II}=0$) to that of the corresponding uniplanar joints, the multiplanar geometrical stiffening effects can be determined.

For joints with $\beta \leq 0.8$, the multiplanar geometrical stiffening effects are within 10%. Especially for joints with $\beta \leq 0.6$, the curves for uniplanar joints and those for the corresponding multiplanar joints with $J_{II}=0$ are about the same.

For $\beta=0.8$, the $2\gamma$ influence is actually the weld effects. For $\beta=1.0$, the $2\gamma$ influence is caused by the use of the ultimate deformation limit which is critical for all the multiplanar joints and for uniplanar joints with $2\gamma=15$ and $2\gamma=24$, while for uniplanar joint with $\beta=1.0$ and $2\gamma=35$, a maximum moment capacity is reached.

For joints with $\beta=1$, the ultimate moment capacity of multiplanar XX-joint with the out-of-plane braces unloaded is much higher than that of the uniplanar X-joint. The quantitative values of the multiplanar geometrical stiffening effects are listed in Table 8.9.

**Table 8.9 The multiplanar geometrical stiffening effects of XX-joints loaded with in-plane bending moments**

| Uniplanar joints | | Multiplanar joints $J_{II}=0$ | | Geometrical parameters | | Multiplanar geometrical effects |
|---|---|---|---|---|---|---|
| No. | $\dfrac{M_{1,ipb,u}}{f_{y0}t_0^2 h_1}$ | No. | $\dfrac{M_{1,ipb,u}(J_{II}=0)}{f_{y0}t_0^2 h_1}$ | $\beta$ | $2\gamma$ | $\dfrac{M_{1,ipb,u}(J_{II}=0)}{M_{1,ipb,u}}$ |
| x1i | 5.71 | xx1ii | 5.72 | 0.4 | 15 | 1.00 |
| x2i | 5.35 | xx2ii | 5.36 | 0.4 | 24 | 1.00 |
| x3i | 5.21 | xx3ii | 5.22 | 0.4 | 35 | 1.01 |
| x4i | 7.56 | xx4ii | 7.61 | 0.6 | 15 | 1.01 |
| x5i | 7.17 | xx5ii | 7.20 | 0.6 | 24 | 1.00 |
| x6i | 7.25 | xx6ii | 7.34 | 0.6 | 35 | 1.01 |
| x7i | 11.80 | xx7ii | 12.94 | 0.8 | 15 | 1.10 |
| x8i | 11.41 | xx8ii | 12.12 | 0.8 | 24 | 1.06 |
| x9i | 10.87 | xx9ii | 11.41 | 0.8 | 35 | 1.05 |
| x10i[*] | 16.85 | xx10ii[*] | 23.38 | 1.0 | 15 | 1.42 |
| x11i[*] | 24.04 | xx11ii[*] | 34.62 | 1.0 | 24 | 1.44 |
| x12i[*] | 29.21 | xx12ii[*] | 47.58 | 1.0 | 35 | 1.63 |
| x13i | 5.43 | xx13ii | 5.44 | 0.2 | 35 | 1.00 |

[*]: Without weld

**The multiplanar load effects**

Comparing the ultimate moment capacity of multiplanar joints with moment ratios $J_{II}$ to that of multiplanar joints with the out-of-plane braces unloaded ($J_{II}$=0), the multiplanar load effects can be determined.

For joints loaded with negative moment ratios, the stiffness and the ultimate moment capacity of the joints are reduced considerably compared to those of the joints with the out-of-plane braces unloaded.

For joints with $\beta\leq0.6$ loaded with positive moment ratios, the ultimate moment capacity gives a slight enhancement compared to that of joints with the out-of-plane braces unloaded except for joints with $2\gamma$=35 and a moment ratio $J_{II}$=1.0 where the ultimate moment capacity is slightly reduced. The reason is that, at the ultimate deformation limit of the joint, the development of the membrane action in the chord is more restrained for joints with a moment ratio $J_{II}$=1 than for joints with other moment ratios, see Figure 8.12.

For joints with $\beta$=0.8 loaded with positive moment ratios, the maximum enhancement in ultimate moment capacity is 20% compared to that of joints with the out-of-plane braces unloaded.

For joints with $\beta$=1.0 loaded with positive moment ratios, the ultimate moment capacity of the joints are unchanged for a moment ratio of $J_{II}$=0.5 or about 10% decreased for a moment ratio of $J_{II}$=1.0 compared to $J_{II}$=0.0.

For multiplanar joints with $\beta$=1, the ultimate moment capacity can be higher than that of the uniplanar joints even for multiplanar joints with negative moment ratios, mainly due to the geometrical stiffening effects.

The quantitative values of the multiplanar load effects are listed in Table 8.10.

**Table 8.10 The multiplanar load effects of XX-joints loaded with in-plane bending moments**

| Joints | β | 2γ | $\dfrac{M_{1,ipb,u}(J_{II})}{M_{1,ipb,u}(J_{II}=0)}$ | | | | |
|---|---|---|---|---|---|---|---|
| | | | $J_{II}=-1.0$ | $J_{II}=-0.5$ | $J_{II}=0$ | $J_{II}=0.5$ | $J_{II}=1.0$ |
| xx1ii | 0.4 | 15 | 0.78 | 0.93 | 1.00 | 1.02 | 1.02 |
| xx2ii | 0.4 | 24 | 0.78 | 0.92 | 1.00 | 1.02 | 1.01 |
| xx3ii | 0.4 | 35 | 0.78 | 0.90 | 1.00 | 1.03 | 0.98 |
| xx4ii | 0.6 | 15 | 0.67 | 0.83 | 1.00 | 1.07 | 1.07 |
| xx5ii | 0.6 | 24 | 0.66 | 0.81 | 1.00 | 1.06 | 1.01 |
| xx6ii | 0.6 | 35 | 0.64 | 0.79 | 1.00 | 1.05 | 0.93 |
| xx7ii | 0.8 | 15 | 0.63 | 0.79 | 1.00 | 1.14 | - |
| xx8ii | 0.8 | 24 | 0.61 | 0.77 | 1.00 | 1.18 | 1.23 |
| xx9ii | 0.8 | 35 | 0.60 | 0.77 | 1.00 | 1.18 | 1.20 |
| xx10ii[*] | 1.0 | 15 | 0.73 | 0.90 | 1.00 | - | - |
| xx11ii[*] | 1.0 | 24 | 0.74 | 0.90 | 1.00 | 1.00 | 0.90 |
| xx12ii[*] | 1.0 | 35 | 0.75 | 0.92 | 1.00 | 0.99 | 0.90 |
| xx13ii | 0.2 | 35 | 0.91 | 0.97 | 1.00 | 1.03 | 1.05 |

[*]: Without weld

## 8.2.5 The ultimate moment capacity of XX-joints loaded with in-plane bending moments

The ultimate moment capacity formulae for multiplanar joints are determined by the following general formulae:

$$M_{1,ipb,u}(J_{II}=0) = c_m \cdot M_{1,ipb,u} \tag{8.12}$$

$$M_{1,ipb,u}(J_{II}) = f(J_{II}) \cdot M_{1,ipb,u}(J_{II}=0) \tag{8.13}$$

Where $M_{1,ipb,u}$ is the ultimate moment capacity of uniplanar X-joint;
$c_m$ is a factor considering the multiplanar geometrical stiffening effects;
$M_{1,ipb,u}(J_{II}=0)$ is the ultimate moment capacity of multiplanar XX-joints with $J_{II}=0$;
$M_{1,ipb,u}(J_{II})$ is the ultimate moment capacity of multiplanar XX-joints with $J_{II}$.

**The factor for the multiplanar geometrical stiffening effects**

According to the numerical results shown in Figure 8.13, the multiplanar geometrical stiffening effects are very small for joints with $\beta \leq 0.8$. Large multiplanar geometrical stiffening effects are found for joints with $\beta = 1.0$. Based on the above observations, a lower bound factor is given by:

$$c_m = 1 + 0.4\beta^8 \tag{8.14}$$

In comparison with axially loaded multiplanar XX-joints, the exponent of $\beta$ in equation (8.14) is increased (i.e. $\beta^8$ v.s. $\beta^4$).

Equation (8.14) is plotted in Figure 8.13.
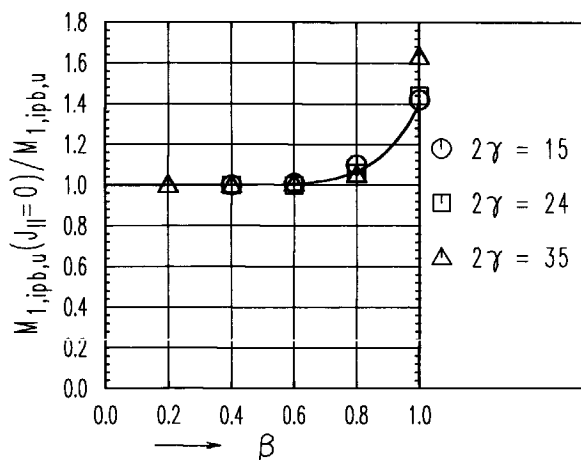


**Figure 8.13    The multiplanar geometrical stiffening effects of joints loaded with in-plane bending moments**

**The function for the multiplanar load effects**

For joints with $\beta \leq 0.8$ loaded with negative moment ratios, the multiplanar load effects are a function of the moment ratios and the $\beta$ values. The function for the multiplanar load effects can be defined as follows:

$$f(J_{II}) = 1 + R_1 \beta J_{II} \qquad\qquad (J_{II} \leq 0) \tag{8.15}$$

The regression constant $R_1$ and the statistical results are listed in Table 8.11. Equation (8.15) is plotted in Figure 8.14.

**Table 8.11  Regression results of equation (8.15)**

| $R_1$ | Mean normalised error | Coefficient of variation CoV | Correlation coefficient $R^2$ |
|---|---|---|---|
| 0.53 | 1.000 | 0.032 | 0.972 |

For joints with $\beta \leq 0.8$ loaded with a positive moment ratio, the maximum multiplanar load effect is within 20%, see Figure 8.14. For joints with $\beta = 0.6$ and $2\gamma = 35$, a small negative influence is found for $J_{II} = 1$ because the membrane action at the ultimate deformation limit for joints with $J_{II} = 1$ is largely reduced. For design recommendations, it is proposed to neglect the relatively small influence of the positive moment ratio. Thus:

$$f(J_{II}) = 1 \qquad\qquad (J_{II} \geq 0) \qquad\qquad\qquad (8.16)$$

For joints with $\beta = 1$, a large negative multiplanar load effect is found for moment ratios $J_{II} < 0$. For moment ratios $J_{II} \geq 0$, the multiplanar load effect is smaller, see Figure 8.15 and Table 8.10. Following regression formula is assumed:

$$f(J_{II}) = 1 + R_1 J_{II} + R_2 J_{II}^2 \qquad\qquad (\beta = 1.0) \qquad\qquad\qquad (8.17)$$

This function differs from equation (8.15) since the behaviour of joints with $\beta = 1.0$ differs from that of joints with $\beta < 1.0$. The regression results are listed in Table 8.12.

**Table 8.12  Regression results of equation (8.17)**

| $R_1$ | $R_2$ | Mean normalised error | Coefficient of variation CoV | Correlation coefficient $R^2$ |
|---|---|---|---|---|
| 0.08 | -0.18 | 0.999 | 0.008 | 0.995 |

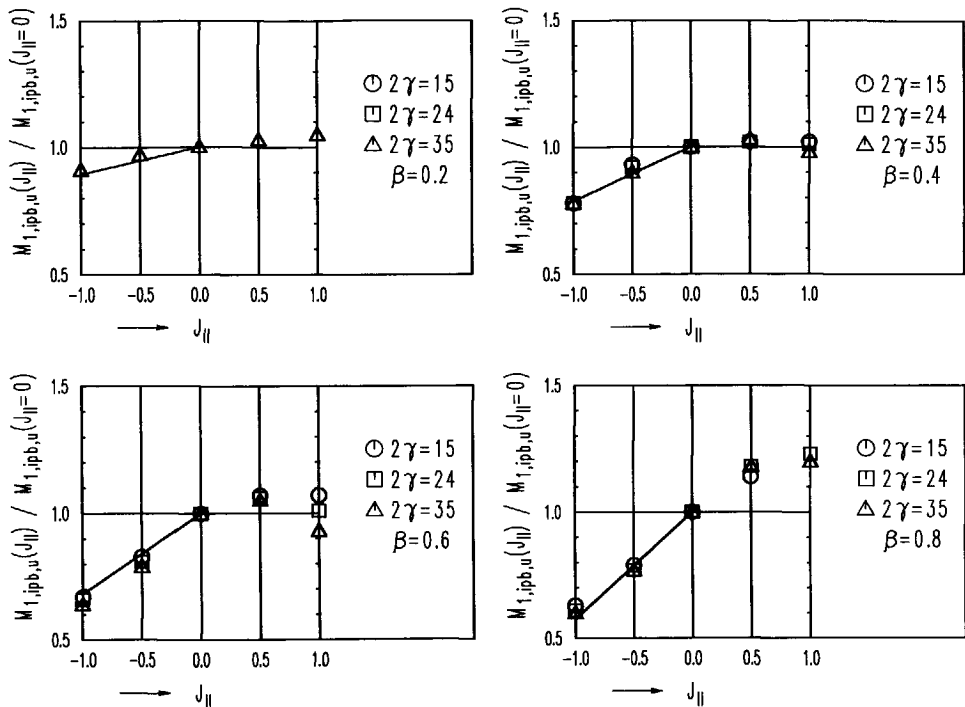**Figure 8.14**        **The multiplanar load effects of XX-joints loaded with in-plane bending moments ($\beta \leq 0.8$)**
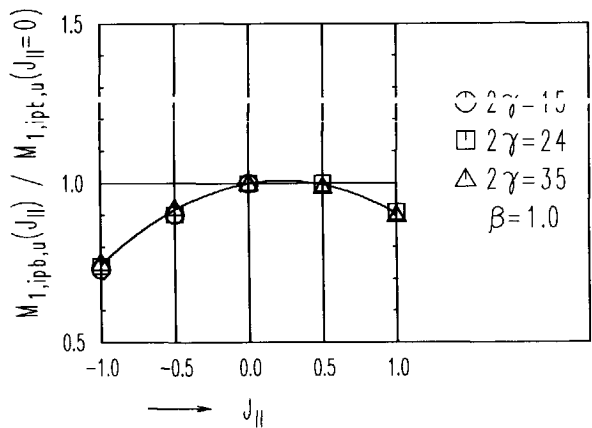


**Figure 8.15**        **The multiplanar load effects of XX-joints loaded with in-plane bending moments ($\beta = 1$)**

## 8.2.6    Conclusions

The static strength and behaviour of multiplanar XX-joints loaded with in-plane bending moments on both in-plane and out-of-plane braces has been studied.

The multiplanar geometrical stiffening effects are very small for joints with $\beta \leq 0.8$, while very large multiplanar geometrical stiffening effects are found for joints with $\beta = 1$.

The multiplanar load effects depend upon the $\beta$ values and the moment ratios. The ultimate moment capacity is decreased with increasing negative moment ratios and $\beta$ values. For joints with a positive moment ratio and $\beta \leq 0.6$, the ultimate moment capacity is hardly changed compared to that of joint with $J_{II}=0$. For joints with a positive moment ratio and $\beta = 0.8$, the maximum multiplanar load effect is about 20%. For joints with a positive moment ratio and $\beta = 1.0$, the negative multiplanar load effect is up to 10% for $J_{II}=1.0$.

Equations (8.15) and (8.16) have been checked for $\beta \leq 0.8$. As limitation for the validity, $\beta = 0.85$ is taken. For $0.85 \leq \beta \leq 1.0$, a linear interpolation is required between equations (8.15) and (8.17) or (8.16) and (8.17).

## 8.3 XX-JOINTS LOADED WITH IN-PLANE BENDING MOMENTS ON THE IN-PLANE BRACES AND AXIAL FORCES ON THE OUT-OF-PLANE BRACES

### 8.3.1 Introduction

Due to asymmetry in deformation, the behaviour of multiplanar XX-joints loaded with a combination of in-plane bending moments and axial forces is more complicated than that of XX-joints loaded with only axial forces or only in-plane bending moments as studied in Sections 8.1 and 8.2. The joint behaviour is largely influenced by the boundary conditions applied on the out-of-plane braces. In this section, two extreme cases of boundary conditions are included for comparison: one with the ends of the out-of-plane braces free to rotate, another one with the ends of the out-of-plane braces fixed in the direction parallel to the length of the chord. Furthermore, some additional calculations have been done with the applied loads always in the direction of the longitudinal axis of the out-of-plane braces which are called "follow force" in the MARC program. The above three boundary conditions are shown in Figure 8.16.
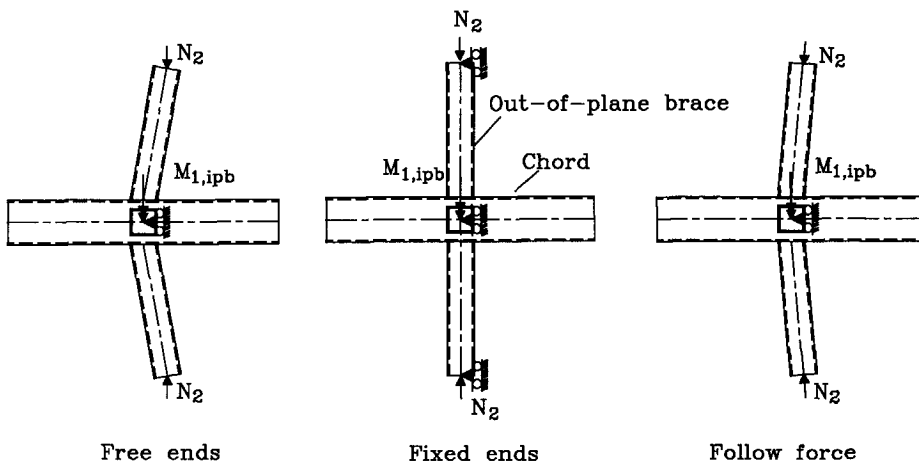


**Figure 8.16 Three different boundary conditions**

Due to the in-plane bending moments on the in-plane braces the out-of-plane braces will rotate. If the ends of the out-of-plane braces are free (free ends in Figure 8.16) and loaded in tension, additional secondary bending moments on the out-of-plane braces occur which reduce the rotation somewhat. Thus, the rotation of the out-of-plane braces is not very much in such a case. If the ends of the out-of-plane braces are free and loaded in compression, the secondary bending moments increase the rotation. As a result, failure of the out-of-plane braces may occur due to a combination of the compression forces and the secondary bending moments in the out-of-plane braces. In such a case, the rotation of the out-of-plane braces reduces largely the ultimate moment capacity of the joints.

If the ends of the out-of-plane braces are restrained (fixed ends in Figure 8.16) in a direction parallel to the chord length, secondary bending moments due to rotation of the out-of-plane braces are prevented. However, reaction forces on the ends of the out-of-plane braces result in secondary bending moments too. Such restraints have been applied in the experimental test for joint DX7, as shown in Figure 3.2, Chapter 3, where it is called "vertical adjustment". Due to the application of the restraints, the ultimate moment capacity of the joints may increase for a large positive load ratio.

If the method of "follow force" (Figure 8.16) is used, all distributed loads on the ends of the out-of-plane braces are formed on the basis of current geometry. Thus, the applied forces on the out-of-plane braces are always in the direction along the longitudinal axis of the out-of-plane braces. As a result, no secondary bending moments on the out-of-plane braces occur.

### 8.3.2   Research programme

The configuration of a multiplanar XX-joint loaded with in-plane bending moments in the in-plane braces and axial forces in the out-of-plane braces is shown in Figure 8.17. The research programme is summarised in Table 8.13. In fact, the same joints as in Section 8.2 are analysed in this section only with different loading and boundary conditions. The load ratio is defined as $J_{IA}=N_2/(M_1/h_1)$. For each multiplanar XX-joint, five load ratios are applied with $J_{IA}$=-1.0, -0.5, 0, 0.5 and 1.0 respectively. If the out-of-plane braces are loaded in compression, the load ratio is defined as positive, as shown in Figure 8.17. There are two groups of joints: the first group with the out-of-plane braces free, the second group with the out-of-plane braces restrained at their ends in the direction parallel to the chord length. In total, there are 120 analyses. The corresponding uniplanar joints which have been studied in Chapter 6 are included in this section for comparison.
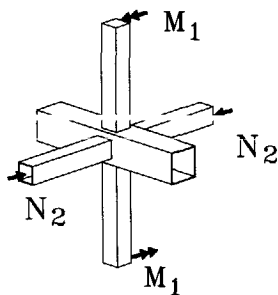


**Figure 8.17**   **Configuration of an XX-joint loaded with in-plane bending moments and axial forces**

**Table 8.13    Research programme for XX-joints loaded with in-plane bending moments and axial forces**

| Uniplanar joints | Multiplanar joints | Nominal dimensions | | Geometrical parameters | |
|---|---|---|---|---|---|
| | | chord | brace | | |
| | | $b_0xt_0$  (mm) | $b_1xt_1$  (mm) | $\beta$ | $2\gamma$ |
| x1i | xx1ia | 150x10 | 60x10 | 0.4 | 15 |
| x2i | xx2ia | 150x6.25 | 60x6.25 | 0.4 | 24 |
| x3i | xx3ia | 150x4.29 | 60x4.29 | 0.4 | 35 |
| x4i | xx4ia | 150x10 | 90x10 | 0.6 | 15 |
| x5i | xx5ia | 150x6.25 | 90x6.25 | 0.6 | 24 |
| x6i | xx6ia | 150x4.29 | 90x4.29 | 0.6 | 35 |
| x7i | xx7ia | 150x10 | 120x10 | 0.8 | 15 |
| x8i | xx8ia | 150x6.25 | 120x6.25 | 0.8 | 24 |
| x9i | xx9ia | 150x4.29 | 120x4.29 | 0.8 | 35 |
| x10i[*] | xx10ia[*] | 150x10 | 150x10 | 1.0 | 15 |
| x11i[*] | xx11ia[*] | 150x6.25 | 150x6.25 | 1.0 | 24 |
| x12i[*] | xx12ia[*] | 150x4.29 | 150x4.29 | 1.0 | 35 |
| $f_{y0}$=355 N/mm$^2$    $l_0$=900 mm    $b_2=b_1=h_1$    $t_2=t_1$    $J_{IA}$=-1, -0.5, 0, 0.5, 1.0 | | | | | |

*: Without weld

### 8.3.3   The FE analysis

For each corresponding joint, the same element meshes are used as in Section 8.2. For the joints with the out-of-plane braces free (first group), the boundary conditions are the same as shown in Figure 8.11. For the joints with the out-of-plane brace fixed (second group), an extra support at the end of the out-of-plane braces is applied in the direction parallel to the chord length (X-direction), besides the boundary conditions applied to the first group. Furthermore, some additional calculations have been done with the method of "follow force" (third group). In the third group, although the end of the out-of-plane brace is also free, the axial load on the out-of-plane brace are formed on the basis of current geometry, thus, no secondary bending moment occurs in the out-of-plane brace.

The same method as described in Section 8.2 is used to apply a pure bending moment on the in-plane brace. Proportional axial load (with a load ratio of $J_{IA}=N_2h_1/M_1$) is applied to the out-of-plane brace at each increment.

### 8.3.4   Numerical results and observations

The results are presented in two groups: group 1 includes the joints with the out-of-plane braces free to rotate; group 2 includes the joints with the out-of-plane braces fixed at the ends in the direction parallel to the chord length. The results from group 3 are presented later on as a comparison. The procedure to determine the ultimate moment capacity of the joint can be found in Figure 4.22, Chapter 4.

### Joints with the out-of-plane brace free (Group 1)

For joints with the out-of-plane braces free, the FE results of the non-dimensional in-plane bending moment vs. chord top face indentation curves are illustrated in Figure 8.18. The ultimate moment capacity of the joints is listed in Table 8.14. For each multiplanar joint, five load ratios are included. The corresponding uniplanar joints are also included as comparison. The results of the multiplanar joints with the out-of-plane braces unloaded are the same as those in Section 8.2. Thus, the multiplanar geometrical stiffening effect is the same as described in the previous section. Observations from Figure 8.18 are :

-       For the joints with small $\beta$ values, the ultimate moment capacity is increased with an increase of the load ratios ($-1 \leq J_{IA} \leq 0.5$). For joints with a load ratio of $J_{IA}=1.0$, the ultimate moment capacity is decreased due to the increased rotation of the out-of-plane braces which results in unfavourable secondary bending moments in the out-of-plane braces. In such a case, the joint fails at the compression side of the out-of-plane braces next to the weld toe.

-       The influence of the load ratio is larger for joints with smaller $\beta$ values ($\beta=0,4$ and 0.6) than that for joints with larger $\beta$ values ($\beta=0.8$ and 1.0) due to the rotation effects. Especially for joints with $\beta=1$, the influence of the load ratio is so small that the curves for different load ratios are overlapped.
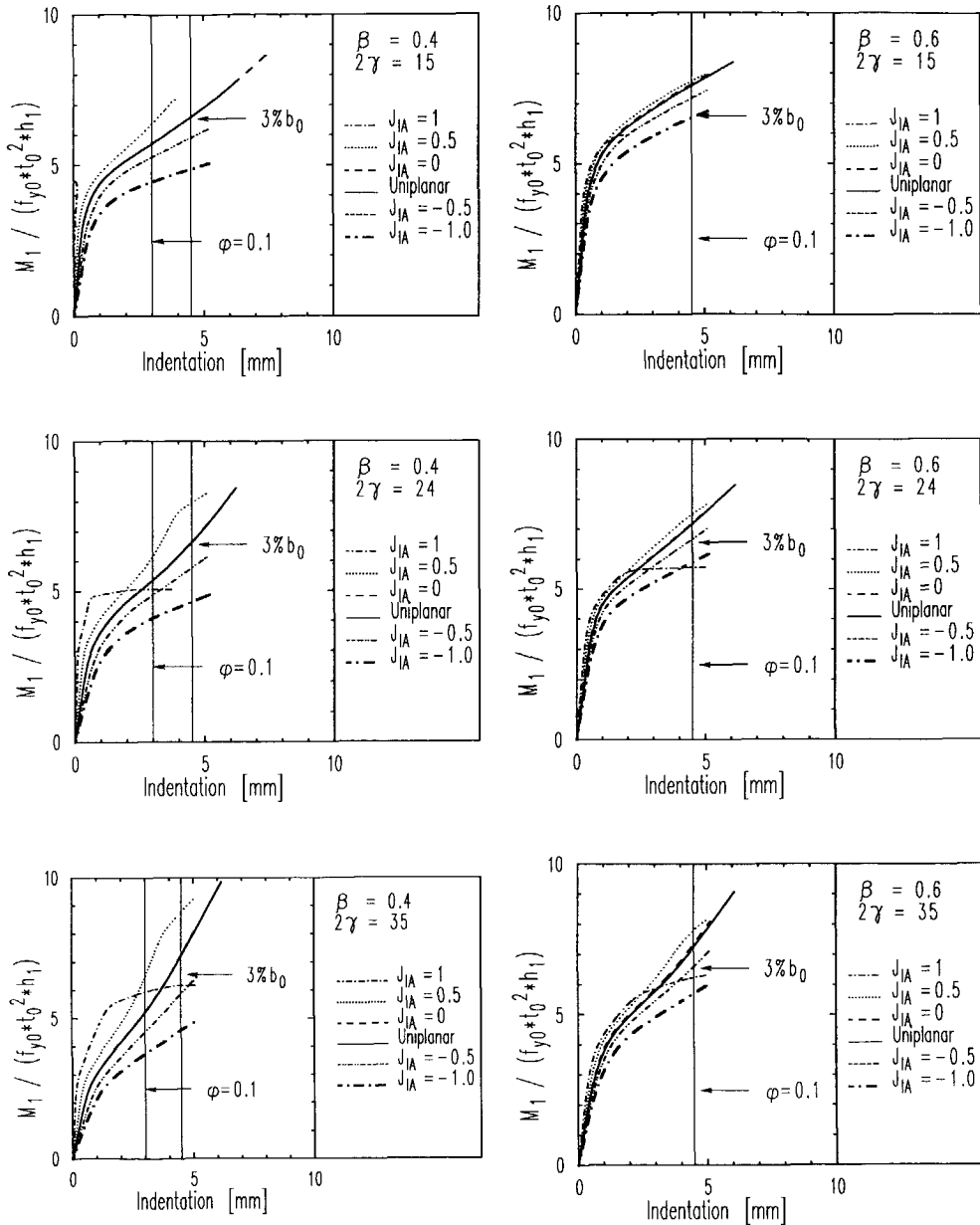
**Figure 8.18** **Numerical results of multiplanar XX-joints with the out-of-plane braces free (Group 1)**
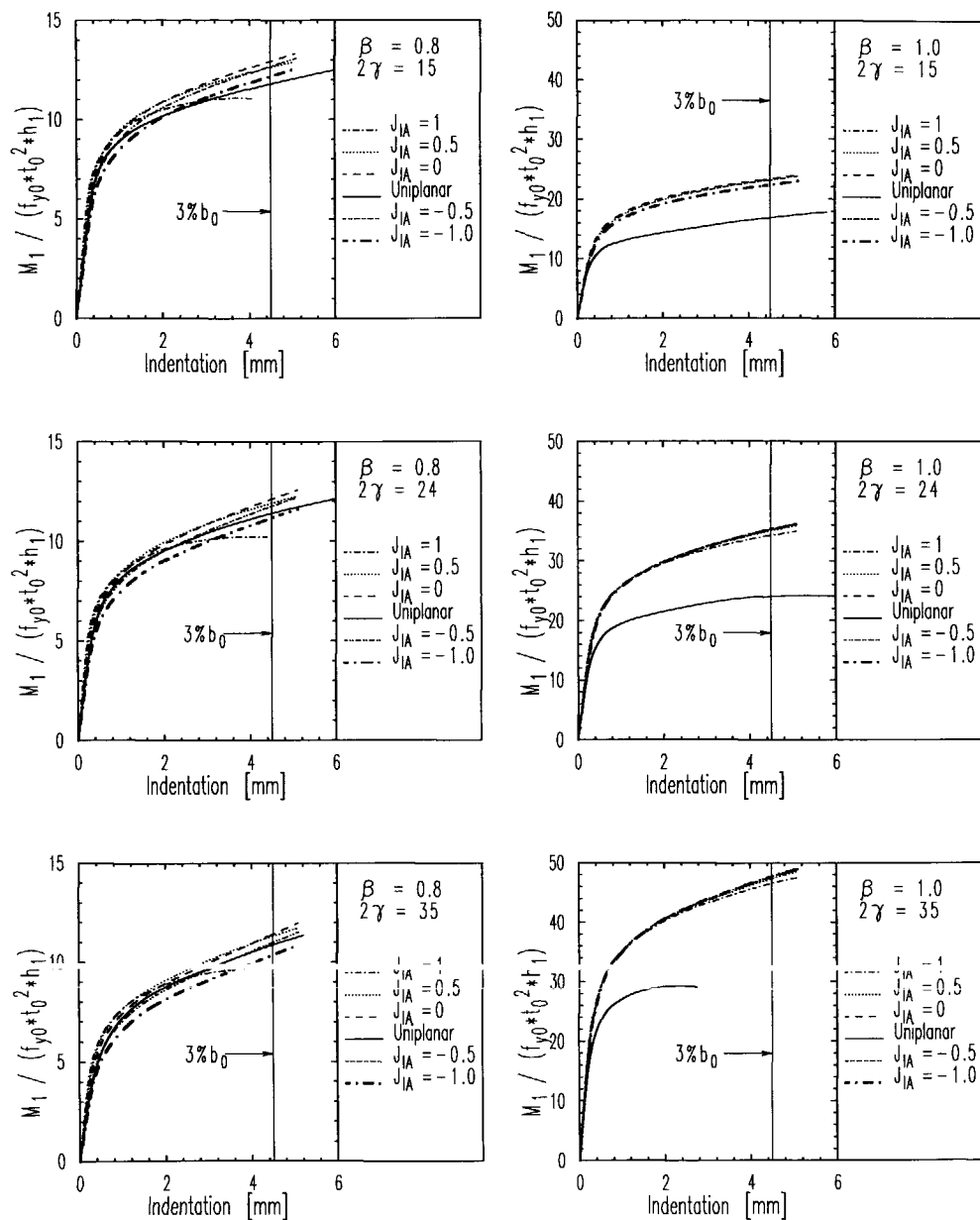
**Figure 8.18** (Group 1 continued)

**Table 8.14    Numerical results of XX-joints loaded with in-plane bending moments and axial forces (out-of-plane braces free)**

| Uniplanar joints | | Multiplanar joints | | | | | |
|---|---|---|---|---|---|---|---|
| No. | $\dfrac{M_{1,ipb,u}}{f_{y0}t_0^2 h_1}$ | No. | $M_{1,ipb,u}(J_{IA})/(f_{y0}t_0^2 h_1)$ | | | | |
| | | | $J_{IA}=-1$ | $J_{IA}=-0.5$ | $J_{IA}=0$ | $J_{IA}=0.5$ | $J_{IA}=1$ |
| x1i | 5.71 | xx1ia | 4.45 | 5.27 | 5.72 | 6.38 | - |
| x2i | 5.35 | xx2ia | 4.09 | 4.86 | 5.36 | 6.15 | 5.05 |
| x3i | 5.21 | xx3ia | 3.75 | 4.51 | 5.22 | 6.48 | 5.95 |
| x4i | 7.56 | xx4ia | 6.49 | 7.14 | 7.61 | 7.71 | 5.95 |
| x5i | 7.17 | xx5ia | 5.90 | 6.66 | 7.20 | 7.50 | 5.72 |
| x6i | 7.25 | xx6ia | 5.72 | 6.62 | 7.34 | 7.79 | 6.25 |
| x7i | 11.80 | xx7ia | 12.18 | 12.68 | 12.94 | 12.63 | 11.07 |
| x8i | 11.40 | xx8ia | 11.18 | 11.76 | 12.12 | 11.92 | 10.22 |
| x9i | 10.87 | xx9ia | 10.35 | 10.99 | 11.41 | 11.31 | 9.79 |
| x10i[*] | 16.85 | xx10ia[*] | 22.36 | 23.18 | 23.38 | - | - |
| x11i[*] | 24.04 | xx11ia[*] | 35.20 | 35.27 | 34.62 | 33.37 | 30.87 |
| x12i[*] | 29.21 | xx12ia[*] | 47.68 | 47.70 | 47.58 | 47.31 | 46.52 |

[*]: Without weld,   ‾: convergency failure.

## Joints with the out-of-plane braces restrained (Group 2)

In order to prevent failure due to the rotation of the out-of-plane braces, the end of the out-of-plane brace is restrained in the direction parallel to the chord length. The numerical results of these joints are shown in Figure 8.19. The ultimate moment capacity of the joints is listed in Table 8.15. Observations from Figure 8.19 are as follows:

-    For multiplanar joints with $\beta \leq 0.6$, very little multiplanar geometrical effects are found compared to the results of the uniplanar joints. For multiplanar joints with $\beta=0.8$ and 1.0, larger multiplanar geometrical effects exist. The multiplanar geometrical effects are somewhat higher than those of joint group 1 (or joints in Section 8.2) depending upon the geometrical parameters.

-    As a general tendency, the ultimate moment capacity of the joints is increased with the increase of the load ratios for joints with $\beta \leq 0.8$. For joints with $\beta=1.0$, the influence of the load ratio is very small which agrees with that for joints with the out-of-plane braces free.

- For multiplanar joints with $\beta \leq 0.8$ and $J_{IA}=1.0$, the ultimate moment capacity of the joints is increased largely due to the restraints on the out-of-plane braces which results in high numerical results.
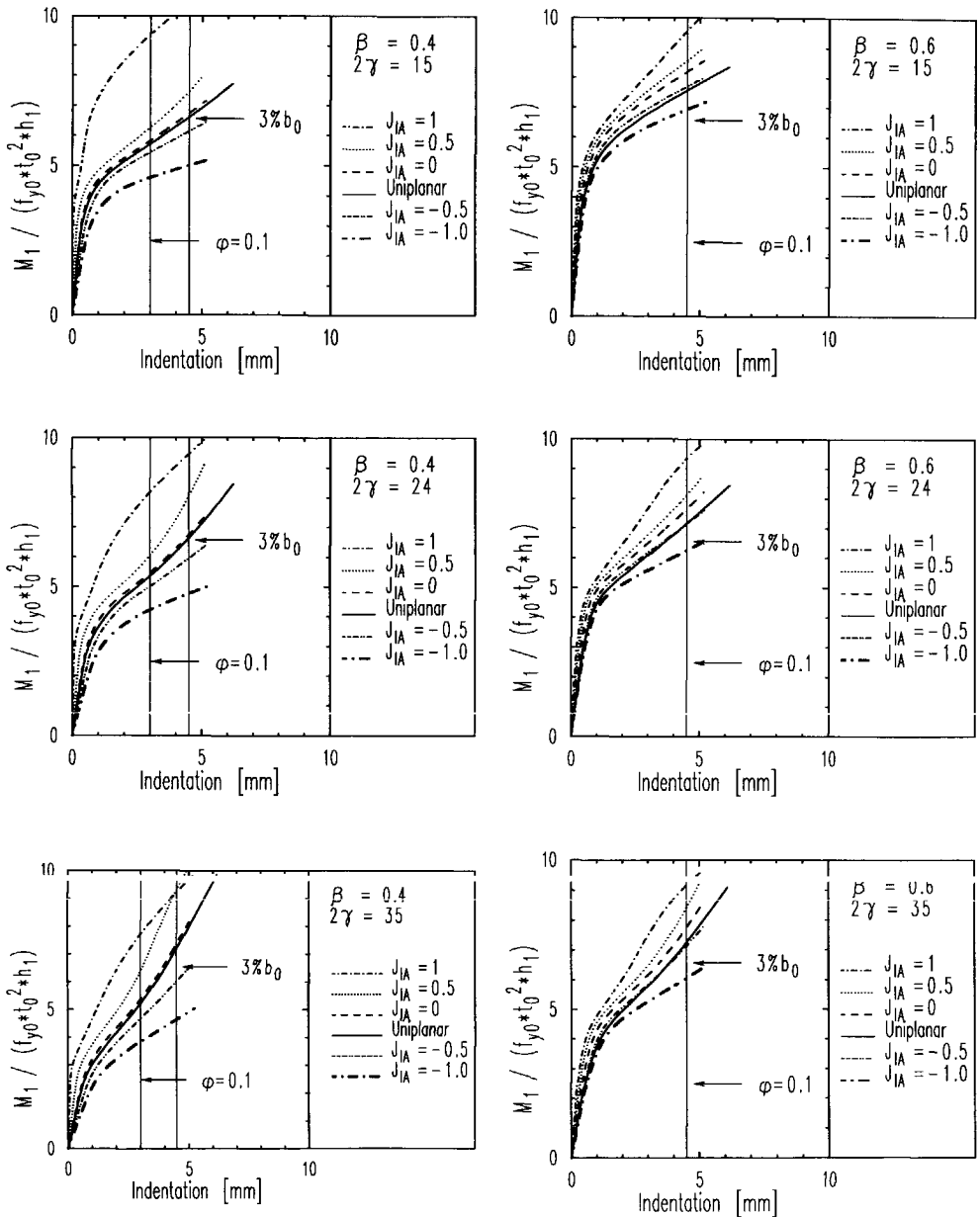


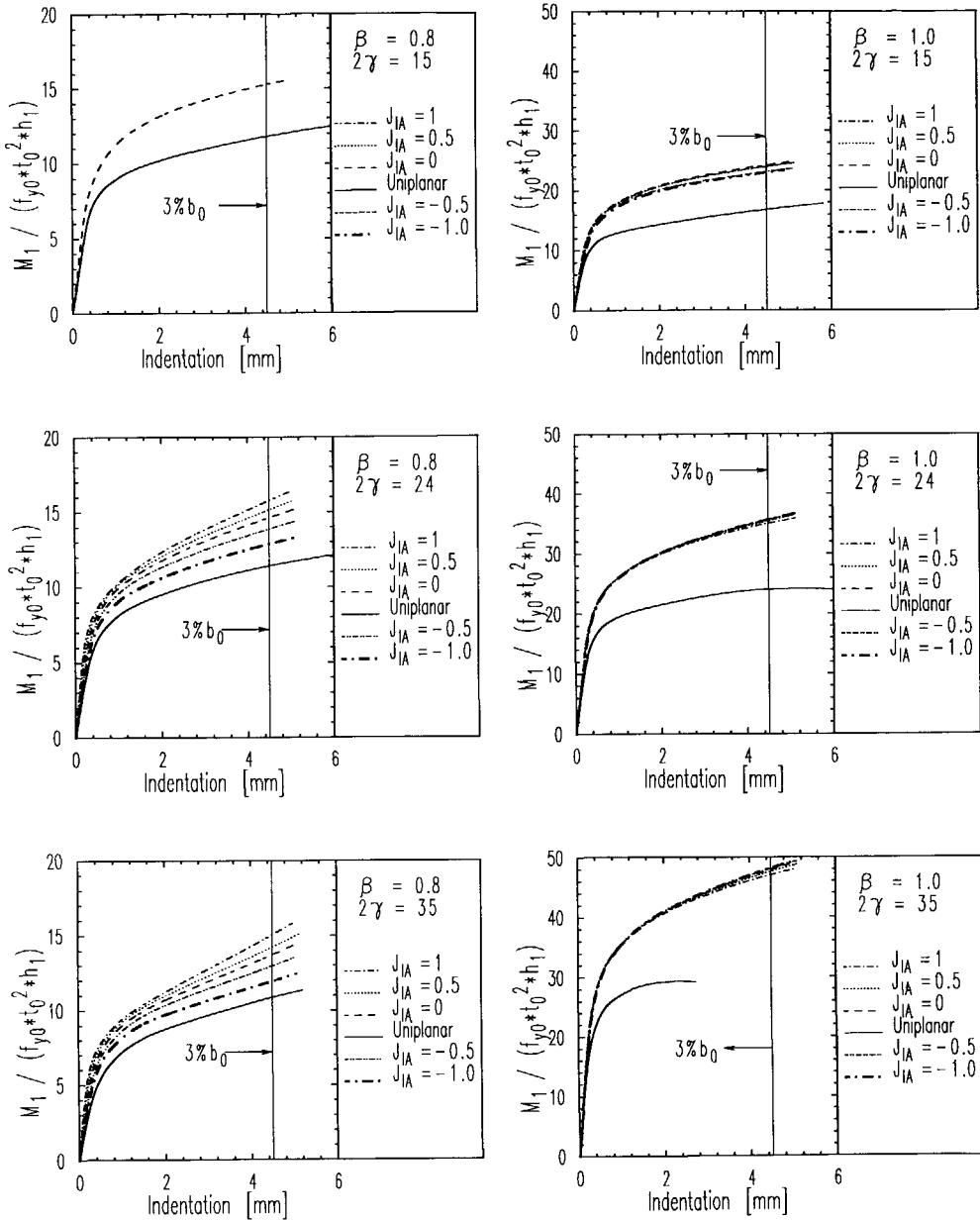**Figure 8.19    Numerical results of multiplanar XX-joints with the out-of-plane braces restrained (Group 2)**

**Figure 8.19** (Group 2 continued)

**Table 8.15    Numerical results of XX-joints loaded with in-plane bending moments and axial forces (out-of-plane braces restrained)**

| Uniplanar joints | | Multiplanar joints | | | | | |
|---|---|---|---|---|---|---|---|
| No. | $\dfrac{M_{1,ipb,u}}{f_{y0}t_0^2 h_1}$ | No. | $M_{1,ipb,u}(J_{IA})/(f_{y0}t_0^2 h_1)$ | | | | |
| | | | $J_{IA}=-1$ | $J_{IA}=-0.5$ | $J_{IA}=0$ | $J_{IA}=0.5$ | $J_{IA}=1$ |
| x1i | 5.71 | xx1ia | 4.60 | 5.44 | 5.83 | 6.25 | 9.37 |
| x2i | 5.35 | xx2ia | 4.22 | 5.01 | 5.46 | 6.05 | 8.17 |
| x3i | 5.21 | xx3ia | 3.84 | 4.67 | 5.36 | 6.36 | 7.70 |
| x4i | 7.56 | xx4ia | 6.93 | 7.69 | 8.19 | 8.56 | 9.56 |
| x5i | 7.17 | xx5ia | 6.27 | 7.16 | 7.66 | 8.13 | 9.35 |
| x6i | 7.25 | xx6ia | 6.05 | 7.13 | 7.75 | 8.41 | 9.16 |
| x7i | 11.80 | xx7ia | - | - | 15.28 | - | - |
| x8i | 11.40 | xx8ia | 12.86 | 13.86 | 14.62 | 15.15 | 15.76 |
| x9i | 10.87 | xx9ia | 11.95 | 12.97 | 13.72 | 14.22 | 15.05 |
| x10i[*] | 16.85 | xx10ia[*] | 23.04 | 24.01 | 24.27 | 24.00 | 23.16 |
| x11i[*] | 24.04 | xx11ia[*] | 35.65 | 35.68 | 35.61 | 35.45 | 35.04 |
| x12i[*] | 29.21 | xx12ia[*] | 48.10 | 48.03 | 47.84 | 47.55 | 47.01 |

[*]. Without weld,    ⁻. Convergency failure.

### 8.3.5    Comparison between the results of joints with different boundary conditions

**Comparison between the results of joints with fixed and free ends**

The influence of the restraints on the out-of-plane braces is shown in Figure 8.20. The vertical axis represents the ratio between the ultimate moment capacities of the joints with fixed and those with free ends of the out-of-plane braces.

For joints with load ratios $J_{IA}$=-1.0, -0.5, 0 and 0.5, the influence of the restraints is about 20% for joints with $\beta$=0.8 and is within 10% for joints with $\beta$=0.4, 0.6 and 1.0 independent of the load ratios, see Figure 8.20. The $2\gamma$ influence is neglectable.

For joints with $J_{IA}$=1.0 and $\beta\leq0.8$, a much larger influence of the restraints is found, see Figure 8.20. When the out-of-plane braces are free to rotate, the ultimate moment capacity of the joints is reduced largely due to the large secondary bending moments on the out-of-plane braces for joints with $J_{IA}$=1.0, see Figure 8.18. Failure occurs at the compression side of the out-of-plane braces close to the weld toe in such a case. However, when the

out-of-plane braces are restrained and rotation is thus avoided, the ultimate moment capacity is increased as shown in Figure 8.19. In practice, the out-of-plane braces are restrained between free and fixed boundary conditions. Thus, the influence of the restraints shown in Figure 8.20 is higher than that in the practice.
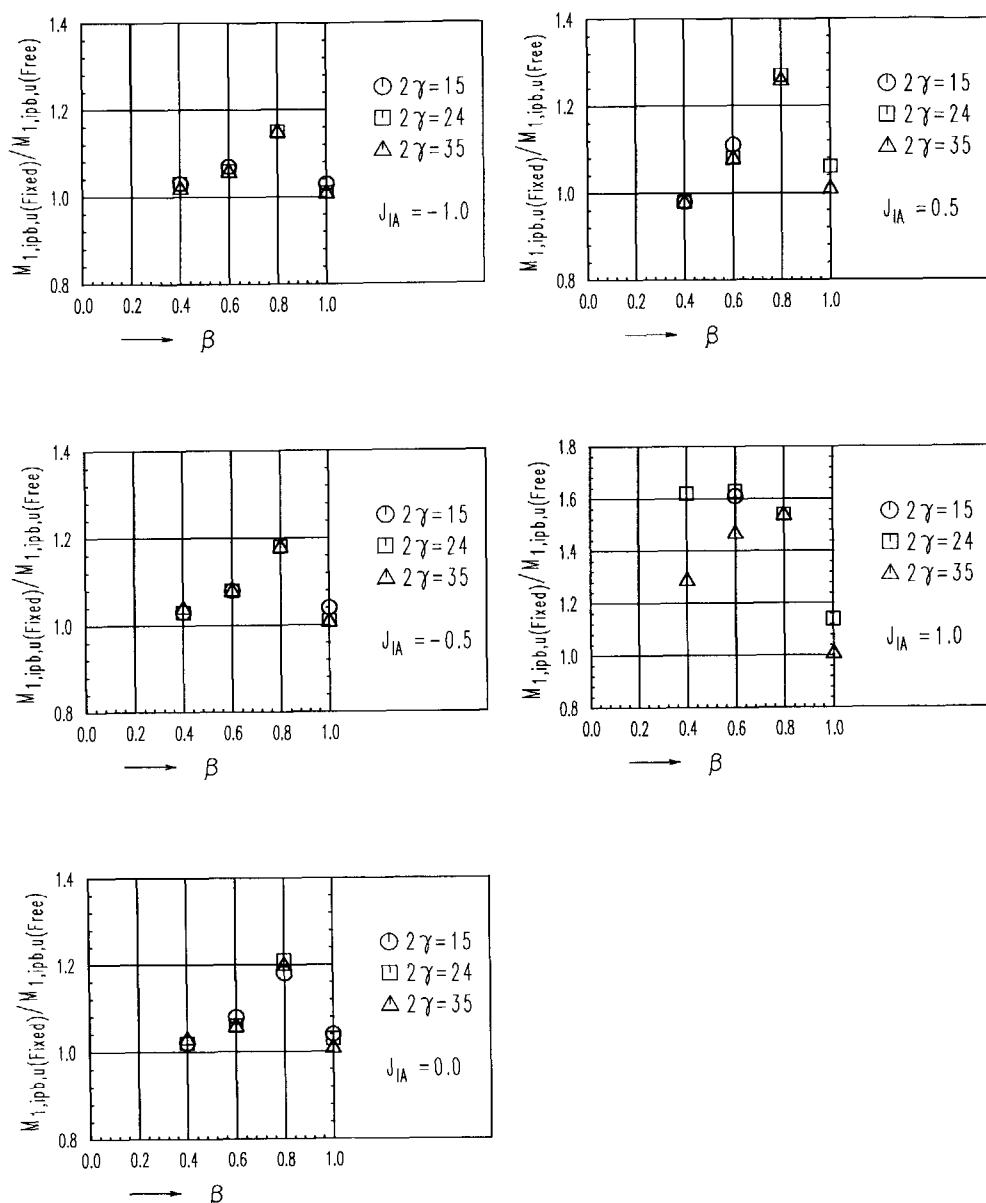


**Figure 8.20   Comparison between the results of joints with fixed and free ends**

**Comparison between the results of joints with fixed ends, free ends and "follow force"**

A comparison between the results of joints with fixed ends, free ends and "follow force" on the out-of-plane braces is shown in Figure 8.21. It can be seen that the ultimate moment capacity of joints with "follow force" is higher than joints with free ends and lower than joints with fixed ends.

For a joint with load ratio $J_{IA}=0.5$ and $\beta=0.6$, the ultimate moment capacity of a joint with "follow force" is 5% higher than that of a joint with free ends and 3% lower than that of a joint with fixed ends. For a joint with load ratio $J_{IA}=0.5$ and $\beta=0.8$, the ultimate moment capacity of a joint with "follow force" is 8% higher than that of a joint with free ends and 15% lower than that of a joint with fixed ends.

For a joint with $J_{IA}=1.0$ and $\beta=0.6$, the ultimate moment capacity of a joint with "follow force" is 62% higher than that of a joint with free ends and only 1% lower than that of a joint with fixed ends. For a joint with $J_{IA}=1.0$ and $\beta=0.8$, the ultimate moment capacity of a joint with "follow force" is 31% higher than that of a joint with free ends and 15% lower than that of a joint with fixed ends.

For low load ratio, the ultimate moment capacity of joints with "follow force" is closer to that of joints with free ends. For high load ratio, it is closer to that of joints with fixed ends.
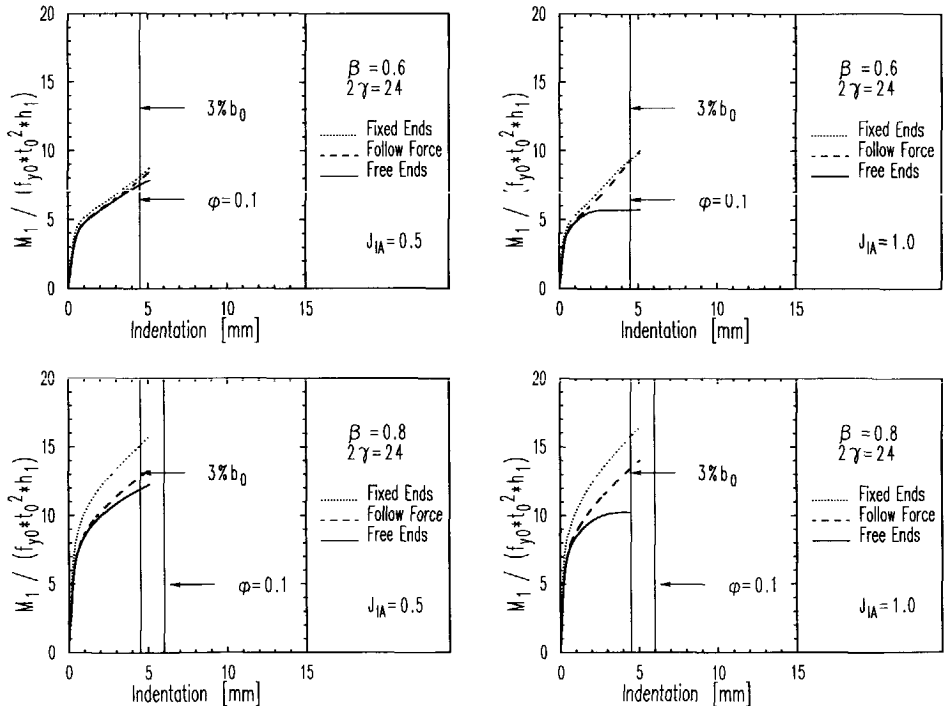


**Figure 8.21    Comparison between the results of joints with fixed ends, free ends and "follow force"**

### 8.3.6 The ultimate moment capacity

Similar to Sections 8.1 and 8.2, the general formulae for the ultimate moment capacity of the joints are determined as follows:

$$M_{1,ipb,u}(J_{IA}=0) = c_m \cdot M_{1,ipb,u} \qquad (8.18)$$

$$M_{1,ipb,u}(J_{IA}) = f(J_{IA}) \cdot M_{1,ipb,u}(J_{IA}=0) \qquad (8.19)$$

Where $M_{1,ipb,u}$ is the ultimate moment capacity of uniplanar X-joints;
$c_m$ is a factor considering the multiplanar geometrical stiffening effects;
$M_{1,ipb,u}(J_{IA}=0)$ is the ultimate moment capacity of XX-joints with load ratio $J_{IA}=0$;
$M_{1,ipb,u}(J_{IA})$ is the ultimate moment capacity of XX-joints with load ratio $J_{IA}$.

#### 8.3.6.1 The factor for the multiplanar geometrical stiffening effects

**Joints with the out-of-plane braces free**

According to definition, the factor for the multiplanar geometrical stiffening effects is defined as the ratio between the ultimate moment capacity of multiplanar XX-joints with $J_{IA}=0$ and that of the corresponding uniplanar X-joints. Joints with $J_{IA}=0$ and the out-of-plane braces free to rotate are exactly the same as joints with $J_{II}=0$ analysed in Section 8.2. Thus, the factor for the multiplanar geometrical stiffening effects in this section should be the same as in Section 8.2:

$$c_m = 1 + 0.4\beta^8 \qquad (8.14)$$

**Joints with the out-of-plane braces fixed**

For joints with the out-of-plane braces restrained to rotate, the multiplanar geometrical stiffening effects are somewhat larger than those of the corresponding joints with the out-of-plane braces free due to the secondary bending moments on the out-of-plane braces. In practice, the boundary conditions of the out-of-plane braces are between fixed and free situations. Thus, equation (8.14) is recommended as a lower bound.

#### 8.3.6.2 The function for the multiplanar load effects

**Joints with the out-of-plane braces free**

The multiplanar load effects for joints with the out-of-plane braces free are illustrated in Figure 8.22.

For joints with negative load ratios ($J_{IA} \leq 0.0$), a clear negative multiplanar load effect is found. The function for the multiplanar load effects is defined as follows:

$$f(J_{IA}) = 1 + R_1(1-\beta)J_{IA} \qquad\qquad (J_{IA} \leq 0) \qquad (8.20)$$

As already discussed, due to the similar influence of the restraints for joints with different load ratios ($J_{IA}$=-1.0, -0.5 and 0 etc.), the multiplanar load effects of joints with and without restraints are similar. Thus, a regression analysis based upon equation (8.20) is carried out using all the numerical results of joint groups 1 and 2. The regression constant $R_1$ and the statistical results are listed in Table 8.16. Equation (8.20) is plotted in Figure 8.22.
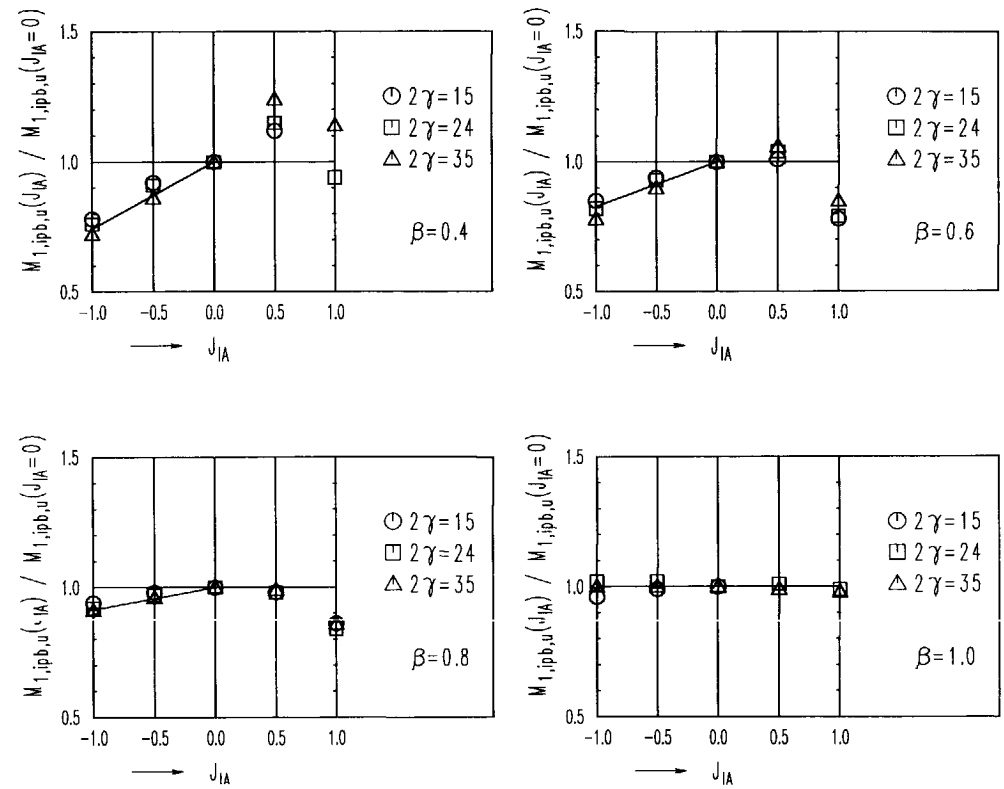


**Figure 8.22    The multiplanar load effects (joints with the out-of-plane braces free)**

**Table 8.16  Regression results of equation (8.20)**

| $R_1$ | Mean normalised error | Coefficient of variation CoV | Correlation coefficient $R^2$ |
|-------|----------------------|------------------------------|-------------------------------|
| 0.43  | 1.003                | 0.025                        | 0.927                         |

For joints with a positive load ratio of $J_{IA}$=0.5, the multiplanar load effect is positive or negligibly small. For joints with a positive load ratio of $J_{IA}$=1.0 and $\beta \leq 0.8$, a negative multiplanar load effect is found in many cases due to the large secondary bending moments on the out-of-plane braces. The influence of the secondary bending moments depends not only on the load of the out-of-plane braces but also on the length of them. If the method of "follow force" is used, the secondary bending moments are excluded and the multiplanar load effects will be positive. For example, for joint with $\beta$=0.6, $2\gamma$=24 and $J_{IA}$=1.0, the multiplanar load effect according to Figure 8.22 is -21%, while if "follow force" is used, the joint ultimate moment capacity is increased by 62% compared to that of the corresponding joint with the out-of-plane braces free, see Figure 8.21. As a result, the multiplanar load effect with "follow force" is 29%. The value of 29% is the ultimate moment capacity of the joint with "follow force" ($J_{IA}$=1.0) divided by that of the joint with the out-of-plane braces free and unloaded.

Similarly, for the joint with $\beta$=0.8, $2\gamma$=24 and $J_{IA}$=1.0, the multiplanar load effect for the joint with the out-of-plane braces free is -16%, while the multiplanar load effect for the joint with "follow force" is 11%. Based upon these considerations, a lower bound of $f(J_{IA})$=1.0 is recommended for joints with $J_{IA} \geq 0.0$.

**Joints with the out-of-plane braces restrained**

The results of joints with the out-of-plane braces restrained are illustrated in Figure 8.23.

For joints with negative load ratios ($J_{IA} \leq 0$), equation (8.20) is applied, because a similar tendency of multiplanar load effects is found. Equation (8.20) is plotted in Figure 8.23.

For joints with positive load ratios ($J_{IA} \geq 0.0$), the multiplanar load effects in Figures 8.22 and 8.23 are about the same for $J_{IA} = 0.5$, while for joints with $J_{IA} = 1.0$, the multiplanar load effect for joints with the out-of-plane braces free (Figure 8.22) is negative and it is positive for joints with the out-of-plane braces restrained (Figure 8.23). Thus, the behaviour of the joints is largely influenced by the boundary conditions of the out-of-plane braces. In practice, the out-of-plane braces are restrained between free and fixed boundary conditions. Based upon Figures 8.21 to 8.23, a lower bound of $f(J_{IA}) = 1.0$ is recommended for joints with $J_{IA} \geq 0.0$.
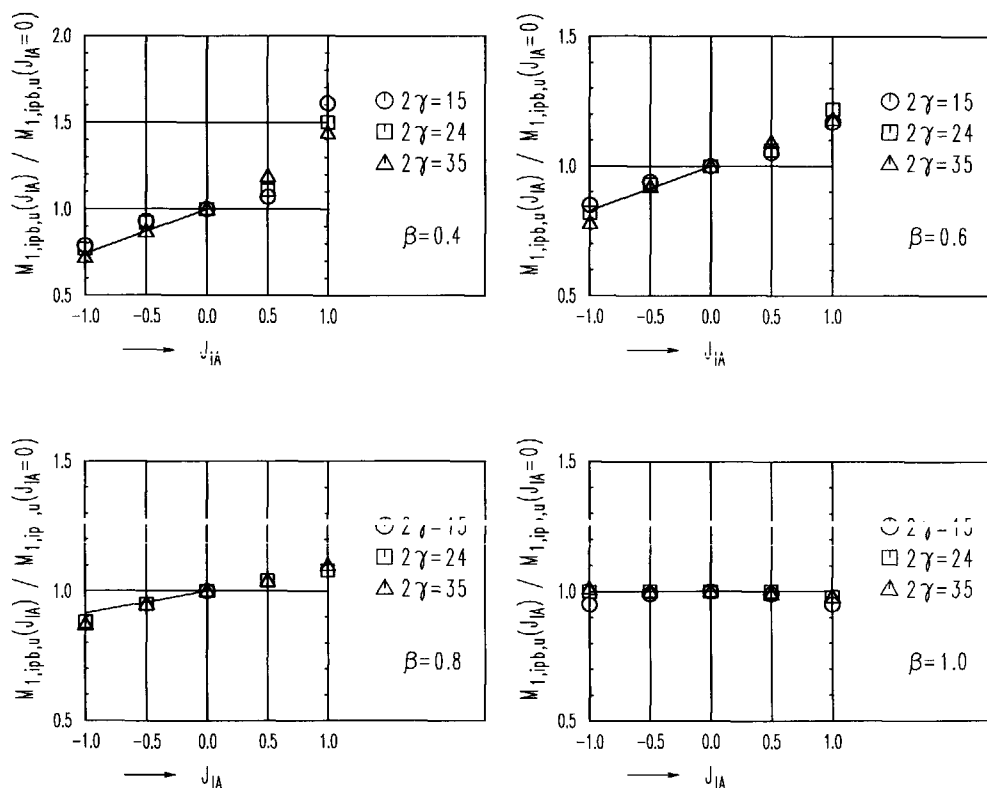


**Figure 8.23**   **The multiplanar load effects (joints with the out-of-plane braces restrained)**

### 8.3.7 Conclusions

The behaviour of multiplanar XX-joints loaded with in-plane bending moments on the in-plane braces and axial forces on the out-of-plane braces has been analysed for different joint geometrical parameters and three groups of boundary conditions. It is summarised as follows:

- For joints loaded with $J_{IA} \leq 0.5$, the maximum influence of the restraints on the ultimate moment capacity is about 20% for joints with $\beta = 0.8$ and is within 10% for joints with other $\beta$ values, see Figure 8.20. This tendency is similar for all the joints with $J_{IA} \leq 0.5$. For joints with $J_{IA} = 1.0$, the influence of the restraints is larger (up to about 60%). In practice, the out-of-plane braces are restrained between free and fixed boundary conditions.

- For the multiplanar geometrical stiffening effects, the same formula is valid as given in Section 8.2.

- For joints loaded with negative load ratios, a clear negative multiplanar load effect is found with the same tendency for joints with and without the out-of-plane braces restrained. Equation (8.20) is recommended as the function for multiplanar load effects.

- For joints loaded with positive load ratios, the multiplanar effects depend upon the value of the load ratios and the boundary conditions. For joints with $J_{IA} = 1.0$, the multiplanar load effects are largely influenced by the boundary conditions. For $J_{IA} = 1.0$, the multiplanar load effects are negative for most of the joints with the out-of-plane braces free and are positive for joints with the out-of-plane braces fixed due to the secondary bending moments. If "follow force" is used with the secondary bending moments excluded, the multiplanar load effects are between the two extreme cases, but still with a positive influence. As a lower bound, a function of $f(J_{IA}) = 1.0$ for the multiplanar load effects is recommended.

# 9      MULTIPLANAR TX-, UNIPLANAR K- AND MULTIPLANAR KK-JOINTS

## 9.1      INTRODUCTION

This chapter deals with the behaviour of multiplanar TX-, Uniplanar K- and multiplanar KK-joints. Due to asymmetric in load and deformation, the behaviour of such joints is more complicated. In Section 9.2, the influence of boundary conditions, the multiplanar geometrical stiffening effects and the multiplanar load effects of TX-joints excluding chord bending are studied. In Section 9.3, the influence of boundary conditions of uniplanar K-joints is discussed. The multiplanar load effect of KK-joints is analysed based upon the available experimental information.

## 9.2      MULTIPLANAR TX-JOINTS

The configuration of a TX-joint is shown in Figure 9.1. Similar to axially loaded uniplanar T-joints, the axial force applied to the in-plane brace is balanced by the reaction forces at the ends of the chord which result in a bending moment in the chord. As already studied in Chapters 5 to 7, due to this bending moment, the ultimate load capacity of the joint is reduced. In order to separate the effect of the chord bending moment from that of the axial load, compensating bending moments can be applied in such a way that the chord bending moment at the intersection of the brace is zero, see Figure 9.1 (b).



(a) Including chord bending          (b)      Excluding  chord     bending  in   the intersection of the brace
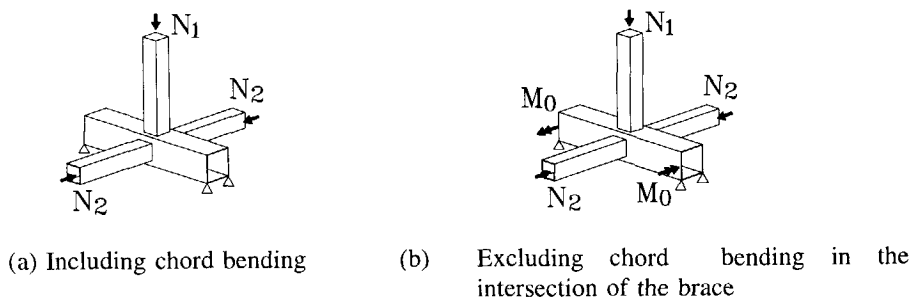
**Figure 9.1   Configuration of a TX-joint**

### 9.2.1    The numerical modelling

-       The FE meshes for each joint analysed in this chapter are generated based on those of the corresponding XX-joints in Section 8.1, Chapter 8. The dimensions and material properties of the joints and the welds are the same as described in Chapter 8.

-       The chord bending moment in the intersection between the brace and the chord is excluded for all the joints analysed in this chapter by applying compensating bending moments at the chord ends with $M_0 = N_0 * h_0 = N_1 * (l_0 - h_1)/4$, see Figure 9.1 (b).

-       Based upon symmetry in load and geometry, a quarter of a joint is analysed. Boundary
        conditions at the planes of symmetry and the end supports of the chord are the same
        as described in Chapter 4. Boundary conditions at the out-of-plane braces are
        discussed in Section 9.2.2.

## 9.2.2   Influence of the boundary conditions

Due to asymmetric in load and deformation, the out-of-plane braces of a TX-joint rotate as
shown in Figure 9.2 (a). If the out-of-plane braces are free and loaded in compression, the
compressive forces enlarge the rotation of the out-of-plane braces, as a result, failure of the
out-of-plane braces may occur due to large secondary bending moments for a large
multiplanar load ratio. In order to prevent rotation of the out-of-plane braces, points A and
D can be tied to points B and C respectively to keep the out-of-plane braces horizontal, see
Figure 9.2 (b). This method also results in secondary bending moments in the out-of-plane
braces. Both methods have been used in the experimental tests and the numerical calibration
in Chapters 3 and 4. Similar to Section 8.3 of Chapter 8, a method to exclude the secondary
bending moments in the numerical study is the use of the so-called "follow force", see Figure
9.2 (c). The method of "follow force" ensures that the axial loads on the out-of-plane braces
are formed on the basis of the current geometry which means that the out-of-plane forces
always follow the axis of the out-of-plane braces during loading.



(a) Out—of—plane braces free          (b) Out—of—plane braces kept
                                          horizontal (restrained)
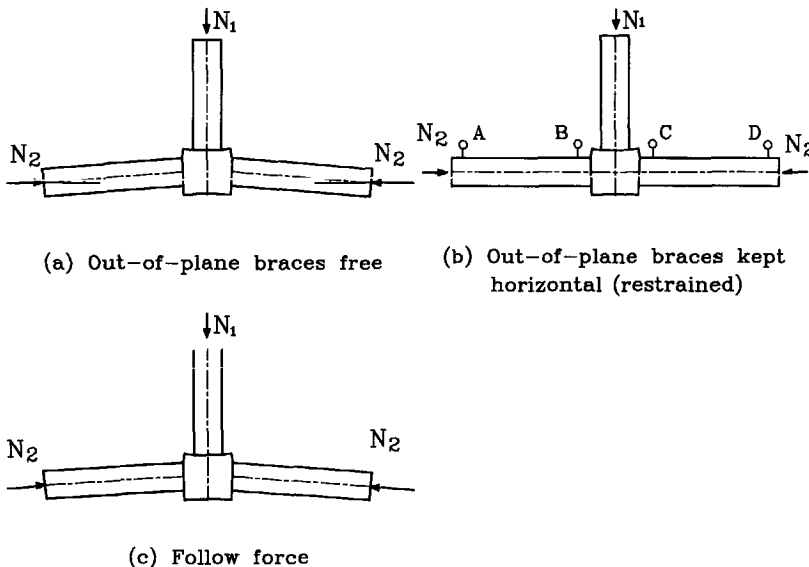
(c) Follow force

**Figure 9.2      Three different boundary conditions on the out-of-plane braces**

A comparison between the results of Figure 9.2 (a) and (b) is illustrated in Figure 9.3 based
upon the experimental and the numerical studies in Chapters 3 and 4. The difference between
the results of (a) and (b) is within 12% for the investigated parameters.
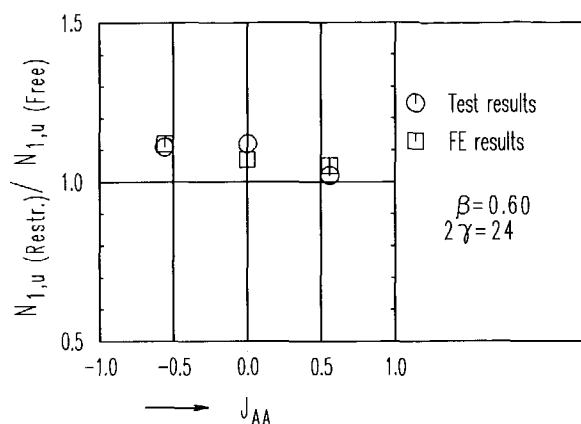
**Figure 9.3**    **Influence of boundary conditions based upon test results and numerical calibration (see Tables 3.8 and 4.4 in Chapters 3 and 4)**

A similar numerical investigation has been done by Crockett (1994) for comparison between boundary conditions (a) and (b). As shown in Figure 9.4, he found a difference of 10% between the two methods except for one joint with a load ratio of $J_{AA}=N_2/N_1=1.0$. For joints with $J_{AA}=1.0$ and boundary condition (a), the large compressive forces on the out-of-plane braces increase their rotation which results in large secondary bending moments. Due to the large secondary bending moments and the compressive forces, failure occurs in the out-of-plane braces. While for joints with $J_{AA}=1.0$ and boundary condition (b), rotation of the out-of-plane braces is prevented. Failure of the out-of-plane braces does not occur.
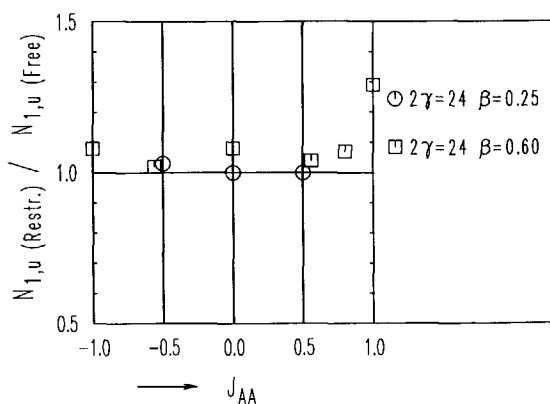


**Figure 9.4**    **Influence of boundary conditions (numerical results of Crockett 1994)**

In Figure 9.5, the numerical results of joints with three different boundary conditions as shown in Figure 9.2 are compared.

**Figure 9.5      Comparison between the results of the three boundary conditions**

For a joint with the out-of-plane braces unloaded ($J_{AA}$=0.0), the numerical results for Figure 9.2. (a) and 9.2. (c) are the same. The difference between the ultimate load capacity of joints with "follow force" and that of joints with the out-of-plane braces kept horizontal (restrained) is 5-7%. The difference between the ultimate load capacity of joints with "follow force" and that of joints with the out-of-plane braces free is 2% for the investigated parameters and load ratios.
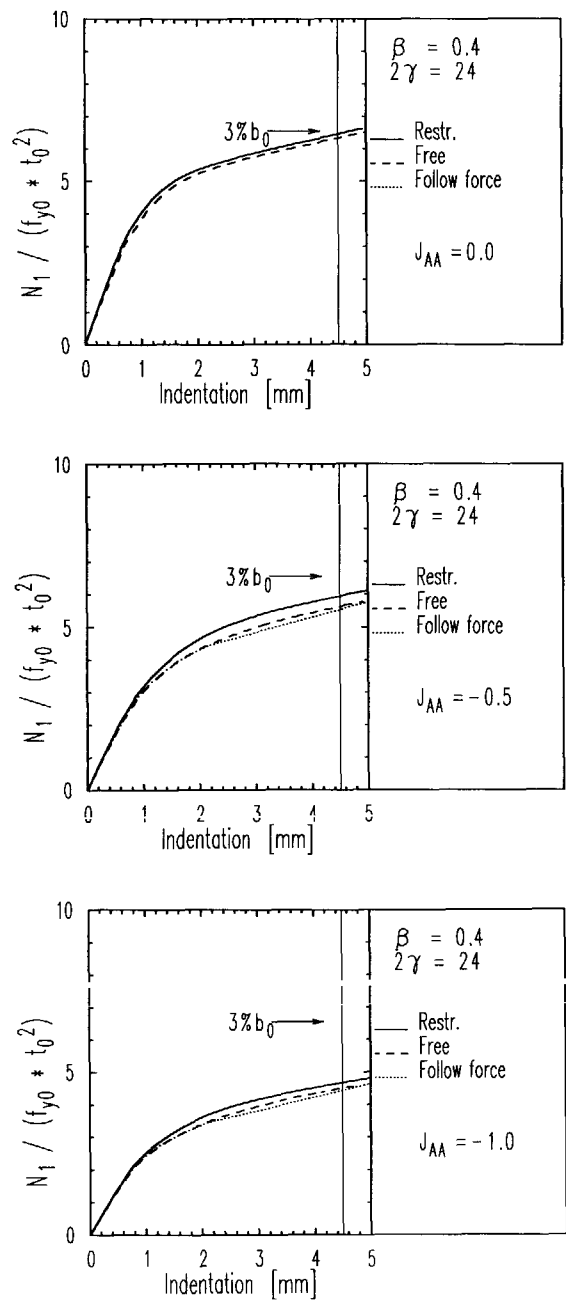
It should be mentioned that the numerical analysis using "follow force" is very time consuming and sometimes fails to convergency. Considering that the multiplanar load effect is a relative value between $N_{1,u}(J_{AA})$ and $N_{1,u}(J_{AA}=0)$ and the influence of the boundary conditions is not very large except for the case $J_{AA}$=1.0, it is acceptable to omit the influence of the boundary conditions upon the multiplanar load effect if the ultimate load capacities are determined using a consistent boundary condition.

### 9.2.3 The numerical results

The numerical results of the parameter study are shown in Figure 9.6. The ultimate load capacity of each joint is given in Table 9.1.

A general tendency is observed from Figure 9.6 and Table 9.1.

For joints with $J_{AA}$=0.0 and $\beta \leq 0.6$, the multiplanar geometrical stiffening effect is negligible, namely, the stiffness and the ultimate load capacity of the joints are almost the same as those of uniplanar T-joints excluding chord bending. For joints with $J_{AA}$=0.0 and $\beta$=0.8, the factor for multiplanar geometrical stiffening effect is 1.26 if the out-of-plane braces are kept horizontal and 1.18 if the out-of-plane braces are free.

For joints with negative load ratios, the ultimate load capacity is reduced considerably.

For joints with positive load ratios, the ultimate load capacity is increased slightly for the investigated parameters.
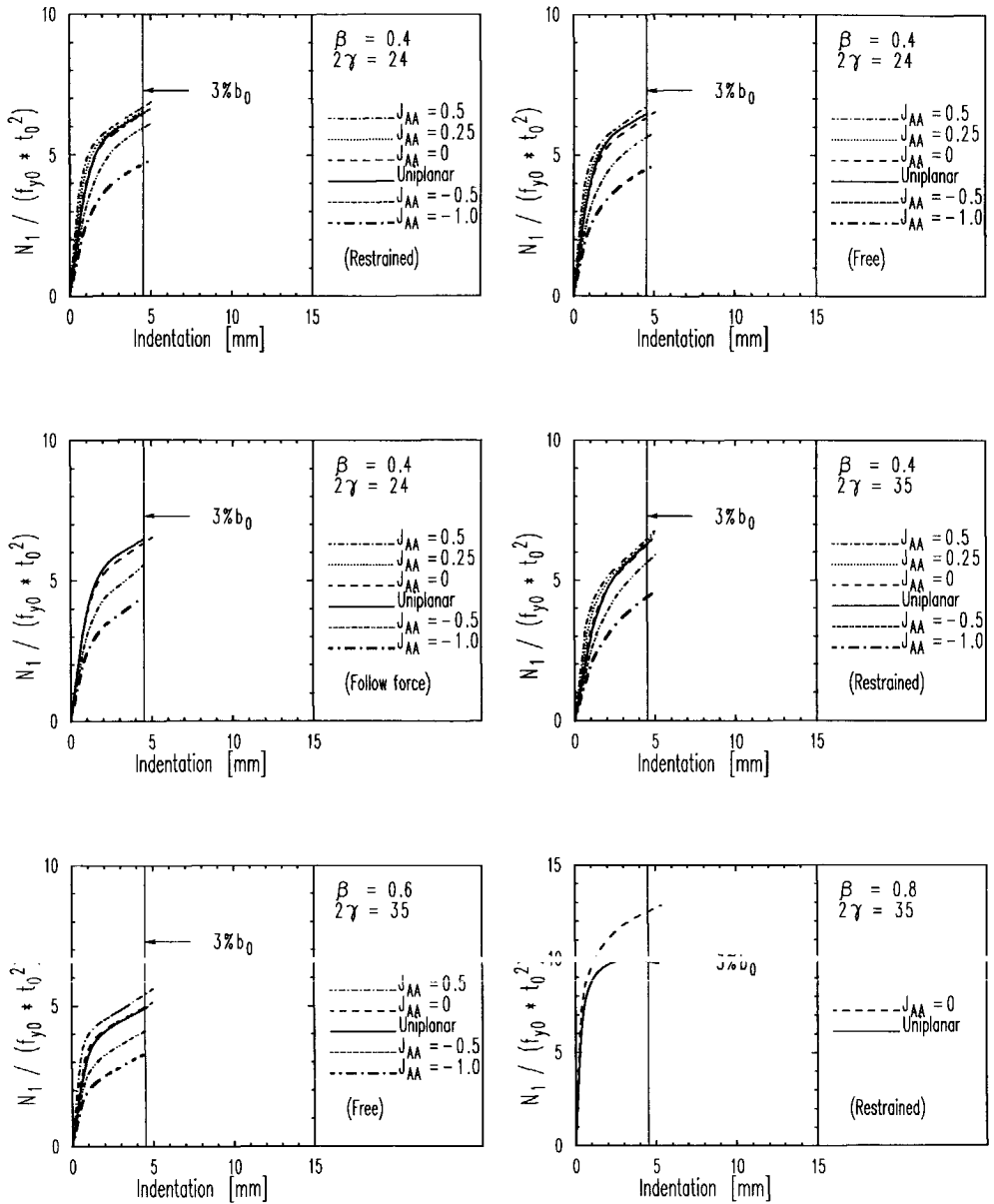
**Figure 9.6  Numerical results of TX-joints**

**Table 9.1    Numerical results of T- and TX-joints excluding chord bending**

| β | 2γ | B.C. | $J_{AA}$ | $N_{1,u}(J_{AA})/(f_{y0}t_0^2)$ | $f(J_{AA})$ | Uniplanar $N_{1,u}/(f_{y0}t_0^2)$ |
|---|---|---|---|---|---|---|
| 0.4 | 24 | Restr. | -1.0 | 4.67 | 0.72 | 6.46 |
| | | | -0.5 | 5.95 | 0.92 | |
| | | | -0.25 | 6.25 | 0.97 | |
| | | | 0.0 | 6.45 | 1.00 | |
| | | | 0.25 | 6.56 | 1.02 | |
| | | | 0.5 | 6.68 | 1.04 | |
| | | Free | -1.0 | 4.51 | 0.71 | |
| | | | -0.5 | 5.63 | 0.89 | |
| | | | -0.25 | 6.04 | 0.96 | |
| | | | 0.0 | 6.33 | 1.00 | |
| | | | 0.5 | 6.73 | 1.06 | |
| | | Follow force | -1.0 | 4.43 | 0.70 | |
| | | | -0.5 | 5.54 | 0.88 | |
| | | | 0.0 | 6.33 | 1.00 | |
| | 35 | Free | -1.0 | 4.39 | 0.70 | 6.29 |
| | | | -0.5 | 5.62 | 0.90 | |
| | | | 0.0 | 6.27 | 1.00 | |
| | | | 0.25 | 6.38 | 1.02 | |
| | | | 0.5 | 6.47 | 1.03 | |
| 0.6 | 35 | Free | -1.0 | 7.02 | 0.67 | 10.45 |
| | | | -0.5 | 8.72 | 0.83 | |
| | | | 0.0 | 10.54 | 1.00 | |
| | | | 0.5 | 11.52 | 1.09 | |
| 0.8 | 35 | Restr. | 0.0 | 26.55 | 1.00 | 21.01 |
| | | Free | 0.0 | 24.79 | 1.00 | |
| $f_{y0}$=355 N/mm$^2$    $b_0$=$h_0$=150 mm    $b_1$=$h_1$ | | | | | | |

The numerical results from Crockett (1994) are given in Table 9.2. The following aspects about his results and the numerical modelling should be known:

-   Crockett used different element types than those used in this thesis. For joints with $\beta$=0.25 and 0.6, the chord and the braces were modelled with 4-noded thick shell elements and the welds were modelled with 6-noded solid elements. For joints with $\beta$=1.0, the joints were modelled with 8-noded thick shell elements.

-   If no maximum load was reached, the ultimate load capacity was determined at the intersection point of two tangent lines (the line of the linear elastic part and that of the plastic part of the load vs. indentation curve). Since this method was used consistently for all uniplanar and multiplanar joints, the results in Table 9.2 can be used as far as for a relative comparison.

-   For joints with $\beta$=0.25 and 0.6, the chord bending moments were not excluded, namely TX-joints as shown in Figure 9.1 (a) were analysed. According to the results of uniplanar T-joints in Table 7.3 of Chapter 7, the influence of the chord bending moment on the ultimate load capacity of the joint is within 7% for joints with $\beta \leq 0.6$ and $\alpha \leq 12$. For the joint geometrical parameters used by him ($\beta$=0.25, 0.6 and $\alpha$=12), it is considered that the influence of the chord bending moments is negligible as far as for a relative comparison.

-   For joints with $\beta$=1.0, the axial load applied to the in-plane brace was balanced by a uniform support at the whole bottom of the chord. As a result, bending moments in the chord were completely excluded.

**Table 9.2    Numerical results from Crockett (1994)**

| $\beta$ | $2\gamma$ | B.C. | $J_{AA}$ | $N_{1,u}(J_{AA})^*$ (kN) | $N_{1,u}(J_{AA})^* / N_{1,u}(J_{AA}=0)^*$ | Uniplanar $N_{1,u}$ (kN) |
|---|---|---|---|---|---|---|
| 0.25 | 24 | Restr. | -0.5 | 71 | 0.90 | 79 |
| | | | 0.0 | 79 | 1.00 | |
| | | | 0.5 | 80 | 1.01 | |
| | | Free | -1.0 | 57 | 0.72 | |
| | | | -0.5 | 69 | 0.87 | |
| | | | 0.0 | 79 | 1.00 | |
| | | | 0.5 | 80 | 1.01 | |
| 0.6 | 24 | Restr. | -1.0 | 162.5 | 0.71 | 195 |
| | | | -0.8 | 170 | 0.74 | |
| | | | -0.56 | 192 | 0.83 | |
| | | | -0.40 | 220 | 0.96 | |
| | | | -0.20 | 222 | 0.97 | |
| | | | 0.0 | 230 | 1.00 | |
| | | | 0.2 | 230 | 1.00 | |
| | | | 0.4 | 235 | 1.02 | |
| | | | 0.56 | 240 | 1.04 | |
| | | | 0.8 | 245 | 1.07 | |
| | | | 1.0 | 245 | 1.07 | |
| | | Free | -1.0 | 150 | 0.71 | |
| | | | -0.56 | 187.5 | 0.88 | |
| | | | 0.0 | 212 | 1.00 | |
| | | | 0.56 | 230 | 1.08 | |
| | | | 0.8 | 230 | 1.08 | |
| | | | 1.0 | 190 | 0.90 | |
| 1.0 | 24 | Free | -0.5 | 1259 | 0.95 | 989 |
| | | | 0.0 | 1321 | 1.00 | |
| | | | 0.5 | 1284 | 0.97 | |
| $f_{y0}=420$ N/mm$^2$ | | $t_0=6.25$ mm | | $b_0=h_0=150$ mm | | $b_1=h_1$ |

Notation:    $N_{1,u}(J_{AA})^*$ means maximum load or load at the intersection point of two tangent lines (the line of the linear elastic part and that of the plastic part of the load vs. indentation curve).

### 9.2.4   The ultimate load capacity

The ultimate load capacity formulae of multiplanar TX-joints excluding the influence of chord bending moments can be built up with the same general formulae as those of XX-joints:

$$N_{1,u}(J_{AA}=0)=c_m \cdot N_{1,u} \tag{8.1}$$

$$N_{1,u}(J_{AA})=f(J_{AA}) \cdot N_{1,u}(J_{AA}=0) \tag{8.2}$$

Where $N_{1,u}$ is the ultimate load capacity of uniplanar T-joints with the influence of chord bending moment excluded, equation (6.1);
$c_m$ is a factor considering the multiplanar geometrical stiffening effects;
$N_{1,u}(J_{AA}=0)$ is the ultimate load capacity of multiplanar TX-joints with a load ratio $J_{AA}=0$;
$N_{1,u}(J_{AA})$ is the ultimate load capacity of multiplanar TX-joints with a load ratio $J_{AA}$;
$f(J_{AA})$ is a function for the multiplanar load effects.

### TX-joints with the out-of-plane braces unloaded

In Section 7.2, it has been concluded that axially loaded T-joints excluding the influence of chord bending moment can be treated as axially loaded X-joints, namely, the same ultimate load capacity formula is used for T- and X-joints. Similarly, the ultimate load capacity of multiplanar TX-joints excluding the influence of chord bending moment can be related to that of XX-joints. In Table 9.3, the results of TX-joints with $J_{AA}=0.0$ are compared with those of the corresponding XX-joints analysed in Chapter 8 (see Table 8.3). It can be seen that the results of TX-joints agree very well with that of XX-joints. Thus, axially loaded TX-joints excluding the influence of chord bending moment can be treated as axially loaded XX-joints. The factor for the multiplanar geometrical effects is defined as equation (8.3):

$$c_m=1+0.4\beta^4 \tag{8.3}$$

Table 9.3    Comparison between the results of axially loaded TX- and XX-joints

| $\beta$ | $2\gamma$ | $J_{AA}$ | $N_{1,u}(J_{AA}=0) / (f_{y0}t_0^2)$ | | (1)/(2) |
|---|---|---|---|---|---|
| | | | TX-joints (1) | XX-joints (2) | |
| 0.4 | 24 | 0.0 | 6.45 (Restr.) 6.33 (Free ) | 6.26 | 1.03 1.01 |
| | 35 | 0.0 | 6.27 (Restr.) 6.17  (Free) | 6.08 | 1.03 1.01 |
| 0.6 | 35 | 0.0 | 10.54 (Free ) | 10.09 | 1.04 |
| 0.8 | 35 | 0.0 | 26.55 (Restr.) 24.79 (Free ) | 25.69 | 1.03 0.96 |

**TX-joints with the out-of-plane braces loaded**

The ultimate load capacity of TX-joints with the out-of-plane braces loaded can be built up according to equation (8.2) which is equal to the function for multiplanar load effect $f(J_{AA})$ multiplied by $N_{1,u}(J_{AA}=0.0)$. Because $N_{1,u}(J_{AA}=0.0)$ is recommended to be the same as for XX-joints, only $f(J_{AA})$ needs to be determined.

The multiplanar load effects from the numerical results of the author and those of Crockett are presented in Tables 9.1 and 9.2.

According to Chapter 8, the function for the multiplanar load effects of XX-joints is:

$$f(J_{AA}) = 1 + 0.37 * J_{AA} \qquad (J_{AA} \leq 0) \tag{8.4}$$

A comparison between equation (8.4) and the results from Tables 9.1 and 9.2 is illustrated in Figure 9.7. It can be seen that for joints with negative load ratios, equation (8.4) is a lower bound for the multiplanar load effects of TX-joints. For joints with positive load ratios, a slightly positive effect is found.
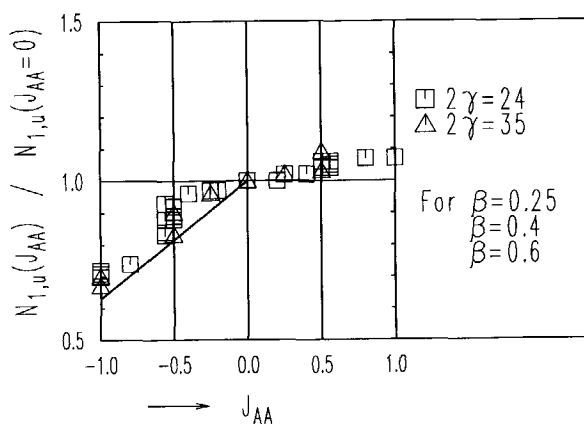


**Figure 9.7  Multiplanar load effects of TX-joints**

Based upon the above observations, it is recommended that equation (8.4) can be used also for TX-joints with $J_{AA} \leq 0.0$. For $J_{AA} \geq 0.0$, $f(J_{AA})=1.0$ is recommended.

For joints with $\beta > 0.6$ and $J_{AA} > 0$, only a few results are available, no formula for the multiplanar load effect is recommended.

## 9.3 UNIPLANAR K- AND MULTIPLANAR KK-JOINTS

Uniplanar K-joints can be found in a Warren truss system and multiplanar KK-joints in a three dimensional triangular truss system. Experimental research (for example by Wardenier 1978) on uniplanar K-joints has shown that different failure modes can exist depending on the joint types, loading conditions and joint geometrical parameters. In the CIDECT design guide (Packer 1992a), different design formulae have been recommended for gap and overlap joints. For RHS K-joints with gap, four design formulae are included which are based upon chord face plastification, chord shear, brace effective width and chord punching shear respectively. Plastic failure of the chord face is the most common failure mode for gap K-joints with small to medium $\beta$ values. Chord shear mechanism is found for gap K-joints with lower chord depth ($h_0 < b_0$) or high $\beta$ values. Brace effective width mechanism is found for gap K-joints with relatively thin walled brace members. For overlap joints, three design formulae depending upon the overlap parameter are included based upon brace effective width failure. As described in Chapter 2, Tables 2.1 and 2.2, the current design formulae for multiplanar KK-joints are equal to that of the corresponding uniplanar K-joints multiplied by a correction factor of 0.9. This recommendation was based upon some initial investigations on multiplanar rectangular hollow section joints (Bauer 1983, 1984, 1985) and Redwood (1983).

Configurations of uniplanar K- and multiplanar KK-joints are shown in Figure 9.8.
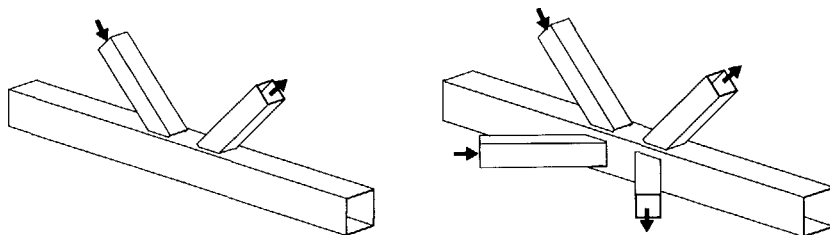


**Figure 9.8   Configurations of K- and KK-joints**

This chapter concentrates on a study of the static behaviour of gap joints with zero or small eccentricities. Following considerations should be taken into account for such joints:

> In design practice, lattice structures can usually be designed assuming pin jointed members. Secondary bending moments can be neglected for static design if the joints and the members of the joints have sufficient rotation capacity. In experimental tests or numerical studies on isolated K- and KK-joints, large secondary bending moments may exist in case of extremely bad boundary conditions (e.g. for a free end compression brace) which should be avoided. In principle, boundary conditions used for isolated K- and KK-joints should reflect the conditions in the girder as close as

possible. The influence of boundary conditions used in the literature is discussed in Section 9.3.1.

-    Plastification of the chord face is the most common failure mode for K-joints with small to medium $\beta$ values. Maximum load capacity of the joints is not reached and joints fail at very large local deformation. The membrane effects for such joints are much larger. An ultimate deformation limit should be used to determine the ultimate load capacity of the joints.

### 9.3.1    Influence of boundary conditions for K-joints

Some representing boundary conditions for isolated uniplanar K-joints used in the existing literature are shown in Figure 9.9. They can be summarised as follows:

-    One chord end restraint: UBC3, UBC4 and UBC5 or two chord ends restraints: UBC1, UBC2 and UBC6.

-    Free ended, pin ended or roll ended braces. Boundary conditions with free ended braces (UBC6) are not recommended because lateral movement of the braces causes very large secondary bending moments which do not reflect the boundary conditions of a K-joint within a frame.

-    Compression chord (UBC1, UBC3, UBC5 and UBC6) or tension chord (UBC2 and UBC4) due to reaction forces at the chord end.

-    Boundary conditions used by Wardenier (1978) for extensive tests on isolated K-joints were similar to UBC5. Later on, four lattice girders (de Koning 1979) were investigated to compare the joint behaviour with that of isolated joints. It was concluded that the load-deformation behaviour of the girder joints was very similar to that observed for similar isolated joints.
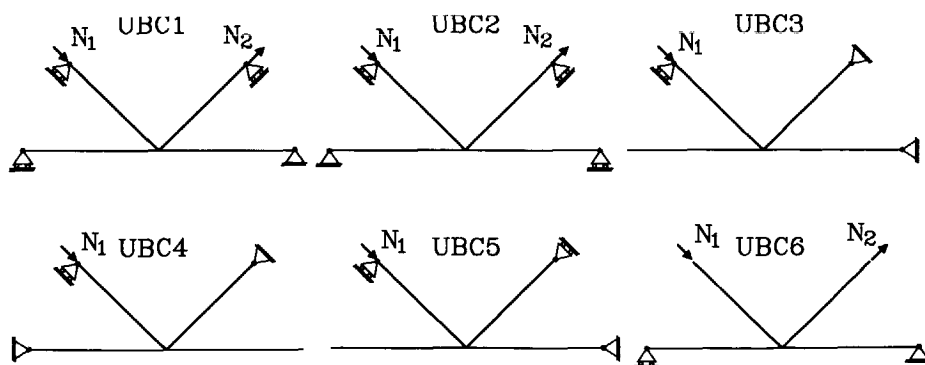


**Figure 9.9    Boundary conditions**

Numerical investigation has been carried out by Liu (1998) in order to study the influence of boundary conditions UBC1 to UBC5 on the static behaviour of uniplanar gap K-joints. This study includes three basic uniplanar K-joints. Each joint analysed five times with boundary conditions UBC1 to UBC5. The joint geometrical and material properties are shown in Figure 9.10 and Table 9.4. The angle of the brace to the chord is 45°. Eight noded thick shell elements are used to model the joints. Fillet welds are included. One material property is used for the chord, the braces and the welds. Both geometrical and material non-linearities are included.
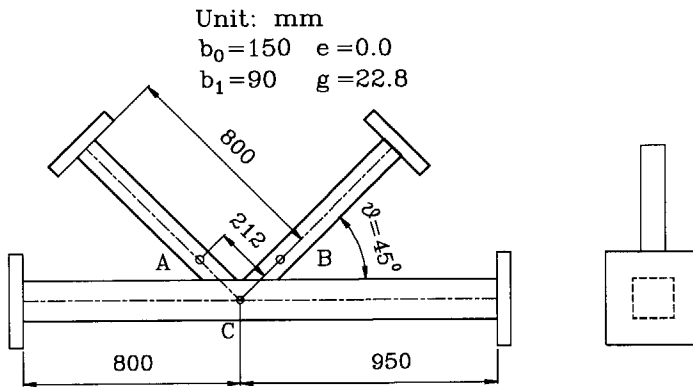


**Figure 9.10  Configuration of joints UBC-15, 25 and 35**

**Table 9.4     Geometrical and material properties**

| Joints | $b_0$ mm | $t_0$ mm | $b_1$ mm | $t_1$ mm | $\beta$ | $2\gamma$ | $f_{y0}$ N/mm$^2$ | $f_{y1}$ N/mm$^2$ |
|--------|----------|----------|----------|----------|---------|-----------|-------------------|-------------------|
| UBC-15 | 150.6 | 9.74 | 89.0 | 8.09 | 0.59 | 15.5 | 355 | 355 |
| UBC-25 | 146.9 | 6.00 | 89.0 | 8.09 | 0.61 | 24.5 | 355 | 355 |
| UBC-35 | 145.1 | 4.20 | 89.0 | 8.09 | 0.61 | 34.5 | 355 | 355 |

**Results of the numerical investigation**

The ultimate load capacity of each joint is determined based upon the ultimate deformation criterion used in this thesis based on the compression brace load versus chord top face indentation. It should be mentioned that the serviceability deformation and the ultimate deformation should be 1%$b_0$/sin($\theta$) and 3%$b_0$/sin($\theta$) respectively for joints with an inclined brace (the relative vertical displacement between point A and C in Figure 9.10) in order to be consistent with those for joints with an orthogonal brace. Comparison of the numerical results of the joints with different boundary conditions with that of the joint with boundary condition UBC5 is given in Table 9.5.

**Table 9.5    Comparison between the numerical results of joints under different BCs**

| Joints | Chord reaction force | $N_{1,u}$ kN | $N_{1,u}/N_{1,u}$(UBC5-15) |
|---|---|---|---|
| UBC1-15 | $C^*$ | 674 | 1.00 |
| UBC2-15 | $T^*$ | 693 | 1.02 |
| UBC3-15 | $C^*$ | 677 | 1.00 |
| UBC4-15 | $T^*$ | 695 | 1.03 |
| UBC5-15 | $C^*$ | 677 | 1.00 |
| Joints | Chord reaction force | $N_{1,u}$ kN | $N_{1,u}/N_{1,u}$(UBC5-25) |
| UBC1-25 | $C^*$ | 307 | 1.00 |
| UBC2-25 | $T^*$ | 338 | 1.10 |
| UBC3-25 | $C^*$ | 308 | 1.00 |
| UBC4-25 | $T^*$ | 338 | 1.10 |
| UBC5-25 | $C^*$ | 307 | 1.00 |
| Joints | Chord reaction force | $N_{1,u}$ kN | $N_{1,u}/N_{1,u}$(UBC5-35) |
| UBC1-35 | $C^*$ | 175 | 1.01 |
| UBC2-35 | $T^*$ | 206 | 1.19 |
| UBC3-35 | $C^*$ | 174 | 1.01 |
| UBC4-35 | $T^*$ | 208 | 1.20 |
| UBC5-35 | $C^*$ | 173 | 1.01 |

Note:  -    UBC1-15 means a joint under boundary condition UBC1 (see Figure 9.9) with 2γ about 15.

  -    "$C^*$" means compression and "$T^*$" means tension.

Following conclusions can be drawn:

-    The boundary conditions used can be divided into two groups: joints with chord in compression (UBC1, 3 and 5) and joints with chord in tension (UBC2 and 4) due to reaction forces. There is hardly any difference between the ultimate load capacities of joints UBC1, 3 and 5. Similarly, the ultimate load capacities of joints UBC2 and 4 are almost the same. Thus, the influence of the boundary conditions is actually due to the sense of the chord reaction force. The reason is that chord compression force reduces the chord membrane action, as a result, the ultimate load capacity is reduced. The influence of the sense of the chord end reaction force on the ultimate load capacity

of the joints depends on the $2\gamma$ values of the joints. For joints with $2\gamma\approx15$, 25 and 35, the influence is 3%, 10% and 20% respectively compared to UBC5. This is logical because for joints with large $2\gamma$ values the membrane effect is largely reduced by the compression reaction force in the chord.

- As long as the lateral movement of the braces is restrained, the difference between the results of one chord end restraint and two chord end restraints can be neglected.

- The results of UBC2 and 4 may be too optimistic for joints with chord end reaction forces in compression. UBC1, 3 or 5 can be used as a basis for further studies of uniplanar K- and multiplanar KK-joints.

### 9.3.2  Multiplanar KK-joints

Information about the static behaviour of multiplanar KK-joints is very limited. The earliest work was done by the Canadians (Bauer 1983 and 1985) and Redwood (1983) to investigate the static behaviour of triangular trusses with tension in the chord. It was concluded that the yield line theory gave a lower bound ultimate load capacity prediction. Furthermore, two tests on multiplanar KK-joints were done by British Steel (1985). Insufficient data was available to develop comprehensive guidelines for such joints. Since then on, no work has been done on multiplanar KK-joints until about the end of the 80's when the ECSC research programme entitled "The Development of Design Methods for the Cost Effective Applications of Multiplanar Connections" was started. As a part of this programme, experimental tests on multiplanar KK-joints have been carried out by British Steel (Yeomans 1993). Calibration of the numerical models for such joints have been done by SCI (O'Connor 1993, SCI 1995).

The specimen configuration of the SCI KK-joints is shown in Figure 9.11. The geometrical and material properties of the joints are outlined in Table 9.6. For multiplanar KK-joints, the chord reaction force is $4*N*cos(\theta)$ if no extra tension forces are applied on the chord end. However, for the corresponding uniplanar K-joints (UBC1, or 3 or 5), the chord reaction force is $2*N*cos(\theta)$. It is known from Section 9.3.1 that the ultimate load capacity of the joints is largely influenced by the chord axial forces. Thus, the ultimate load capacity of multiplanar KK-joints with chord compressive reaction force $4*N*cos(\theta)$ will be much lower than that of their uniplanar counterparts. In order to make the results of multiplanar KK-joints comparable with those of uniplanar K-joints, an additional tension force $2*N*cos(\theta)$ in the multiplanar tests is applied at one end of the chord as shown in Figure 9.11. With the additional tension force, local buckling of the chord is also prevented.
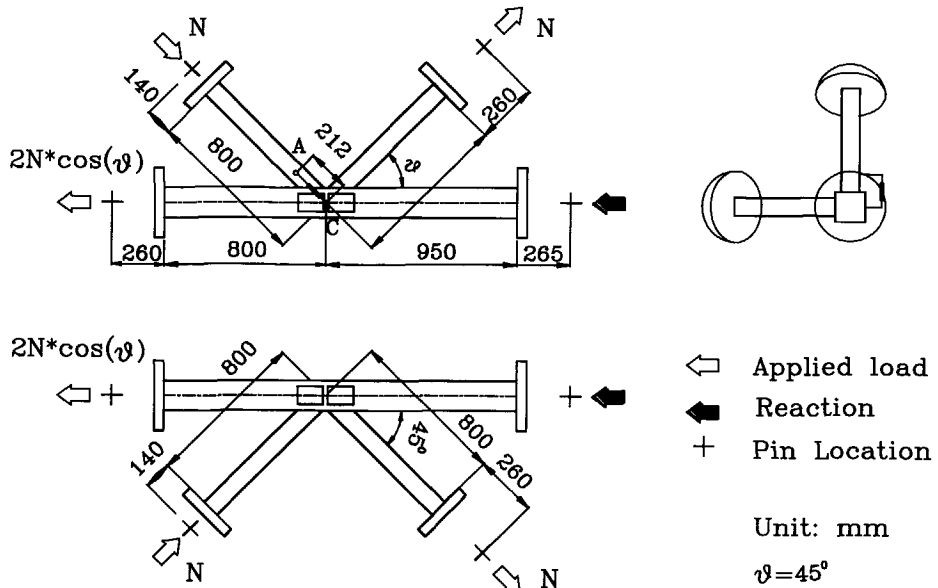
**Figure 9.11    Specimen configuration of KK-joints (SCI 1995)**

**Table 9.6        Measured geometrical and material properties of the test specimen**

| Joints | $b_0$ mm | $t_0$ mm | $g$ mm | $\theta$ | $f_{y0}$ N/mm$^2$ | $\beta$ | $2\gamma$ |
|--------|------|------|-----|------|------|------|------|
| rrkk01 | 149.0 | 4.87 | 65 | 45° | 325 | 0.4 | 30.6 |
| rrkk02 | 149.3 | 6.05 | 65 | 45° | 321 | 0.4 | 24.7 |
| rrkk03 | 151.0 | 9.74 | 65 | 45° | 305 | 0.4 | 15.5 |
| rrkk04 | 149.0 | 4.87 | 30 | 45° | 325 | 0.6 | 30.6 |
| rrkk05 | 149.3 | 6.05 | 30 | 45° | 321 | 0.6 | 24.7 |
| rrkk06 | 151.0 | 9.74 | 30 | 45° | 305 | 0.59 | 15.5 |
| rrkk07 | 149.0 | 4.87 | 13 | 45° | 325 | 1.00 | 30.6 |
| rrkk08 | 149.4 | 6.05 | 13 | 45° | 321 | 1.00 | 24.7 |
| rrkk09 | 150.0 | 9.74 | 13 | 45° | 305 | 1.00 | 15.4 |

The chord face deformation is the change in length of a displacement transducer between two steel offsets attached to the chord center line and to the compression brace center line (the relative displacement between point A and C), see Figure 9.11. The ultimate load capacity of the joints is determined based upon the compressive brace load vs. chord top face indentation

curves. Because no maximum load capacity is reached for the tests, the ultimate deformation criterion has to be used ($3\%b_0/\sin(\theta)$ for an inclined brace). The ultimate load capacity ($N_{u,exp.}$) from the test results is outlined in Table 9.7.

The CIDECT design resistance formula for uniplanar gap K-joints with chord plastification failure is given by:

$$N_{Rd,y} = 8.9\,\beta\gamma^{0.5} \cdot \frac{f_{y0}t_0^2}{\sin(\theta)} \cdot f(n) \qquad (9.1)$$

This design formula was derived from the following ultimate mean test formula (Wardenier 1982a):

$$N_{u,m} = 10.9\,\beta\gamma^{0.5} \cdot \frac{f_{y0}t_0^2}{\sin(\theta)} \cdot f(n) \qquad (9.2)$$

Where f(n) is given as:

$$f(n) = 1.3 - \frac{0.4}{\beta} \frac{N_0}{A_0 f_{y0}} \qquad (9.3)$$

For uniplanar K-joints (UBC1, UBC3 and UBC5 in Figure 9.9) with no extra chord preloading, the chord axial load $N_0$ is equal to the chord reaction force:

$$N_0 = 2 * N_{u,m} \cdot \cos(\theta) \qquad (9.4)$$

Equation (9.4) can also be used for the multiplanar KK-joints shown in Figure 9.11, because extra chord tension loads are applied.

For multiplanar joints with $\beta=1.0$, chord shear failure may occur. Due to the extra tension load in the chord, Figure 9.11, the axial stress in the gap of the chord is zero. Only shear failure needs to be checked. The design resistance of multiplanar joints with chord shear failure is given in the following analytical equation:

$$N_{Rd,sh} = \frac{2\,(h_0 - t_0)\,t_0\,f_{y0}}{\sqrt{3} \cdot \sin(\theta)} \qquad (9.5)$$

According to CIDECT (1992), the design resistance of multiplanar joints is equal to equation (9.1) multiplied by 0.9. A similar method is applied to predict the ultimate mean value of multiplanar joints. In Table 9.7, the predicted design resistance and ultimate mean value for multiplanar joints are compared with the test results.

**Table 9.7** **Comparison between test results and the predicted values**

| Joints | Multiplanar chord face plastification | | Multiplanar shear failure | Exp. results | Comparison | | |
|---|---|---|---|---|---|---|---|
| | $N_{Rd,y}*0.9$ eq.(9.1)*0.9 kN | $N_{u,m}*0.9$ eq.(9.2)*0.9 kN | $N_{Rd,sh}$ eq. (9.5) kN | $N_{u,exp.}$ kN | $\dfrac{N_{u,exp.}}{0.9*N_{Rd,y}}$ | $\dfrac{N_{u,exp.}}{0.9*N_{u,m}}$ | $\dfrac{N_{u,exp.}}{N_{Rd,sh}}$ |
| rrkk01 | 138 | 168 | 375 | 148 | 1.07 | 0.88 | 0.39 |
| rrkk02 | 185 | 226 | 454 | 203 | 1.09 | 0.90 | 0.45 |
| rrkk03 | 333 | 407 | 682 | 392* | 1.18 | 0.96 | 0.57 |
| rrkk04 | 207 | 252 | 375 | 367 | 1.77 | 1.46 | 0.98 |
| rrkk05 | 277 | 338 | 454 | 403* | 1.45 | 1.19 | 0.89 |
| rrkk06 | 494 | 603 | 682 | 673* | 1.36 | 1.12 | 0.99 |
| rrkk07 | 344 | 419 | <u>375</u> | 603* | 1.75 | 1.44 | 1.61 |
| rrkk08 | 460 | 562 | <u>454</u> | 659* | 1.43 | 1.17 | 1.45 |
| rrkk09 | 836 | 1020 | <u>682</u> | 796* | 0.95 | 0.78 | 1.17 |

*:     If the ultimate deformation limit is not reached, the load at the end of the test is taken.

**Comparison with the design resistance**

Table 9.7 shows that for joints rrkk07, rrkk08 and rrkk09 ($\beta$=1.0, $2\gamma$=30.6, 24.7 and 15.4), chord shear failure is critical. For other joints, chord face plastification failure is critical. The ultimate load capacity of the tested results are all higher than the predicted design resistance of multiplanar joints, except for joint rrkk09.

**Comparison with the ultimate mean**

Actually, the ultimate load capacity of the test result should be compared with the predicted ultimate mean value instead of the design resistance. For joints with chord shear failure, no comparison is available for ultimate load capacity due to the lack of formula for such failure mode. For joints with chord plastification failure, test results are compared with the predicted ultimate mean values of KK-joints. For joints rrkk01, rrkk02 and rrkk03 ($\beta$=0.4), the ultimate load capacity of the tested multiplanar joints is lower than that of the predicted ultimate mean value, while for joints rrkk04 to rrkk07, the tested ultimate load capacity is higher than the predicted ultimate load capacity. This means that for joints with lower $\beta$ values ($\beta \leq 0.4$) the factor for the multiplanar load effect is lower than 0.9 while for joints with higher $\beta$ values ($\beta \geq 0.6$), it is higher than 0.9.

It should be mentioned that the above comparison is being made between the prediction equations and experimentally obtained multiplanar tests. The ultimate load capacity obtained from the multiplanar experiments is based upon the ultimate deformation criterion, whereas

the predicted equations are based upon test data which has been analysed based on the "ultimate load capacity" without any deformation limit. Therefore, similar to the study on multiplanar XX- and TX-joints, multiplanar KK-joints need to be analysed based upon the same ultimate criterion, the same geometrical parameters, material properties and boundary conditions as those for uniplanar K-joints before final conclusions can be drawn. Further numerical investigation on multiplanar KK-joints with more geometrical parameters and loading cases is currently undergoing (Liu 1998). The same philosophy as for multiplanar XX- and TX-joints will be used to establish the ultimate load capacity formulae for multiplanar KK-joints.

### 9.3.3   Conclusions

In this section, the influence of the boundary conditions on the ultimate load capacity of uniplanar K-joints is discussed. The ultimate load capacity of the tested KK-joints (SCI 1995) is compared with the design resistance formula and the predicted ultimate mean formula for multiplanar KK-joints. Conclusions can be drawn as follows:

-      In tests or numerical studies on isolated K- and KK-joints, the brace lateral movements should be restrained in order to prevent large secondary bending moments. As long as the lateral movements of the braces are restrained, the influence of the boundary conditions is actually due to the sense of the chord reaction force. If the sense of the chord reaction force is the same, there is no difference between the ultimate load capacities of joints under different boundary conditions. Boundary conditions of UBC1, 3 or 5 are recommended for further numerical parameter study because they give lower values than the tests with chord reaction force in tension.

-      The multiplanar effects of KK-joints depend upon the $\beta$ values and the $2\gamma$ ratios. For joints with small $\beta$ and large $2\gamma$ ratios, the ultimate load capacity of KK-joints may be reduced compared to that of uniplanar K-joints (even larger than 0.9). The ultimate load capacity of multiplanar KK-joints from the experiments is determined based upon the ultimate deformation criterion whereas the predicted ultimate mean formula is based upon the "ultimate load capacity" without any deformation limit. Further study on multiplanar KK-joints is required in order to get more information about the multiplanar effects.

# 10 SUMMARY, CONCLUSIONS AND RECOMMENDATIONS

## 10.1 INTRODUCTION

This PhD study provides new information about the static behaviour of uniplanar and multiplanar connections in rectangular hollow sections. A numerical model which is fully calibrated against the experimental results is developed. This numerical model is further used for a series of extensive parameter studies on uniplanar and multiplanar connections in rectangular hollow sections under different loading conditions. Based upon the numerical studies, the experimental results and the existing and newly developed analytical formulae, design recommendations for the static strength of uniplanar and multiplanar connections in rectangular hollow sections are proposed. Specific conclusions have been drawn for each topic at the end of the appropriate section of the previous chapters. This chapter gives a summary of the main conclusions of the above research work. Furthermore, recommendations for a further study on multiplanar connections in rectangular hollow sections are given.

## 10.2 SUMMARY AND GENERAL CONCLUSIONS

### Experimental work

The experimental research programme consists of uniplanar X-, multiplanar XX-joints, uniplanar T- and multiplanar TX-joints in square hollow sections with a brace to chord width ratio of 0.6 ($\beta$), a chord width to thickness ratio of 24 ($2\gamma$) and a brace to chord thickness ratio of 1.0 ($\tau$), see Table 3.1.

For the uniplanar X- and multiplanar XX-joints, the tests are divided into two groups: the first consists of an axially loaded uniplanar X-joint and three axially loaded multiplanar XX-joints with load ratios between the out-of-plane braces and the in-plane braces of -0,6, 0.0 and 0.6 respectively. The second consists of an uniplanar X-joint loaded with in-plane bending moments and three multiplanar XX-joints loaded with in-plane bending moments on the in-plane braces and axial forces (tension, compression or unloaded) on the out-of-plane braces.

For the uniplanar T- and multiplanar TX-joints, the tests are also divided into two groups: the first consists of an axially loaded uniplanar T-joint and three multiplanar TX-joints with the out-of-plane braces kept horizontal. The second consists of three axially loaded multiplanar TX-joints with the out-of-plane braces free to rotate. The load ratios for multiplanar joints are -0.56, 0.0 and 0.56.

Following conclusions can be drawn:

- For all the experimentally investigated multiplanar joints with $\beta$=0.6, the multiplanar geometrical stiffening effects are minor, except for TX-joints with the out-of-plane braces kept horizontal which results in bending moments on the out-of-plane braces. This conclusion is valid only for multiplanar joints with $\beta$ values smaller than or equal to 0.6. For joints with larger $\beta$ values, higher multiplanar geometrical effects are expected. The reason is that for joints with small to medium $\beta$ values, local

plastification of the chord top face is the governing failure mechanism. While for joints with large $\beta$ values, chord side wall failure occurs.

-   For all the multiplanar joints, the joints loaded with positive load ratios give the highest ultimate load (moment) capacity, while the joints loaded with negative load ratios give the lowest ultimate load (moment) capacity.

-   For axially loaded multiplanar joints, the ultimate load capacity for joints with negative load ratios is considerably reduced.

-   For the multiplanar XX-joint loaded with in-plane bending moments in the in-plane braces and axial compression forces in the out-of-plane braces, the secondary bending moments due to the adjustment of the out-of-plane braces enhance the ultimate moment capacity of the joint.

-   For the first group of axially loaded TX-joints, the out-of-plane braces are kept horizontal during the tests which results in favourable bending moments on the out-of-plane braces. As a result, the ultimate load capacity of the joints is increased. The maximum influence of the adjustment of the out-of-plane braces is 12% for the investigated joints.

## Numerical modelling and calibration

In order to establish a suitable model to simulate the current problem, following aspects have been considered:

-   The choice of the element types.
-   The modelling of the weld and the geometry of the joint as precise as possible.
-   The mesh refinement.
-   The inclusion of material and geometrical non-linearities.

Following conclusions are drawn from the numerical modelling and calibration:

-   Although it is known that solid elements are inadequate to model non-linear behaviour, it has been used, for comparison purposes, to clearly demonstrate the erroneous results. Using solid elements or a combination of solid and shell elements through transition elements to model RHS joints gives, as experienced by using the FE MARC program, an unacceptably high load capacity of the joint compared to the experimental results. The reason is that there are no more than three integration points in each direction of the elements, particularly in the thickness direction. The stress distribution in the elements after yielding can therefore not be described adequately.

-   If the same mesh pattern is used, the numerical results using the 4-noded thick shell elements give higher ultimate loads than those using the 8-noded thin and thick shell elements.

- The weld should be properly included in the numerical model. An 8-noded thick shell element is recommended to model the hollow sections and the welds. For modelling of the fillet weld, an average thickness of the weld can be used, see Figure 4.5. For modelling of the butt weld, the throat thickness of the "fillet" part of the weld has been proved to be suitable.

- For models with $2\gamma$ value higher than 24, an 8-noded thin shell element can give adequately accurate solutions and can be used as an alternative model, in order to save computing time and disc working space if the model is very large (with large number of nodes). Theoretically speaking, an 8-noded thick shell element is more accurate than an 8-noded thin shell element because the transverse shear strain of the element is considered. The recommended numerical model is calibrated for accuracy against the experimental results. This makes it possible to carry out an extensive numerical parameter study.

**Analytical study**

The existing design formula for chord side wall failure of axially loaded full width X-joints ($\beta=1.0$) is very conservative especially for joints with high chord width to thickness ratios. Based upon a so-called "4-hinge yield line and chord web crippling" model (see Figures 5.5, 5.7 and 5.9), a set of new formulae is developed for full width X-joints loaded with axial forces, in-plane and out-of-plane bending moments respectively. This model is also compared with the model including the membrane action in Appendix V. It is found that the membrane effect can be neglected for axially loaded full width X-joints. The membrane effect for full width X-joints loaded with out-of-plane bending moments is also very small, similar to that for axially loaded full width X-joints. For full width X-joints loaded with in-plane bending moments, the membrane effect is larger than that for axially loaded joints which is, however, for simplicity, not taken into account in the recommended formula. The new formulae agree well with the numerical results especially for full width X-joints loaded with axial forces or out-of-plane bending moments.

Based upon a yield line model, the influence of the in-plane bending moments and axial forces in the chord on the ultimate load capacity of the joint is studied analytically. It is concluded that the reduction of the joint ultimate load capacity is caused by the reduction of the plastic moment of the yield lines when a yield line is not parallel to the axial stresses. Furthermore, the compressive axial stresses in the chord reduce the membrane effect of the chord faces, and as a result, the ultimate load capacity of the joint is reduced.

For full width T-joints subjected to an out-of-plane bending moment, failure of the joints is dominated by distortion of the chord section. This failure mechanism is not included in the CIDECT design guide, which is unsafe. Generally, the ultimate moment capacity of full width T-joints loaded with an out-of-plane bending moment is lower than that of the corresponding X-joint if no diaphragm stiffening for the chord is used. In this analytical study, a yield line model given by Niemi is used. Other analytical formulae used in this study are taken from the existing literature.

**Parameter study and analysis**

The recommended numerical model which is adequately calibrated against the experimental results is used for an extensive numerical parameter study. This study includes both uniplanar and multiplanar joints in RHS with different joint configurations and loading cases. For each type of joint and load case, ultimate load (moment) capacity formulae are derived based upon a combination of the numerical results and the analytical studies. For a specific joint type and load case, details can be found in Chapters 6 to 9. General aspects about the numerical parameter study can be found in Chapter 4.

General remarks about the numerical parameter study:

-       The numerical parameter study covers chord face plastification and chord side wall failure. Because cracking is not modelled at this moment, brace effective width and chord punching shear failure are not included in the numerical study. For design, brace effective width failure and chord punching shear failure should be also checked.

-       Because the load-indentation curves are very important in reflecting the joint behaviour, all the numerical results are presented in figures in this thesis. These figures may give very helpful information to future researchers in evaluating the databases. Except for joints with maximum load (moment), there is no internationally uniform definition to describe the ultimate strength of joints which makes it very difficult to compare the results from different researchers if the load-indentation curves are not available. The load-indentation curves are also necessary to give the initial stiffness of joints as well as stiffness at other load levels as information for future researchers.

-       In this thesis, the ultimate load (moment) capacity of the joints is defined as the maximum load (moment) if the deformation at the maximum load (moment) is smaller than the "ultimate" deformation limit, or is defined as the load (moment) at an "ultimate" deformation limit if no maximum load is reached, see Chapter 4. The ultimate strength determined based upon this criterion is used for further regression analyses in combination with the analytical studies. As a result, ultimate strength formulae are developed.

-       The ultimate strength formulae developed in this thesis generally have a very low coefficient of variation and a very high correlation coefficient compared to the numerical results. The mean normalised error between the numerical results and the recommended formulae is close to 1.0.


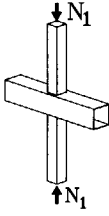**10.3    PROPOSED ULTIMATE STRENGTH FORMULAE**

In the Limit States Design, the design load should not exceed the design strength. The ultimate strength formulae have to be statistically analysed to give the design strength. There are two approaches to obtain the design strength:

1) Using the procedure in Annex Z of EC3 (1993a) to determine the design strength from a given ultimate strength function (ultimate load or moment capacity formula).

2) If the partial safety factor of the joint is known beforehand, the design strength is equal to the characteristic strength divided by the partial safety factor $\gamma_M$ of the joints (Wardenier 1982a).

In Annex Z of EC3 (1993a), a procedure is given in determination of the partial safety factor $\gamma_M$. Nevertheless, the method of Wardenier (1982a) is a very practical way to determine the $\gamma_M$ factor. In his methods, the $\gamma_M$ factor depends on the mode of failure and the way in which the ultimate strength functions are determined. He proposed that if the strength function is based on a lower bound analytical model (e.g. yield line) and justified by tests which show sufficient ductility, a $\gamma_M$=1.0 can be chosen. If the ultimate strength is derived from the ultimate load capacity based on experimental evidence, then due to the greater uncertainties and no additional reserve a $\gamma_M \geq 1.0$ should be taken into account. The value also depends on the deformation capacity of the joint. For example, for ductile joints a $\gamma_M$=1.0 to 1.1 and for less ductile joints $\gamma_M$=1.25 can be adopted. Based upon these considerations, different partial safety factors were recommended for each type of joint and failure mode (Wardenier 1982a).

The results of the research work for each type of joint and load case are presented in ultimate strength formulae and summarised in Tables 10.1 to 10.13.

**Table 10.1    Axially loaded uniplanar X-joints**

|  | **Ultimate load capacity formulae** | **Validity** |
|---|---|---|
| Chord top face plastification | $N_{1,u} = \dfrac{2f_{y0}t_0^2}{1-\beta} \cdot (\eta + 2\sqrt{1-\beta}) \cdot f(\beta,\eta)$    (6.1) <br><br> $f(\beta,\eta) = 0.7 + 0.6\beta + 0.1\eta$    (6.2) | $0.2 \leq \beta \leq 0.85$ <br><br> $15 \leq 2\gamma \leq 35$ <br><br> $0.5\beta \leq \eta \leq 2.0\beta$ |
| Chord side wall failure | $N_{1,u} = 4\kappa\,(\sqrt{\gamma} + \gamma\eta) \cdot f_{y0}t_0^2$    (5.20) <br><br> $\kappa$:   according to EC3 curve-a, using a column slenderness ratio of $1.732*(h_0/t_0-2)$, see also equation (5.13) to (5.17). | $\beta = 1.0$ <br><br> $15 \leq 2\gamma \leq 35$ <br><br> $0.5\beta \leq \eta \leq 2.0\beta$ |
| | Linear interpolation between equations (6.1) and (5.20) + note 2. | $0.85 < \beta < 1.0$ |

Note: 1.    For statistical values see Table 6.5 for equations (6.1) and (6.2) and Table 6.6 for equation (5.20).

      2.    Brace effective width and chord punching shear failures should be checked ~~separately using the CIDECT design guide formulae.~~

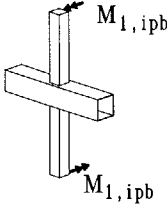$$\kappa = 1/(\phi + \sqrt{\phi^2 + \overline{\lambda}^2}\,) \qquad (5.13)$$

$$\phi = 0.5[1 + 0.21(\overline{\lambda} - 0.2) + \overline{\lambda}^2] \qquad (5.14)$$

$$\overline{\lambda} = \frac{\lambda}{\lambda_E} \qquad (5.15)$$
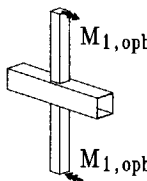
$$\lambda_E = \pi\sqrt{E/f_{y0}} \qquad (5.16)$$

$$\lambda = \sqrt{3}\,(h_0/t_0 - 2) \qquad (5.17)$$

**Table 10.2    Uniplanar X-joints loaded with in-plane bending moments**

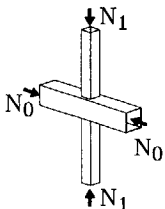|  $M_{1,ipb}$ ... $M_{1,ipb}$ | **Ultimate moment capacity formulae** | **Validity** |
|---|---|---|
| Chord top face plastification | $M_{1,ipb,u} = (\dfrac{2}{\sqrt{1-\beta}} + \dfrac{\eta}{1-\beta} + \dfrac{1}{2\eta}) \, f_{y0}t_0^2 \, h_1 \cdot f(\beta,\eta)$   (6.3) <br><br> $f(\beta,\eta) = 1 + 0.6\beta - 0.25\eta$   (6.4) | $0.2 \le \beta \le 0.85$ <br><br> $15 \le 2\gamma \le 35$ <br><br> $0.5\beta \le \eta \le 2.0\beta$ |
| Chord side wall failure | $M_{1,ipb,u} = \kappa(2\sqrt{\gamma} + \gamma\eta + \dfrac{1}{2\eta}) f_{y0}t_0^2 h_1$   (5.32) <br><br> Where <br><br> $\kappa = \begin{cases} 1 & (\eta \le 1.0) \\[2mm] \dfrac{1}{\phi + \sqrt{\phi^2 + \overline{\lambda}^2}} & (\eta = 2.0) \\[4mm] 1 + (\eta - 1)(\dfrac{1}{\phi + \sqrt{\phi^2 + \overline{\lambda}^2}} - 1) & (1.0 < \eta < 2.0) \end{cases}$   (6.5) <br><br> $\phi, \overline{\lambda}$: see note Table 10.1 | $\beta = 1.0$ <br><br> $15 \le 2\gamma \le 35$ <br><br> $0.5\beta \le \eta \le 2.0\beta$ |
| | Interpolation between equations (6.3) and (5.32) + note 2. | $0.85 < \beta < 1.0$ <br><br> $15 \le 2\gamma \le 35$ <br><br> $0.5\beta \le \eta \le 2\beta$ |

Note:  1.    For statistical values, see Table 6.10 for equations (6.3) and (6.4); Table 6.11 for equation (5.32).

2.    Brace effective width and chord punching shear failures should be checked separately using the CIDECT design guide formulae.

**Table 10.3    Uniplanar X-joints loaded with out-of-plane bending moments**

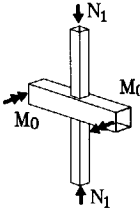| | Ultimate moment capacity formulae | Validity |
|---|---|---|
| $M_{1,opb}$ $M_{1,opb}$ | | |
| Chord face yielding | $M_{1,opb,u} = f_{y0}t_0^2 b_1 \left( \dfrac{\eta(1+\beta)}{2\beta(1-\beta)} + \sqrt{\dfrac{2(1+\beta)}{\beta(1-\beta)}} \; \right) \cdot f(\beta,\eta)$  (6.6)  $f(\beta,\eta) = 1 + 0.5\beta$  (6.7) | $0.2 \leq \beta \leq 0.85$  $15 \leq 2\gamma \leq 35$  $0.5\beta \leq \eta \leq 2.0\beta$ |
| Chord side wall failure | $M_{1,ipb,u} = \kappa \cdot (\sqrt{2(1+2\gamma)} + 2\gamma\eta) \cdot f_{y0}t_0^2 b_1$  (5.44)  $\kappa$:     see Table 10.1 | $\beta = 1.0$  $15 \leq 2\gamma \leq 35$  $0.5\beta \leq \eta \leq 2.0\beta$ |
| | Interpolation between equations (6.6) and (5.44) + note 2 | $0.85 < \beta < 1.0$  $15 \leq 2\gamma \leq 35$  $0.5\beta \leq \eta \leq 2\beta$ |

Note:  1.    For statistical values see Table 6.15 for equations (6.6) and (6.7); Table 6.16 for equation (5.44).
 2.    Brace effective width and chord punching shear failures should be checked separately using the CIDECT design guide formulae.

**Table 10.4**    **Influence of the chord axial preloading**

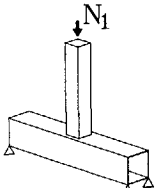| | Reduction function due to chord preloading | Validity |
|---|---|---|
| $N_0$ $N_1$ $N_0$ $N_1$ | | |
| | $$f(n) = \left(1 - n^{\frac{2}{(1+0.004\gamma^2)(1-0.85\beta^3)}}\right)^{0.4} \quad (6.12)$$ $$n = \frac{N_0}{N_{0,Rd}} = \frac{N_0}{A_0 f_{y0}} \quad (6.10)$$ | $0.2 \leq \beta \leq 1.0$ $15 \leq 2\gamma \leq 35$ $\beta = \eta$ $f_{y0} \leq 355 \ N/mm^2$ |

Note: 1.    For statistical values see Table 6.19 in Section 6.4 of Chapter 6.

      2.    The ultimate load capacity of the joint is equal to the ultimate load capacity formula of the corresponding joint with $N_0 = 0.0$, equation (6.1) in Table 10.1, multiplied by this reduction function $f(n)$.

**Table 10.5**     **Influence of the chord bending moment**

| | Reduction function due to chord bending | Validity |
|---|---|---|
| Based upon section classes of EC3 | $$f(J_m) = \left(1 - J_m^{\frac{1}{1-0.85\beta^{1.6}}}\right)^{\frac{1}{3}} \qquad (6.17)$$  $$J_m = \begin{cases} M_0/M_{pl,Rd} & \text{(class 1 or 2)} \quad (5.47) \\ M_0/M_{el,Rd} & \text{(class 3)} \end{cases}$$ | $0.2 \leq \beta \leq 1.0$ |
| Based upon the plastic moment capacity only | $$f(J_m) = \left(1 - (\frac{M_0}{M_{pl,Rd}})^{\frac{2}{(1+0.004\gamma^2)(1-0.85\beta^3)}}\right)^{0.4} \qquad (6.19)$$ | $15 \leq 2\gamma \leq 35$  $\beta = \eta$  $f_{y0} \leq 355$  $(N/mm^2)$ |
| Based upon the elastic moment capacity only | $$f(J_m) = 1 - 0.23(1-0.85\beta)\sqrt{\gamma}\left(\frac{M_0}{M_{el,Rd}}\right)^2 \qquad (6.21)$$ | |

Note:   1.     For statistical values see Tables 6.23, 6.26 and 6.27 for equations (6.17), (6.19) and (6.21) respectively.

       2.     The ultimate load capacity of the joint is equal to the ultimate load capacity formula of the corresponding joint with $M_0 = 0.0$, equation (6.1) in Table 10.1, multiplied by this reduction function $f(J_m)$.

**Table 10.6    Reduction function for T-joints due to chord bending**

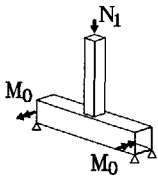|  | **Reduction function due to chord bending** | **Validity** |
|---|---|---|
| Based upon section classes of EC3 | $$f(J_m) = \left(1 - (J_m)^{\frac{1}{1-0.85\beta^{1.6}}}\right)^{\frac{1}{3}} \qquad (6.17)$$ $$J_m = \begin{cases} M_0/M_{v,Rd} & \text{(class 1 or 2)} \\ M_0/M_{v,e,Rd} & \text{(class 3)} \end{cases} \qquad (7.28)$$ | $0.2 \leq \beta \leq 1.0$ |
| Based upon the plastic moment capacity only | $$f(J_m) = \left(1 - (\frac{M_0}{M_{V,Rd}})^{\frac{2}{(1+0.004\gamma^2)(1-0.85\beta^3)}}\right)^{0.4} \qquad (7.30)$$ | $15 \leq 2\gamma \leq 35$ $\beta = \eta$ $f_{y0} \leq 355$ $(N/mm^2)$ |
| Based upon the elastic moment capacity only | $$f(J_m) = 1 - 0.23(1 - 0.85\beta)\sqrt{\gamma}\,(\frac{M_0}{M_{V,e,Rd}})^2 \qquad (7.31)$$ | |
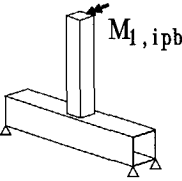
Note: 1.    For statistical values see Tables 6.23, 6.26 and 6.27 for equations (6.17), (7.30) and (7.31) respectively.

2.    The ultimate load capacity of the joint is equal to the ultimate load capacity formula of the corresponding X-joint with $M_0 = 0.0$, equation (6.1) in Table 10.1, multiplied by this reduction function $f(J_m)$.

3.    $M_0$: chord bending moment at the intersection of the brace: $N_1*(l_0-b_1)/4$.

4.    $M_{V,Rd}$: plastic moment resistance reduced by shear, eq. (7.9) or (7.15).

5.    $M_{V,e,Rd}$: elastic moment resistance reduced by shear, eq. (7.21) or (7.25).

**Table 10.7    Axially loaded uniplanar T-joints excluding chord bending moments**

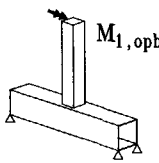| | Ultimate load capacity formulae | Validity |
|---|---|---|
|  | | |
| Chord top face plastification | $N_{1,u} = \dfrac{2f_{y0}t_0^2}{1-\beta}(\eta + 2\sqrt{1-\beta}) \cdot f(\beta,\eta)$  (6.1)<br><br>$f(\beta,\eta) = 0.7 + 0.6\beta + 0.1\eta$  (6.2) | $0.2 \leq \beta \leq 0.85$<br><br>$15 \leq 2\gamma \leq 35$<br><br>$0.5\beta \leq \eta \leq 2.0\beta$ |
| Chord side wall failure | $N_{1,u} = 4\kappa (\sqrt{\gamma} + \gamma\eta) f_{y0}t_0^2$  (5.20)<br><br>$\kappa$: see Table 10.1 | $\beta = 1.0$<br><br>$15 \leq 2\gamma \leq 35$<br><br>$0.5\beta \leq \eta \leq 2.0\beta$ |
| | Linear interpolation between equations (6.1) and (5.20) + note 2. | $0.85 < \beta < 1$ |

Note:  1.    For statistical values see Table 6.5 for equations (6.1) and (6.2) and Table 6.6 for equation (5.20).

2.    Brace effective width and chord punching shear failures should be checked separately using the CIDECT design guide formulae.

3.    $M_0$: moment to compensate the moment in the chord due to $N_1$, see note 3 Table 10.6.

**Table 10.8     Uniplanar T-joints loaded with in-plane bending moments**

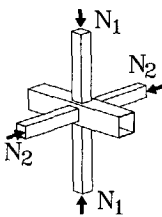|  | Ultimate moment capacity formulae | Validity |
|---|---|---|
| Chord top face plastification | $M_{1,ipb,u} = (\dfrac{2}{\sqrt{1-\beta}} + \dfrac{\eta}{1-\beta} + \dfrac{1}{2\eta})f_{y0}t_0^2 h_1 \cdot f(\beta,\eta)$  (6.3) <br><br> $f(\beta,\eta) = 1 + 0.6\beta - 0.25\eta$  (6.4) | $0.2 \leq \beta \leq 0.85$ <br><br> $15 \leq 2\gamma \leq 35$ <br><br> $0.5\beta \leq \eta \leq 2\beta$ |
| Chord side wall failure | $M_{1,ipb,u} = \kappa\,(2\sqrt{\gamma} + \gamma\eta + \dfrac{1}{2\eta})\,f_{y0}t_0^2 h_1$  (5.32) <br><br> Where <br><br> $\kappa$:    see Table 10.2 | $\beta = 1.0$ <br><br> $15 \leq 2\gamma \leq 35$ <br><br> $0.5\beta \leq \eta \leq 2\beta$ |
| | Linear interpolation between equations (6.3) and (5.32) + note 2. | $0.85 < \beta < 1.0$ <br><br> $15 \leq 2\gamma \leq 35$ <br><br> $0.5\beta \leq \eta \leq 2\beta$ |

Note:  1.   For statistical values, see Table 6.10 for equations (6.3) and (6.4); Table 6.11 for equation (5.32).

2.   Brace effective width and chord punching shear failures should be checked separately using the CIDECT design guide formulae.

**Table 10.9    Uniplanar T-joints loaded with out-of-plane bending moment**

| $M_{1,opb}$ | The ultimate moment capacity | Validity |
|---|---|---|
| Chord top face plastification | $M_{1,opb,u} = f_{y0}t_0^2 b_1 \left( \dfrac{\eta(1+\beta)}{2\beta(1-\beta)} + \sqrt{\dfrac{2(1+\beta)}{\beta(1-\beta)}} \right) \cdot f(\beta,\eta) \quad (6.6)$   $f(\beta,\eta) = 1 + 0.5\beta \qquad (6.7)$ | $\beta \leq 0.85$   $15 \leq 2\gamma \leq 35$   $0.5\beta \leq \eta \leq 2\beta$ |
| Chord distortion failure | $M_{1,opb,u} = 2f_{y0}t_0^2 b_0 \cdot (2\sqrt{\gamma}+1) \cdot f(\alpha) \qquad (7.48)$   where   $f(\alpha) = \left(\dfrac{\alpha_x}{\alpha}\right)^{0.03\gamma} \geq 1.0 \qquad (7.49)$   $\alpha_x = 2*(2\sqrt{\gamma}+1) \qquad (7.47)$ | $\beta = 1.0$   $15 \leq 2\gamma \leq 35$   $\beta = \eta$   $h_0 = b_0$ |

Note:   1.    For statistical values, see Tables 7.14 and 7.15 for equation (7.48).

2.    Brace effective width and punching shear failures should be checked separately using the CIDECT design guide formulae.
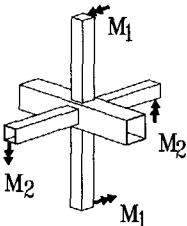
**Table 10.10   Axially loaded multiplanar XX-joints**

| | Multiplanar XX-joints | Validity |
|---|---|---|
| $\begin{array}{c}\downarrow N_1 \\ N_2 \\ N_2 \\ \uparrow N_1\end{array}$ | | |
| General formulae | $N_{1,u}(J_{AA}=0) = c_m \cdot N_{1,u}$ (8.1) <br><br> $N_{1,u}(J_{AA}) = f(J_{AA}) \cdot N_{1,u}(J_{AA}=0)$ (8.2) <br><br> where, $J_{AA} = N_2 / N_1$ | |
| Multiplanar geometrical stiffening factor | $c_m = 1 + 0.4\beta^4$ (8.3) | $0.2 \leq \beta \leq 1.0$ <br><br> $15 \leq 2\gamma \leq 35$ |
| Multiplanar load function | $f(J_{AA}) = 1 + 0.37 J_{AA}$ $\quad (J_{AA} \leq 0)$ (8.4) <br><br> $f(J_{AA}) = 1 + (0.03 + \frac{2}{\gamma}\beta + 0.3\beta^2)J_{AA}$ $\quad (J_{AA} \geq 0)$ (8.5) | $0.2 \leq \beta \leq 0.85$ <br><br> $15 \leq 2\gamma \leq 35$ |
| | $f(J_{AA}) = 1 - \frac{3}{\gamma}J_{AA}^2$ $\quad (-1.0 \leq J_{AA} \leq 1.0)$ (8.6) | $\beta = 1.0$ <br><br> $15 \leq 2\gamma \leq 35$ |
| | Linear interpolation between equations (8.4) and (8.6) or (8.5) and (8.6). | $0.85 < \beta < 1.0$ |

Note: 1.   $N_{1,u}$ is the ultimate load capacity of uniplanar X-joints, see equation (6.1) in Table 10.1.
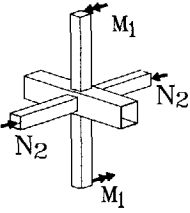
2.   For the statistical values of equations (8.4) and (8.5), see Tables 8.5 and 8.6.

**Table 10.11   Multiplanar XX-joints loaded with in-plane bending moments**

|  | Multiplanar XX-joints | Validity |
|---|---|---|
| General formulae | $M_{1,ipb,u}(J_{II}=0) = c_m \cdot M_{1,ipb,u}$     (8.12) <br><br> $M_{1,ipb,u}(J_{II}) = f(J_{II}) \cdot M_{1,ipb,u}(J_{II}=0)$     (8.13) <br><br> where, $J_{II} = M_2 / M_1$ | |
| Multiplanar geometrical stiffening factor | $c_m = 1 + 0.4\beta^8$     (8.14) | $0.2 \leq \beta \leq 1.0$ <br><br> $15 \leq 2\gamma \leq 35$ |
| Multiplanar load function | $f(J_{II}) = 1 + 0.53\,\beta\,J_{II}$    $(J_{II} \leq 0)$    (8.15) <br> $f(J_{II}) = 1.0$    $(J_{II} \geq 0)$    (8.16) | $0.2 \leq \beta \leq 0.85$ <br><br> $15 \leq 2\gamma \leq 35$ |
| | $f(J_{II}) = 1 + 0.08\,J_{II} - 0.18\,J_{II}^2$    $(-1.0 \leq J_{II} \leq 1.0)$   (8.17) | $\beta = 1.0$ <br><br> $15 \leq 2\gamma \leq 35$ |
| | Linear interpolation between equations (8.15) and (8.17) or (8.16) and (8.17). | $0.85 < \beta < 1.0$ |

Note: 1.   $M_{1,ipb,u}$ is the ultimate moment capacity of uniplanar X-joints, see equation (6.3) in Table 10.2;

      2.   For the statistical values of the above equations, see Section 8.2, Chapter 8.

**Table 10.12   Multiplanar XX-joints loaded with in-plane bending moments and axial forces**

|  | Multiplanar XX-joints | Validity |
|---|---|---|
| General formulae | $M_{1,ipb,u}(J_{IA}{=}0) = c_m \cdot M_{1,ipb,u}$   (8.18)<br><br>$M_{1,ipb,u}(J_{IA}) = f(J_{IA}) \cdot M_{1,ipb,u}(J_{IA}{=}0)$   (8.19)<br><br>where, $J_{IA} = N_2{*}h_1 / M_1$ | |
| Multiplanar geometrical stiffening factor | $c_m = 1 + 0.4\beta^8$   (8.14) | $0.2 \leq \beta \leq 1.0$<br><br>$15 \leq 2\gamma \leq 35$ |
| Multiplanar load function | $f(J_{IA}) = 1 + 0.43(1-\beta)J_{IA}$     $(J_{IA} \leq 0)$   (8.20)<br><br>$f(J_{IA}) = 1$     $(J_{IA} \geq 0)$   (8.21) | $0.2 \leq \beta \leq 1.0$<br><br>$15 \leq 2\gamma \leq 35$ |

Note:  1.  $M_{1,ipb,u}$ is the ultimate moment capacity of uniplanar X-joints, see equation (6.3) in Table 10.2;

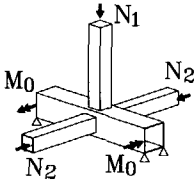2.  For the statistical values of equation (8.20), see Table 8.16, Chapter 8.

**Table 10.13  Axially loaded multiplanar TX-joints excluding chord bending moments**

|  | Multiplanar TX-joints | Validity |
|---|---|---|
| General formulae | $N_{1,u}(J_{AA}=0)=c_m \cdot N_{1,u}$         (8.1) <br><br> $N_{1,u}(J_{AA})=f(J_{AA}) \cdot N_{1,u}(J_{AA}=0)$   (8.2) <br><br> where, $J_{AA}=N_2/N_1$ | |
| Multiplanar geometrical stiffening factor | $c_m=1+0.4\beta^4$            (8.3) | $0.2 \le \beta \le 1.0$ <br><br> $15 \le 2\gamma \le 35$ |
| Multiplanar load function | $f(J_{AA})=1+0.37J_{AA}$      $(J_{AA} \le 0)$   (8.4) <br><br> $f(J_{AA})=1.0$                 $(J_{AA} \ge 0)$ | $\beta \le 0.6$ |
| | Only a few results are available, no formula for the multiplanar load effect is recommended. | $\beta > 0.6$ and <br><br> $J_{AA} > 0.0$ |

Notation:      1.     $N_{1,u}$ is the ultimate load capacity of uniplanar X-joints or T-joints excluding chord bending, see equation (6.1) in Table 10.1.

                 2.     $M_0$ is the moment to compensate the moment in the chord due to $N_1$: $N_1*(l_0-h_1)/4$.

## 10.4   RECOMMENDATIONS FOR FURTHER RESEARCH WORK

-   Further study is required on axially loaded or moment loaded multiplanar TX- and KK-joints in rectangular hollow sections.

-   Some investigations on the static behaviour of multiplanar KK-joints are under way which include the study on the influence of the boundary conditions, the influence of the chord preloading and the multiplanar effects (Liu 1998a and 1998b). However, after this, parameter studies are necessary to complete the evidence and to set up design recommendations.

-   The ultimate strength formulae developed should be considered as basic formulae which need further simplifications for design rules.

-   The establishment of an international database (similar to that for joints in circular hollow sections, Makino 1996) including experimental and numerical results of multiplanar connections in rectangular hollow sections is required in order to further evaluate proposals for new ultimate strength formulae for multiplanar connections in a proper manner.

# 11 REFERENCES

**Some relevant literature before 1982**

Barentse J. (1976)
"Onderzoek naar de statische sterkte van T-verbindingen samengesteld uit buisprofielen en belast door centrische drukkrachten" (in Dutch), Stevin II report no. 6-77-7, Delft University of Technology, The Netherlands.

Davies G. and Roper C.G. (1975)
"Gap Joints with Tubular Members, A Yield Line Approach", Building Science, Vol. 10, 1975.

Davies G. and Roper C.G. (1977)
"Gap Joints with Tubes - A Yield Line Modified by Shear Approach", Building and Environment, Vol. 12, 1977.

Eastwood W. and Wood A.A. (1970a)
"Welded Joints in Tubular Structures Involving Rectangular Sections, Conference on Joints in Structures, Session A Paper 2, University of Sheffield, U.K., 1970.

Eastwood W. and Wood A.A. (1970b)
"Recent Research on Joints in Tubular Structures", Canadian Structural Engineering Conference, Toronto, Canada, 1970.

Eastwood W. and Wood A.A. (1971)
"The Static Strength of Welded Joints in Structural Hollow Sections", Construction Steelwork, U.K, 1971.

Edwards M and Giddings T.W. (1974)
"The Behaviour of Welded joints in Complete Lattice Girders with RHS Chords", CIDECT report 74-3-E.

Johansen K.W. (1962)
"Yield Line Theory", Cement and Concrete Association, London, 1962.

Kato B. and Nishiyama G. (1981)
"The Static Strength of RR-Joints with Large b/B Ratio", IIW Doc. XV-459-80.

Koning C.H.M. de and Wardenier J. (1976)
"Supplement Test Results of Welded Joints in Structural Hollow Sections with Rectangular Boom", Stevin Report no. 6-76-5, Faculty of Civil Engineering, Delft University of Technology, The Netherlands.

Koning C.H.M de and Wardenier J. (1979)
"Tests on Welded Joints in Complete Girders Made of Square Hollow Sections", Stevin report 6-79-4. Faculty of Civil Engineering, Delft University of Technology,

The Netherlands.

Mouty J. (1978)
        "Behaviour of Welded Joints of Square and Rectangular Tubular Structures - a
        Theoretical Approach Based on the Method of Yield Lines", IIW Doc. XV-426-78.

Redwood R.G. (1965)
        "The Behaviour of Joints Between Rectangular Hollow Structural Members". Civil
        Engineering and Public Works Review, Vol. 60, No. 711, 1965. pp. 1463-1469.

Roberts T.M. and Rockey K.C. (1979)
        "A Mechanism Solution for Predicting the Collapse Loads of Slender Plate Girders
        When Subjected to In-Plane Patch Loading", Proceedings of Institution of Civil
        Engineers, Part 2, 1979, pp. 155-175.

Packer J.A. (1978)
        "Theoretical Behaviour and Analysis of Welded Steel Joints with RHS Chord Sections.
        PhD thesis, University of Nottingham, UK.

Stewarts and Lloyds (1965)
        "The Local Crushing Strength of RHS Conjunctions", Report C/E.64/65.1, August
        1965.

Terrington J.S. (1970)
        "Combined Bending and Torsion of Beams and Girders; The Calculation of Stresses
        in Beams and Girders due to Simultaneous transverse Bending", Publication British
        Constructional Steelwork Association.

Wardenier J. and Koning C.H.M. de (1974)
        "Ultimate Strength of Welded Lattice Girder Joints in Structural Hollow Sections",
        - influence prestressing,
        - scale effects,
        - influence of cold formed - hot formed RHS,
        Stevin II report no. 6-74-8, Delft University of Technology, The Netherlands.

Wardenier J. and Koning C.H.M. de (1976)
        "Investigation into the Static Strength of Welded Lattice Girder Joints in Structural
        Hollow Sections". Part 1: Rectangular hollow sections.
        Stevin II report no. 6-76-4, Delft University of Technology, The Netherlands.

Wardenier J. and Stark J.W.B. (1978)
        "The Static Strength of Lattice Girder Joints", Stevin report 6-78-4. Faculty of Civil
        Engineering, Delft University of Technology, The Netherlands.

Wardenier J. (1982a)
        "Hollow Section Joints", Delft University Press, The Netherlands.

Wardenier J., Stolle P. and Dool P.W. (1982b)
"The Strength and Behaviour of Plate to I-Chord Connections", Stevin Report No. 6-82-6, Department of Civil Engineering, Delft University of Technology, The Netherlands.

Yura J.A. (1981)
"Ultimate Capacity of Circular Tubular Joints"
Journal of the Structural Division, Proceedings of the American Society of Civil Engineers. ASCE, Vol. 107, No. ST10, October, 1981, pp. 1965-1984.

Zoetemeijer P. (1982)
"A Limit State Design Method for Stiffened Columns and Flush End-Plates" (in Dutch), Stevin Report No. 6-82-4, Department of Civil Engineering, Delft University of Technology, the Netherlands.


**Literature after 1982**

Bakker, M., C., M. (1992)
"Web Crippling of Cold-Formed Steel Members", PhD thesis, Eindhoven, The Netherlands.

Bauer D., Glebe M, Redwood R.G. and Harris P.J. (1983)
"Tests of HSS Triangular Truss Segments", Proceedings Structure Division, Canadian Society of Civil Engineering, Annual Conference, Ottawa, 1983, pp.203-220.

Bauer D. and Redwood R.G. (1984)
"Tests of HSS Double T-joints", CIDECT Report No. 5W/2-84/3-E, 1984, 51p.

Bauer D. and Redwood R.G. (1985)
"Joints for Triangular Trusses Using Rectangular Tubes", ASCE Structural Division, Structural Engineering Congress '85, Proceedings of Symposium on Hollow Structural Sections in Building Construction, 1985.

Bauer D. and Redwood R.G. (1988)
"Triangular Truss Joints Using Rectangular Tubes", Journal of Structural Engineering, Proceedings of the American Society of Civil Engineers, 114(2), pp. 408-24.

Bauer D. and Redwood R.G. (1989)
"Design of Tension Chord Joints in Triangular Trusses", Proceedings of Pacific Structural Steel Conference, Queensland, Australia.

Burdekin F.M. and Laham S.A. (1993)
"Experimental and Finite Element Studies into the Ultimate Behaviour of Cracked and Uncracked Rectangular Hollow Section Fillet Welded K-joints with Gap", Tubular Structures V, Proceedings of the Fifth International Symposium, Nottingham, United

Kingdom, pp. 691-702.

British Steel (1985)
"The Development of Recommendations for the Design of Welded Joints between Steel Structural Hollow Sections and H-sections", Commission of the European Communities, Report EUR 9462EN, 1985.

Cofer W.F. and Will K.M. (1992)
"A Finite Element Technique for the Ultimate Strength Analysis of Tubular Joints", Engineering Computations, Pineridge Press Ltd, Vol. 9, pp. 345-358.

Coutie M.G., Davies G., Bettison M. and Platt J. (1983)
"Development of Recommendations for the Design of Welded Joints between Steel Structural Hollow Sections or Between Steel Structural Hollow Sections and H Sections", Final Report, Part 3: three dimensional joints. Report on ECSC Contract 7210 SA/814, University of Nottingham, UK, 1983.

Crockett P. (1994)
"Finite Element Analysis of Welded Tubular Connections", PhD. Thesis, Department of Civil Engineering, University of Nottingham, UK, 1994.

Czechowski A. (1989)
"Design Rules for RHS Trusses", Proceedings of the Third International Symposium, Lappeenranta, Finland, pp. 46-53.

Davies G. and Panjeh shahi (1984)
"Tee Joints in Rectangular Hollow Sections (RHS) under Combined Axial Load and Bending", Proceedings of International Science and Technology Conference Metal Structures Vol. 3, Gdansk 1984.

Davies G. and Roodbaraky (1986)
"The Effect of Angle on the Strength of RHS Joints", International Meeting on Safety Criteria in Design of Tubular Joints", Tokyo, 1986.

Davies G. and Packer J.A. (1987a)
"Analysis of Web Crippling in a Rectangular Hollow Section", Proceedings of Institution of Civil Engineers, Part 2, 1987, 83, Dec. 785-798.

Davies G. and Wardenier (1987b)
"The Static Strength of Joints in RHS", Proceedings of Safety Criteria in Design of Tubular Structures, 1987.

Davies G. and Roodbaraky (1989)
"Use of Finite Elements as a Tool in Evaluating the Strength of Joints in Rectangular Hollow Sections", Tubular Structures III, Proceedings of the Third International Symposium on Tubular Structures, Lappeenranta, Finland, pp. 214-223.

Davies G. and Morita K. (1991a)
"Three Dimensional Cross Joints under Combined Axial Branch Loading", Tubular Structures IV, Proceedings of the 4th International Symposium on Tubular Structures, Delft The Netherlands, pp. 324-333.

Davies G, Coutie M.G. and Bettison M. (1991b)
"The Static Strength of Multiplanar Hollow Section Joints-Tee Joints",
Research agreement 7210/SA/830, Technical report No. 1, Number SR91030, University of Nottingham, UK.

Davies G., Coutie M.G. and Bettison M. (1992a)
"The Static S.strength of Multiplanar Hollow Section Joints - Tee Joints", Research agreement 7210/SA/830, Technical report No. 2, Number SR91051, University of Nottingham, UK.

Davies G., Coutie M.G. and Bettison M. (1992b)
"The Static Strength of Multiplanar Hollow Section Joints - Tee Joints", Research agreement 7210/SA/830, Technical report No. 3, Number SR92035, University of Nottingham, UK.

Davies G., Coutie M.G. and Bettison M. (1993a)
"The Behaviour of Three Dimensional Rectangular Hollow Section Tee Joints under Axial Branch Loads", Tubular Structures V, Proceedings of the Fifth International Symposium, Nottingham, United Kingdom, pp. 429-436.

Davies G. and Crockett P. (1993b)
"An Interaction Diagram for Three-Dimensional T-joints in Rectangular Hollow Sections under Both In-plane and Out-of-plane Axial Loads", Tubular Structures V, Proceedings of the Fifth International Symposium, Nottingham, United Kingdom, pp. 741-748.

Davies G. and Crockett P. (1994)
"Effect of the Hidden Weld on RHS Partial Overlap K Joint Capacity", Tubular Structures VI, Proceedings of the Sixth International Symposium on Tubular Structures, Melbourne, Australia, pp. 573-579.

Davies G. and Kelly R. (1996a)
"Effect of Angle on the Strength of Overlapped RHS K- and X-joints", Tubular Structures VII, Proceedings of the Seventh International Symposium on Tubular Structures, Miskolc, Hungary, pp. 123-130.

Davies G. and Crockett P. (1996b)
"The Strength of Welded T-DT Joints in Rectangular and Circular Hollow Section under Variable Axial Loads", Journal of Steel Research", Vol. 37, No. 1 pp 1-31, 1996, Elsevier Science Ltd.

Giddings T.W. and Wardenier J. (1985a)
    "The Strength and Behaviour of Statically Loaded Welded Connections in Structural
    Hollow Sections", Monograph No. 6 (Draft), CIDECT, Paris, France, 1985.

Giddings T.W. (1985b)
    "Development of Design Recommendations for Hollow Section Joints", Proceedings
    of Symposium oh Hollow Structural Sections in Building Construction", ASCE
    Structural Division, Structural Engineering Congress '85.

Giddings T.W. and Wardenier J. (1986)
    "The Strength and Behaviour of Statically Loaded Welded Connections in Structural
    Hollow Sections", Monograph No. 6, British Steel Corporation, Corby, U.K., 1986.

Kok A.W.M. (1991)
    "Numerical Mechanics", Text book b18, Delft University of Technology, The
    Netherlands.

Koning C.H.M de and Wardenier J. (1983)
    "The Static Strength of Welded K-joints with a Rectangular Chord", Stevin report No.
    6.83.04, Delft University of Technology, 1983.

Koning C.H.M de and Wardenier J. (1984)
    "The Static Strength of Welded Joints Between Structural Hollow Sections or Between
    Structural Hollow Sections and H Sections, Part 2. Joints between Rectangular Hollow
    Sections", Stevin report No. 6.84.19, Delft University of Technology, 1983.

Koning C.H.M. de, Liu D.K., Puthli R.S. and Wardenier J. (1992)
    "The Development of Design Methods for the Cost-Effective Applications of
    Multiplanar Joints", Experimental and numerical investigation on the static strength
    of multiplanar welded DX- and X-joints in R.H.S., Stevin report No. 6.92.28, Delft
    University of Technology, The Netherlands.

Koskimäki M. and Niemi E. (1989)
    "Finite Element Studies on the Behaviour of Rectangular Hollow Section K-joints",
    Tubular Structures III, Proceedings of the Third International Symposium on Tubular
    Structures, Lappeenranta, Finland, pp. 28-37.

Kurobane Y., Wardenier J. and Back J. de (1984)
    "Ultimate Strength Design of Tubular Structures", Proceedings of the Second
    International Conference on Welding of Tubular Structures, New York, USA,
    pp.439-450.

Li G. (1987)
    "Analysis of Box Girder and Truss Bridges", China Academic Publishers, Beijing,
    1987.

Linderman R.R. (1990)
"Review of Design Criteria for Rectangular Tube Connections", New Zealand Heavy Engineering Research Associations, Manukau City, NZ 15p.

Liu D.K., Puthli R.S. and Wardenier J. (1993)
"Static Strength of Multiplanar DX-joints in Rectangular Hollow Sections", Tubular Structures V, Proceedings of the Fifth International Symposium, Nottingham, United Kingdom, pp. 419-428.

Liu D.K., Yu Y. and Wardenier J. (1998a)
"Effect of Boundary Conditions and Chord Loads on the Strength of RHS Uniplanar Gap KK-joints" (to be published), Tubular Structures VII, Proceedings, 7th International Symposium on Tubular Structures, Singapore.

Liu D.K., Yu Y. and Wardenier J. (1998b)
"Effect of Boundary Conditions and Chord Loads on the Strength of RHS Multiplanar Gap KK-joints" (to be published), Tubular Structures VII, Proceedings, 7th International Symposium on Tubular Structures, Singapore.

Lu L.H., Winkel G.D. de, Yu Y. and Wardenier J. (1994)
"Ultimate Deformation Limit for Tubular Joints", Tubular Structures VI, Proceedings of the 6th International Symposium on Tubular Structures, 1994, Melbourne, Australia, pp. 341-347.

Lu, L.H., Wardenier, J. (1995)
"The Static Strength of Uniplanar and Multiplanar Connections between I-beams and RHS columns Loaded by In-plane Bending Moments", ICSAS Proceedings of the Third International Conference on Steel and Aluminium Structures, Istanbul, Turkey, page 457-464.

Makino Y., Kurobane Y. and Ochi K. (1984)
"Ultimate Capacity of Tubular Double K-joints", Proceedings of the International Conference on Welding of Tubular Structures, Boston, USA, 1984, pp. 451-8.

Makino Y., Kurobane Y., Ochi K., Vegte G.J. van der and Wilmshurst S.R. (1996)
"Database of Test and Numerical Analysis Results for Unstiffened Tubular Joints", IIW Doc. XV-E-96-220, held on Milskilc, Hungary, 1996.

Marshall P.W. (1991)
"Impact of International Developments on A.W.S. D1.1", Tubular Structures IV, Proceedings of the 4th International Symposium on Tubular Structures, Delft The Netherlands, pp. 486-503.

McGilvray I. (1994)
"The Architectural Design of Tubular Structures", Tubular Structures VI, Proceedings of the 6th International Symposium on Tubular Structures, 1994, Melbourne, Australia, pp. 3-9.

Murray N.W. (1984)
> "The Effect of Shear and Normal Stresses on the Plastic Moment Capacity of Inclined Hinges in Thin-Walled Steel Structures", Festschrift Roik, Inst. für Konstruktiven Ingenieurnau, Ruhr Univ. Bochum. Metteilung Nr 84(3), pp.237-248.

Nakai H., Yoo, C. (1988)
> "Analysis and Design of Curved Steel Bridges", McGraw - Hill, New York, 1988.

Mitri H.S., Scola S. and Redwood R.G. (1987)
> "Experimental Investigation into the Behaviour of Axially Loaded Tubular V-joints", Proceedings of the Canadian Society for Civil Engineering Annual Conference, Montreal, Canada, 1987.

Niemi E. (1986)
> "Load Capacity of Rectangular Hollow Section T-joints Subjected to Out-of-plane Bending", Publication No. 39, University of Lappeenranta, Finland 1986.

Niemi E. (1989)
> "Behaviour of Rectangular Hollow Section K-joints at Low Temperature", Tubular Structures II, Proceedings of the Third International Symposium, Lappeenranta, Finland, pp. 19-27.

O'Connor M.A. (1993)
> "Static Strength of Multiplanar K-joints in Rectangular Hollow Sections: Numerical Modelling", Tubular Structures V, Proceedings of the Fifth International Symposium, Nottingham, United Kingdom, pp. 749-756.

Owen J.S., Davies G. and Kelly R.B. (1996)
> "A Comparison of the Behaviour of RHS Bird Beak T-joints with Normal RHS and CHS Systems', Tubular Structures VII, Proceedings of the Seventh International Symposium on Tubular Structures, Miskolc, Hungary, pp. 173-180.

Packer J.A. (1983)
> "Development in the Design of Welded HSS Truss Joints with RHS Chords", Canadian Journal of Civil Engineering, Vol. 10, No. 1, pp. 92-103.

Packer J.A., Birkemoe P.C. and Tucker W.J. (1984a)
> "Canadian Implementation of CIDECT Monograph No. 6", IIW Doc. XV-584 and IIW Doc. XV-E-84-072 and CIDECT Report No. 5AJ-84/9-E, University of Toronto, Toronto, Canada, 1984.

Packer J.A. (1984b)
> "Web Crippling of Rectangular Hollow Sections", Journal of Structural Engineering, Vol. 110, No. 10, October, 1984, pp. 2357-2373.

Packer J.A. (1985)
> "Welded Connections with Rectangular Tubes", Proceedings of Symposium oh Hollow

Structural Sections in Building Construction", ASCE Structural Division, Structural Engineering Congress '85.

Packer J.A. (1987)
"Review of American RHS Web Crippling Provisions", Journal of Structural Engineering, Proceedings of Society of Civil Engineers, 1987, 113, Dec., No. 12.

Packer J.A. and Davies G. (1989)
"On the Use and Calibration of Design Standards for SHS Joints", The Structural Engineer, Vol. 67, No. 21, pp.377-386.

Packer J.A., Wardenier J. Kurobane Y., Dutta D. and Yeomans N. (1992a)
"Design Guide for Rectangular Hollow Section (RHS) Joints under Predominantly Static Loading", Verlag TÜV Rheinland GmbH, Köln 1992.

Packer J.A. and Henderson J.E. (1992b)
"Design Guide for Hollow Structural Section Connections", Canadian Institute of Steel Construction, Toronto, Canada, 348 pp.

Packer J.A., Henderson J.E. and Wardenier J. (1992c)
"Load Resistance Factor Design of Welded Box Section Trusses", American Institute of Steel Construction National Steel Construction Conference, 1991.

Packer J.A. (1993)
"Overview of Current International Design Guidance on Hollow Structural Section Connections", Proceedings of International Offshore and Polar Engineering Conference (ISOPE), 1993.

Panjeh Shahi E. (1983)
"The Behaviour of RHS Tee Joints Under Axial Load and Bending moment", Master Thesis, University of Nottingham, the U.K.

Partanen T. (1989)
"On Convergency of Yield Line Theory and Nonlinear FEM Results in Plate Structures", Tubular Structures IV, Proceedings of the 4th International Symposium on Tubular Structures, Delft, The Netherlands, pp. 313-323.

Partanen T. and Björk T. (1993)
""On Convergency of Yield Line Theory and Experimental Test Capacity of RHS K- and T-joints", Tubular Structures V, Proceedings of the Fifth International Symposium, Nottingham, United Kingdom, pp. 353-363.

Paul J.C., Valk C.A.C. van der, Wardenier J. (1989)
"The Static Strength of Circular Multiplanar X-joints", Tubular Structures III, Proceedings of the Third International Symposium on Tubular Structures, Lappeenranta, Finland, pp. 73-80.

Puthli R.S. (1981)
"Geometrical Non-Linearity in Collapse Analysis of thick Shells, with Application to Tubular Steel Joints"", Heron Publication Vol. 26, no.2, 1981, Delft, The Netherlands.

Rasmussen K.J.R., Teng F. and Young B. (1993)
"Tests of K-joints in Stainless Steel Square Hollow Sections", Tubular Structures V, Proceedings of the Fifth International Symposium, Nottingham, United Kingdom, pp. 373-381.

Redwood R.G. and Bauer D. (1983)
"Behaviour of HSS Triangular Trusses and Design Considerations", Proceedings Canadian Symposium on HSS, 1983, CIDECT, 40p.

Reusink J.H. and Wardenier J. (1989)
"Simplified Design Charts for Axially Loaded Joints of Square Hollow Sections", Tubular Structures III, Proceedings of the Third International Symposium on Tubular Structures, Lappeenranta, Finland, pp. 54-61.

Rondal J., Würker K.-G., Dutta D., Wardenier J. and Yeomans N. (1992)
"Structural Stability of Hollow Sections", Verlag TÜV Rheinland GmbH, Köln 1992.

SCI (The Steel Construction Institute 1989)
"The Development of Design Methods for the Cost-Effective Applications of Multiplanar Connections", Phase I: State-of-the-art Technical/Economic Review and Programme Definition Study, Final report to ECSC, Document Number SCI-RT-075.

SCI (The Steel Construction Institute 1995)
"The Development of Design Methods for the Cost-Effective Applications of Multiplanar Connections", Phase II: Static Strength of RHS Joints, SCI Document No. SCI-RT-439.

Sedlacek G., Wardenier J., Dutta D., Grotmann D. (1991)
"Evaluation of Test Results on Hollow Section Lattice Girder Connections in Order to Obtain Strength Functions and Suitable Model Factors", Background report to Eurocode 3 "Common unified rules for steel structures".

Szlendak J. and Brodka J. (1983)
"Investigation into the Static Strength of Welded T Moment Unreinforced Joints in Rectangular Hollow Sections", IIW Doc. XV-538-83.

Szlendak J. (1984)
"Face and Web Failure of M-N Loaded T, X RHS Joints", Welding of Tubular Structures", Pergamon Press 1984.

Szlendak J. and Brodka J. (1985)
"Yield and Buckling Strength of T, Y and X Joints in Rectangular Hollow Section Trusses", Proceedings of Institution of Civil Engineers, Part 2, 1985.

TS&MD (1992)
>"Multiplanar RHS KK-Joints - Draft Final Report" - Ref No. P011.S.05 -3, British Steel General Steels - Welded Tubes, Corby, UK.

Vegte G.J. van der, Koning C.H.M. de, Puthli R.S., Wardenier J. (1991).
>"Numerical Simulation of Experiments on Multiplanar Tubular Steel X-joints", International Journal of Offshore and Polar Engineering, Vol. 1, No.3.

Vegte G.J. van der (1995)
>"The Static Strength of Uniplanar and Multiplanar Tubular T- and X-joints", Delft University Press, The Netherlands.

Wardenier J. (1985)
>"IIW Recommendations - Present and Future", IIW Proceedings of International Meeting on Safety Criteria in Design of Tubular Structures", Tokyo, 1985.

Wardenier J. (1988)
>"Modified Eurocode 3 Design Recommendations for Hollow Section Lattice Girder Joints", Proceedings of a State-of-the-art Workshop on Connections in Steel Structures, Behaviour, Strength and Design", Cachan, France.

Wardenier J. (1989)
>"Welded Joints between Hollow Sections", Narayanan Elsevier Science Publishers Ltd. ISBN 1-85166-288-X.

Wardenier J and Packer J.A. (1991)
>"Static Design of Joints between Structural Hollow Sections", Building in Steel, London, the U.K., 1991.

Wardenier J. and Packer J.A. (1993)
>"Connections between Hollow Sections", Constructional Steel Design, An International Guide, Edited by Patrick J. Dowling, John E. Harding and Reidar Bjorhovde.

Winkel, G.D. de, Wardenier, J. (1994)
>"Parametric Study on The Static Behaviour of I-beam to Tubular Column Connections Under In-plane Bending Moments", Tubular Structures VI, Proceedings of the 6th International Symposium on Tubular Structures, Melbourne, Australia, page 317-324.

Yeomans N.F. (1989)
>"Full Width Joints in Rectangular Hollow Section Virendeel Girders", Tubular Structures III, Proceedings of the Third International Symposium on Tubular Structures, Lappeenranta, Finland, pp. 38-45.

Yeomans N.F. (1993)
>"Rectangular Hollow Section Double K-joints - Experimental Tests and Analysis", Tubular Structures V, Proceedings of the Fifth International Symposium, Nottingham, United Kingdom, pp. 437-445.

Yu Y., Liu D.K., Puthli R.S. and Wardenier J. (1993a)
"The Development of Design Methods for the Cost-Effective Applications of Multiplanar Joints", Numerical investigation into the static strength of multiplanar welded T-joints in R.H.S., Stevin report No. 6.92.37, Delft University of Technology, The Netherlands.

Yu Y., Liu D.K., Puthli R.S., Wardenier J. (1993b)
"Numerical Investigation into the Static Behaviour of Multiplanar Welded T-joints in RHS", Tubular Structures V, Proceedings, 5th International Symposium on Tubular Structures, pp. 732-740, Nottingham, United Kingdom.

Yu Y., Puthli R.S., Wardenier J. (1994a)
"A Study on the Modelling of Fillet Welded Joints in Rectangular Hollow Sections (RHS)", Proceedings, 5th International Conference on Steel Structures, pp. 347-354, Jakarta, Indonesia.

Yu Y., Puthli R.S., Wardenier J. (1994b)
"Influence of the Types of Welds on the Static Strength of RHS T- and X-joints Loaded in Compression", Tubular Structures VI, Proceedings, Sixth International Symposium on Tubular Structures, pp. 957-605, Australia.

Yu Y., Wardenier J. (1995)
"Influence of the Chord Bending Moments on the Ultimate Capacity of RHS T-joints", Proceedings, 5th International Offshore And Polar Engineering Conference, volume IV, pp. 37-44, The Hague, The Netherlands.

Yu Y., Wardenier J. (1996a)
"Parameter Study on the Static Strength of Multiplanar XX-joints in Rectangular Hollow Sections Loaded with In-plane Bending Moments", Proceedings, Sixth International Offshore and Polar Engineering Conference (ISOPE), vol. IV, pp. 105-112, Los Angles, California, USA.

Yu Y., Wardenier, J. (1996b)
"Parameter Study on the Static Strength of Axially Loaded Multiplanar XX-joints in Rectangular Hollow Sections", Proceedings, 15th International Conference on Offshore Mechanics and Arctic Engineering (OMAE), ASME, vol. III, pp. 225-232, Florence, Italy.

Yu Y., Wardenier J. (1996c)
"Analytical and Numerical Investigations on the Static Strength of Full Width Rectangular Hollow Section X-joints under Different Load Cases", Tubular Structures VII, Proceedings, 7th International Symposium on Tubular Structures, pp. 197-204, Miskolc, Hungary.

Yu Y., Wardenier J. (1996d)
"Influence of the Chord Bending Moments on the Ultimate Load Capacity of X-joints in Rectangular Hollow Sections", Tubular Structures VII, Proceedings, 7th

International Symposium on Tubular Structures, pp. 205-212, Miskolc, Hungary.

Yu, Y., Wardenier J. (1998)
"The Static Behaviour of Multiplanar XX-joints Loaded with In-plane Bending Moments and Axial Forces" (to be published), Tubular Structures VIII, Proceedings, 8th International Symposium on Tubular Structures, Singapore.

Zhang Z.L., Shen Z.Y. and Chen X.C. (1989)
"Nonlinear FEM Analysis and Experimental Study of Ultimate Capacity of Welded RHS Joints", Tubular Structures III, Proceedings of the Third International Symposium on Tubular Structures, Lappeenranta, Finland, pp. 232-240.

Zhang Z.L. and Niemi E. (1993)
"Studies of the Behaviour of RHS Gap K-joints by Non-linear FEM", Tubular Structures V, Proceedings of the Fifth International Symposium, Nottingham, United Kingdom, pp. 364-372.

Zhang Z.L. and Niemi E. (1994)
"Assessment of Ductile Crack Development in Welded (Tubular) Joints", Tubular Structures VI, Proceedings of the Sixth International Symposium on Tubular Structures, Melbourne, Australia, pp. 671-676.

Zhao, X. L., Hancock, G.J. (1991)
"T-joints in Rectangular Hollow Sections Subjected to Combined Actions," Journal Of Structural Engineering, Vol. 117, No. 8, 1991, pp 2250-2276. 44.

Zhao X.L. (1992)
"The Behaviour of Cold-formed Rectangular Hollow Section Beams under Combined Actions", PhD Thesis, School of Civil Mining Engineering, University of Sydney.

Zhao X.-L. and Hancock G.J. (1993a)
"A Theoretical Analysis of the Plastic-Moment Capacity of an Inclined Yield line under Axial Force", Thin-walled Structures, vol. 15, no. 3, 1993, pp. 185-208.

Zhao X.-L. and Hancock, G.J. (1993b)
"Experimental Verification of the Theory of Plastic Moment Capacity of an Inclined Yield Line under Axial Forces", Thin-walled Structures, vol. 15, no. 3, 1993, pp. 209-234.

Zhao X.L. (1996)
"Verification of the Deformation Limit for T-joints in Cold-formed RHS Sections", Tubular Structures VII, Proceedings of the Seventh International Symposium on Tubular Structures, Miskolc, Hungary, pp. 213-222.

## Design Recommendations

AIJ (Architectural Institute of Japan 1990).
"Recommendations for the Design and Fabrication of Tubular Structures in Steel", 3rd. ed., AIJ, Tokyo, Japan.

AWS (American Welding Society 1992)
"Structural Welding Code - Steel", ANSI/AWS D.1.1-92 Chapter 10, AWS, Miami, USA.

CIDECT (see also Packer 1992a)

CISC (Canadian Institute of Steel Construction, See also Packer 1992b)

EC3 (1992)
"Design of Steel Structures", Part 1 General Rules and Rules for Buildings, Volume 1, Chapters 1 to 9 + Background document of Chapter 3.

EC3 (1993a)
Annex Z, "Determination of Design Resistance From Tests", 1993.

EC3 (1993b)
Annex K, "Hollow Section Lattice Girder Connections", 1993.

IIW (International Institute of Welding Subcommission XV-E 1981)
"Design Recommendations for Hollow Section Joints - Predominantly Statically Loaded, 2nd. ed., IIW DOC. XV-491-81, International Institute of Welding Annual Assembly, Oporto, Portugal.

IIW (International Institute of Welding Subcommission XV-E 1989)
"Design Recommendations for Hollow Section Joints - Predominantly Statically Loaded, 2nd. ed., IIW DOC. XV-701-89, International Institute of Welding Annual Assembly, Helsinki, Finland, 1989.

## Finite element packages used

MARC Analysis Research Corporation, Versions K5 and K6, Palo Alto, U.S.A.

SDRC "I-DEAS Finite Element Modelling User's Guide", Structural Dynamics Research Corporation, Ohio, U.S.A.

# SAMENVATTING

## De Statische Sterkte van Verbindingen van Rechthoekige Buisprofielen

Rechthoekige buisprofielen (RHS) vinden veel toepassing, onder meer in industriële gebouwen, torens, masten, bruggen, kranen en mechanische werktuigen met verschillende typen en verbindingsconfiguraties. Tot het einde van de tachtiger jaren was er weinig informatie beschikbaar op het gebied van het statisch gedrag van ruimtelijke verbindingen. Daarnaast zijn voor verbindingen in één vlak onder gecompliceerde belastingsgevallen slechts weinig gegevens beschikbaar. Dit onderzoeksprogramma richt zich op het vaststellen van basisformules voor de statische sterkte van dergelijke verbindingen.

Dit proefschrift bevat de resultaten van analytisch, experimenteel en numeriek onderzoek naar de statische sterkte van gelaste verbindingen tussen rechthoekige stalen buisprofielen.

In de analytische studie zijn sterkteformules opgesteld voor X-verbindingen waarvan de wandstaven even breed zijn als de randstaaf, en belast door een axiale kracht of een buigend moment in het vlak of uit het vlak. Deze analytische modellen zijn gebaseerd op zowel het "4-scharnier" vloeilijn model als op plooi van de lijven van de randstaaf. Verder is de invloed van buigende momenten in de randstaaf op de uiterste sterkte van de verbinding analytisch onderzocht.

In het experimentele programma zijn de sterkte en stijfheid van ruimtelijke verbindingen onderzocht en vergeleken met die van vergelijkbare verbindingen met staven in één vlak. Hierbij is de geometrie-invloed en de belastingsinvloed nader bepaald.

Voor de verbindingen is een numeriek model ontwikkeld en gecalibreerd met de proefresultaten. Bij de calibratie van dit model zijn het elementtype, de lasmodellering en het materiaal- en geometrisch niet-lineair gedrag nader beschouwd.

Het eindige elementen model is verder gebruikt voor een uitgebreide parameterstudie van X- en T-verbindingen en ruimtelijke XX- en TX-verbindingen met verschillende belastingsgevallen. Verder zijn aanvullende studies verricht naar de invloed van de randvoorwaarden op de sterkte van K-verbindingen. Gebaseerd op de analytische formules en experimentele en numerieke resultaten zijn voor de beschouwde verbindingen voorstellen gedaan voor de sterkteformules die als basis kunnen dienen voor rekenregels voor de statische sterkte van vlakke en ruimtelijke verbindingen van rechthoekige buisprofielen.

**Trefwoorden**

Statische Sterkte, Rechthoekige Buisprofielen, Ruimtelijke Verbindingen, Gelaste Verbindingen, Analytisch, Experimenteel, Numeriek.

# CURRICULUM VITAE

| | | |
|---|---|---|
| Name | : | Yanrong Yu |
| Born | : | On April 22, 1961, in Pingshan, Hebei, China. |

Sept. 1978 - Aug. 1982 : Undergraduate study at the Department of Bridge and Road Engineering, Chongqing University of Architecture and Engineering, Chongqing, China.
Graduate thesis: Deflections of partially prestressed concrete beams.

Aug. 1982 - Oct. 1988 : Assistant lecturer and lecturer at Hebei university of Technology, Tianjin, China.

Nov. 1988 - Oct. 1989 : Study at the Faculty of Civil Engineering, Delft University of Technology, within the framework of an exchange programme between China and The Netherlands.

Nov. 1989 - Mar. 1990 : Dutch language course, Delft University Language Center.

May 1990 - Feb. 1992 : Graduate study at the Faculty of Civil Engineering, Delft University of Technology.
Thesis: Influence of corner radii and weld dimensions on the stress concentration factors of T and X joints in rectangular hollow sections.

Mar. 1992 - Aug. 1997 : Research assistant for a PhD degree at the Faculty of Civil Engineering, Delft University of Technology.
Thesis: The static strength of uniplanar and multiplanar connections in rectangular hollow sections.

Sept. 1997 - date : Structural engineer, Arcadis Bouw/Infra, in The Hague, The Netherlands.
Project: Design and calculation of the steel roof structure of the Football Stadium Tunis.